Imperial College of Science and Technology

University of London

Department of Electrical Engineering

A STUDY OF CERTAIN ASPECTS OF THE STEADY STATE AND TRANSIENT ELECTROMAGNETIC BEHAVIOUR OF MULTI-REGION INDUCTION DEVICES

by

Mohammad Hamed Shaker El-Markabi

B.Sc.(Eng.), M.Sc.(Eng.), M.I.E.E.E.

Thesis submitted for the degree of
Doctor of Philosophy of the
University of London

May, 1978

M.H.S. EL-MARKABI

A Study of Certain Aspects of the Steady State and Transient Electromagnetic Behaviour of Multi-region Induction Devices

---

Abstract

Many practical electromagnetic induction devices can be idealized and represented by one of three general mathematical models. Multi-region cylindrical, multi-layer planar and multiple-shell spherical structures. This thesis is concerned with utilizing the transmission line modelling technique in order to derive general electromagnetic equivalent circuits for these models. The flow and potential functions of these circuits are in general magnetic and electric field components rather than currents and voltages.

Double non-uniform transmission lines, coupled at their terminals by complex turns ratio transformers, have been used to describe the mathematical model of a multi-region cylindrical structure excited by a travelling wave two-dimensional surface current sheet. Bessel functions, usually associated with the non-uniform lines, are avoided by replacing the transmission lines by a large number of 'micro-T circuits in cascade.

The effect of motion of the different regions in a multilayer planar model excited by two-dimensional current sheet has been modelled by injecting dependent voltage or current sources at the interface coupling circuits in a double T.L. network.

The finite excitation length effect has been considered for a circumferentially excited multi-region cylindrical model, using a Fourier integral method together with the T.L. modelling technique. The model so obtained has been used to calculate the input impedance of a finite length solenoid when it is either air-cored or closely encircling an infinitely long conducting cylinder.

The electromagnetic field has been calculated for a multiple-shell spherical model when placed in a uniform magnetic field and when it is excited by a single phase, infinitesimally thin spherical coil.

The transient field problem of the one-dimensional excitation version of the above mentioned general mathematical models has been tackled by solving the appropriate electromagnetic equivalent circuits using circuit analysis computer packages.

Finally, the validity of most of the developed circuits has been checked against either published or experimental results.

ACKNOWLEDGEMENTS

This work has been carried out under the supervision of Dr. E. M. Freeman. For the invaluable help, inspiration, guidance and constant encouragement throughout the work, the author expresses his sincere gratitude to Dr. Freeman.

Thanks are also due to Mr. C. J. Carpenter, for many stimulating discussions and the keen interest he maintained during the progress of the work.

The author wishes to extend appreciation to all his colleagues in the Machines Laboratory, especially Dr. A. M. Issawi, Dr. D. A. Lowther for many fruitful discussions and Dr. T. G. Bland who kindly revised the typescript of this thesis.

He would also like to acknowledge the help of Miss E. Boden throughout the course of the work.

The author would like to express his thanks to Messrs. R. B. Owen and C. Johnson for their skillful technical help, and to Miss C. Holt of the Mineral Technology Department, Imperial College, for typing the manuscript.

The author is grateful to the Ministry of Higher Education, Egypt for the financial support which made this work possible.

Finally, special mention is due to the author's wife, Zeinab El-Saadi, for her patience, understanding and invaluable assistance, both tangible and intangible, without which, this work would have been extremely difficult.

بسم الله الرحمن الرحيم

الحمد لله الذى هدانا لهذا وما كنا

لنهتدى لولا أن هدانا الله

In the name of God, Most Gracious,
Most Merciful

Praise be to God, who hath guided us to this,
never could we have found guidance, had it not
been for the guidance of God.

CONTENTS

Abstract 2
Acknowledgements 3
List of Symbols 12

Chapter 1
Introduction 17

Chapter 2
Three dimensional electromagnetic field analysis of infinitely long, concentric multi-region circular-cylinder induction devices excited by two dimensional surface current-sheets. 25

2.1 Introduction 25
2.2 Superconducting generator - a brief review 27
2.3 The concept of a current sheet 37
2.3.1 One-dimensional current sheet 38
2.3.2 Two-dimensional current sheet 38
2.3.3 Three-dimensional current sheet 43
2.4 Mathematical model of a two-dimensional current sheet 45
2.5 Field equations -formulation and analytical solution 48
2.6 Transmission line representation 54
2.6.1 Equations of non-uniform transmission lines 54
2.6.2 Equivalent T.L. 56
2.6.3 E-wave equivalent T.L. 59
2.6.4 H-wave equivalent T.L. 61
2.6.5 Expressions for the electromagnetic field components in terms of the equivalent double T.L. quantities 62

2.7 Surface wave impedance expressions 66
2.8 Application of the boundary conditions 70
2.9 Micro-T circuit formulation 80
2.9.1 Elements of the micro-T circuit of the E-line 85
2.9.2 Elements of the micro-T circuit of the H-line 85
2.9.3 Simplifications for conducting and non-conducting regions 88
2.10 Expressions of the electromagnetic field components in a Laplacian-region: (non-conducting region) 91
2.11 Special case: one-dimensional excitation current sheet 95
2.12 Macro-T circuit representation of E- and H-lines 97
2.13 The equivalent four-terminal network of an annular conducting region bounded by two non-conducting regions 103
2.14 Experimental model 108
2.14.1 Description of the excitation winding test-rig 108
2.14.2 Excitation current-sheet expressions 110
2.14.3 Equivalent circuit and method of computation 113
2.14.4 Test results and computer calculations 119
2.15 Conclusions 131

Chapter 3
Three dimensional electromagnetic field analysis of a multi-layer planar model excited by a two-dimensional surface current sheet. 134

3.1 Introduction 134

3.2	Linear induction motor - historical review	135
3.3	One-dimensional analysis	138
	3.3.1 Finite thickness model	138
	3.3.2 Finite width model	139
	3.3.3 Finite length model	140
3.4	Two-dimensional analysis	141
	3.4.1 Finite excitation models	141
	(i) Finite thickness and width model	141
	(ii) Finite thickness and length model	142
	(iii) Finite length and width model	144
	3.4.2 Finite excitation and finite stator iron length model	144
3.5	'Three'-dimensional analysis	145
	3.5.1 Finite excitation model	146
	3.5.2 Finite excitation and finite iron length model	147
3.6	Numerical methods	148
3.7	Mathematical model	150
3.8	Theory	152
	3.8.1 Maxwell equations	152
	3.8.2 H-field governing equation	153
	3.8.3 E-field governing equation	155
3.9	Transmission line modelling	156
	3.9.1 Equivalent circuit with voltage sources	157
	3.9.2 Equivalent circuit with current sources	162
	3.9.3 The micro-T circuits of E- and H-lines	166
3.10	Some special cases	168
	3.10.1 The coupling circuit between two adjacent non-conducting regions	168
	3.10.2 One-dimensional excitation	170

3.10.3 The equivalent four-terminal network of a conducting region stationary in the frame of reference and bounded by two infinitesimally thin non-conducting layers 172

3.11 Conclusions 178

Chapter 4

Induction devices having circumferentially directed excitation current - The infinitely long model 180

4.1 Introduction 180

4.2 Review of previous work 184

4.3 Mathematical model and fields of application 186

4.3.1 The mathematical model 186

4.3.2 Fields of application 188

4.4 Field equations 189

4.4.1 Assumptions and formulation 189

4.4.2 Methods of solution 191

4.5 Purely algebraic manipulation method 192

4.6 Transfer matrix surface impedance method 194

4.7 Mirco-T circuit method 197

4.7.1 Theory 197

4.7.2 Non-conducting region equivalent circuit 198

4.7.3 Conducting region equivalent circuit 201

4.8 Criteria for the choice of the thickness of the sub-regions in a conducting region 203

4.9 Boundary conditions 208

4.10 Calculation of the terminal impedance from the surface wave impedance 210

4.11 Conductivity measurement 212
4.11.1 Experimental set up 214
4.11.2 Equivalent circuit and method of computation 215
4.11.3 Choice of the test frequency 219
4.11.4 Approximate representation of very thin conducting tubes 223
4.12 Test results: diagrams and discussions 225
4.13 Conclusions 231

Chapter 5
Induction devices having circumferentially directed excitation currents - Finite length model 235

5.1 Introduction 235
5.2 Theory 244
5.2.1 Mathematical model 244
5.2.2 Excitation current expression 246
5.2.3 Transmission line modelling and equivalent circuit 250
5.3 Calculation of the terminal input impedance of the excitation coil 254
5.4 Current density distribution 259
5.5 Normalised terminal impedance of finite length, air-cored solenoidal coil 263
5.5.1 Simple expressions for the input wave impedance of non-conducting innermost and outermost regions 263
5.5.2 Expressions for the Nagaoka factor derived from the surface wave impedance 265
5.5.3 Nagaoka factor in terms of complete elliptic integrals 267
5.6 Computations and comparison with the published material 269

5.6.1 Nagaoka factor and terminal impedance 269
5.6.2 Axial distribution of the surface current density 280
5.6.3 Radial distribution of the circumferential current density 285
5.7 Conclusions 290

Chapter 6
Electromagnetic field solution of a concentric multiple-region spherical structure excited by a one-dimensional current sheet or a uniform magnetic field. 293

6.1 Introduction 293
6.2 Mathematical model 297
6.3 Field equations 299
6.3.1 Formulation 299
6.3.2 Solution of the field equations 300
6.4 Excitation current sheet 302
6.5 Transmission line modelling 306
6.5.1 Micro-T circuit representation 308
6.5.2 Transfer matrix representation of non-conducting spherical shells 312
6.5.3 Innermost and outermost non-conducting regions: Input impedance 315
6.5.4 Choice of the sub-region thickness Δr 318
6.6 Expression for the power flow over a spherical surface 321
6.7 Special case: Spherical multiple-shell model in a uniform magnetic field 323

6.8 Applications 330
6.8.1 Magnetic shielding 330
6.8.2 Eddy current screening 335
6.9 Conclusions 350

Chapter 7
Transients in layered structures 353

7.1 Introduction 353
7.2 Objective of the present work 355
7.3 Brief review of published material 356
7.4 Transmission-line modelling 359
7.5 Catalogue of micro-T circuits 362
7.6 Analytical solutions of some one-dimensional planar models 365
7.6.1 Micro-T circuits - New concept 366
7.6.2 Analytical expressions 369
7.7 Calculations and experimental results 371
7.7.1 Analytical check 371
7.7.2 Experimental model 374
7.8 Conclusions 378

Chapter 8

Conclusions and suggestions for future work. 379

References 387
Appendix 405
List of papers accepted for publication 409

LIST OF SYMBOLS

A = Constant in chapters 2, 4 and 6

A_n, A'_n = constants in chapter 6

a = excitation radius in chapters 4 and 5

a = outer radius of spherical shell in chapter 6

a_m = element of transfer matrix in chapter 4

$\bar{B}$ = flux density vector

B = constant in chapter 4

b = outer radius of conducting tube in chapter 4

b = inner radius of spherical shell in chapter 6

b_m = element of transfer matrix in chapter 4

C = capacitance

C = constant in chapter 4

C_{1h}, C_{1e}, C_i, C_v = constants in chapter 2

C_n, C'_n = constants in chapter 6

$C_{1,n}$, $C_{2,n}$, $C_{3,n}$, $C_{4,n}$ = elements of transfer matrix in chapter 6

c = inner radius of conducting tube in chapter 4

c_m = element of transfer matrix in chpater 4

D = constant in chapters 2 and 4

D' = constant in chapter 2

d = penetration depth $\{d=(1/\omega\mu\sigma)^{\frac{1}{2}}\}$

d_m = element in transfer matrix in chapter 4

$\bar{E}$	= electric field strength vector
$E(k)$	= complete elliptic integral of the second kind
e'_x, e'_y, e''_y	= form functions in chapter 3
erf	= error function
erfc	= complementary error function
f	= frequency
g_{11}, g_{22}, g_{33}	= metric coefficients in Appendix A
$\bar{H}$	= magnetic field strength vector
h''_x, h'_y, h''_y	= form functions in chapter 3
I	= current
I', I"	= equivalent T.L. currents in chapters 2 and 3
I^r	= 'transformed' T.L. current in chapter 2
I_r, I_s	= receiving end and sending end currents of a T.L.
I_o, I_1, I_α, $I_{\alpha+1}$, $I_{\alpha-1}$	= modified Bessel functions of the first kind
$\bar{J}$	= current density
j	= square root of minus one
$\bar{K}$	= linear current density
K_o, K_1, K_α, $K_{\alpha+1}$, $K_{\alpha-1}$	= modified Bessel functions of the second kind
$K(k)$	= complete elliptical integral of the first kind
Kr	= integration kernel in chapter 5
L	= inductance
L_o	= inductance of an air-cored, infinitely long solenoid per unit length

l = axial length of solenoid coil in chapters 4 and 5

m = order of spatial harmonic

N = number of turns in chapter 5

n = order of spatial harmonic

P_n^m, Q_n^m = first and second kinds of associated Legendre functions of order (n) and degree (m)

Q = transformation factor in chapter 3

R = resistance

R = radius in chapter 6

$R(r)$ = r-dependent function in chapter 6

r = radius

r_e = excitation radius

r, θ, z = circular-cylinder coordinate system

r, θ, ϕ = spherical coordinate system

$\bar{S}$ = complex Poynting vector

s = slip

T = coupling transformer complex turns ratio in chapters 2 and 3

T = number of turns in chapter 4

t = time

V = voltage

V', V'' = equivalent T.L. voltages in chapters 2 and 3

$\bar{v}$ = linear velocity vector

v_x = linear velocity in the x-direction

W = Wronskian in chapter 5

W	= power in chapter 6
X	= reactance
x, y, z	= rectangular cordinate system
Y	= admittance
Y', Y''	= surface wave admittance/unit length
Z	= impedance
Z', Z''	= surface wave impedances/unit length
Z_o', Z_o''	= characteristic surface wave impedances
Z_s	= surface wave impedance in chapter 4
$Z_T(\Omega)$	= tensorial surface wave impedance in chapter 5
Z_t	= terminal impedance
α	= wave number in chapters 2 and 3
α	= spherical coil angle in chapter 6
β	= wave number in chapters 2 and 3
γ, γ_o	= propagation constants
$\Delta r, \Delta z$	= elementary thicknesses in the r- and z-directions respectively
δ	= skin depth $=(2/\omega\mu\sigma)^{\frac{1}{2}}$
ε	= per unit electric field component in chapter 5
ε	= error in chapter 4
ε	= permittivity
η	= filling factor defined in chapter 4
$\Theta_n(\theta)$	= nth surface zonal harmonic
μ	= permeability

σ	= conductivity
$2\tau = l$	= axial length of solenoidal coil in chapter 5
Ω	= spatial harmonic frequency
ω	= angular frequency
∇_t	= Nabla operator in the transverse direction ($\nabla_t \equiv \nabla - \delta/\delta z$)
Re	= real part
Im	= imaginary part
$\hat{}$	= peak value
*	= complex conjugate

All other symbols are defined in the text

Chapter 1

Introduction

The importance of applying Maxwell field equations for solving electrical machines problems has been well known since the end of last century. Many referecnces can be found in an interesting review paper by Nasar[1.1], and in the discussion[1.2].

In general, the electrical machines are so complicated in geometry that an exact analytic solution of these equations is quite impracticable, even if the effects of non-linearity and hysteresis in iron are ignored. Usually the machine has to be idealized to the point where the actual physical structure can be replaced by a mathematical model which is amenable to analysis. The practical designer can then use the idealized solution to give him general guidance on the problem he has in hand.

There is no doubt that the numerical methods, such as the finite difference or finite element techniques which have been developed successfully in the past two decades, are capable of solving many field problems specially in these cases where the idealized models fail to represent the physical structures accurately. But of course this will be on the expense of the cost of solution and computer time.

In this thesis we will be concerned with solving the field problem for models of that class of electrical devices where the currents are induced, by electromagnetic induction, in the conducting regions due to the alteration of excitation currents in nearby windings. These devices are referred to, throughout the text, as 'induction devices'. The geometries considered are particularly amenable for modelling as multi-region cylindrical, multi-layer planar or multiple-shell spherical, mathematical models.

The method of solution pursued in this work is essentially a 'computer-aided analytical technique'. Numerical methods are not considered, except for the solution of the transient V and I using ECAP/SPICE.

The theory of an electromagnetic device is usually presented in one of two ways. Either the device is represented by an 'electric' equivalent circuit, or analytical expressions are derived from electromagnetic field theory. These are the 'circuit' and 'field-theory' approaches respectively.

The circuit approach, when applied directly, involves the determination of lumped parameters. These parameters are usually chosen in order to indicate both the effects of changes in the physical structure of the device on the components of the circuit, and also the effects on the device characteristics due to changing the circuit parameters. In many simple cases, this equivalent electric circuit can be obtained to match the terminal characteristics of the device as obtained by measurements.

Alternatively, analysing the electric-current and magnetic flux paths, i.e. solving the field equations, and constructing an 'electromagnetic' equivalent circuit, from which an electric current may be obtained by appropriate transformation, yields similar results. The second technique is preferable to the first because it allows more information about conditions in the material that may be

subject to electric and magnetic stresses, also it eliminates many approximations.

The resulting equivalent circuit has proved to be extremely useful and can give a fairly deep insight into the behaviour of the electromagnetic device. Engineers are trained to interpret equivalent circuits, and once the circuit elements have been obtained, the amount of calculation required for a given set of conditions is relatively small.

The rest of this thesis is devoted to developing the appropriate electromagnetic equivalent circuits, starting from Maxwell equations, for a wide range of practical problems.

The idea of developing electromagnetic equivalent circuits from Maxwell field equations may go back to 1916 when Professor Howe[1.3] drew attention to the similarity between the telephone transmission line formulae and skin depth problems. It seems that nobody took this analogy any further for at least twenty years. In 1937, Schelkunoff (ref. 1.4) published a paper in which he stressed the similarity between the equations which govern the plane electromagnetic waves propagation, and the equations which govern the distribution of the voltage and current over continuous transmission lines. Realizing this similarity,

Schelkunoff constructed a T.L. 'electromagnetic' equivalent circuit in which the flow and potential quantities were field components rather than voltages and currents. The input impedance to this line is a ratio between field components and so it has been known as the 'wave impedance'. Since then, this concept of wave impedance has been a corner stone of micro-wave theory[1.5].

Kron[1.6, 1.7] took this concept a step further and developed a three-dimensional equivalent circuit to represent the tensor-density form of Maxwell field equations in a very general way. Then he showed that his complicated equivalent circuit could be reduced, under some special cases, to the single transmission lines obtained earlier by Schelkunoff.

For some time the concept of wave impedance has been extensively utilized for high frequency applications. With reference to low frequency applications, Cooper[1.8] analysed the operation of inductors and transformers in terms of the field impedance (i.e. wave impedance). Similarly, Welsby[1.9] utilized the same concept in order to study the harmonic distortion of the electromagnetic field in a ferromagnetic medium due to hysteresis.

Arguing that the induction motor, like all other electrical devices, must obey the laws of electricity and magnetism as formulated by Maxwell equations of the electromagnetic

field, Cullen and Barton[1.10] published their stimulating paper in which they introduced the concept of wave impedance in the context of induction machine theory. They modelled an induction motor using two regions, and replaced each region by an equivalent transmission line. The slotting effect has been introduced by considering anisotropic permeability and conductivity.

Greig and Freeman[1.11], then Freeman[1.12] generalised the Cullen and Barton model by introducing the concept of transfer matrices in order to deal with a multilayer model.

The literature now is rich in the publications where the concepts of wave impedance and transmission line representation are used for low frequency applications[1.13-1.21].

The main objective of the present work is to utilize the same concepts in order to analyse some mathematical models which have not been considered before. The thesis is set out as follows:

Chapter 2: The mathematical model of a multilayer cylindrical structure excited by a two-dimensional surface current sheet (in the axial and circumferential directions) has been considered. Although this model has been considered sometime ago by Eastham and Alwash[1.22] to model transverse flux tubular motors, the analysis reported by them is not strictly correct. Due to the fact that the r- and θ-directed components of the electric field vector $\bar{E}$ are cross coupled through the vector

Helmholtz equation, the neglect of any one of them, on the basis that there is no excitation current in its direction, is not 'generally' valid. The analysis developed in this chapter has been carried out without any assumption regarding the neglect of any component of the electric and magnetic field vectors.

Chapter 3: The analysis of a multilayer planar model, excited by a two dimensional current sheet, has been reported. This analysis differs from any other reported in the literature in two respects:

(a) The effect of motion has been introduced explicitly, and not implicitly through the concept of slip frequency adopted by others[1.17]

(b) The normal current (to the excitation surface) has not been assumed zero (see for example the work by Williamson[1.23]). The equivalent network developed in this chapter is then capable of representing the general case when two adjacent different 'conducting' regions are in relative motion.

Chapter 4: The field problem of an infinitely long solenoidal coil immersed in a multiregion cylindrical structure has been considered. This problem in particular

has been solved before as indicated in the literature review. However, the main contribution of the reported work lies in simplifying the computation procedure by avoiding the calculation of Bessel functions of complex arguments. In addition a simple method is proposed by which the conductivity of conducting solid cylinders or tubes could be obtained to an estimated accuracy of 1%.

Chapter 5: The analysis reported in chapter 4 has been taken a step further by studying the finite length effect of the excitation coil. The Fourier integral method, together with a T.L. equivalent network has been utilized to calculate the input impedance of a finite length coil when it is closely encircling a solid conducting cylinder and when it is air-cored. Comparison between published results and calculations based on the theory developed, has been reported. The induced eddy currents in the conducting rod have also been determined.

Chapter 6: The model of a multiple-shell spherical structure, excited by either an infinitesimally thin spherical coil or a uniform external magnetic field, has been considered. An electromagnetic equivalent circuit has been developed, and comparison between calculated results and both closed form solution and experimental results have been reported.

Chapter 7: The transient field problem of some one-dimensional multilayer mathematical models has been

considered. Making use of the circuit analysis computer packages, the transient solution is made possible by solving the electromagnetic equivalent circuit problems.

An introduction has been written for each chapter in which some of the important practical applications which can be represented by the mathematical model are listed. A literature review has been included in each chapter whenever possible.

CHAPTER 2

Three Dimensional Electromagnetic Field Analysis of Infinitely Long, Concentric Multiregion Circular-Cylinder Induction Devices Excited by Two-Dimensional Surface Current-Sheets.

2.1 Introduction

A search through the literature shows that in general the solution of the field equations in cylindrical coordinate systems has been reported by many authors. The excitation current is usually represented by a current sheet which is restricted to either an axial or a circumferential direction. For instance, Piggott[2.1] solved the field in an annular air-gap of a squirrel-cage induction motor, the excitation had been assumed to be in the axial direction only, and the rotor induced currents had been represented by an equivalent linear current sheet. For a more complicated mathematical model, Freeman solved the field equations for a multilayer cylindrical structure considering an axial[2.2] or circumferential[2.3] excitation current sheet. The tedious and cumbersome task of matching the boundary conditions at the layer interfaces had been elegantly tackled by the transfer matrix representation[2.4]. It is worth mentioning that, in a recent paper by Kirtley[2.5], a method for matching the boundary conditions in a multilayer, axially excited cylindrical structure, has been suggested. This method is very much like that reported by Freeman some

years earlier. Hughes and Miller[2.6] solved for the field of an air-cored, axially excited, machine. Their model is essentially a special case of the general multilayer model by Freeman.

Hammond[2.7] derived the field solution of an air-cored cylindrical structure, excited by a two-dimensional surface current sheet, which has axial and circumferential components. The magnetic field obtained by Hammond is three dimensional . Lawrenson and Ralph[2.8, 2.9] perhaps were the first to derive a complete field solution in a cylindrical coordinate system where both the magnetic field and the induced eddy current each had three components. Although their solution is general, it is very compolicated and may be extremely difficult to apply specially when more than one conducting region is involved. The determination of the constants, which appear in their expressions, by satisfying the boundary conditions at the interfaces, is a formidable problem.

Eastham and Alwash[2.10], studying a transverse flux tubular motor, solved the field equations in a cylindrical coordinate system. They assumed a multilayer model with axial and circumferential current sheets. Freeman[2.11] developed a network model based on their results. One of the assumptions adopted in their solution is not strictly correct, which is the assumption of zero radial electric field component everywhere, and consequently no radial induced eddy current in any conducting region. This assumption is only an approximation and, as will be shown later, it can be reasonably applied

when the radii are very large as compared with the radial thicknesses of the different annular layers of the mathematical model.

Recently, the superconducting turbo-generator emerged as one of the promising solutions for obtaining very large power economically from a single generator unit. This generator could be represented by the basic mathematical model considered in this chapter, and because of its practical importance, section 2.2 will be devoted to a brief review of the literature relating to this generator.

2.2 Superconducting Generator - A Brief Review

The demand for electrical power throughout the world has been roughly doubling every decade. The increased demand has been met by a great increase in the power output per generator, made possible by significant advances in their design particularly in cooling the windings and better utilization of materials.

Today single generators rated at 1200 MVA are in service and higher rated units have been ordered for installation in a few years time. In a recent paper by Parker and Towne of Westinghouse Co., U.S.A. (reference 23), a graph shows the estimated growth of generator ratings between the years 1980 and 2000. They anticipated that by the end of this century, the maximum unit rating may amount to about 4000 MVA. It appears that present technology will provide for ratings up

to about 2500 MVA[2.23].

The output equation of an a.c. generator is usually written in the form:

$$kVA = k\ B\ A\ n\ V$$

where

kVA = generator rating

B = air-gap flux density

A = armature current loading

V = generator volume

n = rotational speed

k = proportionality constant

It is obviously clear that an attempt to increase the rating of an a.c. generator can be effected by increasing any of the right hand side variables of the above output equation. The rotational speed (n) is limited by the frequency, and cannot be increased more than 3000 r.p.m. (for a 50 Hz 2-pole machine). The volume V is limited by mechanical considerations such as the maximum peripheral speed, which limits the machine diameter for a certain rotor speed, and the sag and vibrations of the rotor, which limits its axial length. It is also limited by the transportation and shipping weight requirements. The current loading A is limited by thermal considerations and by the forces existing in the end windings under short circuit conditions.

It seems then that the flux density B can play a major

role in increasing the generator rating for a certain frame size.

In the conventional a.c. generator, the 3-phase stator winding is usually accommodated in a slotted iron structure. The removal of approximately half the stator air-gap periphery, due to slotting, concentrates the main flux in the teeth. Consequently the air-gap flux density will be mainly limited by the saturation of the teeth. Thus, it has been thought that removing the stator winding from the slotted iron will approximately double the air-gap working flux density, hence the rating of a certain frame size can be approximately doubled. Davies[2.12] revived this idea, originally suggested by Horsely[2.13] also be Morgan and Wilkins[2.14], of using a slotless stator winding a.c. generator. Fully slotless machines have been described by Airchholzer[2.15]. Spooner[2.16] gave an interesting comparative study between those slotless a.c. generators and their conventional counterparts. Sometimes these slotless machines are referred to in the literature as machines with air-gap windings.

With the introduction in the mid 1960's of stable multifilamentary, type II superconductors capable of carrying large currents in high d.c. magnetic fields, came the realization of the potential improvements that could result from their application to the field winding of high power electrical a.c. generators.

Superconductivity removes the direct connection between rotor ampere-turns and copper losses, and hence the ampere-turns are limited by available materials rather than by cooling and efficiency limitations. Hence replacing the rotor copper conductor by a superconductor permits the rotor current density to be increased and consequently the corresponding airgap flux density.

With a superconductor it is possible to get magnetic fields of >5 Tesla at $4^{\circ}K$. This increased magnetic field capability, to a level beyond the saturation level of iron, means that the iron can be removed from the rotor leaving more space available for the winding and thus resulting in a reduction in rotor diameter. Also, the stator teeth can be removed leading to an "air-gap machine".

Towards the end of 1960's and by the early 1970's, projects were started in different research laboratories in U.S.A., Russia and U.K. in order to demonstrate the feasibility and practicality of employing superconductors in large a.c. machines (e.g. references 2.17 - 2.23). With this new technology of removing the iron from the machine structure, new types of problems, which did not exist before in the conventional machines, have been introduced. For instance, the machine torques are exerted now directly on the windings, so they have to be designed to withstand these torques, and torque transmitting means must be provided. The field winding being placed on the rotor, the problem of designing a rotating

cryostat, which cools the superconductor to about $5^{o}K$, arises. To overcome this, a team in CERL, U.K. suggested a stationary field, rotating armature system[2.22], but this configuration immediately raises the problem of collecting a very high power through slip rings. This in turn resulted in research aiming to develop liquid metal slip rings capable of handling this large power.

The basic cross-sectional configuration, widely accepted by most researchers, of an A.C. two pole generator with superconducting field winding is shown in Fig.(2.1). The field winding, being kept at $4^{o}K$, is required to be thermally insulated from the armature winding, which is kept at the ambient temperature, hence a 'thermal radiation shield' is introduced which completely encloses the field winding. In order to protect the cryogenic environment of the field winding from A.C. fluctuations in the flux linking the field winding, an 'electromagnetic shield' is introduced in the airgap space. At steady state, such fluctuations are typically caused by negative sequence currents due to unbalanced loads and by the stator winding space harmonics. Faults and other transient conditions also lead to time varying magnetic fields at the rotor. A secondary role of this shield, is to act as a damper winding for the mechanical oscillations of the rotor. The damping effectiveness of any damper winding is a function of both its time constant and the frequency of the rotor oscillations to be damped. In order to obtain maximum damping the time constant of the damper winding should be

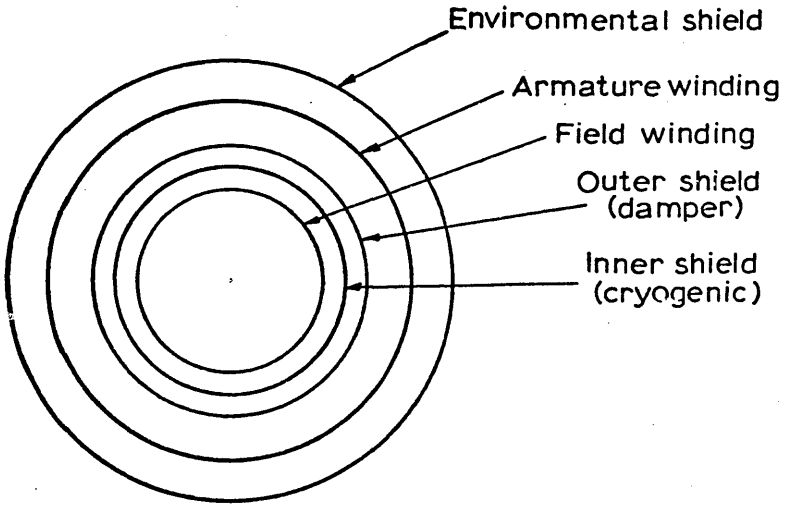


Fig. 2·1 Schematic cross section of a double shield superconducting machine.
(Taken from ref. 2·25)

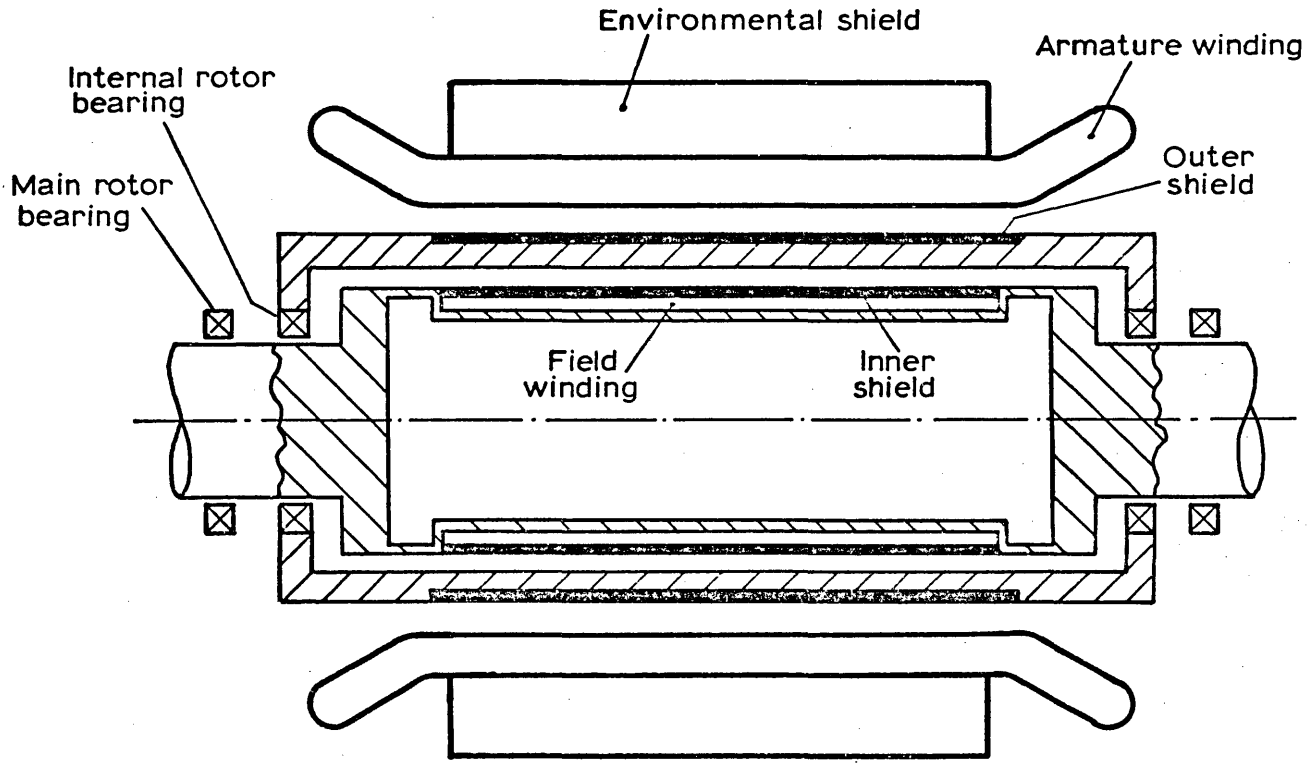


Fig. 2·2 Superconducting alternator with an inertial-shell
(Taken from ref. 2·27)

'tuned' to the range of swing frequencies to be damped.

These two functions of the shield have conflicting requirements. The best electromagnetic shield should have a very long time constant. Effective damping should not be too long[2.25].

A possible resolution of the conflict between damping and shielding functions is represented by the double shielding concept originally introduced by Luck and Thullen[2.24], and then theoretically investigated by Furuyama and Kirtley[2.25], and more recently by Lawrenson et al[2.26]. This double shielding consists of two concentric shells. The outer shield, which operates at about the ambient temperature, serves as a damper and as the primary magnetic shield, and it serves to absorb the very large (of the order of ten per unit) alternating torque and crushing loads associated with faults. The exact form of this shield is not yet completely clear. It has been suggested that this shield may be constructed from a strong non-magnetic steel cylindrical structure that completely encloses the field winding. The electrical shielding from asynchronous fields is supplied by a layer of high conductivity material at either the inner or the outer surfaces of the supporting steel cylinder. The inner shield, which operates at 20 - 40^{o}K, is cryogenic. It serves as the radiation shield and as the final stage in the magnetic shielding system.

In an attempt to relieve some of the stresses that occur during a fault, Dagalakis and Kirtley[2.27, 2.28] suggested that the outer shield could be mounted on its own bearings, thus making it able to rotate independently of the rotor winding. During normal operation, free to rotate on its own bearing, it would behave as a drag-cup induction motor with essentially no load, and would thus rotate at nearly synchronous speed. During fault conditions, however, the strongest component of the alternating fault torques with fundamental or twice fundamental frequency, will simply accelerate and decelerate the freely rotating shield, and it will not be transmitted to the rotor, shafts, couplings and turbine. If the inertia of the shield is large enough, the angular excursion during the fault conditions will be relatively small. Dagalakis and Kirtley gave the name 'inertial electromechanical', or simply 'inertial', to this freely rotating outer shield.

Finally, in order to exclude the large field of the superconducting generator from the surroundings, the stator structure is enclosed in an outer shield. This shield is usually termed the 'environmental' shield, and it may be constructed from either laminated iron or conducting material.

The arrangement of the supreconducting generator with double shielding where the outer shield is an inertial shield is shown in Fig. (2.2).

In order to study the damping, screening and the forces associated with the superconducting generators, it is generally required to solve for the magnetic field components as well as the induced eddy currents in the different conducting regions. As it has been indicated before, there are at least one or two conducting layers in the air gap between the stator and rotor windings, together with an outer laminated iron or conducting layer. Furthermore, any of these layers could be constructed from one or more materials having different conductivities. The mathematical model which can be thought of to represent this structure is then of multi-layer cylindrical form. An idealised representation of the three phase stator winding may be single surface current sheet acting at the mean radius of the winding itself. A better representation, but of course slightly complicated, is obtained by considering more than one surface current sheet distribution along a radial direction, with each representing a certain radial thickness of the stator winding. In fact this representation can be implemented easily after developing the transmission line analogue of the multi-layer model as will be shown later.

Since the air-gap is comparable with the radii involved in the structure of this type of problem, the field equations have to be solved in a cylindrical polar coordinate system. The cartesian representation is no longer valid.

After this brief review of the published material, the

rest of the Chapter will be devoted to the development of a three-dimensional electromagnetic field solution for a multi-layer cylindrical structure excited by a two dimensional surface current sheet. This mathematical model is basic to the solution of wide variety of problems. For example, the problems of superconducting turbo-alternator screening, transverse flux tubular motors, eddy currents losses in screened-rotor induction motors[2.29], drag-cup rotor and sleeve rotor motors, all can be represented by this multi-layer mathematical model.

The transmission line modelling technique will be utilized in order to obtain an equivalent network, hence simplifying the solution. In order to check the validity of the results, an experimental model has been built and comparison between the experimental and theoretically calculated results shows remarkable agreement.

The two dimensional current sheet has been obtained using a three-phase winding wound helically around a tube of insulating material. The winding has only a single layer. Its radial thickness is very much smaller than the radii or the thicknesses of the conducting layers which were either inserted inside or placed concentrically outside the helical winding.

2.3 The Concept of a Current Sheet

The theoretical treatment in this chapter can be applied to many different practical applications which can be represented by the mathematical model illustrated later in section (2.4). Of course, the different applications will impose different forms of expression for the excitation current.

The complicated geometry of the individual excitation coils of a machine makes it difficult to describe them analytically . Hence the complete winding has to be essentially represented by a simplified equivalent current distribution. This current distribution is usually referred to in the literature as a 'current sheet'.

The concept of replacing the actual machine conductors by an infinitesimally thin current sheet may be attributed to Hague[2.31]. Saunders[2.32], following Hague, replaced the slot current of a slotted structure by a uniform elementary current sheet acting at the slot opening. The contribution of all the elementary current sheets gives the harmonic series of the resultant equivalent current sheet produced by the excitation winding.

The methods employed to replace an actual cylindrical machine by an equivalent current sheet may be divided in general into three main categories:

i) One-dimensional current sheet, which is either in the axial or the circumferential directions.

ii) Two-dimensional current sheet, which has components in both the axial and the circumferential directions.

iii) Three-dimensional current sheet, which has components in the radial, circumferential and axial directions in general.

2.3.1 One-dimensional current sheet

The excitation winding can be represented by either an axial or circumferential current sheet. This is commonly done when the device is either axially or circumferentially excited provided that the finite length effects are to be ignored. Typical examples are: the winding of an induction motor which can be replaced by an axial sheet rotating in the circumferential direction at synchronous speed, while the winding of a 3-phase tubular motor[2.33] can be represented by a circumferential current sheet which travels along in the axial direction.

2.3.2 Two-dimensional current sheet

The assumption of an infinitely long mahcine is not of course valid. However, it can be justified in the cases where the axial length/diameter is large enough. In an

actual machine, the axial excitation current has a return path through the end winding, and it does not extend to infinity as is assumed in the one-dimensional model. Many researchers tried to model the finite length effect, to a first approximation, by a two-dimensional current sheet. The model usually chosen to represent the finite length machine consists of an infinite array of machines[2.34] arranged as shown schematically in Fig. (2.3) on a common axis.

The impressed current sheet components are now assumed to have both axial and circumferential variations. The infinite succession of these machines has the great advantage that the excitation current sheet can be expressed in terms of a Fourier series. Each two adjacent machines are assumed to be oppositely excited in order to satisfy mathematically the physical property that the induced eddy currents are confined to the rotor dimensions, and not flowing form one machine to another. Wood and Concordia[2.34] assumed that the separation S between the adjacent machines of Fig.(2.3) is zero, hence the axial variation of both components of the exciting current sheet will be given as shown in Fig. (2.4).

Hammond[2.7] dealing with the excitation finite length effects considered the same arrangement of infinite succession of machines on a common axis, however, he allowed the separation S to be large enough such that the field due to any one

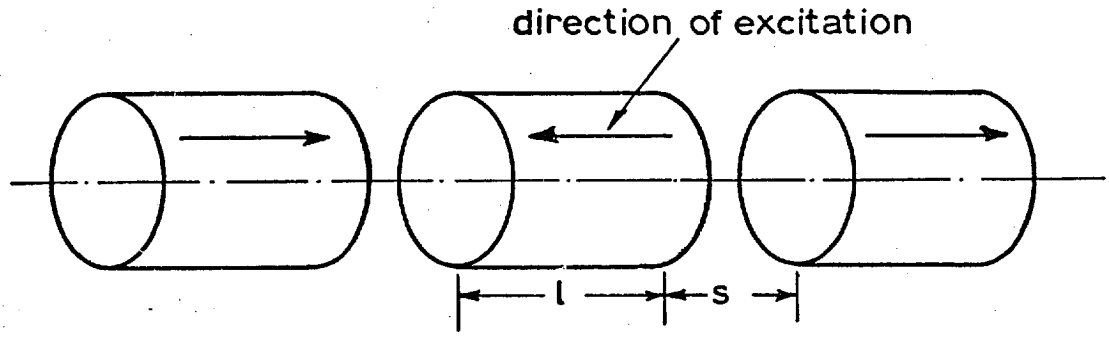


Fig. 2·3 Array of an infinite number of machines arranged on a common axis

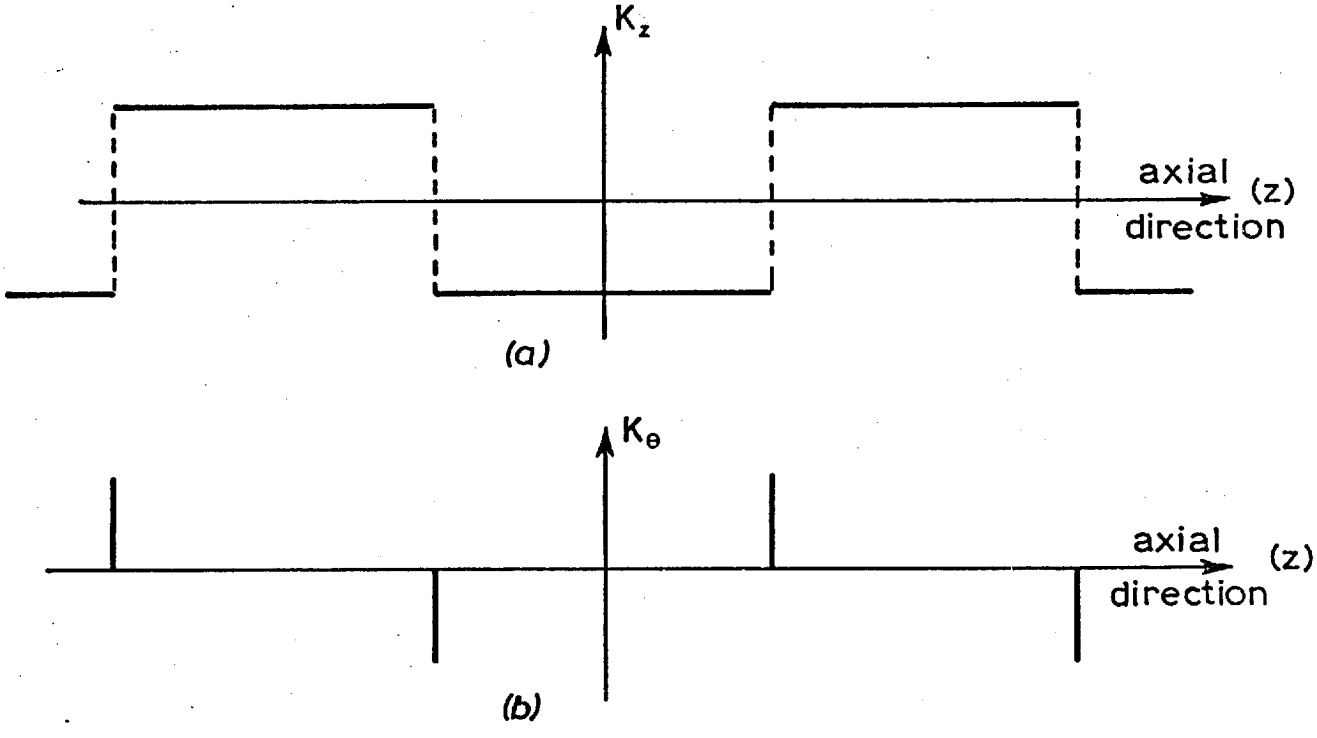


Fig. 2·4 Current sheet waveforms
(a) axial (b) circumferential

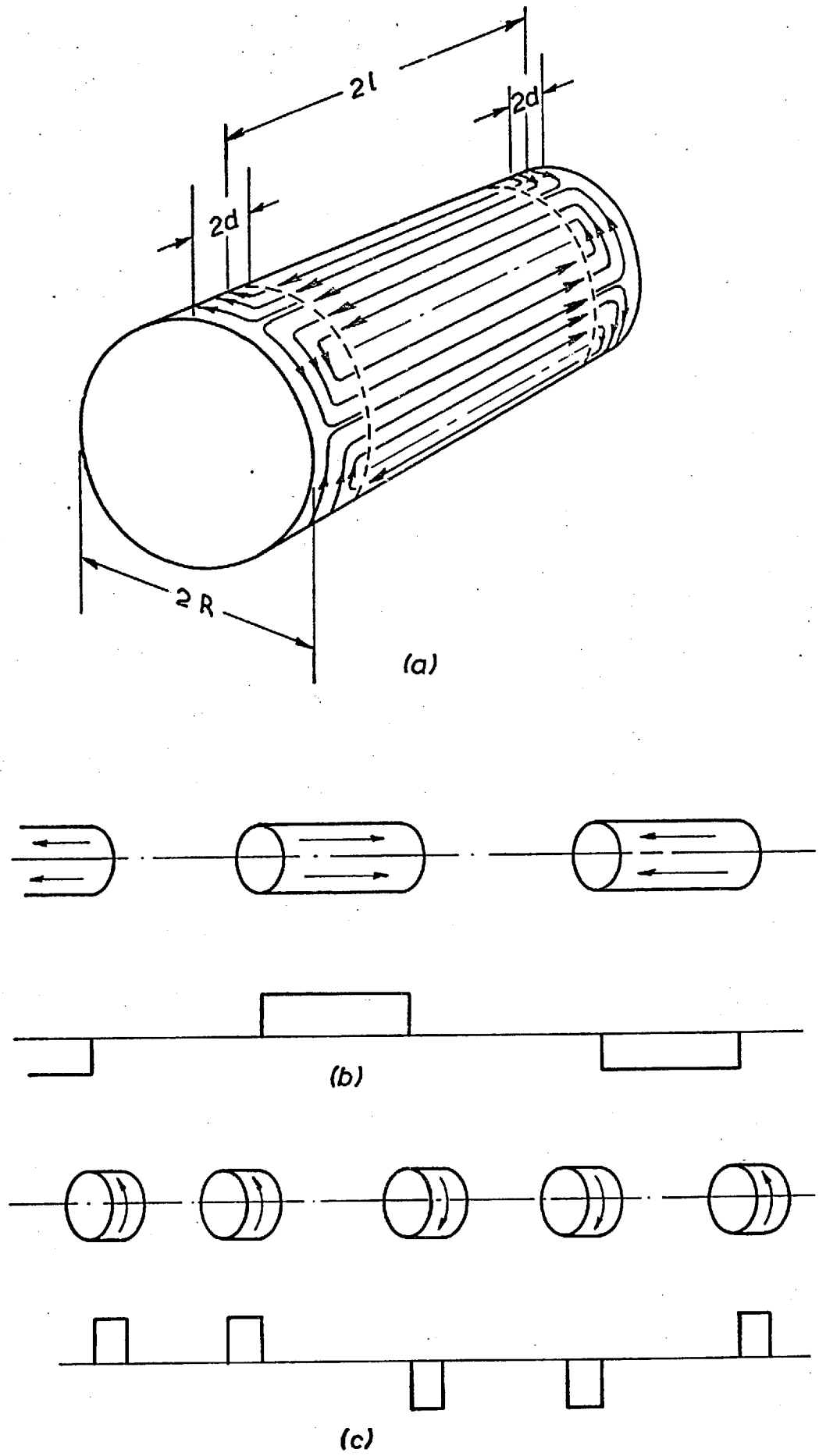


Fig 2·5 A tubular current made up of an axial section and two end rings.
(Taken from ref. 2·7)

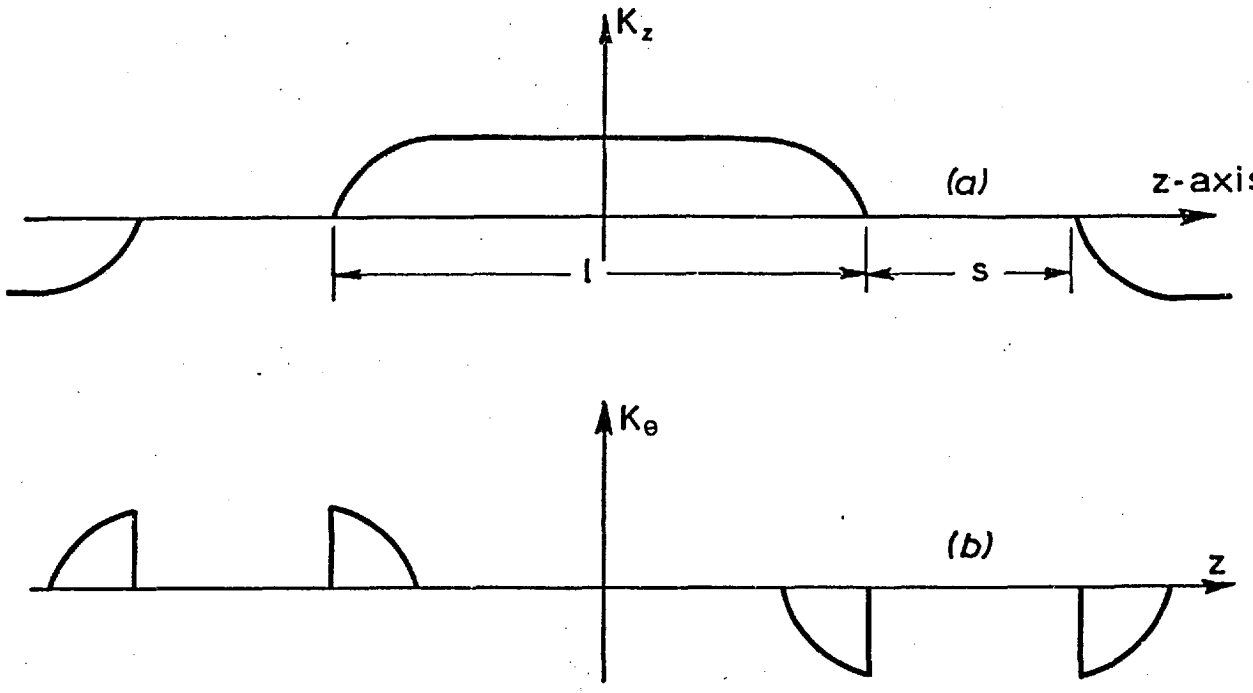


Fig. 2·6 Current sheet components of a diamond winding
(a) axial component (b) circumferential component

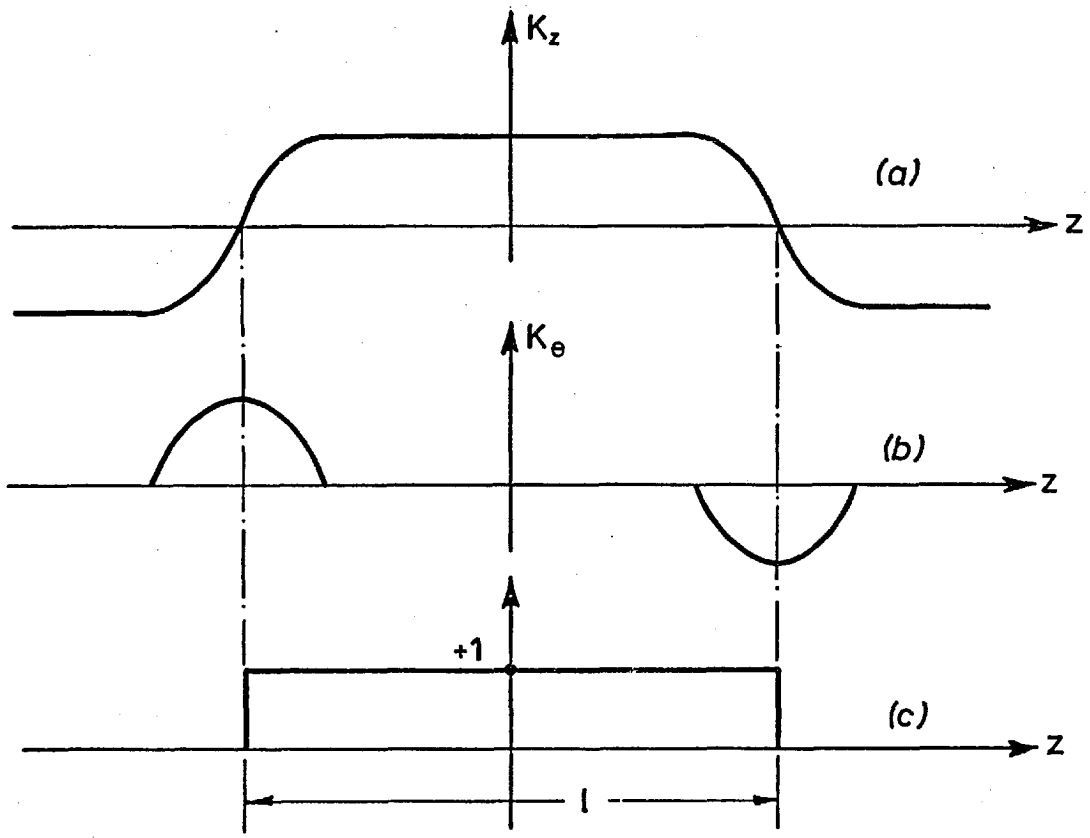


Fig. 2·7 Alternative distribution of current sheet components of a diamond winding.
(a) axial (b) circumferential
(c) modulating waveform to represent an isolated winding

current sheet will not affect the field of the adjacent machine. In other words, the mutual inductance between the windings of adjacent machines should be negligible. It should be noticed here that Hammond considered an air-cored mahcine and he was interested in calculating the magnetic field in the absence of any conducting regions. In his analysis, Hammond modelled the current sheet of a concentric winding as shown in Fig. (2.5).

Of course, the axial distribution of the axial and circumferential current sheets will depend to a great extent on the type of winding. For instance, the current sheet component of a diamond winding can be sketched as in Fig. (2.6).

In order to simulate the actual case of an isolated machine, the separation S must be large. Alternatively, one can model this mathematically by assuming no separation between the different machines, analyse the current sheet wave forms as shown in Fig. (2.7 - a and b), then use the modulating function Fig. (2.7 - c) in order to confine the excitaion to the axial length (of the winding and its overhang) only.

2.3.3 Three-dimensional current sheet

Although it is beyond the scope of the analysis reported in this thesis, the consideration of a three dimensional

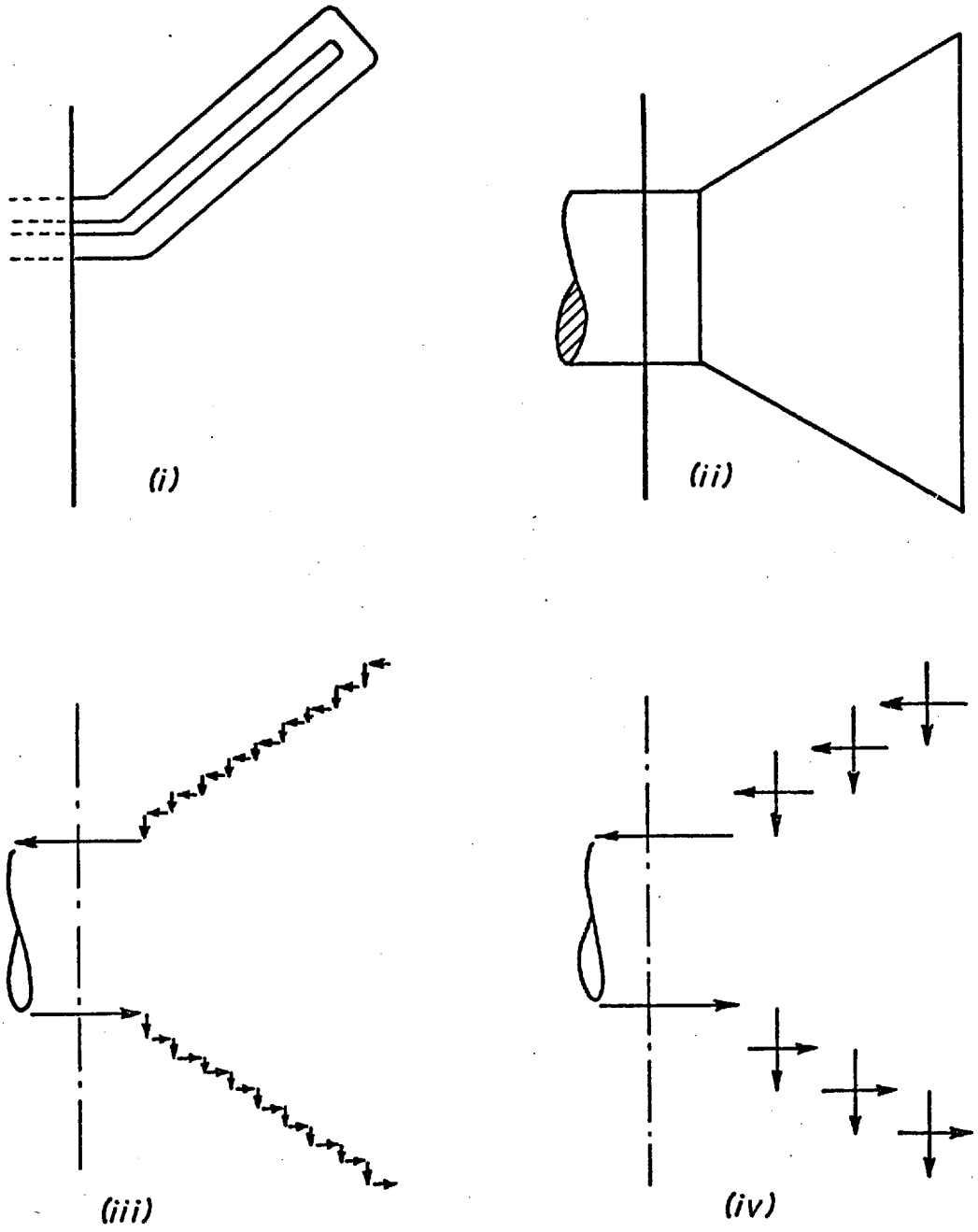


Fig. 2·8 Simplified representation of end winding (Taken from ref. 2·35)

current sheet is mentioned here for completeness.

The need for a three-dimensional current sheet usually arises when modelling the end winding of turbine generators[2.35, 2.36]. Ashworth and Hammond[2.35] demonstrated how the end winding could be represented by a current sheet in the shape of a cylinder and a cone. Then they replaced the 'conical' current sheet by a large number of steps as shown in Fig. (2.8). As a further simplification, these steps were combined into a number of tubes and discs. Expressions of the current sheet components in this case are given in reference (2.35).

2.4 Mathematical Model of a Two-Dimensional Current Sheet

Consider a set of N infinitely long concentric circular-cylindrical regions as shown in Fig. (2.9). Each region is assumed linear, homogenous and isotropic with single valued parameters. The excitation current sheet is assumed to be infinitesimally thin, and located on the boundary surface between any two adjacent regions. For generality, the current sheet is assumed to have two components in the axial and in the circumferential directions. Their expressions are given, in general, by equation (2.1). each individual application will be merely a special case of this form.

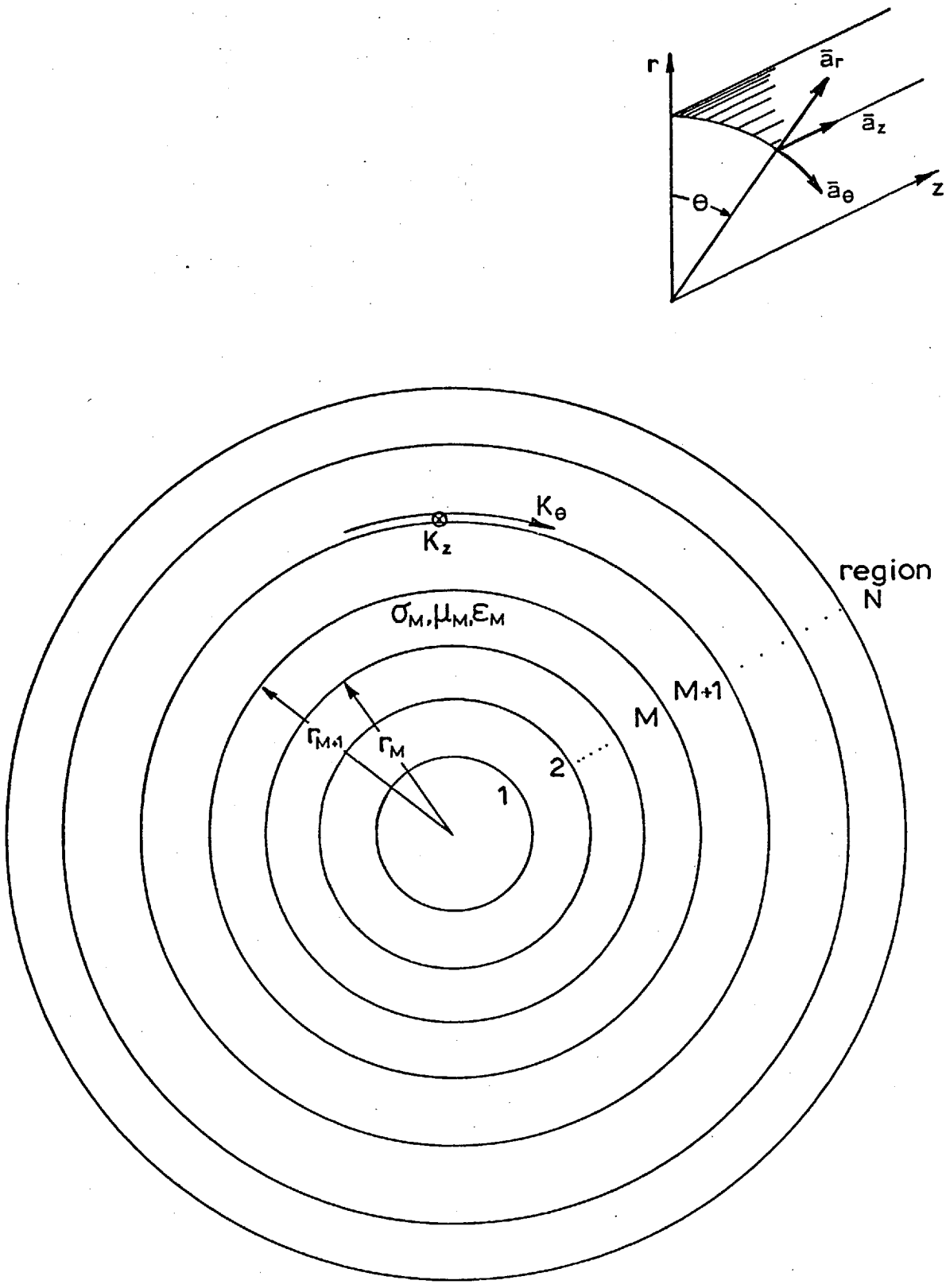


Fig. 2·9 Mathematical model

$$K_\theta = \sum_{m=-\infty}^{\infty} \sum_{n=-\infty}^{\infty} (\hat{K}_\theta)_{m,n} \cdot \exp\{j(\omega t - \beta_m z + \alpha_n \theta\}$$

$$K_z = \sum_{m=-\infty}^{\infty} \sum_{n=-\infty}^{\infty} (\hat{K}_z)_{m,n} \cdot \exp\{j(\omega t - \beta_m z + \alpha_n \theta\} \qquad (2.1)$$

Both components act at the same radius (r). The relation between the complex amplitudes of the surface sheet components can be obtained from the equation $\nabla.\bar{K} = 0$, thus:

$$(\hat{K}_\theta/\hat{K}_z)_{m,n} = r\beta_m/\alpha_n \qquad (2.2)$$

The positive and negative signs before $(\beta_m z)$ and $(\alpha_n \theta)$ are quite arbitrary, they can be all +ve or all -ve or they can be interchanged. The upper and lower limits of (m) and (n) as well as the amplitudes $(\hat{K}_\theta)_{m,n}$ and $(\hat{K}_z)_{m,n}$ will be defined according to the special practical application.

For instance, the finite length excitation problem in superconducting turbo-generators can be studied assuming current sheet expressions of the form:

$$K_\theta = \sum_{m=1,3..}^{\infty} \hat{K}_{\theta m} \cos(\beta_m z).\exp\{j(\omega t \pm \alpha\theta)\}$$

$$K_z = \sum_{m=1,3..}^{\infty} \hat{K}_{zm} \sin(\beta_m z).\exp\{j(\omega t \pm \alpha\theta)\} \qquad (2.3)$$

The amplitudes can be obtained by the standard Fourier

series technique from the spatial waves shown in Fig. (2.6) for example.

It should be noted that the consideration of an isolated exciting current sheet will result in replacing the summation sign in equation (2.3) by an integral operator. Instead of having discrete spatial frequencies in the z-direction, the current sheet will be represented by a continuous spectrum of spatial harmonics. In other words, the excitation will be expressed in a Fourier integral space rather than a Fourier series space. To demonstrate this clearly, a complete treatment in a Fourier integral domain is given in Chapter 5 for solving the problem of the finite length circumferential excitation in a multi-layer cylindrical structure.

2.5 Field Equations; Formulation and Analytical Solution

Maxwell equations:

$$\nabla \times \bar{E} = -\frac{\delta \bar{B}}{\delta t}$$

$$\nabla \times \bar{H} = \sigma E + \varepsilon \frac{\delta \bar{E}}{\delta t} \qquad (2.4)$$

Where $\bar{E}$ is measured in a reference frame fixed in the region considered.

By taking the curl of the above equations, and substituting for $\nabla.\bar{H} = 0$ and $\nabla.\bar{E} = 0$ (no free space charge), we get for a steady state sinusoidal excitation:

$$\nabla^2 \begin{bmatrix} \bar{E} \\ \bar{H} \end{bmatrix} = j\omega\mu\sigma_c \begin{bmatrix} \bar{E} \\ \bar{H} \end{bmatrix} \qquad (2.5)$$

Where:

$\sigma_c = \sigma + j\omega\varepsilon$, will be called the 'complex conductivity'

For low frequency applications, $\sigma >> \omega\varepsilon$, the displacement current can be neglected and the term σ_c reduces to σ. However, σ_c will be kept throughout the next sections for the sake of generality. The results can then be applied to a wide range of different problems, e.g. from screening of superconducting generators to studying the inhomogeneously filled circular waveguides[2.37]. Considering only the (m,n) component of the double Fourier series which represents the excitation current sheet, the excitation function becomes:

$$\begin{bmatrix} K_\theta \\ K_z \end{bmatrix}_{m,n} = \begin{bmatrix} \hat{K}_\theta \\ \hat{K}_z \end{bmatrix} . \exp\{j(\omega t - \beta_m z + \alpha_n \theta)\} \qquad (2.6)$$

The separation of variable technique, which will be adopted to solve this problem, necessitates that the exponential term which appears in equation (2.6) should appear with all the components of both electric and magnetic fields. This in turn permits replacing some differential operators, which appear in the Maxwell field equations (2.4) or the vector Helmholtz equation (2.5), by simple multipliers as follows:

$$\left.\begin{aligned} \frac{\delta}{\delta t} &= j\omega \\ \frac{\delta}{\delta z} &= -j\beta_m = -j\beta \\ \frac{\delta}{\delta \theta} &= j\alpha_n = \alpha \end{aligned}\right\} \qquad (2.7)$$

The suffices m and n are removed for brevity . The general solution for equation (2.5) then becomes

$$\bar{E}(r,\theta,z,t) = \{E_r(r)\,\bar{a}_r + E_\theta(r)\,\bar{a}_\theta + E_z(r)\,\bar{a}_z\}.\exp\{j(\omega t - \beta z + \alpha\theta)\} \qquad (2.8)$$

Substituting from relations (2.7), and expanding equation (2.5) in the circular-cylindrical coordinate system we get:

$$\left[\frac{d^2}{dr^2} + \frac{1}{r}\frac{d}{dr} - \{(\alpha^2 + 1)/r^2 + \gamma^2\}\right].E_r - 2\alpha j/r^2 .E_\theta = 0 \qquad (2.9a)$$

$$\left[\frac{d^2}{dr^2} + \frac{1}{r}\frac{d}{dr} - \{(\alpha^2 + 1)/r^2 + \gamma^2\}\right].E_\theta + 2\omega j/r^2 .E_r = 0 \qquad (2.9b)$$

$$\left[\frac{d^2}{dr^2} + \frac{1}{r}\frac{d}{dr} - \{\alpha^2/r^2 + 1\}\right]\cdot E_z = 0 \qquad (2.9c)$$

Where

$$\gamma = \beta^2 + j\omega\mu\sigma_c$$

Similar equations apply for the components of the magnetic field. The equation in E_z is the modified Bessel differential equation, its solution is standard and is given in terms of Bessel functions as follows:

$$\left.\begin{aligned} E_z(r) &= C_{1e}\, I_\alpha(\gamma r) + C_{2e}\, K_\alpha(\gamma r) \\ \text{Similarly} & \\ H_z(r) &= C_{1h}\, I_\alpha(\gamma r) + C_{2h}\, K_\alpha(\gamma r) \end{aligned}\right\} \qquad (2.10)$$

Where all the C's are separation constants ,which can be determined from the application of the boundary conditions. They are in general complex quantities. The solution for the r- and θ-components of the field vectors is not direct as for the z-component. Multiply equation (2.9b) by $j = \sqrt{-1}$ and subtract from (2.9a). Similarly multiply (2.9a) by j and subtract from (2.9b). We get:

$$\left[\frac{d^2}{dr^2} + \frac{1}{r}\frac{d}{dr} - \{(\alpha^2 - 2\alpha + 1)/r^2 + \gamma^2\}\right].\left[E_r - jE_\theta\right] = 0 \qquad (2.11a)$$

$$\left[\frac{d^2}{dr^2} + \frac{1}{r}\frac{d}{dr} - \{(\alpha^2 + 2\alpha + 1)/r^2 + \gamma^2\}\right].\left[E_\theta - jE_r\right] = 0 \qquad (2.11b)$$

Now, the solution of equations (2.11a) and (2.11b) will be given in terms of modified Bessel functions of orders $(\alpha - 1)$ and $(\alpha + 1)$ respectively.

And the solutions of the field components will be given generally by:

$$E_r(r) = (A\, I_{\alpha-1} + D\, K_{\alpha-1}) + j(A'\, I_{\alpha+1} + D'\, K_{\alpha+1})$$

$$E_\theta(r) = j(A\, I_{\alpha-1} + D\, K_{\alpha+1}) + (A'\, I_{\alpha+1} + D'\, K_{\alpha+1})$$

$$E_z(r) = \gamma/j\beta \;.\; \{(A + jA')\, I_\alpha - (D + jD')\, K_\alpha\} \qquad (2.12)$$

Where:

- I's and K's are the modified Bessel functions of argument (γr), the argument is omitted from the equations for brevity.

- A, A', D, and D' are separation constants.

It is worth mentioning that this mathematical manipulation to get expressions of $E_r(r)$ and $E_\theta(r)$, although simple and direct, it seems that nobody has used it. It was thought to have been originated by the author, until recently it came to his knowledge that a similar technique was published some years ago in a discussion article by Endean and Allen[2.9].

A similar mathematical model has been considered to model 'a helical winding tubular motor' by Eastham and Alwash[2.10]. The solution for the field components has been given in a transfer matrix form. Later, Freeman[2.11] developed the T.L. analogue for this particular motor according to the equations derived by the above authors. In fact, Eastham and Alwash obtained a solution for the axially directed component of the electric field vector exactly as the solution given by equation (2.10). In an attempt to get the other field components, they assumed that the radial field component E_r was zero, then applied $\nabla.\bar{E} = 0$, knowing E_z, the authors got an expression for E_θ. Actually the solution for E_θ so obtained is not correct, and even if E_r is assumed zero, this solution does not satisfy the circumferentially directed component of the vector Helmholtz equation which is given by (2.9b). The solution should be in terms of modified Bessel functions of order $\sqrt{(\alpha^2 + 1)}$ and not (α) as they quoted.

The main disadvantage of the purely analytical solution obtained in this section lies in the determination of the separation constants. Moreover, the complexity increases as the number of regions increases.

In the following sections, another technique will be adopted instead of the purely analytical one, namely the transmission line modelling technique. This technique has been used extensively in the field of microwaves to study wave

propogation and its related problems. The transmission line representation, as will be shown later, has the main advantage of dealing with a large number of regions in a simple and routine way.

2.6 Transmission Line Representation

2.6.1 Equations of non-uniform transmission lines

Let V and I represent, respectively, the voltage and current at any point distant (r) from the sending end terminals of a non-uniform transmission line. If Z is the variable (i.e. distance dependent) series impedance per unit length, then the impedance of a length dr is (Zdr) and the corresponding potential difference across it due to current I is:

$$-dV = I Z dr$$

Therefore

$$\frac{dV}{dr} = - IZ \qquad (2.13a)$$

the negative sign signifying the V decreases as the distance r increases.

Now, if Y is the variable shunt admittance per unit length, the corresponding change in the input current to an elementary section of the T.L. whose length is (dr), is given by:

$$-dI = VY\,dr$$

Therefore

$$\frac{dI}{dr} = -VY \tag{2.13b}$$

Eliminating I then V between equations (2.13a) and (2.13b) we get:

$$\frac{d^2V}{dr^2} - \frac{1}{Z}\frac{dZ}{dr}\frac{dV}{dr} - ZYV = 0 \tag{2.14}$$

and

$$\frac{d^2I}{dr^2} - \frac{1}{Y}\frac{dY}{dr}\frac{dI}{dr} - ZYI = 0 \tag{2.15}$$

Equations (2.14) and (2.15) represent, respectively, the distribution of the potential difference and the current along a non-uniform transmission line whose series impedance and shunt admittance are functions of the distance (r).

According to the functional dependence of Z and Y on the distance (r), this transmission line is given a particular name[2.38]. For instance, if Y is linearly proportional to (r), while Z is inversely proportional to the distance (r), this non-uniform line is known in the literature as the "Heaviside-Bessel" line[2.39]. In general, if Z is proportional to r^{α}, and Y is proportional to r^{β}, where α and β are constants, the solution for V and I is always in form of Bessel function[2.38].

The similarity between the two equations (2.14) and (2.15) of a non-uniform T.L.,and equation (2.9c) of the axial component of the electric (or the magnetic) field vector suggests

the construction of an equivalent T.L., with series and shunt elements, the distribution of V and I along its length can be related to E_z and H_z of the electromagnetic field. This idea of course is not new as indicated in the introduction. It was suggested by the author to Freeman as indicated by Freeman in reference (2.57).

2.6.2 Equivalent transmission line:

Since Schelkunoff[2.40], in the late 1930's, introduced the concept of wave impedance in the theory of wave propagation, the common practice is that the electric field in volt/metre and the magnetic field in ampere/ meter are made analogous to V and I respectively. This of course has been done to keep the ratio between E/H and V/I as having the dimension of impedance.

Consequently, the equation (2.14) will be compared with the differential equation in E_z, while equation (2.15) is to be compared with the D.E. in H_z in order to find the equivalent T.L. element.

Comparing V and E_z,

$$\left.\begin{aligned} &\frac{d^2V}{dr^2} - \frac{1}{Z}\frac{dZ}{dr}\frac{dV}{dr} - (ZY)V = 0 \\ &\frac{d^2}{dr^2}E_z + \frac{1}{r}\frac{d}{dr}E_z - (\alpha^2/r^2 + \gamma^2)E_z = 0 \end{aligned}\right\} \quad (2.16)$$

The term by term comparison between the above two equations yields:

$$V \equiv E_z \tag{2.17a}$$

$$-\left(\frac{dZ}{dr}\right).\left(\frac{1}{Z}\right) \equiv \frac{1}{r} \tag{2.17b}$$

$$ZY \equiv \left(\frac{\alpha^2}{r^2} + \gamma^2\right) \tag{2.17c}$$

Equation (2.17b) is an ordinary differential equation, its solution is given by:

$$Z = \frac{\text{constant}}{r} \tag{2.18a}$$

Substituting in (2.17c),

$$Y = \frac{r}{\text{constant}} \left\{\frac{\alpha^2}{r^2} + \gamma^2\right\} \tag{2.18b}$$

Thus the distribution of the axial component of the electric field vector in the radial direction is exactly similar to the distribution of the potential difference along a non-uniform transmission line whose series impedance and shunt admittance per unit length are given by the equations (2.18a) and (2.18b) respectively.

Comparing I and H_z equations given below :

$$\left.\begin{aligned} &\frac{d^2I}{dr^2} - \frac{1}{Y}\frac{dY}{dr}\frac{dI}{dr} - (ZY)\,I = 0 \\ &\frac{d^2}{dr^2}H_z + \frac{1}{r}\frac{d}{dr}H_z - (\alpha^2/r^2 + \gamma^2)H_z = 0 \end{aligned}\right\} \tag{2.19}$$

Similarly the term by term comparison between equations (2.19) shows that:

$$I \equiv H_z \tag{2.20a}$$

$$-\left(\frac{dY}{dr}\right).\left(\frac{1}{Y}\right) \equiv \frac{1}{r} \tag{2.20b}$$

$$ZY \equiv \left(\frac{\alpha^2}{r^2} + \gamma^2\right) \tag{2.20c}$$

following the previous steps,

$$Y = \frac{\text{constant}}{r} \tag{2.21a}$$

$$Z = \frac{r}{\text{constant}} \left\{\frac{\alpha^2}{r^2} + \gamma^2\right\} \tag{2.21b}$$

Hence, the distribution of the axial component of the magnetic field vector $\bar{H}$ in the radial direction is exactly similar to the current distribution along a non-uniform transmission line whose shunt admittance and series impedance per unit length are given by equations (2.21a) and (2.21b) respectively.

The above discussion shows that E_z and H_z are equivalent to the voltage and current of two different transmission lines each having the same propagation constant but different series and shunt elements. The transmission line whose potential difference is E_z will be called the E-line or the single primed line. All the quantities which are related to it will

be singly primed as V', I', Z', Y'. While the transmission line whose current is H_z will be called the H-line or the doubly primed line. All the quantities which are related to it will be doubly primed such as V", I", Z", Y".

The decomposition of the main field into two basic modes, as shown in Appendix A, where each mode depends only on one scalar quantity E_z or H_z, is quite compatible with the double transmission lines concept obtained above. Since, in this case, all the information about the distribution or propagation of each mode can be represented or obtained from the corresponding equivalent transmission line, as will be shown later in the following sections.

2.6.3 E-wave equivalent transmission line:

The electric and magnetic fields components of the E-wave are obtained in Appendix A for a generalised cylindrical coordinates system. The equations which correspond to the circular-cylinder coordinate system are given by:

$$\left.\begin{aligned} E'_r &= j\beta/\gamma^2 \cdot \frac{d}{dr} E_z && \text{(a)} \\ E'_\theta &= j\beta/\gamma^2 \cdot j\alpha/r \cdot E_z && \text{(b)} \\ E_z' &= E_z && \text{(c)} \\ H'_r &= -\sigma_c/\gamma^2 \cdot j\alpha/r \cdot E_z && \text{(d)} \end{aligned}\right\} \quad (2.22)$$

$$H'_\theta \doteq \sigma_c/\gamma^2 \cdot \frac{d}{dr} E_z \qquad \text{(e)}$$

$$H'_z = 0 \qquad \text{(f)} \qquad \Big\} \ (2.22)$$

If the above equations are going to relate the field components to an equivalent voltage and current of a transmission line whose potential difference V' is equal to E_z, the H'_θ, which is given by equation (2.22e), will be represented by the current I' flowing in this equivalent transmission line. This is clearly obvious since H'_θ has the units of ampere/metre, and it is proportional to the rate of change of voltage with respect to the distance.

Equation (2.22e) is rearranged to satisfy equation (2.18a) which gives the functional relation of the series impedance per unit length of the equivalent transmission line and the radial distance (r) as follows:

from (2.18a);

$$Z' = \text{constant}/r$$

from (2.22e);

$$\frac{d}{dr} E_z = \frac{dV'}{dr} = -(\gamma^2/\sigma_c) H'_\theta$$

$$= -Z'I'$$

$$= -\ \text{const.}/r \ . \ I'$$

Therefore

$$H'_\theta = -\sigma_c/\gamma^2 \ . \ \text{const.}/r \ . \ I'$$

This constant is arbitrary, it is convenient to choose it equal to (γ^2/σ_c), hence the relation between $H'_\theta(r)$ and I' becomes:

$$H'_\theta(r) = -1/r \cdot I'(r) \tag{2.23}$$

And the series impedance per unit length of the E-line will be given by:

$$Z' = \gamma^2/\sigma_c r \tag{2.24}$$

The shunt admittance per unit length of the E-line can be obtained from (2.18b) and (2.24), it will have the form:

$$Y' = \sigma_c r/\gamma^2 \cdot \{\alpha^2/r^2 + \gamma^2\} \tag{2.25}$$

2.6.4 H-wave equivalent transmission line

Similarly, the H-wave field components deduced from Appendix (A) for a circular cylinder coordinate system can be written in the form:

$$\left.\begin{aligned} H''_r &= j\beta/\gamma^2 \cdot \frac{d}{dr} H_z && \text{(a)} \\ H'' &= j\beta/\gamma^2 \cdot j\alpha/r \cdot H_z && \text{(b)} \\ H''_z &= H_z && \text{(c)} \end{aligned}\right\} \tag{2.26}$$

$$E''_r = j\omega\mu/\gamma^2 \cdot j\alpha/r \cdot H_z \qquad (d)$$

$$E''_\theta = -j\omega\mu/\gamma^2 \cdot \frac{d}{dr} H_z \qquad (e)$$

$$E''_z = 0 \qquad (f)$$

} (2.26)

Following the same argument as for obtaining the elements of the E-line, the series impedance and the shunt admittance per unit length are given for the H-line in the form:

$$Y'' = \gamma^2/j\omega\mu r \qquad (2.27)$$

$$Z'' = j\omega\mu r/\gamma^2 \cdot \{\alpha^2/r^2 + \gamma^2\} \qquad (2.28)$$

because

$$H''_z(r) = I''(r) \qquad (2.29)$$

therefore

$$E''_\theta(r) = \frac{1}{r} V''(r) \qquad (2.30)$$

where

$V''(r)$ is related to $I''(r)$ by the relation:

$$\frac{dI''}{dr} = -Y'' V''(r)$$

2.6.5 Expressions for the electromagnetic field components in terms of the equivalent double transmission line quantities

It has been shown above in Sections (2.6.2), (2.6.3) and (2.6.4) that the distribution of the electromagnetic field

components in any one circular-cylindrical region of the mathematical model shown in Fig. (2.9) can be obtained from the distribution of voltages and currents along an equivalent double transmission line whose elements (i.e. series impedances and shunt admittances) are functions of the radial distance (r) as well as the region parameters.

The expressions for the electromagnetic field components of any one region can then be obtained in terms of the voltages and currents of the equivalent T.L. from equations (2.22) to (2.30), keeping in mind that the solution for each field component is simply the superposition of the solution of its corresponding modes.

The expressions can be summarised in the following general equations:

for an excitation current sheet flowing in the boundary surface between any two adjacent regions and having the expression;

$$\bar{K} = \sum_{m,n} \{\hat{K}_\theta \bar{a}_\theta + \hat{K}_z \bar{a}_z\}_{m,n} \cdot \exp\{j(\omega t - \beta_m z + \alpha_n \theta)$$

the electric field components will be given by;

$$E_r(r) = \sum_{m,n} (\omega\mu\alpha_n/\gamma^2_m r) \cdot \{(\gamma^2_m \beta_m/j\omega\mu\sigma_c\alpha_n) I'_{m,n}(r) - I''_{m,n}(r)\}$$

(2.31a)

$$E_\theta(r) = \sum_{m,n} 1/r \cdot \{-\alpha_n\beta_m/\gamma_m^2 \cdot V'_{m,n}(r) + V''_{m,n}(r)\} \quad (2.31b)$$

$$E_z(r) = \sum_{m,n} V'_{m,n} \quad (2.31c)$$

$$\bar{E}(r,\theta,z,t) = \sum_{m,n} \{E_r \bar{a}_r + E_\theta \bar{a}_\theta + E_z \bar{a}_z\}_{m,n} \cdot \exp\{j(\omega t - \beta_m z + \alpha_n \theta)\} \quad (2.31d)$$

and the magnetic field component will be given by;

$$H_r(r) = \sum_{m,n} -(\beta_m/\omega\mu r) \cdot \{(j\omega\mu\sigma_c\alpha_n/\gamma_m^2\beta_m) \cdot V'_{m,n}(r) + V''_{m,n}(r)\} \quad (2.32a)$$

$$H_\theta(r) = \sum_{m,n} -(\alpha_n\beta_m/\gamma_m^2 r) \cdot \{(\gamma_m^2/\alpha_n\beta_m) \cdot I'_{m,n}(r) + I''_{m,n}(r)\} \quad (2.32b)$$

$$H_z(r) = \sum_{m,n} I''_{m,n}(r) \quad (2.32c)$$

$$\bar{H}(r,\theta,z,t) = \sum_{m,n} \{H_r \bar{a}_r + H_\theta \bar{a}_\theta + H_z \bar{a}_z\}_{m,n} \cdot \exp\{j(\omega t - \beta_m z + \alpha_n \theta)\} \quad (2.32d)$$

where:

$$\gamma_m^2 = \beta_m^2 + j\omega\mu\sigma_c$$

$$\sigma_c = \sigma + j\omega\varepsilon$$

$$= \text{'Complex conductivity'}$$

The $V_{m,n}$'s and the $I_{m,n}$'s are the distributed voltages and currents on the equivalent double transmission line shown

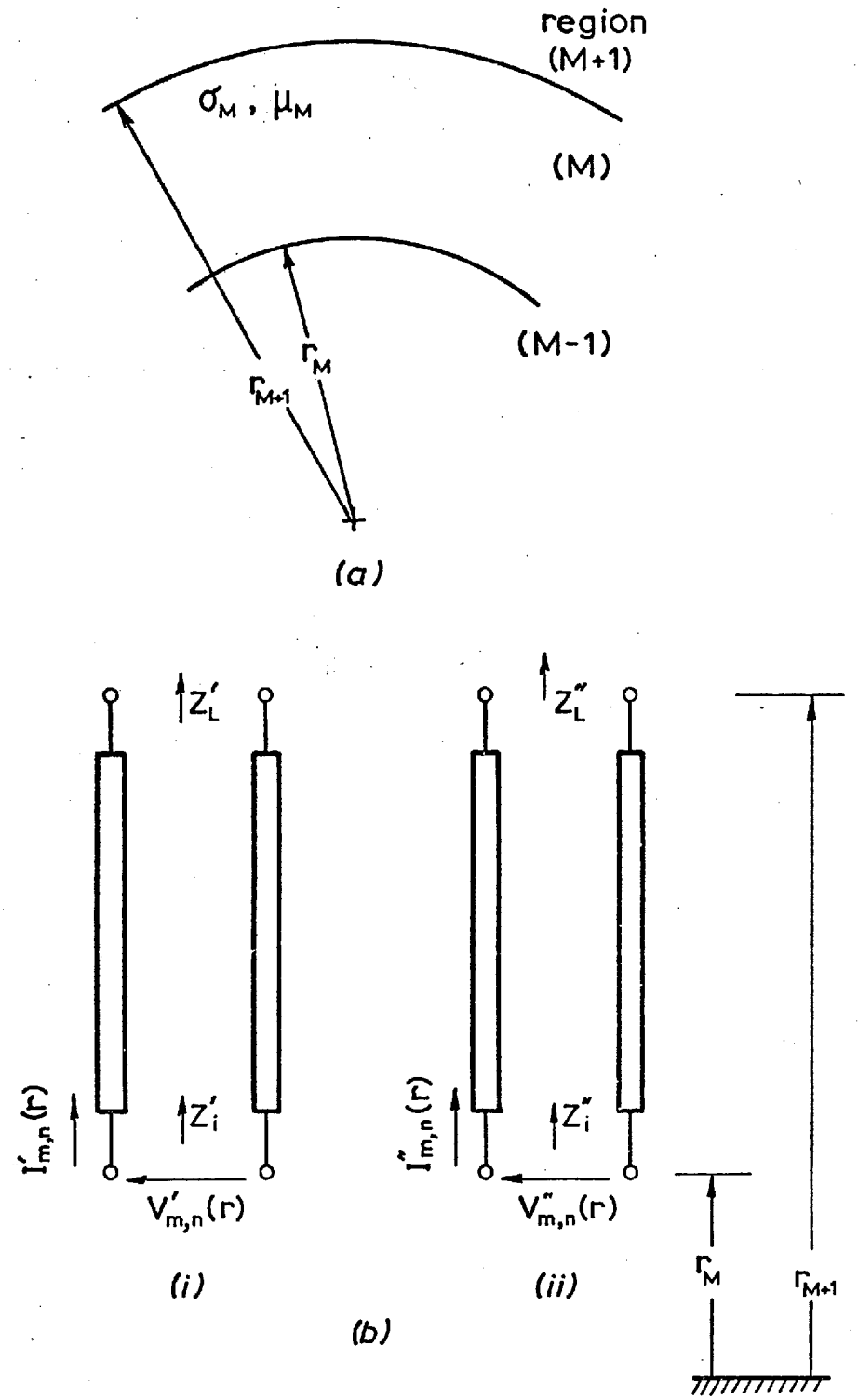


Fig. 2·10 The m,n-spatial harmonic equivalent transmission line of an annular region.

(a) Annular region

(b) Equivalent double T.L.

(i) E-line

(ii) H-line

schematically in Fig. (2.10).

Although, to the author's knowledge, the study of the electromagnetic behaviour of multiregion concentric circular-cylindrical induction devices in terms of double transmission line equivalent circuits as derived in this Chapter, is original, and has not been attempted before, similar double transmission line representations have been reported in the literature of some other branches of science. For instance, Clarricoats et al[2.37,2.41-.43] studying circular waveguides containing an axial circularly cylindrical region, with material differing from those of the surrounding annulus, developed what they called 'transverse equivalent-network' which is composed of a double T.L. Acoustic wave propagation in uniform isotropic regions is another example where the double transmission line equivalent circuit was found to be very helpful and efficient in studying the acoustical effects in these regions[2.44,2.45].

2.7 Surface Wave Impedance Expressions

Consider a general region (M), as shown in Fig. (2.10), whose inner and outer radii are r_M and r_{M+1} respectively. The region is assumed isotropic, homogeneous and linear having conductivity, permeabillity and permittivity, σ_M, μ_M and ε_M respectively.

Consider only an m,n-spatial harmonic excitation. The suffices m,n will be omitted from all expressions for brevity. The voltages and currents of the E-and H- lines are given by:

$$V'(r) = C_{1e}(I_\alpha(\gamma r) + C_v K_\alpha(\gamma r)) \quad (2.33)$$

$$I''(r) = C_{1h}(I_\alpha(\gamma r) + C_i K_\alpha(\gamma r)) \quad (2.34)$$

$$\frac{dI''}{dr} = -\gamma^2/j\omega\mu r \cdot V''(r) \quad (2.35)$$

$$\frac{dV'}{dr} = -\gamma^2/\sigma_c r \cdot I'(r) \quad (2.36)$$

(i) Input impedance of the H-line

$$\text{Let } Z''_o = j\omega\mu/\gamma^2 \quad (2.37)$$

$$= \text{The T.L. characteristic wave impedance.}$$

From equations (2.34), (2.35) and (2.36), we get:

$$V''(r) = -Z''_o.(\gamma r).C_{1h}\{\dot{I}_\alpha(\gamma r) + C_i \dot{K}_\alpha(\gamma r)\} \quad (2.38)$$

where:

$\dot{I}_\alpha(\gamma r)$ and $\dot{K}_\alpha(\gamma r)$ are the first derivatives of $I_\alpha(\gamma r)$ and $K_\alpha(\gamma r)$ w.r.t. (γr) respectively.

The surface wave impedance at any radius (r) inside the

region looking in the direction of the increase of (r) is given by:

$$Z''(r) = V''(r)/I''(r)$$
$$= -Z_o.(\gamma r).\{\dot{I}_\alpha(\gamma r) + C_i \dot{K}_\alpha(\gamma r)\}/$$
$$\{I_\alpha(\gamma r) + C_i K_\alpha(\gamma r)\} \qquad (2.39)$$

Substituting for (r), in equation (2.39), once by r_M then by r_{M+1}, noticing that:

$$Z''(r_M) = Z''_{i,M}$$

and

$Z''(r_{M+1}) = Z''_{L,M}$, and eliminating the separation constant C_i, we get:

$$Z''_{i,M} = Z''_{o,M}.S(y_o,y_1).\{Z''_{o,M}.R(y_1,y_o) - Z''_{L,M}\}/$$
$$\{Z''_{o,M}.S(y_1,y_o) - Z''_{L,M}\} \qquad (2.40)$$

Where:

$$S(y_o,y_1) = y_o.\{\dot{I}_\alpha(y_o) K_\alpha(y_1) - I_\alpha(y_1) \dot{K}_\alpha(y_o)\}/$$
$$\{I_\alpha(y_1) K_\alpha(y_o) - I_\alpha(y_o) K_\alpha(y_1)\}$$

$$R(y_1,y_o) = y_1.\{\dot{I}_\alpha(y_1) \dot{K}_\alpha(y_o) - \dot{I}_\alpha(y_o) \dot{K}_\alpha(y_1)\}/$$
$$\{\dot{I}_\alpha(y_o) K_\alpha(y_1) - I_\alpha(y_1) \dot{K}_\alpha(y_o)\}$$

$S(y_1,y_o)$ can be obtained by interchanging y_o and y_1 in the expression of $S(y_o,y_1)$ above.

$y_o = \gamma_M r_M$

$y_1 = \gamma_M r_{M+1}$

$Z''_{L,M}$ = terminating impedance of the H-line

Similar expressions are obtained by Clarricoats, Olver and Wong[2.41].

(ii) Input admittance of the E-line

$$\text{Let } Y'_o = \sigma_c/\gamma^2 \qquad (2.41)$$

= The E-line characteristic surface wave admittance.

From equations (2.33), (2.36) and (2.41), we get:

$$I'(r) = -Y'_o.(\gamma r).C_{1e}\{\dot{I}_\alpha(\gamma r) + C_v \dot{K}_\alpha(\gamma r)\} \qquad (2.42)$$

Following similar steps for the H-line input impedance we get:

$$Y'_{i,M} = Y'_{o,M}.S(y_o,y_1).\{Y'_{o,M}.R(y_1,y_o) - Y'_{L,M}\}/\{Y'_{o,M}\,S(y_1,y_o) - Y'_{L,M}\} \qquad (2.43)$$

Where:

$Y'_{i,M}$ and $Y'_{L,M}$ are the input and load admittances respectively of the E-line.

The functions $R(y_1,y_o)$, $S(y_o,y_1)$ and $S(y_1,y_o)$ are as defined before.

2.8 Application of the Boundary Conditions

In section (2.6), it has been shown that the decomposition of the main electromagnetic field to two basic modes permits the representation of the field components by equivalent voltages and currents of double transmission lines. Each line will represent one of these modes. The lines extend along the radial direction ,and each has a length equal to the annular region thickness. The fact that the two modes are functions in two different scalar quantitites, E_z and H_z, leads to the important result which is the two lines are not coupled along their length.

However, the continuity conditions of the electric and magnetic fields vectors at the interfaces between the adjacent layers will related the voltages and currents of these two lines at the terminal points.

The boundary conditions can be expressed mathematically in the form:

$$\left.\begin{aligned} \bar{n} \times (\bar{E}_2 - \bar{E}_1) &= 0 \\ \bar{n} \times (\bar{H}_2 - \bar{H}_1) &= \bar{K} \end{aligned}\right\} \quad (2.44)$$

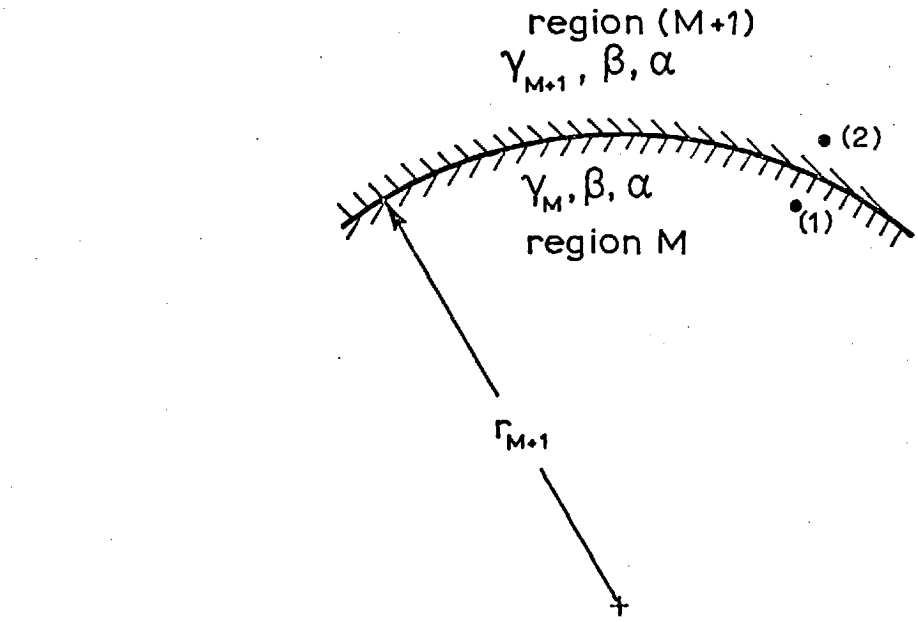
Where:

$\bar{E}_1$, $\bar{E}_2$ and $\bar{H}_1$, $\bar{H}_2$ are the electric and magnetic fields respectively at both sides of a boundary between two adjacent regions. These two expressions state that the tangential

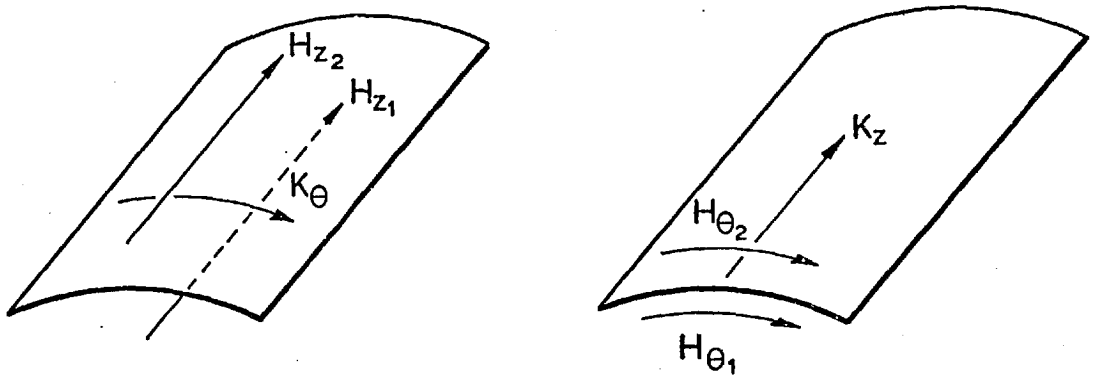
component of the electric field is continuous, while the discontinuity in the tangential component of the magnetic field in a certain direction is equal to the component of the surface current sheet perpendicular to that direction. In other words, E_θ and E_z are continuous at the boundary layer, and the components H_θ and H_z are alsc continuous with allowance for the current sheet if it exists.

The continuity of E_z, with reference to equation (2.31c), ensures that the output voltage $V'_{m,n}$ of the E-line of a certain region is equal to the input voltage to the E-line which corresponds to the following (or adjacent) region. That is to say that the E-lines of the consecutive regions are all connected in cascade. In a similar manner, in the event of no current sheet flowing between two adjacent regions, H_z will be continuous, hence $I''_{m,n}$ as revealed from equation (2.32c). Consequently, the H-lines are to be connected in series for this case.

Consider now two adjacent annular regions (M) and (M+1) as shown in Fig. (2.11a). Each is characterised by its own γ_m, i.e. γ_M and γ_{M+1} respectively . Let there be a current sheet $\bar{K}_{m,n}$, having two components $(K_\theta)_{m,n}$ and $(K_z)_{m,n}$ flowing in the boundary surface between the two regions, as shown in Fig. (2.11b). As before, we shall consider one harmonic component (m,n) at a time, and the suffices will be dropped for brevity.



(a)



(b)

Fig. 2·11 Boundary conditions

$$H_{\theta_1} - H_{\theta_2} = - K_z$$

$$H_{z_1} - H_{z_2} = K_\theta$$

Equation (2.44b), when applied to the points (1) and (2) of the sketch shown in Fig. (2.11a) yields:

$$(H_\theta)_1 - (H_\theta)_2 = -K_z \tag{2.45a}$$

$$(H_z)_1 - (H_z)_2 = K_\theta \tag{2.45b}$$

a) Continuity of E_z

Therefore $V_1' = V_2'$ (2.46)

b) Continuity of H_z

Substituting for H_{z1} and H_{z2} of equation (2.45b) from equation (2.32c), we get:

$$I_2'' = I_1'' - K_\theta \tag{2.47}$$

c) Continuity of E_θ

From (2.31b), and since E_θ is continuous, hence:

$$V_2'' - V_1'' = (\alpha\beta/\gamma_2^2) \cdot V_2' - (\alpha\beta/\gamma_1^2) \cdot V_1' \tag{2.48}$$

but, from equation (2.46), V' is always continuous,

$$V_2'' - V_1'' = V_1' \cdot \alpha\beta.\{1/\gamma_2^2 - 1/\gamma_1^2\} \tag{2.49}$$

It should be noted that the continuity of the normal component of the flux density vector across the boundary surface B_r, is satisfied by equation (2.49).
This can be realised as follows:

$$B_r = -\beta/\omega r \,.\, \{(j\omega\mu\sigma_c\alpha/\gamma^2\beta).\, V' + cV''\}$$

from $B_{r1} = B_{r2}$,

$$V_2'' - V_1'' = V_1' (\alpha/\beta) \,.\, \{(j\omega\mu\sigma/\gamma^2)_1 - (j\omega\mu\sigma/\gamma^2)_2\}$$

$$= V_1' \,.\, \alpha\beta \,.\, \{1/\gamma_2^2 - 1/\gamma_2^2\}$$

which is the same as (2.49).

d) Continuity of H_θ

Substituting for $(H_\theta)_1$ and $(H_\theta)_2$ from equation (2.32b) into (2.45a) we get:

$$I_1' + (\alpha\beta/\gamma_1^2)\, I_1'' = (\alpha\beta/\gamma_2^2)\, I_2'' + rK_z + I_2' \qquad (2.50)$$

Equations (2.46) - (2.50) represent the coupling relations between the two basic modes of the main electromagnetic field.

The equivalent circuit which satisfy these equations is shown in Fig. (2.12). The transformers which appear in

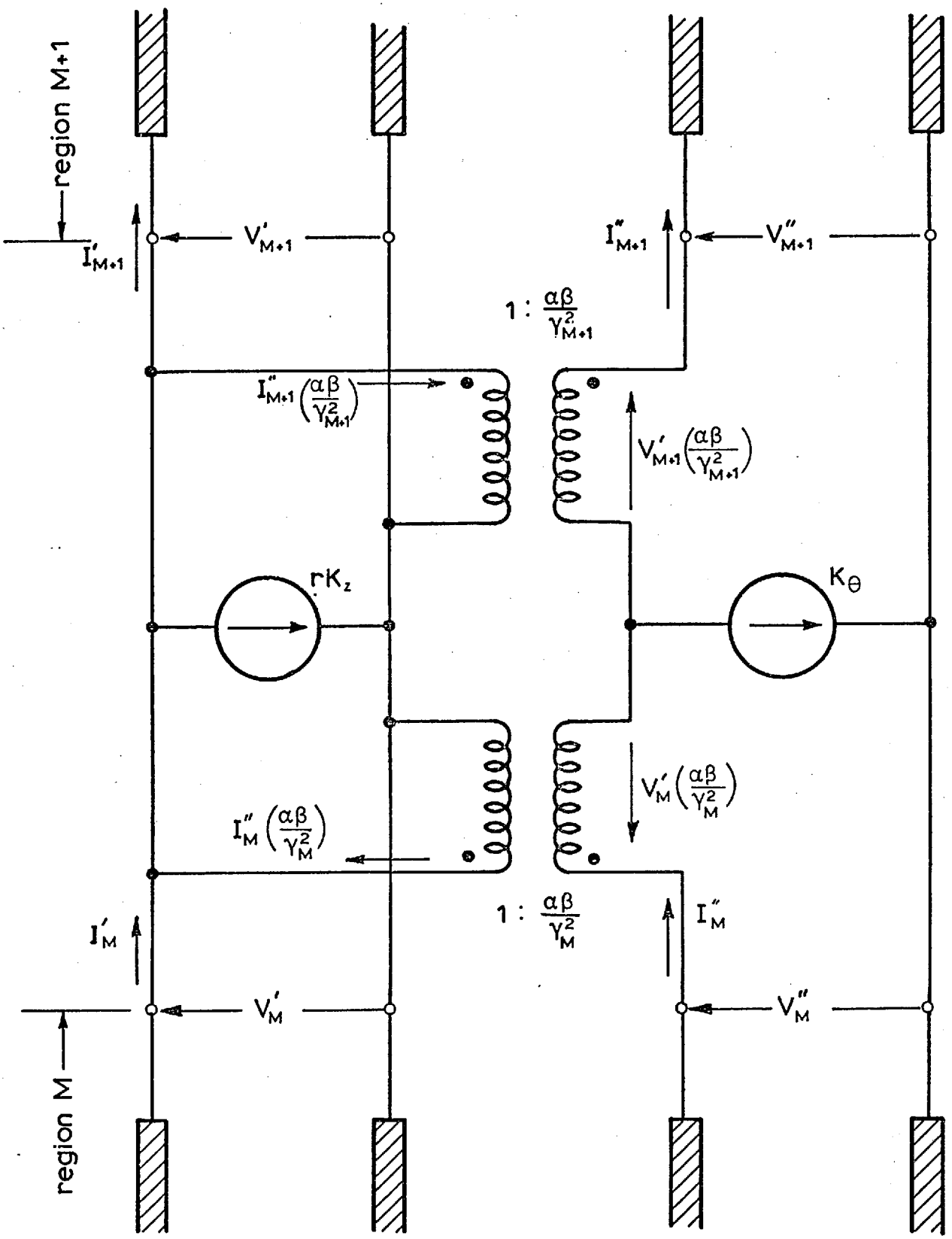


Fig. 2·12 Interface general equivalent circuit.

the circuit, although ideal, have in general 'complex' turns ratios.

In conclusion, the equivalent double T.L.s, which represent two adjacent regions, are coupled at its terminals in order to satisfy the continuity relations at the interfaces between these two regions. The coupling is in general effected by ideal transformers which may have complex turns ratios.

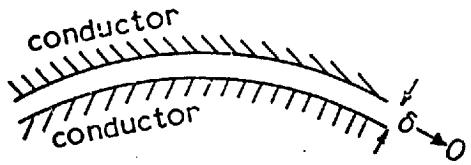
Fig. (2.12) represents the equivalent network of the interfaces for a general case. For practical applications, however, some special cases could be considered, which lead to a simplified representation.

A catalogue of equivalent networks is shown in Fig. (2.13) for cases (i) to (v) for different interfaces:

(i)	Conductor/Conductor	without current sheet
(ii)	Conductor/Non-conductor	without current sheet
(iii)	Conductor/Non-conductor	with current sheet
(iv)	Non-conductor/Non-conductor	without current sheet
(v)	Non-conductor/Non-conductor	with current sheet
(vi)	Conductor/Conductor	with current sheet

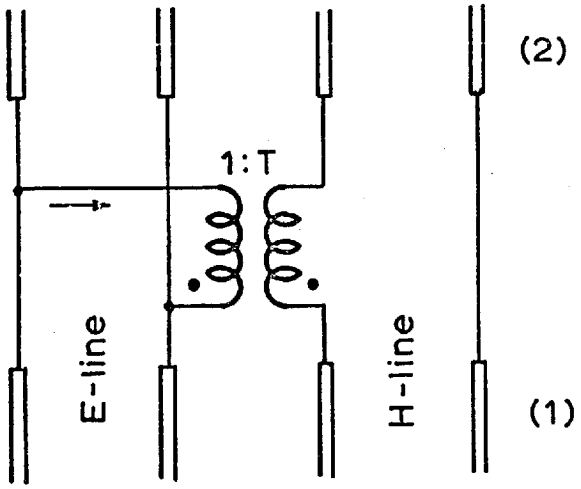
Note: Case (vi) is shown in Fig. (2.12).

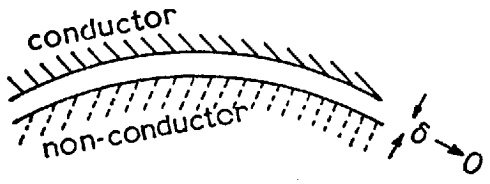
For all the above cases, the displacement current has been neglected, and the expression of (γ) is given by:



$$T = \alpha\beta\left[\frac{1}{\gamma_2^2} - \frac{1}{\gamma_1^2}\right]$$

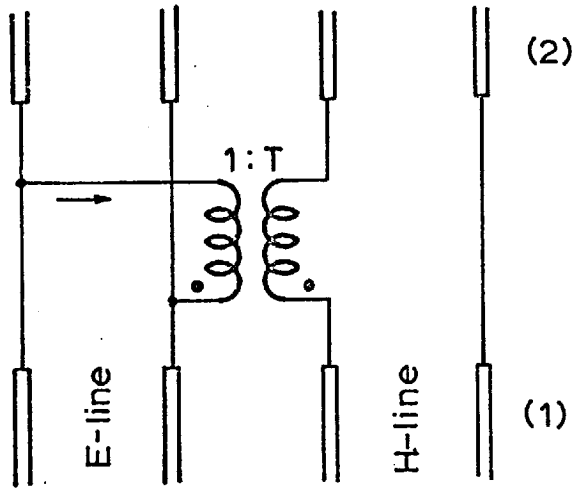
(i) Conductor/conductor interface

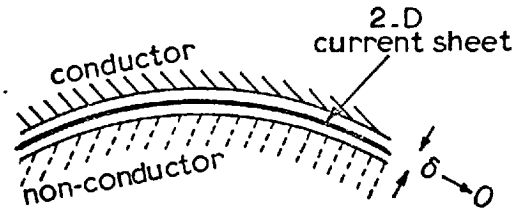




$$T = \alpha\beta\left[\frac{1}{\gamma_2^2} - \frac{1}{\gamma_1^2}\right]$$

(ii) Cond./non-cond. interface





$$T_1 = \frac{\alpha}{\beta} \qquad , T_2 = \frac{\alpha\beta}{\gamma_2^2}$$

(iii) Cond./non-cond. interface with 2-D current sheet.

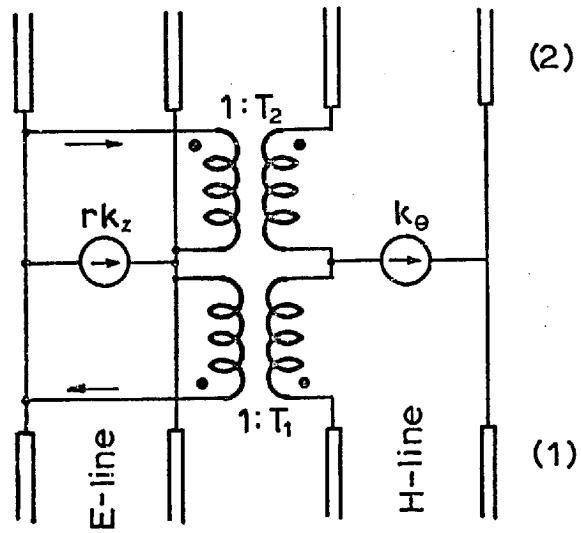
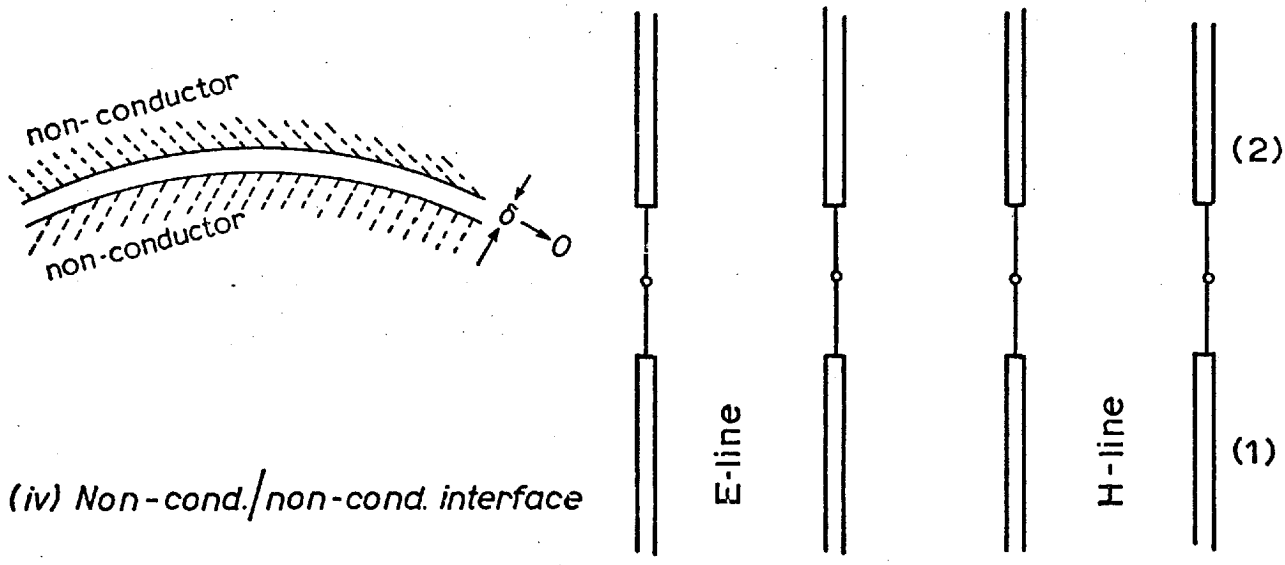
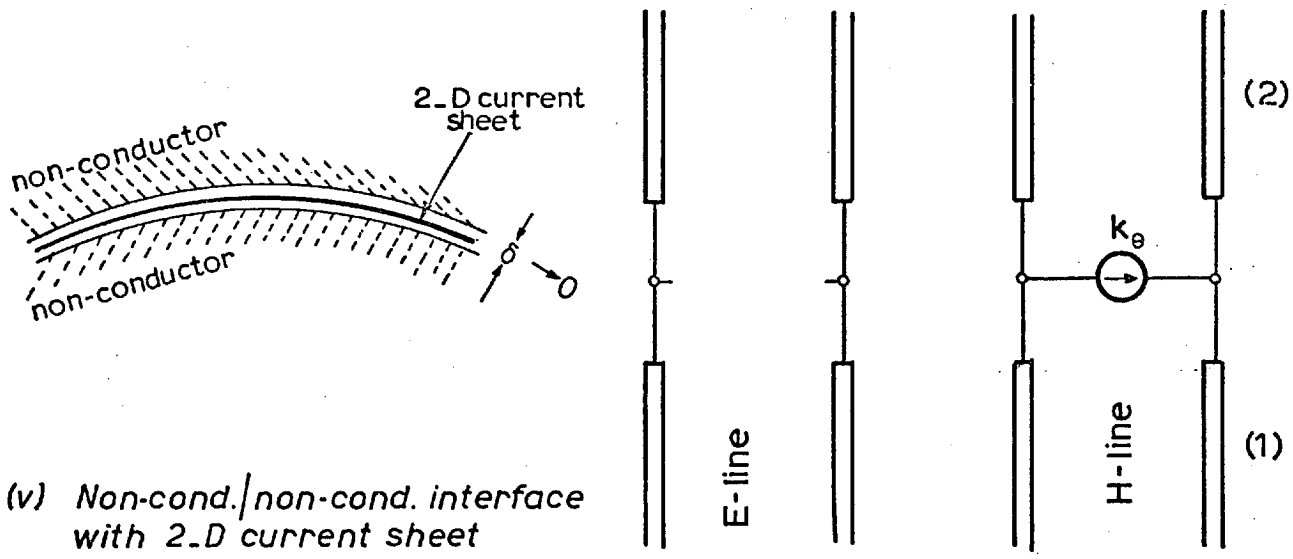


Fig. 2·13 Catalogue of equivalent networks for the interfaces.



(iv) Non-cond./non-cond. interface



(v) Non-cond./non-cond. interface with 2-D current sheet

Fig. 2·13 continued

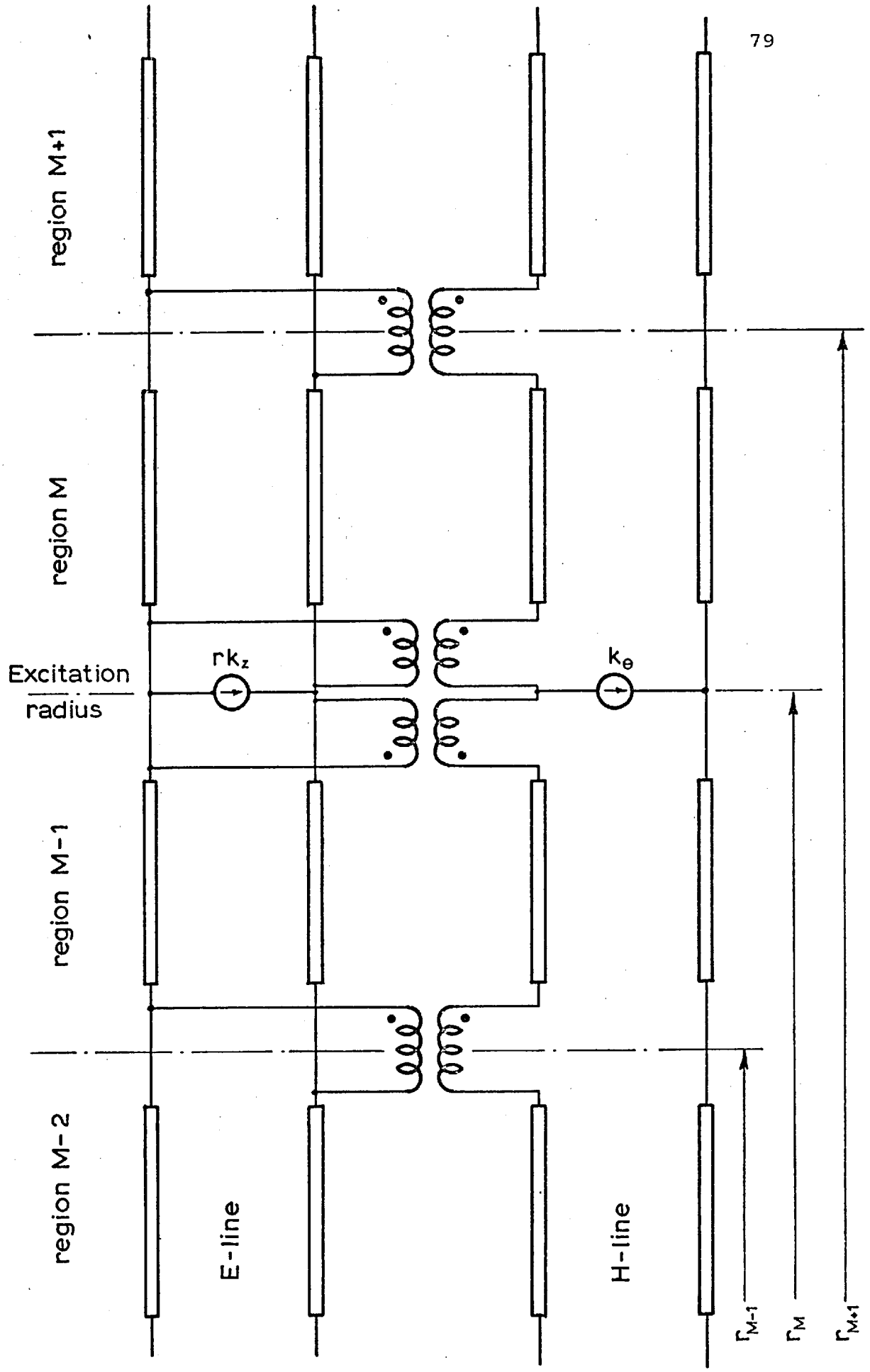


Fig. 2·14 Equivalent double T.L. network of a multiregion circular-cylindrical induction device.

$$\gamma^2 = \beta^2 + j\omega\mu\sigma$$

Fig. (2.14) represents the equivalent network of a general multiregion device as defined by the mathematical model of section (2.4). Only one 2-D current sheet is shown, but any number of excitation current sheets can be inserted in the equivalent network, as appropriate, without any restrictions.

2.9 Micro-T Circuit Formulation

So far, it has been shown that an analogy exists between this field problem, which is described by the mathematical model of section (2.4), and a double transmission line system. The expressions of the surface wave impedances and admittances of the individual sections of the complete equivalent network shown in Fig. (2.14), are given, in terms of modified Bessel functions, by equations (2.40) and (2.43) of section (2.7). In section (2.8), the coupling circuits between the E- and H-lines are developed in order to satisfy the boundary conditions at the regions interfaces. The distribution of the electric and magnetic field vectors, in the radial direction, at any region in the mathematical model, can be obtained by solving for the equivalent voltages and currents along the double transmission lines. The $\bar{E}$ and $\bar{H}$ components can then be related to the V's and I's through equations (2.31) and (2.32).

The main difficulty in the above mentioned procedure lies in using the developed expressions of the input surface wave impedance and admittance. The expressions are in general complicated functions in terms of the modified Bessel functions which can have general complex arguments.

The arguments of the modified Bessel functions which appear in equations (2.40) and (2.43) are either real, for the non-conducting regions, or complex, for the conducting regions, which are lying in the first octant of the complex plane. Modified Bessel functions of real arguments or with arguments which lie on the 45^{o} ray in the complex plane, (in this later case, the modified Bessel function is expressible in terms of Kelvin functions), are generally tabulated for a wide range of the order and the argument of the function. Also there are some polynomial approximations which can be used for the numerical calculation of these functions[2.46].

On the other hand, the functions having complex arguments mentioned above, have rarely been used, hence the literature on calculation methods is sparse.

Freeman and Smith[2.3], dealing with similar problem of calculating the modified Bessel function of complex argument having the same nature found that:

(i) For arguments with real part less than 5.0, downwards recurrence proved to be satisfactory[2.46].

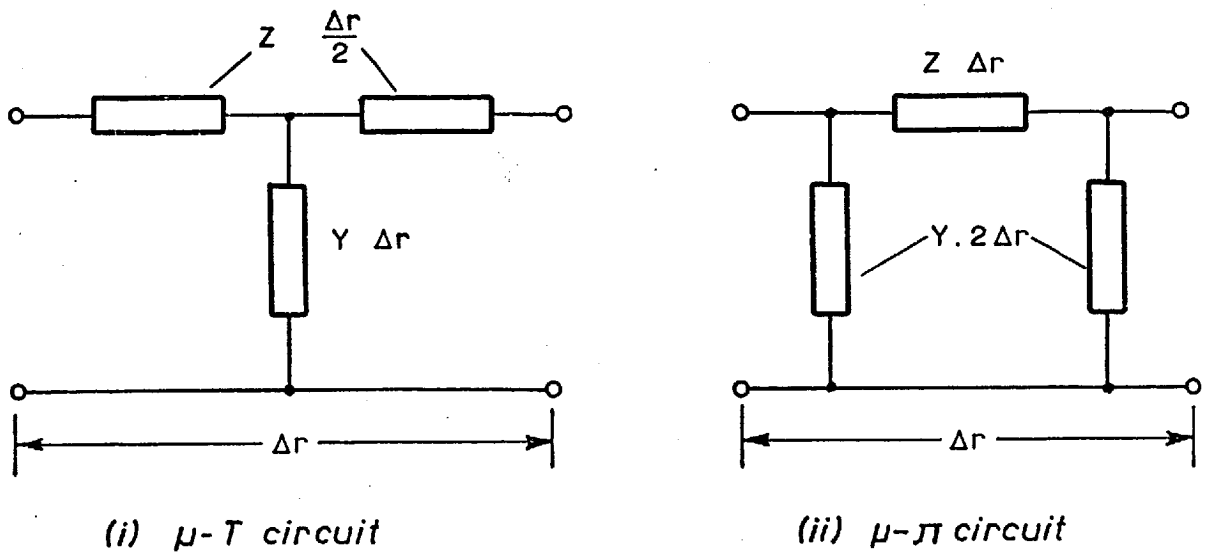
(ii) When the modulus of the argument exceeds 18.0, the asymptotic expansions can be used.

(iii) In the intervening region, a method which employs the Poisson summation formula, is adequate.

Another snag in the expressions given by equations (2.40) and (2.43) from the computational point of view, lies in the form of the functions $S(y_o,y_1)$, $S(y_1,y_o)$ and $R(y_1,y_o)$. Each of these functions is a ratio of differences between terms, which will be very small if y_o and y_1 are near to each other, i.e. if the annular region is narrow and (γ) is not very large. Pfaler[2.47,.48] got around a similar problem by transforming the Bessel differential equation and devising new fundamental solutions other than modified Bessel functions, he called these new functions "modified cylindrical functions" or "annular functions".

In this section, another technique will be adopted in order to calculate the electromagnetic field distribution and hence the surface wave impedance at any point in the model. This technique, which will be termed the 'Micro-T circuit' technique, as will be shown later will avoid the necessity of calculating Bessel functions of any kind. The idea is to discretize the continuous transmission line, which represent the basic unit in building the equivalent network, to a large number of elementary sections connected in cascade.

If each section has a small enough elementary length, Δr, equation (2.13) of the T.L. can be satisfied by the voltage and current relationships of either of the following circuits:



(i) μ-T circuit (ii) μ-π circuit

Fig. 2·15 Elementary equivalent circuit

In fact the idea of lumping the continuous transmission line, i.e. replacing it by a large number of elementary T- or π-circuits is not new. It has been used before for building analogue networks for solving certain field problems. For instance, Roberts[2.49,.50] investigated the eddy current problems involving two-dimensional fields by constructing an

analogue network composed of sections of T- and π-circuits. He introduced the effects of non-linearity in the magnetic material, by adding biased bridge-rectifier circuits into the network. Oberretl[2.51], studying the eddy-current problems in flat plates made of non-linear magnetic materials, has built a non-linear network consisting of semiconductor diodes, capacitors and resistors. It is worth mentioning here that, specially selected silicon Zener diodes have been used by Oberretl in order to simulate, to high degree of accuracy, the magnetisation curves of electrical sheet steels and solid iron. Beland and Richard[2.52], lumped a non-uniform transmission line, whose equation is a special case of equaton (2.13), in order to derive the expression of the shunt and series elements required to simulate this line. O'Kelly and Salih[2.53], similarly repalced a continuous transmission line by a number of π-circuits in cascade.

In order to develop the elements of the micro-T circuit which will represent an elementary distance Δr of either the E- or the H-transmission lines, the technique of 'Continued-Fraction expansions' will be used. The theory of these fractions is a well-developed branch of mathematics[2.54] and has been extensively used in the field of network synthesis[2.55]. For our purposes, a function G may be expressed by a continued fraction in the form:

$$G = b_1 + \cfrac{a_2}{b_2 + \cfrac{a_3}{b_3 + \ddots + \cfrac{a_n}{b_n}}}$$

For the special case when each of the a_r equal to unity, G is said to be expanded in a 'simple continued fraction' form.

2.9.1 Elements of the micro-T circuit of the E-line

Equations (2.24) and (2.25) represent the series impedance and shunt admittance per unit length of the E-line. Multiplying each equation by Δr, to represent an elementary distance Δr and rewriting it again expressing the R.H.S. in a simple continued fraction form, we get:

$$Z'.\Delta r = j\omega\mu\Delta r/2 + 1.0/\{(r\sigma/\beta^2\Delta r) + (j\omega\epsilon r/\beta^2\Delta r)\} \quad (2.51)$$

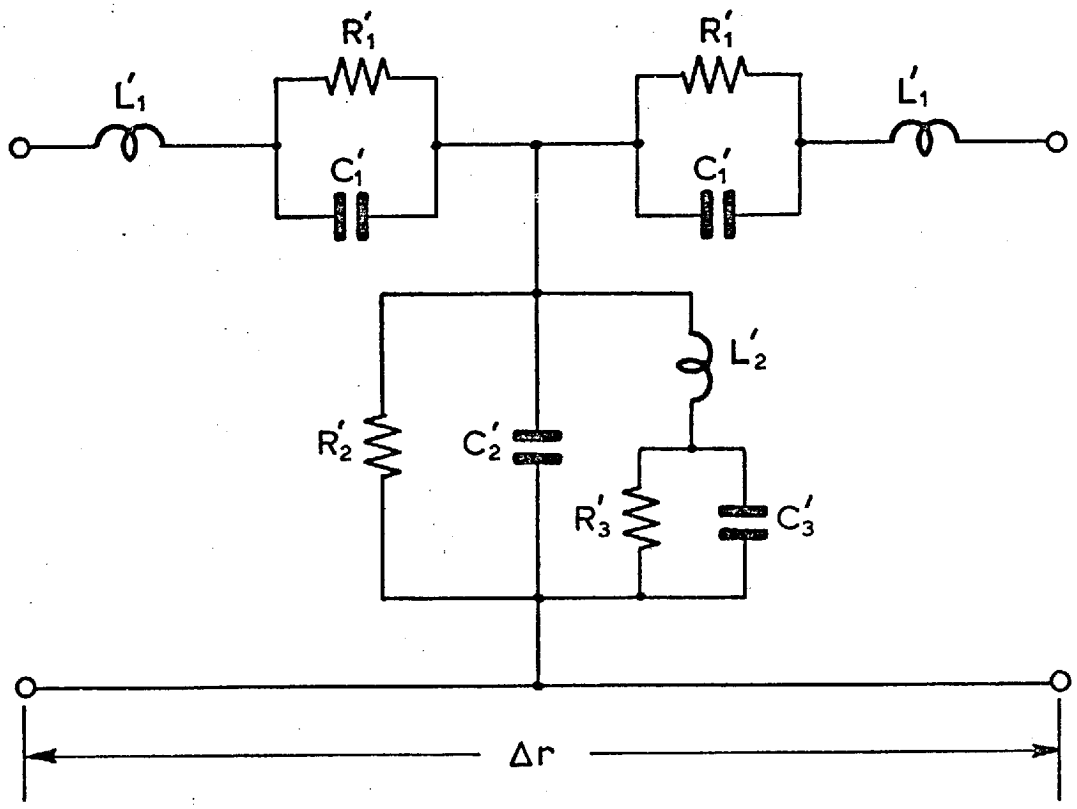
$$Y'.\Delta r = \sigma r\Delta r + j\omega\epsilon r\Delta r + 1.0/\{(j\omega\mu r/\alpha^2\Delta r) + 1.0/[(\sigma\alpha^2\Delta r/r\beta^2) + (j\omega\epsilon\alpha^2\Delta r/r\beta^2)]\} \quad (2.52)$$

2.9.2 Elements of the micro-T circuit of the H-line

Following section (2.9.1), the impedance and admittance of an elementary distance Δr of the H-line are given by:

$$Z''.\Delta r = j\omega\mu r\,\Delta r + 1.0/\{(r\sigma/\alpha^2\Delta r) + (r\beta^2/j\omega\mu\alpha^2\Delta r) + (j\omega r\epsilon/\alpha^2\Delta r)\} \quad (2.53)$$

$$Y''.\Delta r = (\sigma\Delta r/r) + (\beta^2\Delta r/j\omega\mu r) + (j\omega\epsilon\Delta r/r) \quad (2.54)$$



$$L'_1 = \frac{\mu}{r}\,(\Delta r/2) \quad , \quad L'_2 = \mu r \frac{1}{\alpha^2}\,(1/\Delta r)$$

$$C'_1 = \varepsilon r \frac{1}{\beta^2}\,(2/\Delta r)$$

$$C'_2 = \varepsilon r\,(\Delta r)$$

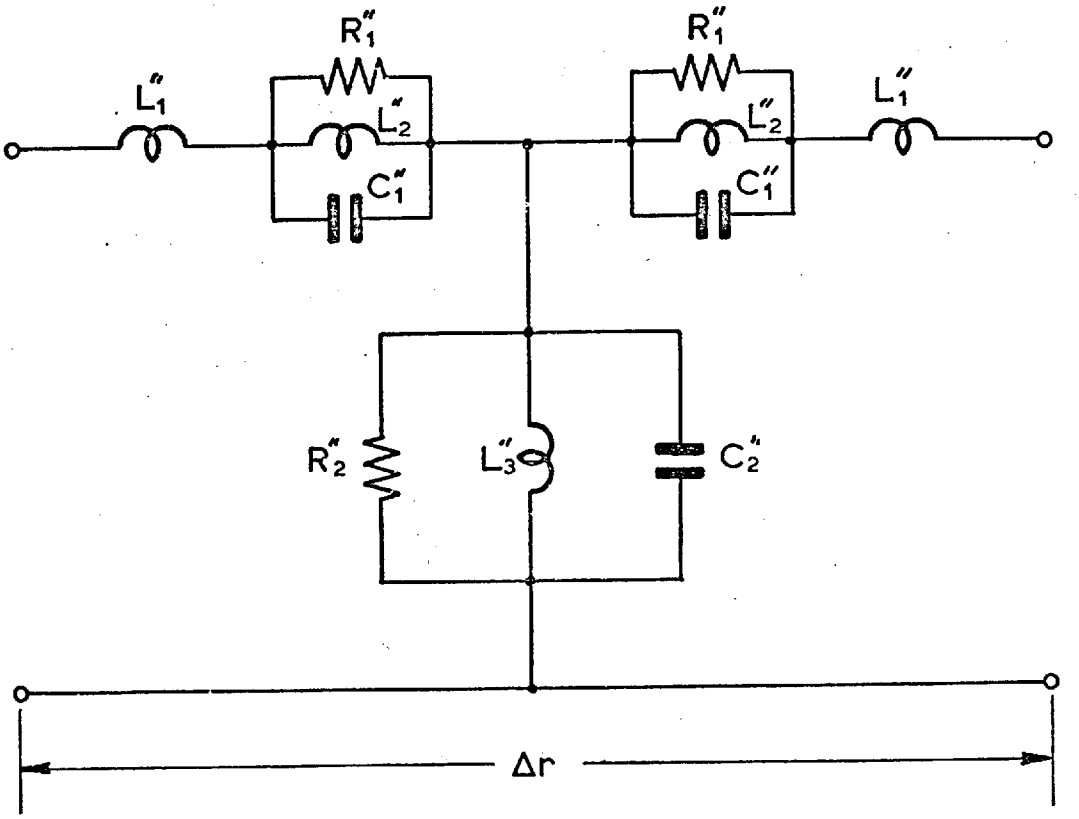
$$C'_3 = \frac{\varepsilon}{r}\frac{\alpha^2}{\beta^2}\,(\Delta r)$$

$$R'_1 = \frac{\beta^2}{\sigma r}\,(\Delta r/2)$$

$$R'_2 = \frac{1}{r\sigma}\,(1/\Delta r)$$

$$R'_3 = \frac{r}{\sigma}\frac{\beta^2}{\alpha^2}\,(1/\Delta r)$$

Fig. 2·16 The micro-T circuit of the E-line.



$$L_1'' = \mu r\ (\Delta r/2)$$

$$L_2'' = \frac{\mu}{r}\ \frac{\alpha^2}{\beta^2}\ (\Delta r/2)$$

$$L_3'' = \mu r\ \frac{1}{\beta^2}\ (1/\Delta r)$$

$$C_1'' = \varepsilon r\ \frac{1}{\alpha^2}\ (2/\Delta r) \qquad C_2'' = \frac{\varepsilon}{r}\ \Delta r$$

$$R_1'' = \frac{\alpha^2}{r\sigma}\ (\Delta r/2) \qquad R_2'' = \frac{r}{\sigma}\ (1/\Delta r)$$

Fig. 2·17 The micro-T circuit of the H-line.

2.9.3 Simplifications for conducting and non-conducting regions

The equivalent micro-T circuits of the E- and H-lines, as well as the expressions of the individual elements in terms of the field quantities , are shown in Figures (2.16) and (2.17) respectively. These circuits include elements which represent the effects of the displacement current, namely, the capacitances. As it is the practice throughout the course of this chapter to consider the general case whenever possible, then simplify according to the nature of the problem in hand, another set of mirco-T circuits can be derived from the general circuits of Figs. (2.16) and (2.17), to represent either a conducting region or an air (i.e. non-conducting) region. An equivalent micro-T circuit of a conducting region shown in Fig. (2.18) has been obtained from the general circuits of Figs. (2.16) and (2.17) by neglecting the displacement current. This can be effected by removing the capacitive branches from the circuits.

For a non-conducting region, the resistances R_1'' and R_2'', of the H-line micro-T circuit, will be open circuited. The capacitors C_1'' and C_2'' are proportional to the permittivity of the region (ε), both are shunting inductive elements whose values are proportional to the permeability μ. The shunting effect of these capacitors is negligible and they can be removed from the circuit without any loss of accuracy. On the other hand, when the resistive elements R_1', R_2' and R_3'

of the E-line micro-T circuit are removed, the capacitive elements will appear in series with the inductance elements of this circuit as shown in Fig. (2.19). In this case, the inductances are to be neglected with respect to capacitors.

Since the values of all the capactive elements are proportional to the permittivity (ε), then as ε approaches zero, the impedance to the flow of the current I'(r) will be very large, reaching infinity in the limit. The equivalent circuit becomes just an open circuit as indicated in part (a-iii) of Fig. (2.19).

Although the current flowing in the ladder network which represents the E-line of a non-conducting region is almost negligible, there is certainly a voltage distribution along the length of this network. This is because of the large value of the impedance elements (capacitive impedance in this case). A close investigation of the expressions of the field components, when written for a non-conducting region, reveals that the magnetic field components will be dependent mainly on the voltage and current of the H-line only. On the other hand ,the components of the electric field vector will depend on voltages and currents of both E- and H-lines. This in turn will lead to the conclusion that, as far as the calculations of the magnetic field vector components are concerned, the E-line of any non-conducting region can be considered as as open circuit. However, in the case when the electric field

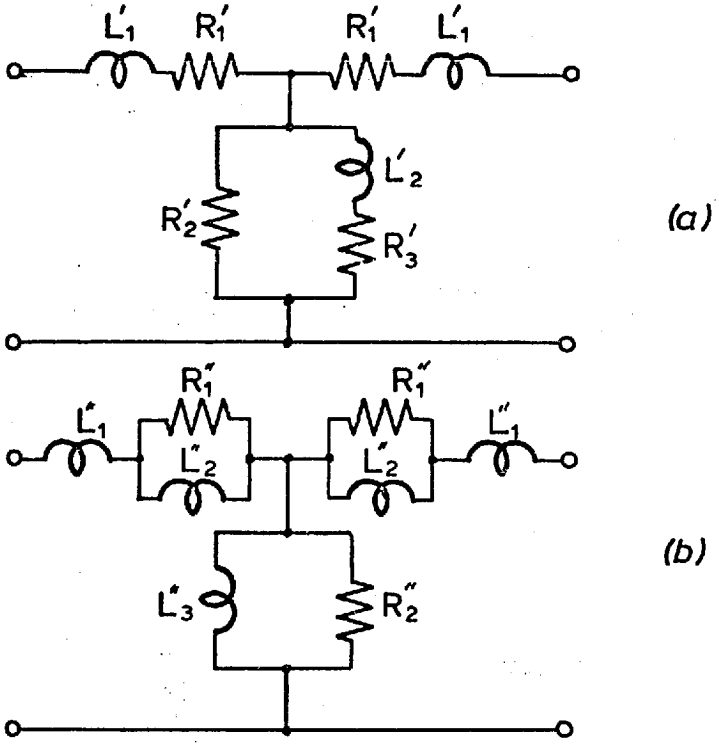


Fig. 2·18 Micro-T equivalent circuit of a conducting region
(a) E-line (b) H-line

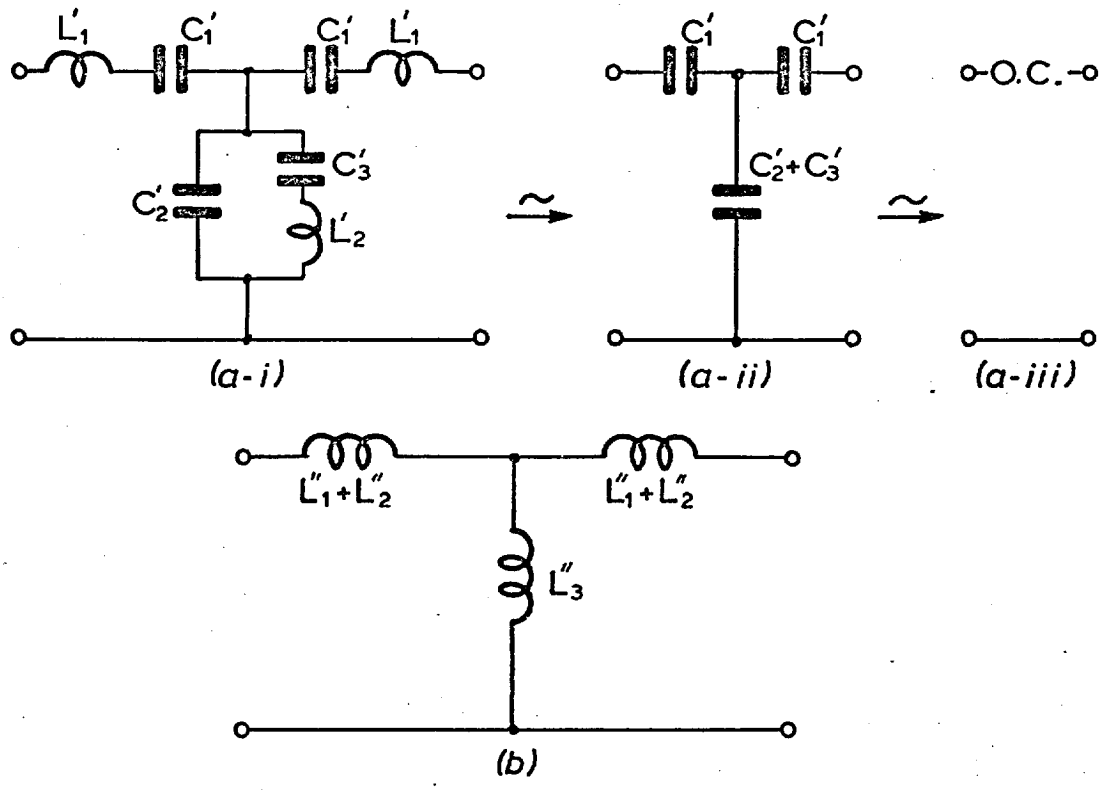


Fig. 2·19 Micro-T equivalent circuit of a non-conducting region (with finite permeability)
(a) E-line (b) H-line

components are required, removing the E-line of the non-conducting region and assuming it to be an open circuit will indeed result in incorrect answer. This might not be immediately obvious, hence the next section will be devoted to a more thorough investigation of this point.

2.10 Expressions of the Electromagnetic Field Components in a Laplacian-region: (Non-Conducting Region)

Usually, for low frequency applications, the distribution of the magnetic field vector components in a non-conducting region are of major importance, while the components of the E-field are not usually required to be calculated. However, to make the work of this chapter complete, we will derive the expressions of the components of the both fields.

The general expressions of the field components are given in section (2.6.5) in terms of the voltages and the currents of the double T.L. equivalent network. For a conducting region, there is no problem, the corresponding expressions can be deduced from the general ones by merely substituting for: (γ^2) by $(\beta^2 + j\omega\mu\sigma)$, and for σ_c by σ. For a non-conducting region, the current $I'(r)$ was found by inspection to be very small if the displacement current is to be neglected. It reaches zero as the premittivity ε approaches zero. The expressions of the field components can be obtained

in this case by substituting for (γ^2) by (β^2), and (σ_c) by $(j\omega\varepsilon)$ and then taking the limit as ε approaches zero, keeping in mind that:

$$\lim_{\varepsilon \to 0} I'(r) = 0$$

while,

$$\lim_{\varepsilon \to 0} \frac{I'(r)}{\varepsilon} \neq 0$$

Thus, the expressions of the electric and magnetic field components of a non-conducting region are given by:

$$\left.\begin{aligned} H_r(r) &= -(\beta/\omega\mu r) \cdot V'' \\ H_\theta(r) &= -(\alpha/\beta r) \cdot I'' \\ H_z(r) &= I'' \end{aligned}\right\} \quad (2.55)$$

$$\left.\begin{aligned} E_r(r) &= \mp(\beta/\omega r) \lim_{\varepsilon \to 0} (I'/\varepsilon) - (\omega\mu\alpha/\beta^2 r) I'' \\ E_\theta(r) &= -(\alpha/\beta r) V' + (1/r) V'' \\ E_z(r) &= V' \end{aligned}\right\} \quad (2.56)$$

The expression of $E_r(r)$ given by equation (2.56) could be written, by virtue of equation (2.36), in terms of $V'(r)$ instead of $I'(r)$ as follows:

$$E_r(r) = (-1/j\beta)\frac{dV'}{dr} - (\omega\mu\alpha/\beta^2 r)\ I'' \qquad (2.57)$$

As will be shown later, it is straight forward to calculate the distribution of I" and V" in either the conducting or non-conducting regions from the double T.L. equivalent network. Also the values of the voltage V' and I' can be obtained directly for the conducting regions from the same network. However, the values of V'(r) for non-conducting regions can be obtained from the equivalent network only at the boundary surfaces. The double T.L. network as developed has an open circuit representing the non-conducting regions E-line.

In order to find the distribution of V'(r) as well as its derivative with respect to the radius (r), recall equation (2.10). V'(r) is given by:

$$V'(r) = C_{1e}\ I_\alpha(\beta r) + C_{2e}\ K_\alpha(\beta r)$$

Now, the constants C_{1e} and C_{2e} can be easily calculated from the values of V'(r) at the inner and outer radii of the non-conducting region. The modified Bessel fucntions which appear in this case have real arguments. Their calculation is easy and straight forward.

However, as we mentioned before, the Bessel functions can always be eliminated by devising the appropriate T.L. . V'(r) satisfies the equation:

$$\left[\frac{d^2}{dr^2} + \frac{1}{r}\frac{d}{dr} - \{\alpha^2/r^2 + \beta^2\}\right] V'(r) = 0 \qquad (2.58)$$

This equation can be thought of as a non-uniform T.L.. equation whose micro-T circuit elements are related by:

$$\left.\begin{aligned} ZY &= \left(\frac{\alpha^2}{r^2} + \beta^2\right) \\ \frac{dZ}{dr} &= -\frac{Z}{r} \end{aligned}\right\} \qquad (2.59)$$

The solution of equations (2.59) is given by:

$$\left.\begin{aligned} Z &= \frac{\text{Constant}}{r} \\ Y &= \frac{r}{\text{Constant}}\left(\frac{\alpha^2}{r^2} + \beta^2\right) \end{aligned}\right\} \qquad (2.60)$$

Apparently, there is an infinite number of equivalent T.L.s which have the same voltage distribution along their length. If the constant which appears in equations (2.60) is chosen to be $(\beta^2/j\omega)$, the micro-T circuit which represent the non-uniform T.L. will be as shown in Fig. (2.20).

The equivalent T.L. will be called the 'transformed E-line' to differentiate it from the E-line developed before. The special choice of the constant of equation (2.60) results in making the current I^r equal to the quantity $\text{Lim}\left(\frac{I'}{\varepsilon}\right)$. It is worth mentioning that the micro-T circuit shown in Fig. (2.20) can be considered as a 'per unit' referred circuit

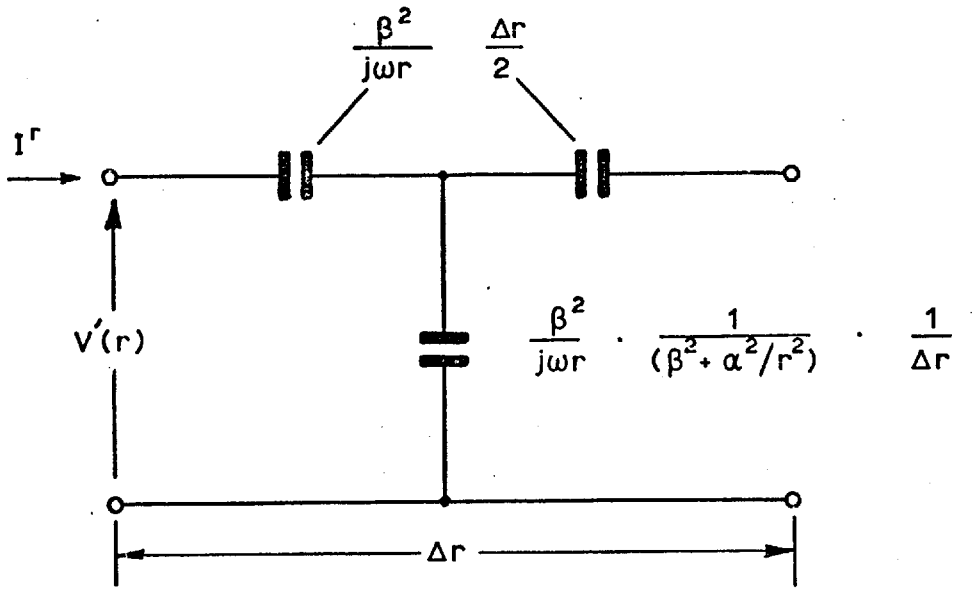


Fig. 2·20 Micro-T circuit of the transformed E-line of a non-conducting region.

of that one shown in (a-ii) of Fig. (2.19) by taking the base voltage as unity, the base current as (ε), hence the base impedance as ($1/\varepsilon$).

2.11 Special Case: One-Dimensional Excitation Current Sheet

So far, the developed double T.L. equivalent network represents the case when the excitation current sheet has two components, in the axial and circumferential directions. The E- and H-lines are excited by current sources whose magnitude is given by ($r_e K_z$) and (K_θ) respectively. Moreover, the two lines are coupled at the interfaces by ideal

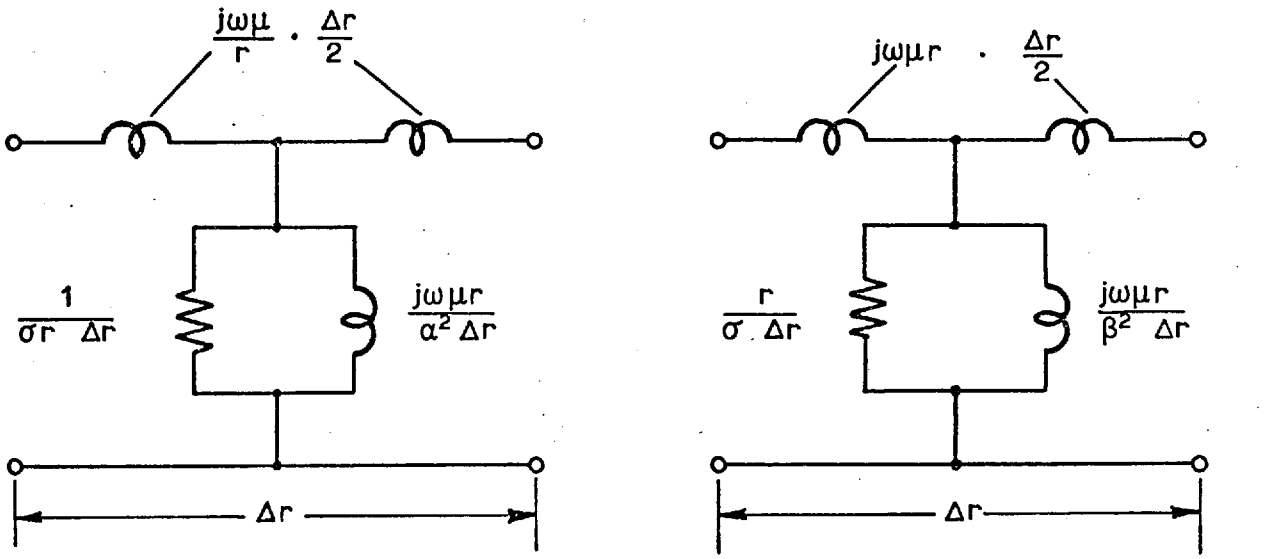
transformers whose turns ratios are in general complex and proportional to the quantity ($\alpha\beta$).

Now, if the excitation current is one-dimentional having a component in the axial direction only.

i.e. $K_\theta = 0$, $\beta = 0$

Since $\beta = 0$, this means no coupling between the two lines. The condition that $K_\theta = 0$ indicates no excitation to the H-line. Hence, we will be left with the E-line only. The micro-T circuit in this case can be obtained from the general form of Fig. (2.16)by substituting for (β) by zero. The capacitive branches will be open circuited ($\beta^2 = 0$. while ε is a very small quantity) while the two resistive branches R_1' and R_3' will be short circuited. The micro-T circuit of the equivalent T.L. representing the axially excited multiregion cylindrical model is then given by Fig. (2.21a). Similarly, if we have a circumferential excitation current sheet, both (K_z) and (α) will be zero. We will be left with the H-line, and the micro-T circuit will be as shown in Fig. (2.21b).

These two equivalent micro-T circuits, which are derived as special cases of the double transmission line circuit, are exactly similar to those obtained by Freeman (2.56 - 2.57).



a. Axial excitation

b. Circumferential excitation

Fig. 2·21 Micro-T circuit for one-dimensional excitation.

2.12 Macro-T Circuit Representation of E- and H-lines

The discretization of the E- and H-lines of each annular region in the mathematical model described in Section (2.4), to a large number of the so called 'micro-T circuits' connected in cascade, eliminates the need for expressing the field solution in terms of Bessel functions. The choice of the number of regions which represent any one line is of great importance, since the main source of computational errors is due to lumping the transmission line into a discrete number

of T-sections. As the number of these T-sections increases, the discretisation error decreases, but of course this will be at the expense of increasing the computational time. A number of micro-T circuits would be considered adequate to represent one transmission line if there is no appreciable change in the calculated results when the same T.L. is replaced by larger number of the T-sections.

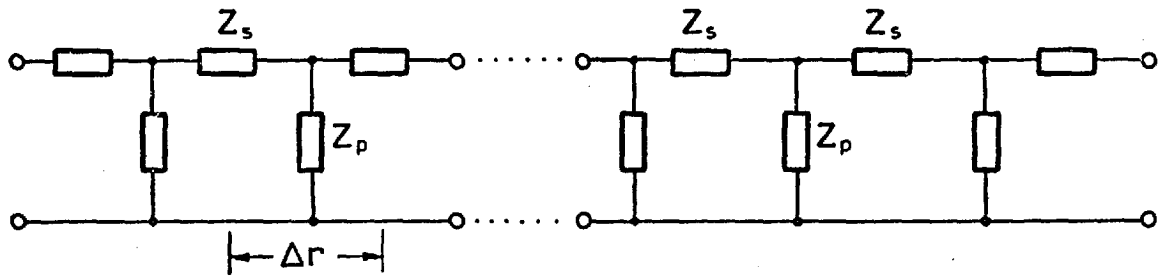


Fig. 2·22 Equivalent circuit of lumped T.L.

Consider the lumped transmission line shown in Fig.(2.22), in which each elementary length Δr has been replaced by T-circuit. The series and parallel impedances which appear in the equivalent circuit are given in general in the form:

$$\left.\begin{aligned} Z_s &= Z\,\Delta r \\ Z_p &= 1/(Y.\Delta r) \end{aligned}\right\} \quad (2.61)$$

Where Z and Y are the series impedance and parallel admittance per unit length of the transmission line. The sub-region thickness Δr can be obtained from:

$$\Delta r = \frac{1}{\sqrt{ZY}} \sqrt{|Z_s|/|Z_p|} \qquad (2.62)$$

For both the E- and H-lines, the quantity $\sqrt{ZY}$ is given by equation (2.20c), hence Δr will be given generally for either of the two lines, in the form:

$$\Delta r = d.\{1 + d^4(\beta^2 + \alpha^2/r^2)^2\}^{-1/4} \sqrt{|Z_s/Z_p|} \qquad (2.63)$$

Where (d) is the penetration depth and is equal to $(\omega\mu\sigma)^{-\frac{1}{2}}$. In fact, a study for estimating the sub-region thickness Δr such that the overall discretization error is limited to well below 1% has been presented in Chapter 4 of this thesis in case of circumferential excitation model. To avoid repetition, only the result will be quoted here. Keeping the ratio $|Z_s|/|Z_p|$ equal to or less than approximatley 1/1000 will limit the maximum error to less than 1%. Consequently, the subregion thickness can be chosen according to the relation

$$\Delta r = 0.03d\{1 + d^4(\beta^2 + \alpha^2/r^2)^2\}^{-1/4} \qquad (2.64)$$

The important observation revealed from the expression of Δr is its dependance on the radius (r). The effect of radius (r) on the subregion thickness is mainly manifested for annular regions of very small radii.

To simplify the programming, Δr has been taken to be constant all over the region, and its value will be calculated

from equation (2.64), substituting for r in the expression by the geometric mean radius of the region. Regions characterised by larger outer/inner radii ratio can be divided into two or more main sub-regions.

The transmission line being replaced by a string of certain number of micro-T circuits connected in cascade, the distribution of the voltage and current along its length can be obtained if its terminal values are known. The terminal quantitites at both sides of the transmission line, however, can be related through 'one' T-circuit instead of many. This 'one' T-circuit is equivalent to the number of the micro-T circuits in cascade. To distinguish this T-circuit from the micro-T circuit, it will be called the 'macro-T' circuit throughout the text.

If Z_A, Z_B and Z_C are the impedances of the 'Macro-T' circuit, shown in Fig. (2.23c), which represent either an E- or H-line of an annular region, their values can be calculated from the following relations[2.58]:

$$\left.\begin{aligned} Z_C &= \pm \sqrt{Z_{sO}(Z_{rO} - Z_{rs})} \\ Z_A &= Z_{sO} - Z_C \\ Z_B &= Z_{rO} - Z_C \end{aligned}\right\} \quad (2.65)$$

Where the impedances Z_{sO}, Z_{ss}, Z_{rO} and Z_{rs} are:

Z_{sO} = sending end impedance with O.C. receiving end.

Z_{ss} = sending end impedance with S.C. receiving end.

Z_{rO} = receiving end impedance with O.C. sending end.

Z_{rs} = receiving end impedance with S.C. sending end.

and they can be obtained from the cascade connection of micro-T circuits shown in Fig. (2.23b) by satisfying the proper terminal conditions then adding the impedances in series and in parallel, as appropriate, till reaching the input terminals. It should be noted that the incorrect choice of the sign of the impedance Z_C will result in reversing the sign of the output voltage and current of the macro-T circuit. This difficulty can simply be overcome as follows:

- Calculate Z_A, Z_B and Z_C from expressions (2.65), assuming a +ve sign for Z_C.

- For an input voltage and current, say 1.0 per unit, calculate the output voltage and current for the macro-T circuit.

- For the same input condition, calculate the output for the equivalent network of cascaded micro-T circuits fo Fig. (2.23b). Compare the two outputs,

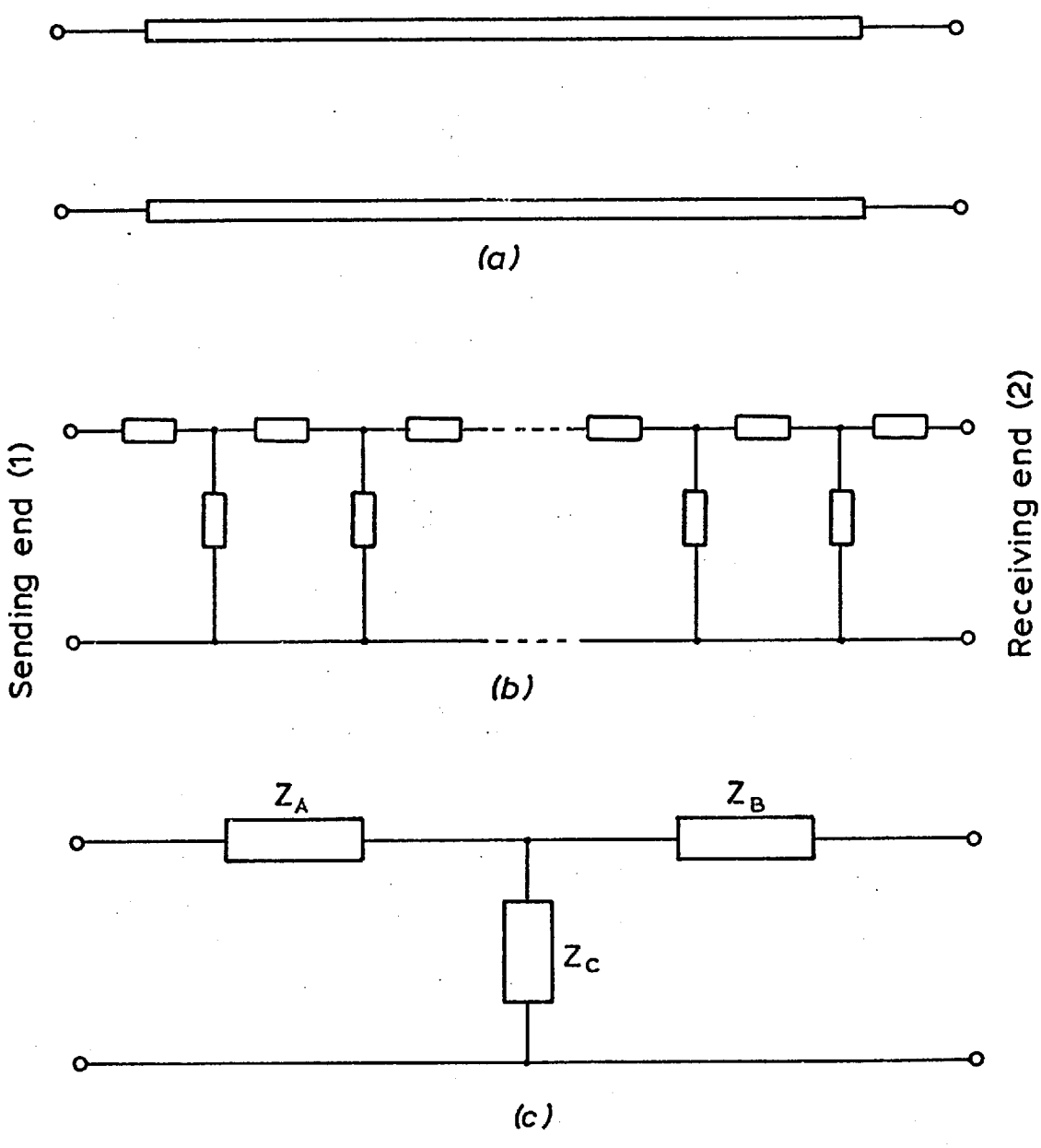


Fig. 2·23 Evolution of macro-T circuit

(a) Continuous line

(b) Equivalent network of number of micro-T circuits in cascade

(c) Equivalent macro-T circuit of the T.L.

they must have the same magnitude and phase. However, if there is 180° phase difference, the -ve sign should be taken in front of Z_c.

It is worth mentioning that for a non-conducting region, the positive sign is always correct for Z_c. The 'sign test' needs to be done only for the conducting regions.

The author would like to acknowledge that the importance of the choice of the sign of Z_c for conducting regions has been drawn to his attention by Mr. K.Y.K. Wu[2.59].

2.13 The Equivalent Four-Terminal Network of an Annular Conducting Region Bounded by Two Non-Conducting Regions

In many practical applications, which can be mathematically modelled as shown in Fig. (2.9), the conducting annular region is usually bounded by two non-conducting regions. This, as will be shown later in this section, can result in some simplification in the form of the equivalent network of this region.

The equivalent network is shown in Fig. (2.24a), the coupling transformers at the interfaces are connected in such a way that they will have the same complex turns ratio T, where T is given by:

$$T = \text{transformer complex turns ratio}$$
$$= \alpha\beta\left(1/\beta^2 - 1/\gamma^2\right)$$
$$= j\omega\mu\sigma\alpha/\beta\gamma^2 \qquad (2.66)$$

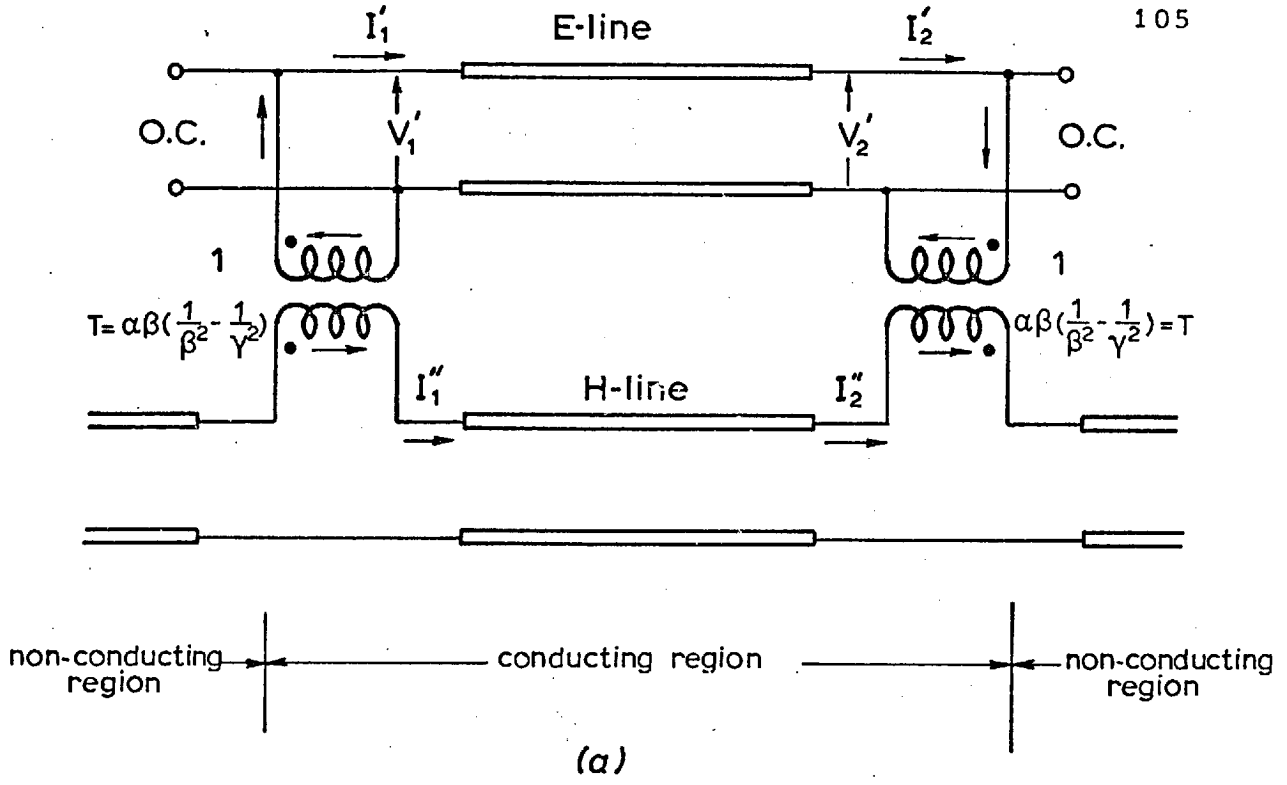
The E-lines of the non-conducting regions at both sides of the annular conducting region are shown in the figure as open-circuited. This has been fully discussed in sections (2.9) and (2.10). The positive directions of the voltage and current at the different points in the equivalent network, are indicated by the arrows in the figure.

Referring all the quantities of the E-line, through the complex turns ratio transformers, to the H-line side, and replacing each line with its equivalent macro-T circuit as defined in section (2.12), we get the equivalent network shown in Fig. (2.24b). The voltage and current of the referred E-line are (T) and (1/T) times their unreferred values respectively. The referred marco-T circuit elements are T^2 times their original values.

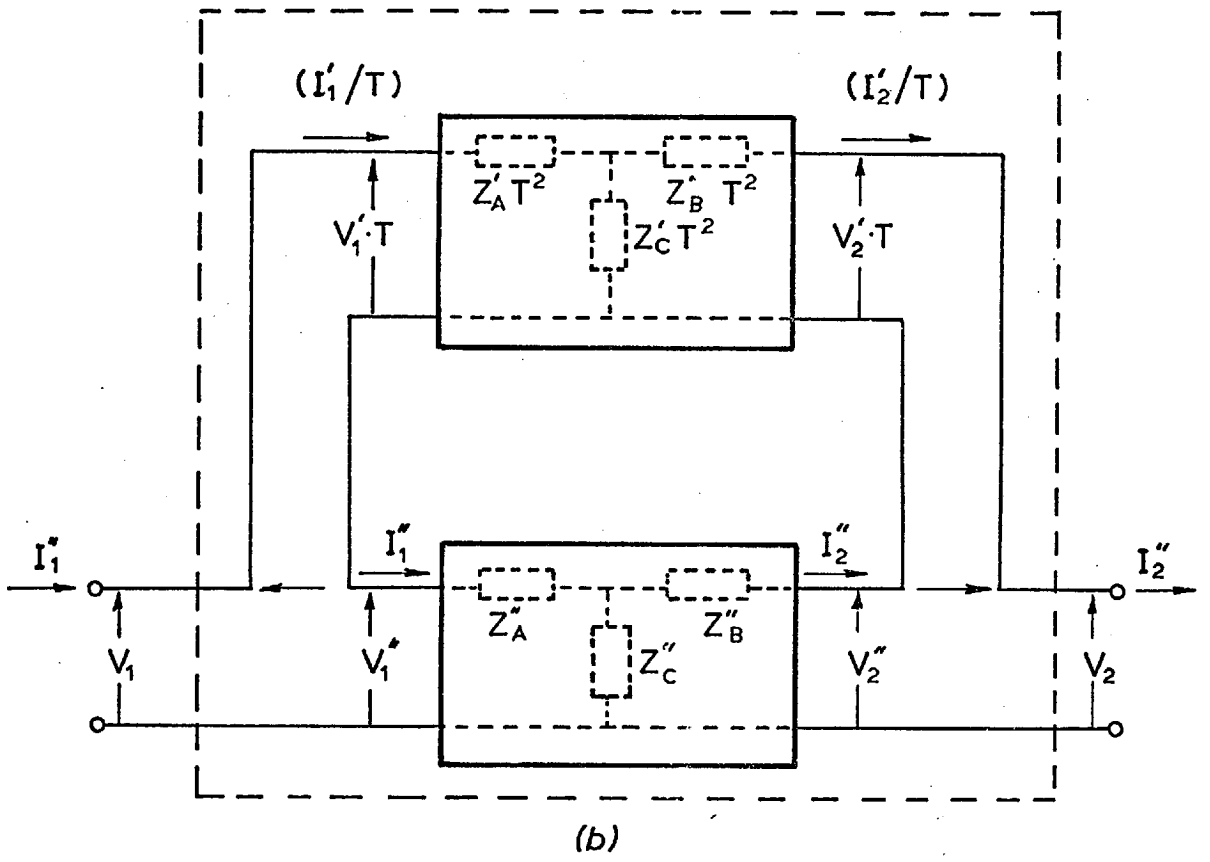
In an attempt to derive one T-circuit for the conducting region in order to relate V_1 and I_1'' to V_2 and I_2'' as they appear in Fig. (2.24b), we proceed as follows:

$$V_1 = V_1'' + T.\, V_1'$$

$$I_1'' = I_1'/T$$



(a)



(b)

Fig. 2·24 Equivalent network of a conducting region bounded by 2 non-conducting regions.

(a) Original network

(b) Referred network to the H-line side

$$V_2 = V_2'' + T.V_2' \qquad (2.67)$$

$$I_2'' = I_2'/T$$

The voltages and currents at both sides of each T-circuit are related by the impedance matrix (A) such that:

$$\begin{bmatrix} V_i \\ \\ V_o \end{bmatrix} = \begin{bmatrix} (Z_A + Z_C) & -Z_C \\ \\ Z_C & -(Z_B + Z_C) \end{bmatrix} \begin{bmatrix} I_i \\ \\ I_o \end{bmatrix} \qquad (2.68)$$

Where the subscripts (i) and (o) stand for input and output respectively.

Hence

$$\begin{bmatrix} V_1'' \\ \\ V_2'' \end{bmatrix} = [A]'' \begin{bmatrix} I_1'' \\ \\ I_2'' \end{bmatrix} \qquad (2.69a)$$

and

$$T. \begin{bmatrix} V_1' \\ \\ V_2' \end{bmatrix} = T^2 [A]'. \frac{1}{T} \begin{bmatrix} I_1' \\ \\ I_2' \end{bmatrix} \qquad (2.69b)$$

Adding (2.69a) and (2.69b), and substituting from (2.67)

$$\begin{bmatrix} V_1'' \\ \\ V_2'' \end{bmatrix} + T \begin{bmatrix} V_1' \\ \\ V_2' \end{bmatrix} = \begin{bmatrix} V_1 \\ \\ V_2 \end{bmatrix}$$

$$= \{[A]'' + T^2\ [A]'\} \cdot \begin{bmatrix} I_1'' \\ \\ I_2'' \end{bmatrix} \qquad (2.70)$$

That is to say the two T-circuits shown in Fig. (2.24b) reduce to only one T-circuit whose elements are given by:

$$\left.\begin{aligned} Z_A &= Z_A'' + T^2\ Z_A' \\ Z_B &= Z_B'' + T^2\ Z_B' \\ Z_C &= Z_C'' + T^2\ Z_C' \end{aligned}\right\} \qquad (2.71)$$

The distribution of the induced eddy currents in the conducting region is often of interest. These expressions of current density can be directly obtained from equations (2.31) of the electric field vector by multiplying it by the conductivity σ. Thus, the induced eddy currents due to (m,n) spatial excitation harmonic will be in the form:

$$\left.\begin{aligned} J_r &= (\omega\mu\sigma\alpha/\gamma^2 r) \cdot \{(I'/T) - I''\} \\ J_\theta &= (\sigma/r) \cdot \{V'' - (\beta^2/j\omega\mu\sigma) \cdot (T.V')\} \\ J_z &= (\sigma/T) \cdot \{T.V'\} \end{aligned}\right\} \qquad (2.72a)$$

And the magnetic field components will be given by:

$$\left.\begin{aligned} H_r &= \pm(\beta/\omega\mu r) \,.\, \{T.V' + V''\} \\ H_\theta &= -(\alpha\beta/\gamma^2 r) \,.\, \{(j\omega\mu\sigma/\beta^2).\ (I'/T) + I''\} \\ H_z &= \{I''\} \end{aligned}\right\} \quad (2.72b)$$

2.14 Experimental Model

In order to verify the theoretical model developed in the previous sections of this chapter, an experimental model was constructed. The flux density components are measured and compared with the corresponding calculated values for different cases, namely:

(i) In the absence of a conducting region

(ii) With a conducting region inserted inside the excitation winding.

(iii) With a conducting region encircling the excitation winding.

2.14.1 Description of the test rig

The excitation winding is a single-layer, helical winding wound on a circular-cylindrical "Paxolin" tube. The particulars of the winding are given below, the devloped

diagram as well as a schematic diagram are shown in Fig. (2.25).

Particulars of the helical winding:

Number of phases	3
Number of axial poles	6
Number of circumferential poles	2
Axial pole pitch	15 cm
Circumferential pole pitch	16.15 cm
Number of conductors/pole/phase	15
Number of helical coils per phase	1
Number of helical turns per coil	15
Conductor diameter	2.337 mm
Rated phase current	20 amps
Paxolin tube outer diameter	10.2 cm
Paxolin tube inner diameter	9.6 cm
Paxolin tube axial length	91.5 cm
Overall axial length of the winding, including the over hangs	106.5 cm
The average winding resistance per phase	0.33 Ω

Two conducting regions are used throughout the tests, one at a time, their inner and outer diameters are as indicated below. The one which fits inside the excitation winding will be called the 'inner screen', while the other which will encircle the excitation winding will be called the 'outer screen'.

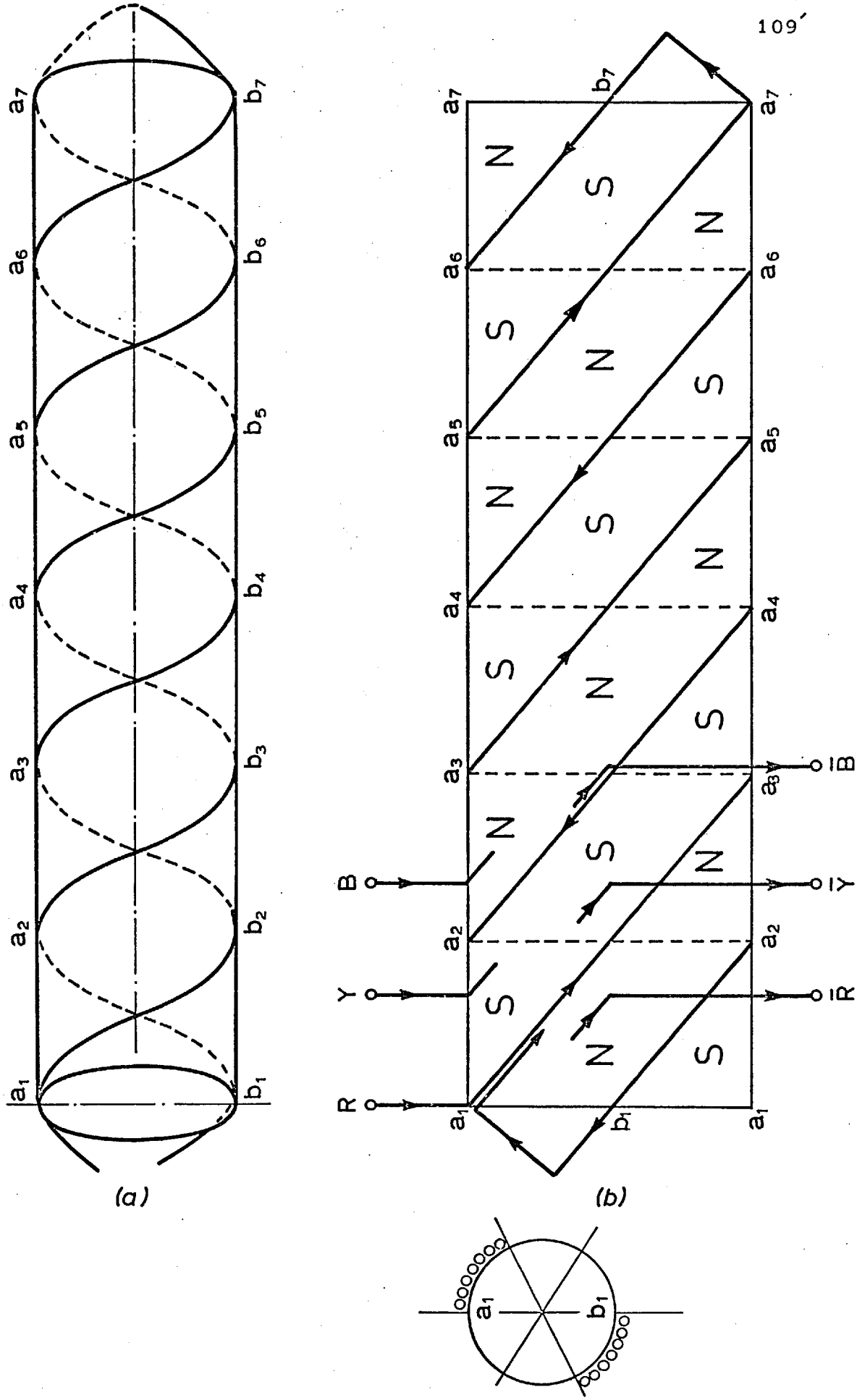


Fig. 2·25 Single-layer, current-sheet, helical winding
(a) Schematic diagram (b) Developed diagram

The inner screen 'inner/outer' diameter ratio = 3.8/7.6 cm

The outer screen 'inner/outer'diameter ratio = 13.28/15.14 cm.

Both screens were aluminium tubes. The conductivity of each one was obtained experimentally as indicated in Chapter 4 to an estimated accuracy of 1%.

The measurement of the three components of the magnetic flux density at any point was achieved by the use of three search coils wound on each other such that the axes of all three were mutually perpendicular. Ideally all the three search coils should have had the same cross sectional area and number of turns, and the area should have been as small as possible. However, due to the form of construction, the area of each coil had to differ slightly from the area of the other two. Each coil has been calibrated using a Gauss-meter. Since the excitation winding has only a small number of ampere turns, the output signal from the search coils had to be amplified before being measured by a digital volt-meter.

2.14.2 Excitation current sheet expressions

The current sheet wave forms are shown diagramatically in Fig. (2.26). In this figure, the phase belts of one phase only are drawn, and the arrows indicate the direction of the current flow. The pulsating current-sheet waveform

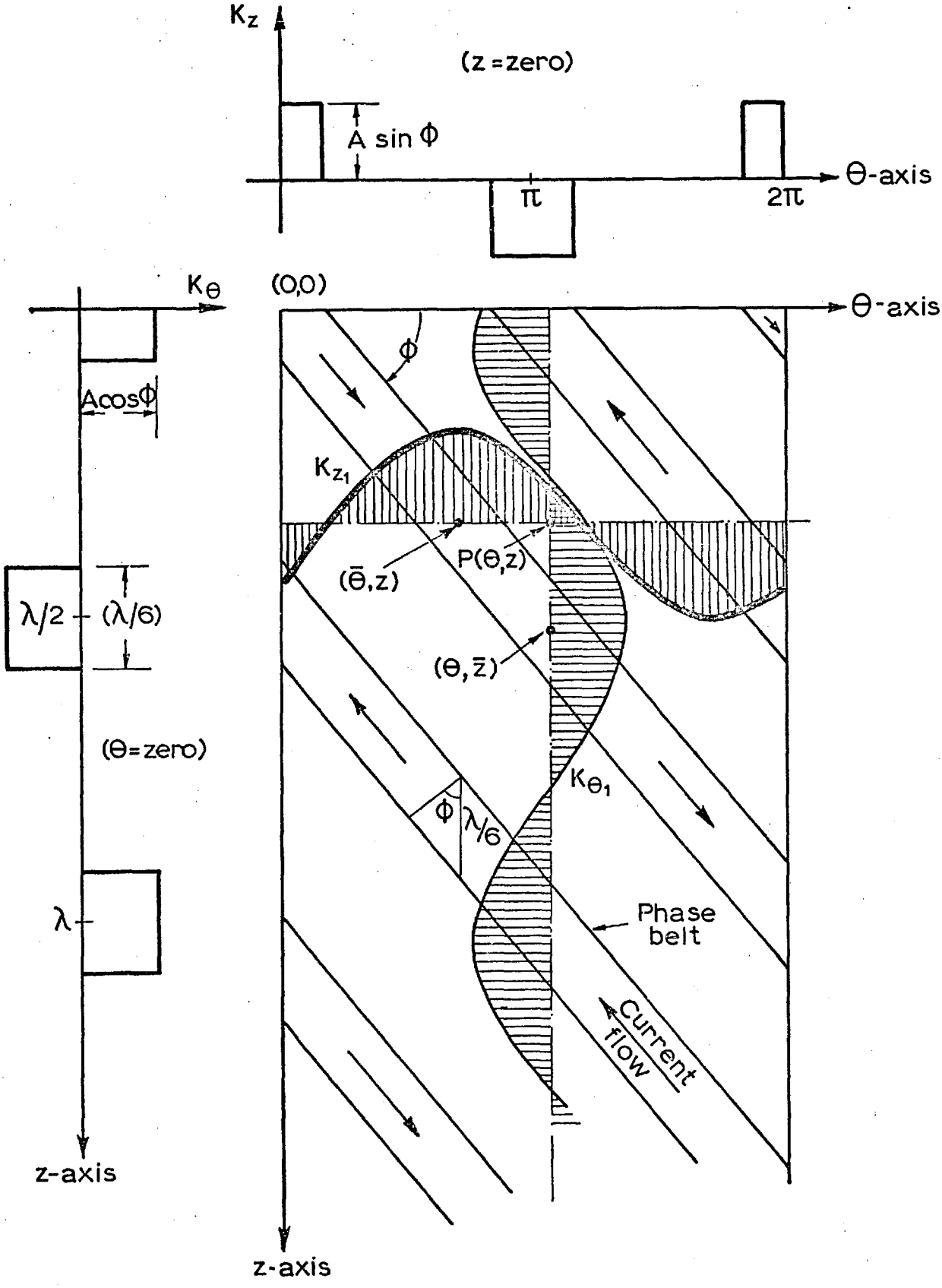


Fig. 2·26 Two dimensional current-sheet

of one phase, has a magnitude, whose r.m.s. value is A, which extends uniformly over the width of the phase belt, and its sign is defined by the direction of the current in the corresponding phase belt.

A is given by:

$$A = \frac{N\ I}{(\lambda/6)\ \cos\ \phi} \qquad \text{ampere/m} \qquad (2.73)$$

Where:

- N number of conductors in the phase belt, and is equal to 15 in our case
- I r.m.s. value of the phase current
- ϕ angle between the helical winding conductors and the θ-direction.

This current sheet is directed along the winding conductors. It can be resolved in both the θ- and z-directions by multiplying it by $(\cos\ \phi)$ and $(\sin\ \phi)$ respectively. The variation of the single phase axially- and azimuthally-directed current sheets along the θ-,(for zero value of z), and z-axes, (for zero values of θ), respectively, are shown in Fig. (2.26).

At any point $P(\theta,z)$, it can be easily shown that, the travelling wave current sheet components produced by the three phase helical winding will have the form:

$$K_\theta = \frac{3}{2} \cdot \frac{4}{\pi} \cdot A.\cos\ \phi \sum_{h=1,3,5,..}^{\infty} \frac{\sin(h\ \pi/6)}{h}\ \exp\{j(\omega t - h.\frac{2\pi}{\lambda}.z + h\theta)\} \qquad (2.74a)$$

$$K_z = \frac{3}{2} \cdot \frac{4}{\pi} \cdot A \sin\phi \sum_{h=1,3,5,..}^{\infty} \frac{\sin(h\,\pi/6)}{h} \cdot$$

$$\exp\{(j(\omega t - h\,\frac{2\pi}{\lambda}\,z + h\theta)\} \qquad (2.74b)$$

The two current sheet components satisfy the divergence equation $\nabla.\bar{K} = 0$.

2.14.3 Equivalent circuit and method of computation

The helical winding described above in section (2.12.1) was tested in order to provide experimental confirmation for the theoretical model developed in this chapter.

The model contains basically one annular conducting region, an excitation surface current sheet, an annular air-gap between the excitation surface and the conducting region and finally the inner most and the outermost air regions. This configuration requires to be represented by at least a four-region mathematical model. However, the computed results which are to be reported in this chapter, have been calculated for nine or ten regions instead of four. This increased number of regions is due to the fact that each of the inner-most and the outermost air regions was considered as consisting of three of four subregions. This has been done in order to introduce, although partially, the effect of variable (r) on calculating the mirco-T circuit elementary thickness Δr of each region. Since Δr is assumed constant for each region

and it has been calculated from its expression given by equation (2.64), where (r) of this expression is to be replaced by the geometric mean radius of the annular region considered.

Fig. (2.27) illustrates both the 9-region mathematical model and its corresponding equivalent network. The innermost and the outermost air-gap regions are replaced by three and four regions respectively. The innermost air-gap region no. 1 in the network, has been assumed as an annular region of an inner radius very nearly equal to zero ($r \simeq 0.0001$ mm), in order to eliminate the possibility of having an infinite result when dividing by this radius. The terminating impedance to this particular region is shown as a short circuit in the equivalent network. Computed results show no difference whether this impedance is open circuit or short circuit. Similarly, if the outermost air-gap region's outer diameter is taken to be large enough, in order to ensure a practically zero value for either the electric or the magnetic fields, the field distribution has been found invariant for either an open circuit or short circuit terminating impedances.

The conducting region has been repalced, in the equivalent circuit, by its four-terminal netwrok derived in section (2.13). However, the double macro-T circuits representing the E- and H-lines of this region are shown since this circuit is the one which permits the calculation of the distribution

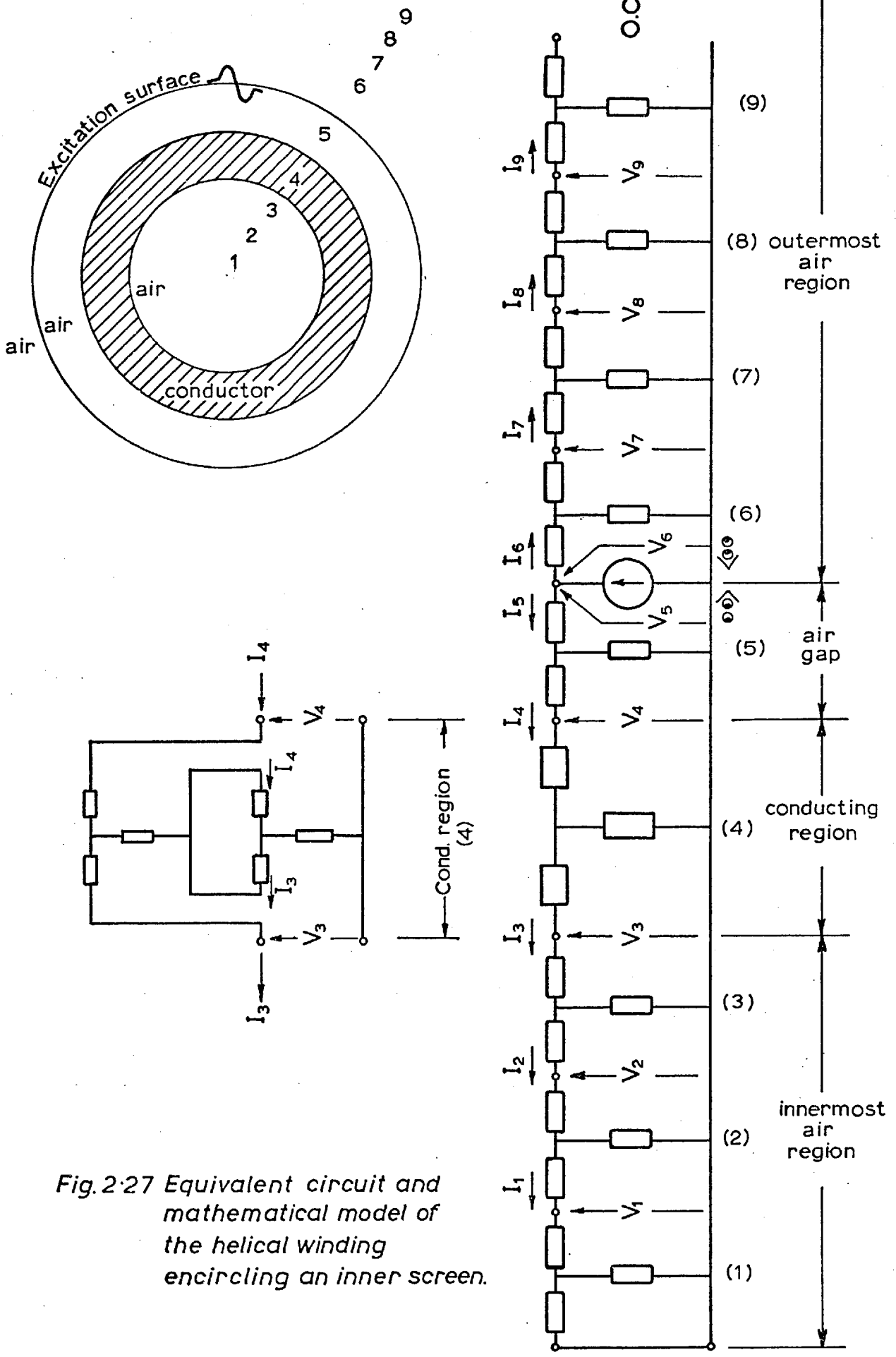


Fig. 2·27 Equivalent circuit and mathematical model of the helical winding encircling an inner screen.

of both the induced eddy currents and the magnetic field components inside the conducting region. A computer program has been written for calculating the distribution of the induced eddy currents in the conducting region as well as the distribution of the magnetic field components at any required region of the model. The method of calculation can be summarized in the following steps.

1. Calculate the elements of the equivalent marco-T circuit of each region, i.e. Z_A, Z_B and Z_C, as explained before in section (2.12).

2. Keeping in mind the shape of the equivalent network of Fig. (2.27), calculate the input impedances looking in the directions inward and outward from the excitation terminals. Let these impedances be designated by Z_{00} and Z_{00} respectively.

3. For a 1.0 p.u. excitation current source, calculate the voltages and currents at the excitation terminals, i.e. V_5, V_6 , I_5 and I_6, from the following relations:

$$\left.\begin{aligned} V_5 &= V_6 = (Z_{00} // Z_{00}) \cdot 1.0 \\ I_5 &= 1.0 \cdot Z_{00}/(Z_{00} + Z_{00}) \\ I_6 &= 1.0 \cdot Z_{00}/(Z_{00} + Z_{00}) \end{aligned}\right\} \quad (2.75)$$

4. The 'interface' voltages and currents can be obtained from the transfer matrices of the macro-T circuits of

the different regions, starting from the excitation terminals, where these voltage and currents are known. The transfer matrix of one macro-T circuit, which relates the output to the input quantities is given by:

$$\begin{bmatrix} V \\ I \end{bmatrix}_{\text{output}} = \begin{bmatrix} (1 + Z_B/Z_C) & Z_C - Z_A Z_B/Z_C \\ -1/Z_C & (1 + Z_A/Z_C) \end{bmatrix} \cdot \begin{bmatrix} V \\ I \end{bmatrix}_{\text{input}} \qquad (2.76)$$

5. <u>For an air-gap region</u>:

Knowing the terminal voltage and current at either end of the macro-T circuit of an air-gap region, the distribution of the voltage and current at any distance along the equivalent H-line of this region can be calculated as follows:

(i) Replace the region by a string of a suitable number of micro-T circuits in cascade.

(ii) Starting from the terminals where V and I are known, which are also the supply quantities of the first micro-T circuit, the voltage and current along these T-circuits can be calculated from its transfer matrices. The transfer matrix of each micro-T circuit is similar to that of equation (2.76) but with $Z_A = Z_B = Z_s/2$.

The far end terminal V and I can then be checked against the corresponding values obtained from step (4).

The distribution of the magnetic field components in this region can be obtained from equations (2.55).

6. For a conducting region

The distribution of $\bar{J}$ and $\bar{H}$ vectors inside the conducting region are obtained from equations (2.72), which are given in terms of the voltages and currents of the H-line and the transformed E-line. Each of these two lines is represented by its equivalent macro-T circuit. Once the voltage and current at one side of each macro-T circuit are known, the whole procedure of step (5) is to be repeated for the appropriate micro-T circuit. The input and output currents of each of the two macro-T circuits of the conducting region are known, hence the input voltage of each circuit can be obtained from the relation:

$$V_{in} = I_{in}(Z_A + Z_C) - I_{out} Z_C$$

Where the suffices (in) and (out) stand for the input and output respectively.

It should be noted that in both cases when the cascade connnection of a large number of micro-T circuits is replaced by one macro-T circuit, or when the distribution of the voltage and current along the length or a lumped transmission line is required, the following assumption has been adopted throughout the computer program:

The elements of any one micro-T circuit, which represent the basic unit in constructing the T.L., are calculated for a constant radius (r) equal to the mean radius of this particular micro-T circuit.

2.14.4 Test results and computer calculations

The three-phase helical winding was supplied from a balanced three-phase, variable frequency, a.c. generator. The flux density distribution along the axial direction and in the radial direction has been measured using search coils as described above. The tests were done for three different configurations.

i) An air-cored helical winding, where the flux density distribution both inside and outside the winding was measured. The experimental as well as the computed results are shown in Figs. (2.28 a, b and c).

ii) The helical winding encircles an aluminium tube whose inner and outer radii are 1.9 cm and 3.8 cm respectively. The experimental and the computed results are shown in Figs. (2.29 a. b.and c) for a supply frequency of 50 Hz.

iii) The helical winding is enclosed by an aluminium tube whose inner and outer radii are 6.64 cm and 7.75 cm

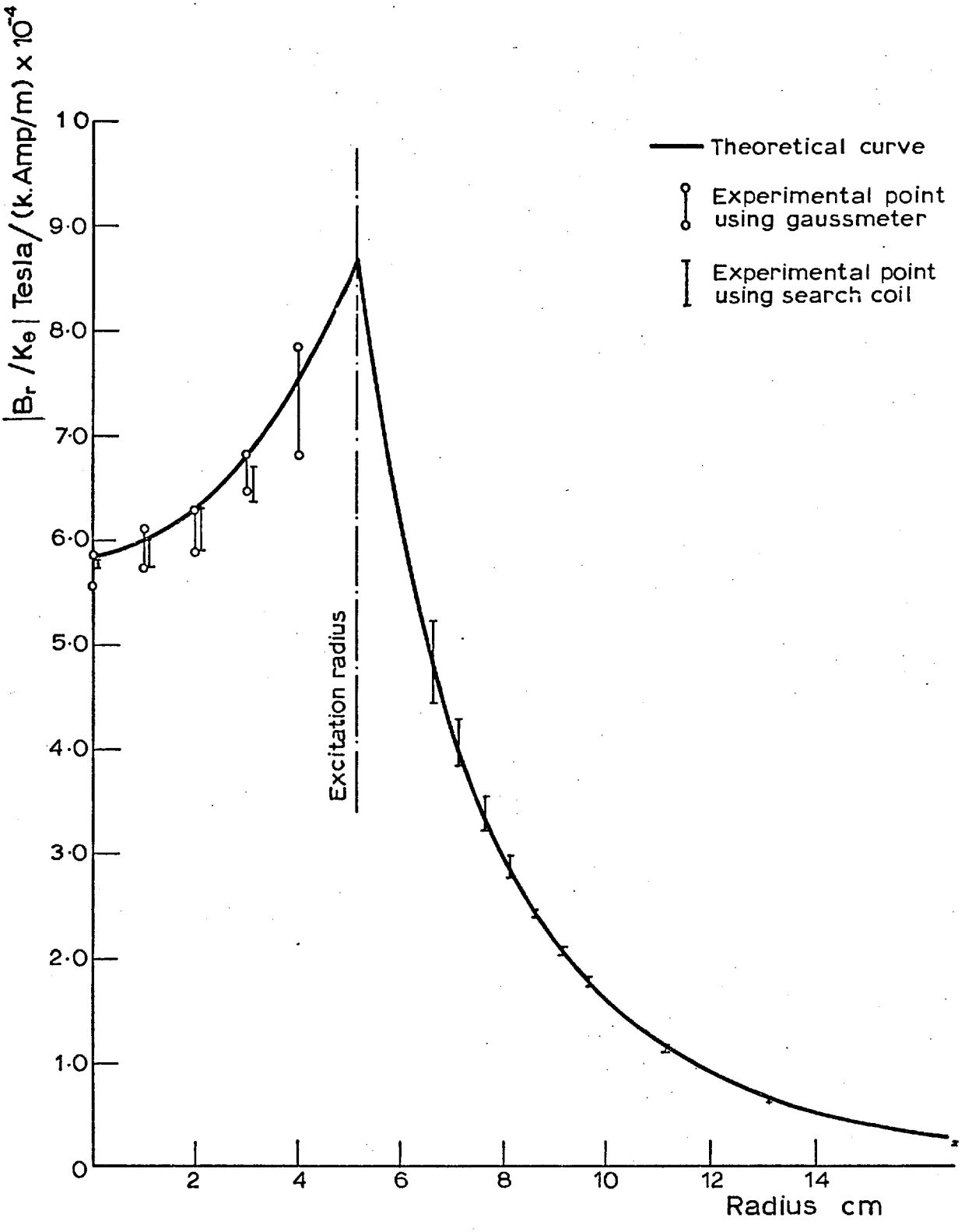


Fig. 2·28a Radial distribution of the flux density radial component of an air-cored helical winding.

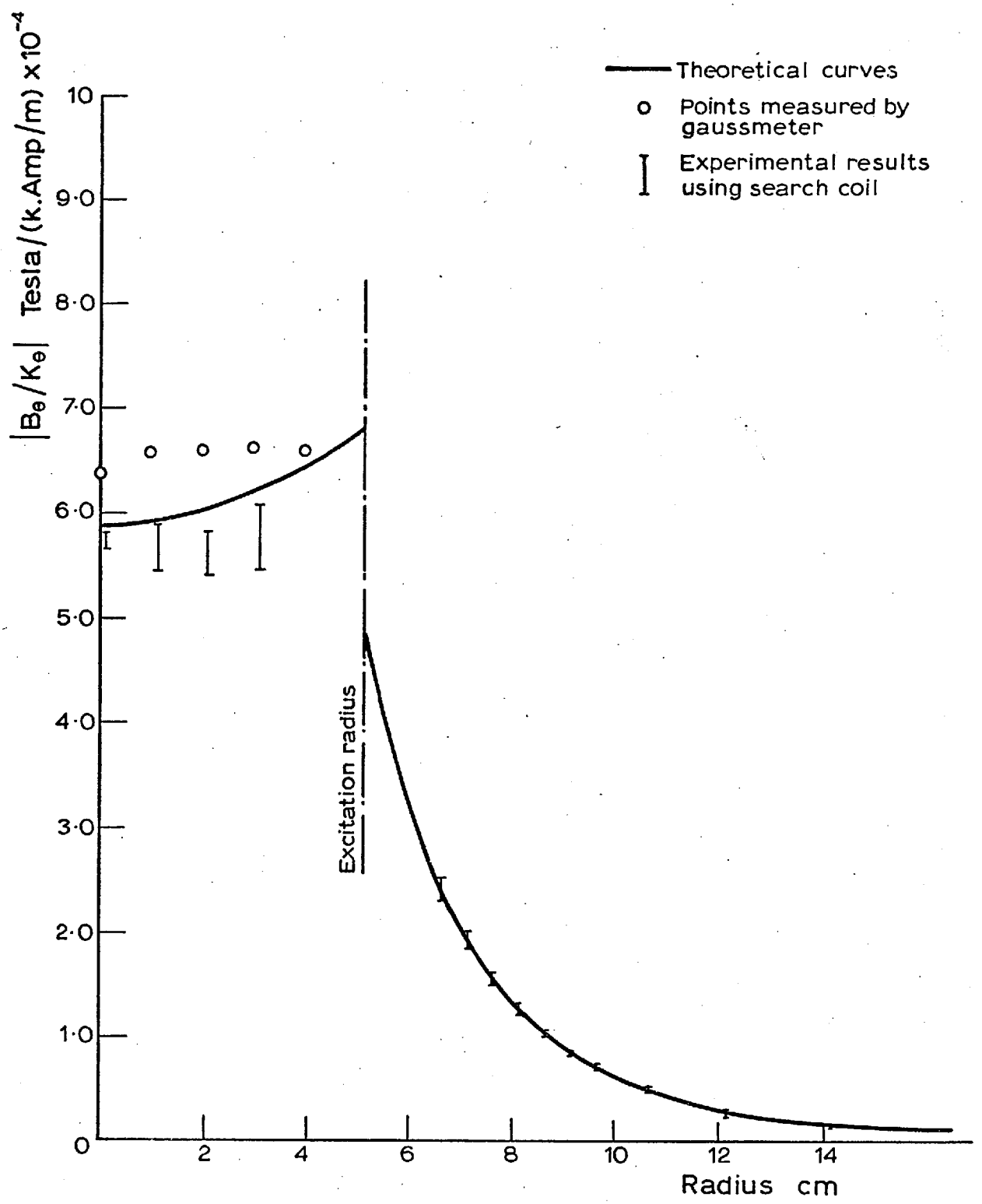


Fig. 2·28b Radial distribution of the flux density circumferential component of an air-cored helical winding.

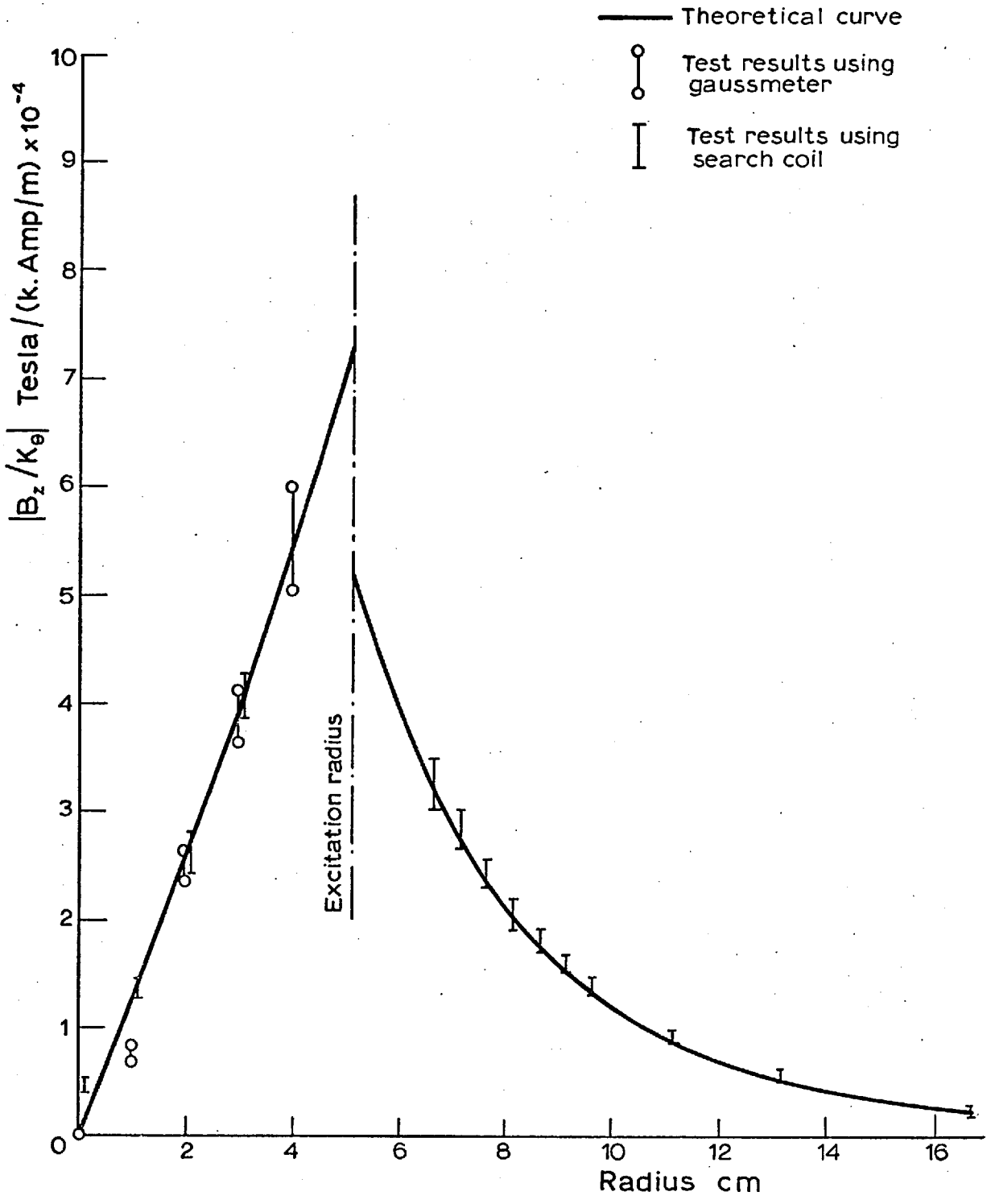


Fig.2·28c Radial distribution of the flux density axial component of an air-cored helical winding.

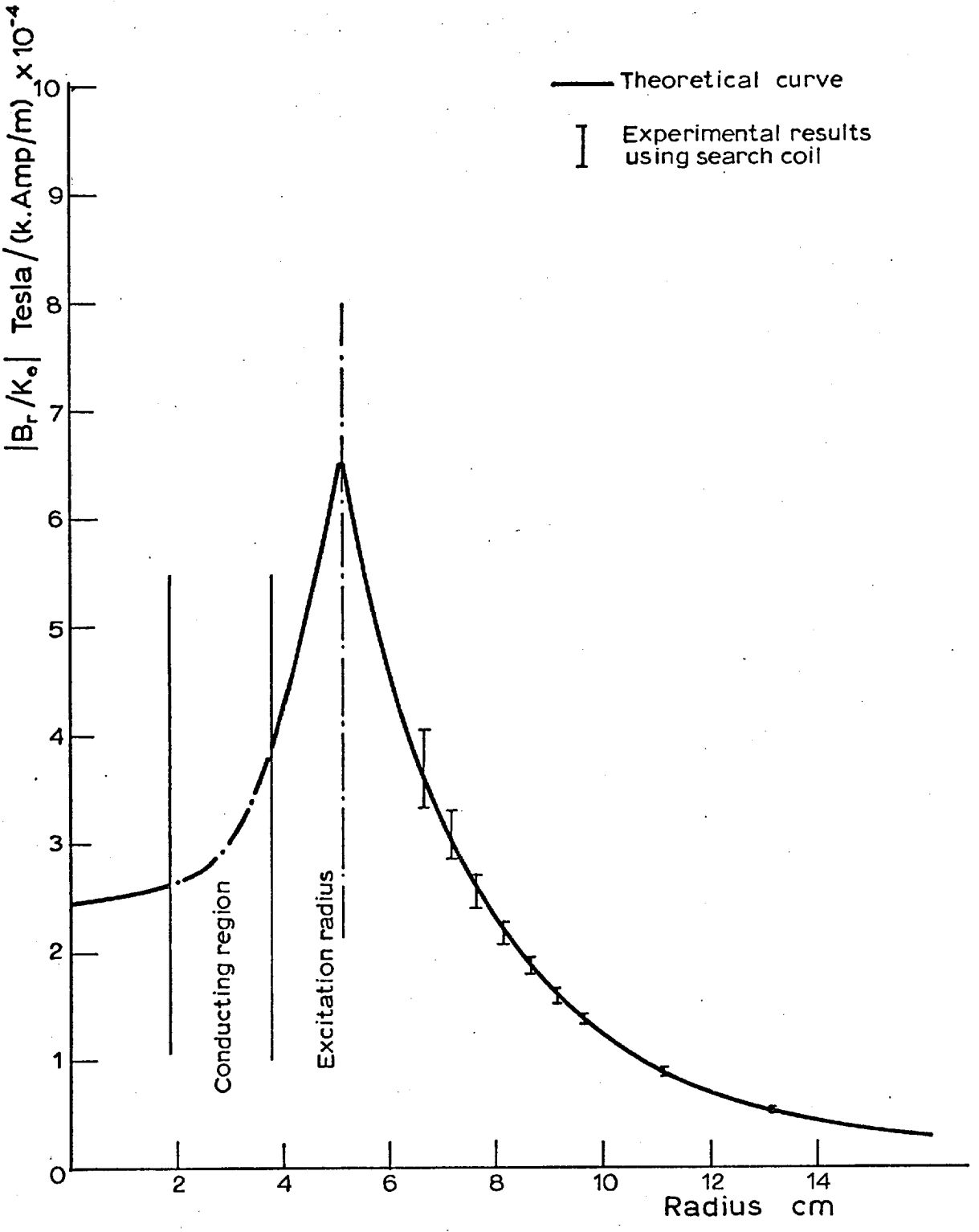


Fig. 2·29a Radial distribution of the flux density radial component of a helical winding encircling conducting tube.

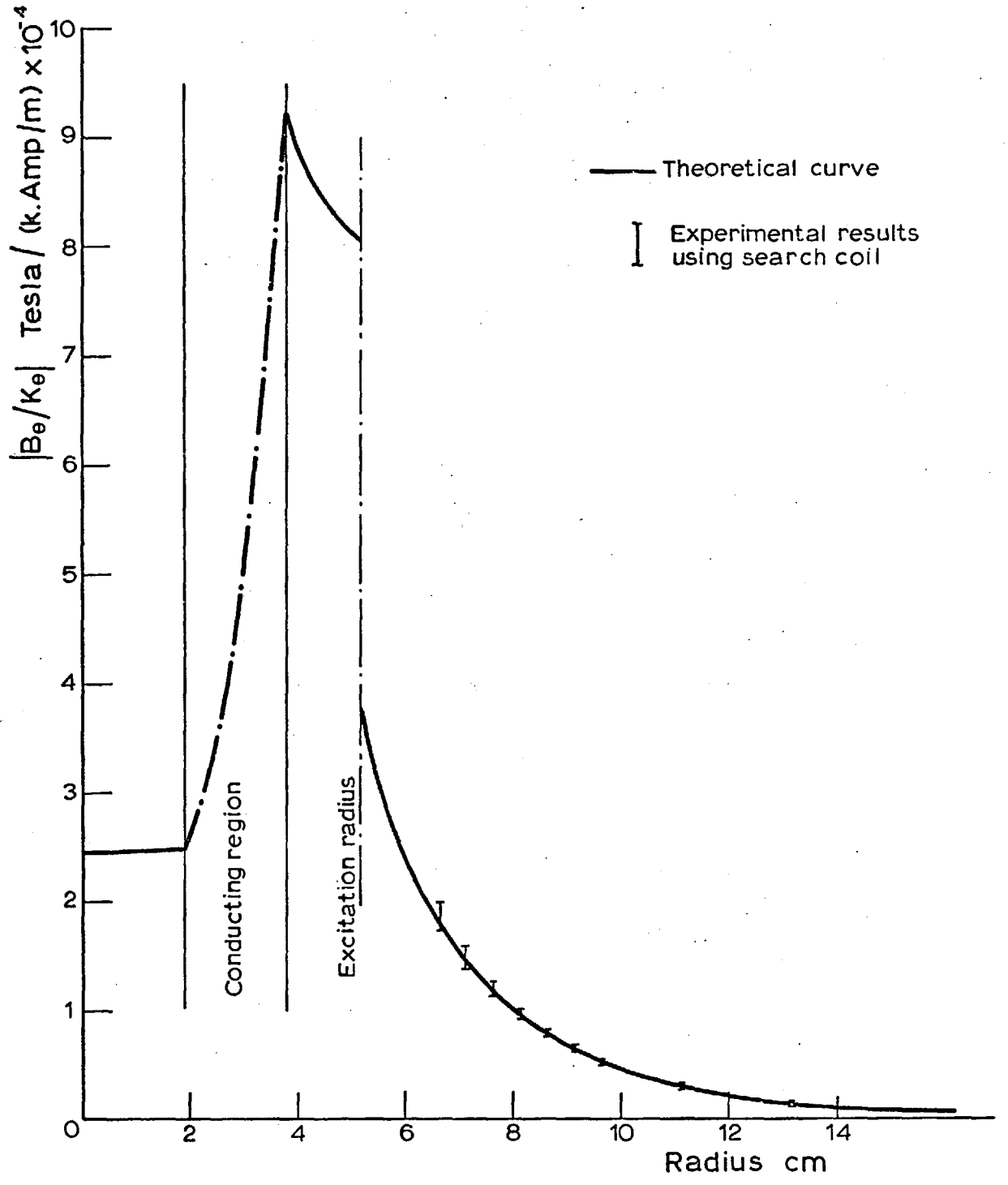


Fig. 2·29b Radial distribution of the flux density circumferential component of a helical winding encircling conducting tube.

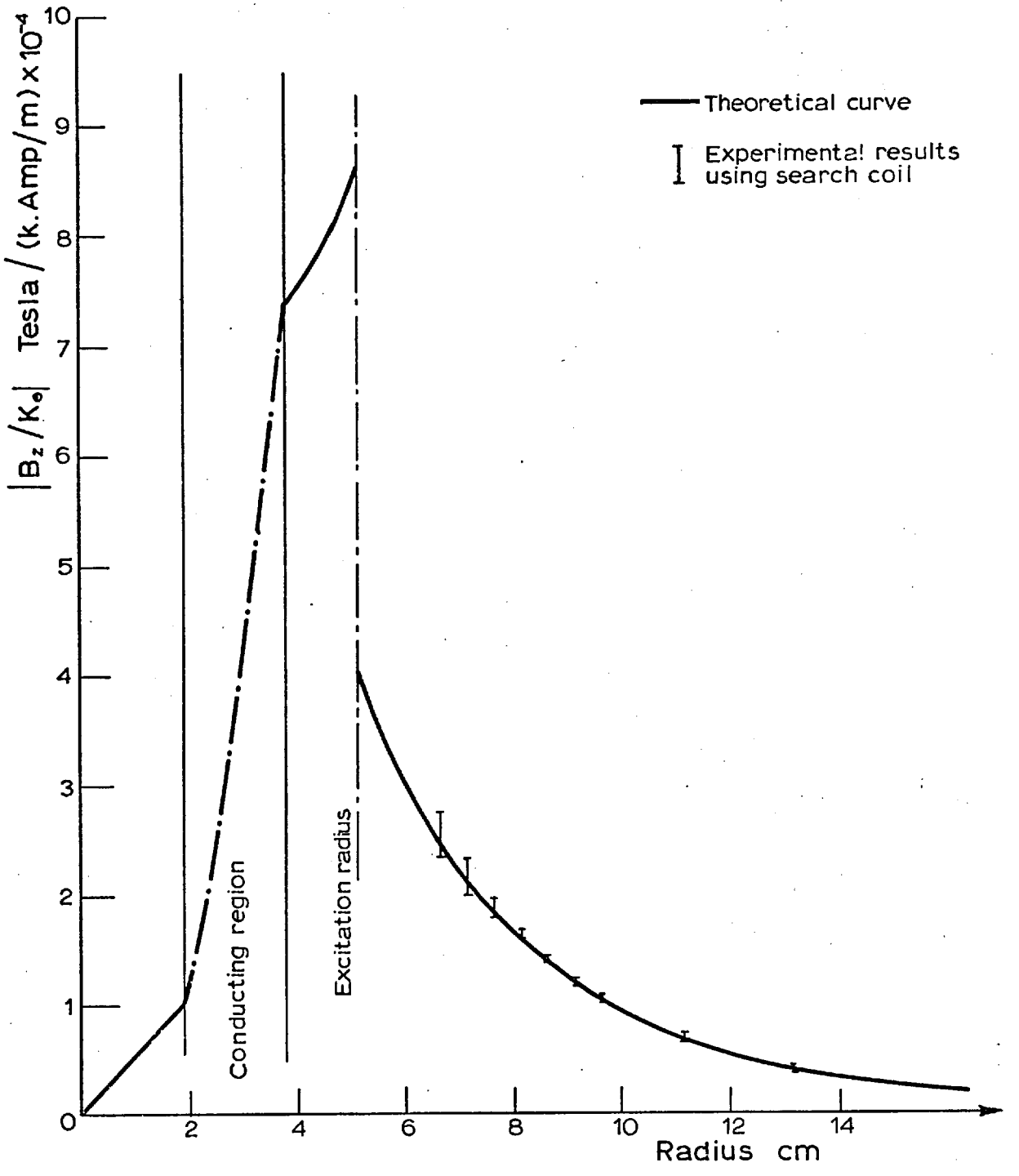


Fig. 2·29c Radial distribution of the flux density axial component of a helical winding encircling conducting tube.

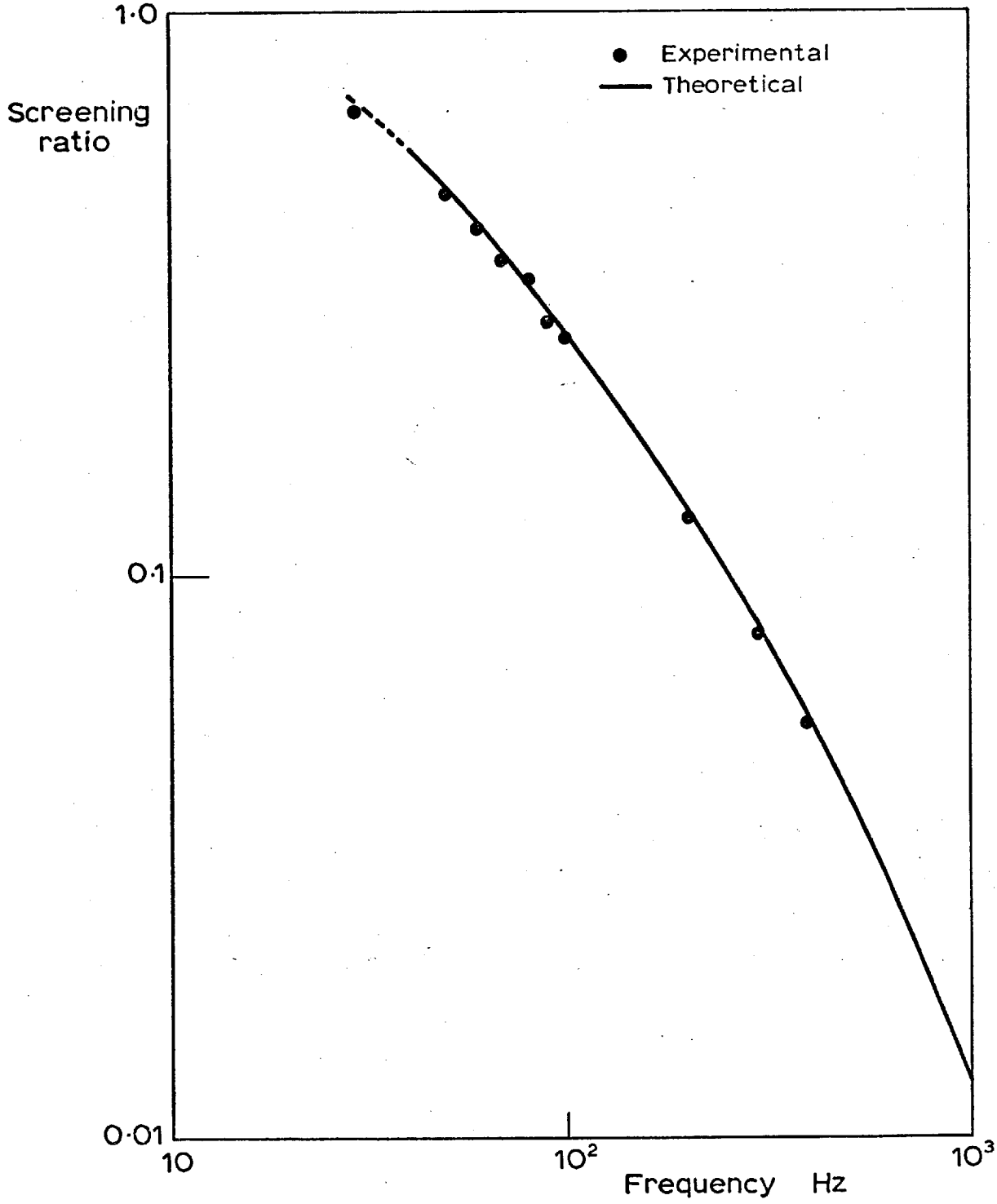


Fig. 2·30 Screening ratio of helical winding enclosed by a conducting screen.

respectively. The screening ratio for different supply frequencies was measured and calculated, and both sets of results are plotted in Fig. (2.30).

Comparison between the theoretical and experimental results for all tests show that, the difference between the computed flux density components and the average value of the measured results does not exceed 3% for all points outside the helical winding. On the other hand, for the points inside the helical winding, this max. difference becomes about 5% for the axial and radial flux components and reaches 7.5% for the circumferential component. The larger difference between the theoretical and experimental results occurs inside the helical winding, and it is believed that this happens because this region is characterised by small radii, consequently any slight angular displacement in positioning the search coil will be responsible for introducing this error. As we go outside the winding, the angular position of the search coils is not so critical, hence less difference between experimental and theoretical results is observed.

The good agreement between the experimental results and the theoretical results computed from the double transmission line equivalent circuit emphasizes the effectiveness of the theoretical mathematical model, and its associated equivalent circuit, in describing practical models.

The radial distribution of the induced eddy current in the conducting region has been calculated from the T.L. network according to equations (2.72a). In order to have a feel for the relative magnitude of the induced current components, the ratios J_r/J_θ and J_z/J_θ have been plotted in Figs. (2.31 and 2.32) for different cases. For example, in Fig. (2.31) the current ratios are plotted for a conducting tube encircled by a 3-phase helical winding having an angle of 45°. The excitation and the outer radii of the conducting tube are kept constant at 5.14 and 5.00 cms respectively, while different values of the inner radius of the conducting tube are considered. For a small values of inner radius, the radial component of the induced eddy current can be as much as 35% of the other two components. In order to examine the effect of the tube inner radius on the induced eddy current radial distribution, different tubes having different inner radii, but the same wall thickness, are considered. The current ratio curves are plotted in Fig. (2.32) for three different cases where the inner radius was 2, 5 and 15 cms. The excitation radius for each case has been taken equal to the inner radius of the corresponding tube. Again, Fig. (2.32) clearly demonstrates that the induced radial current has an appreciable value for small radii. As the radius increases, the curvature decreases and so the radial current decreases. Theoretically as $r \to \infty$, the induced radial current will approach zero.

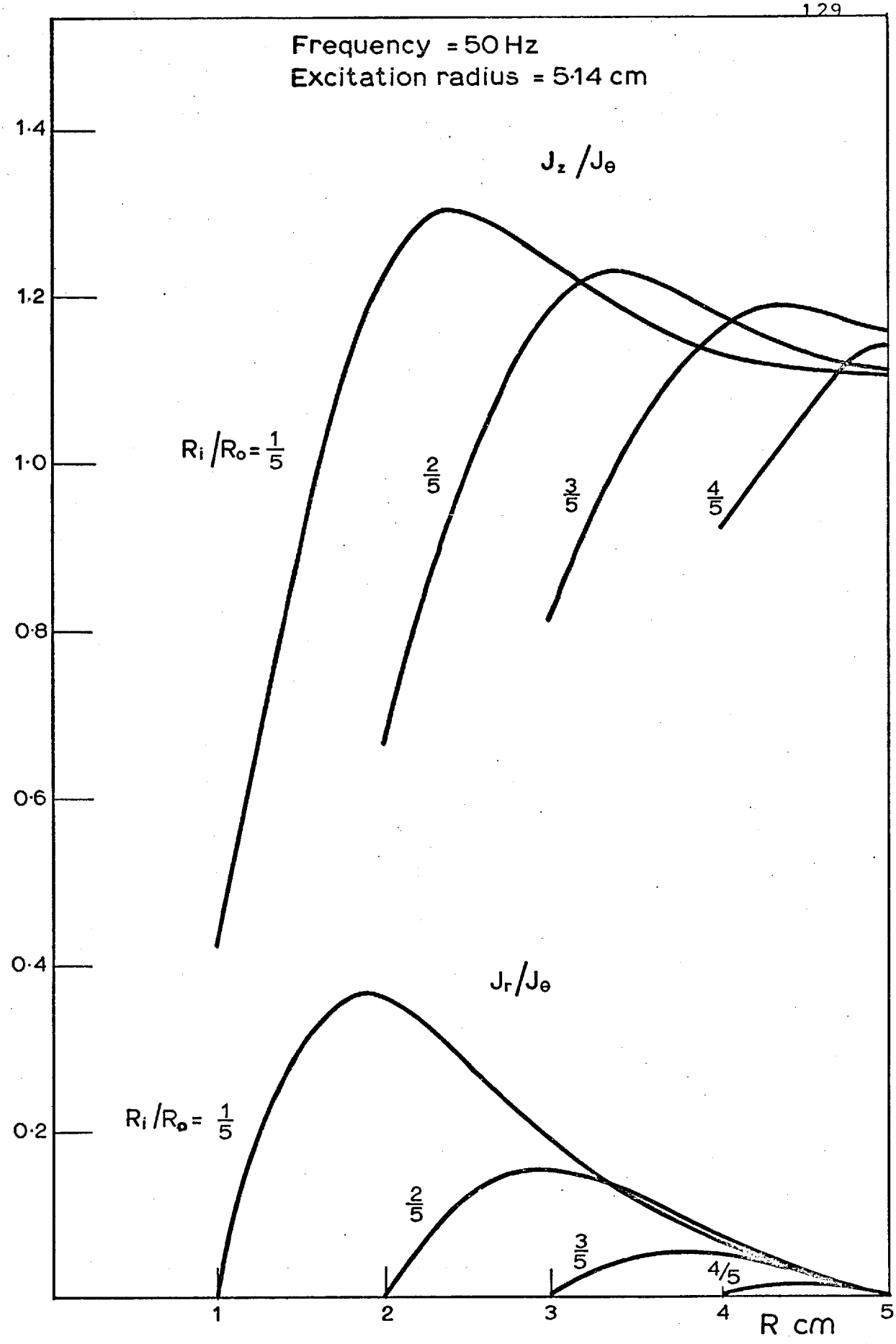
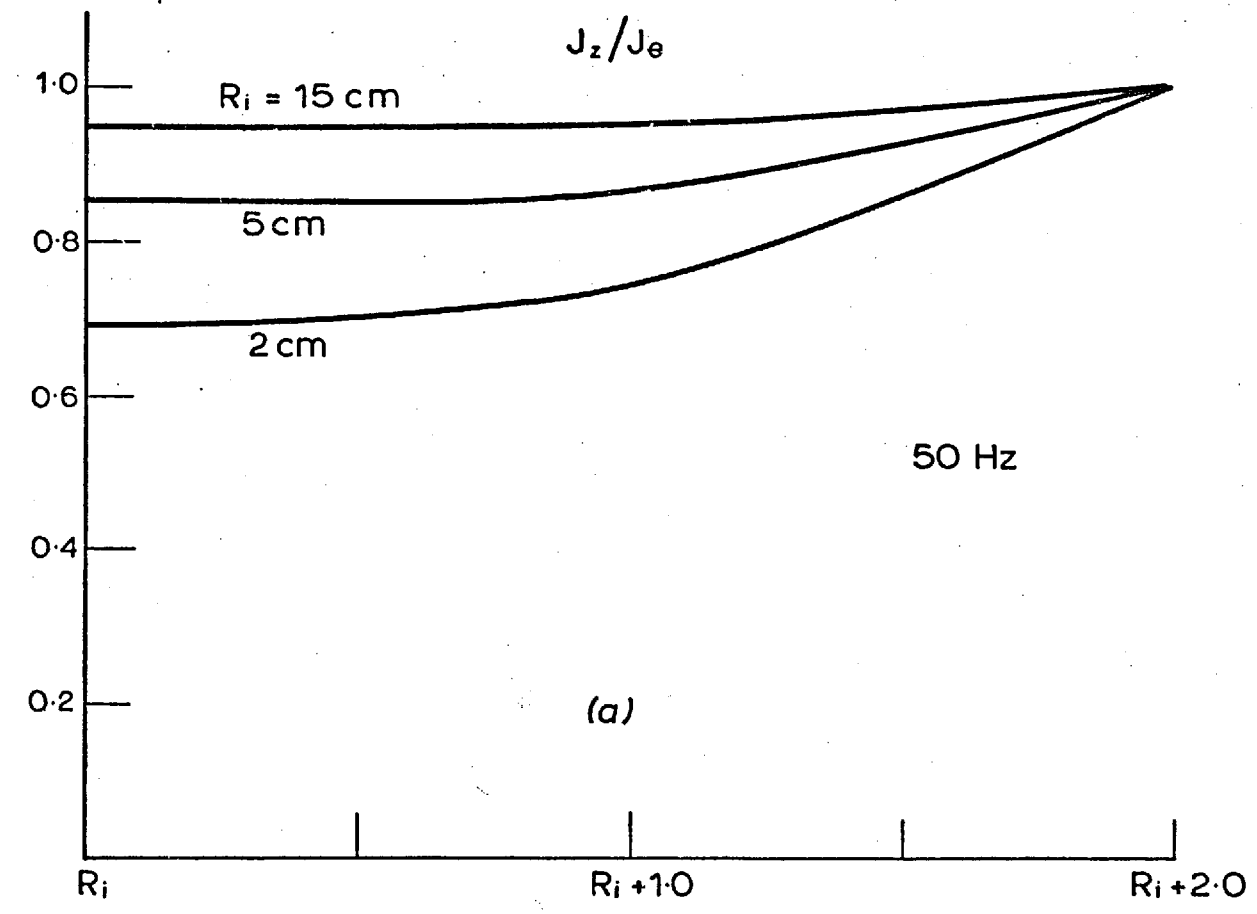


Fig. 2·31 Current ratio radial distribution in conducting cylinders encircled by a helical winding.



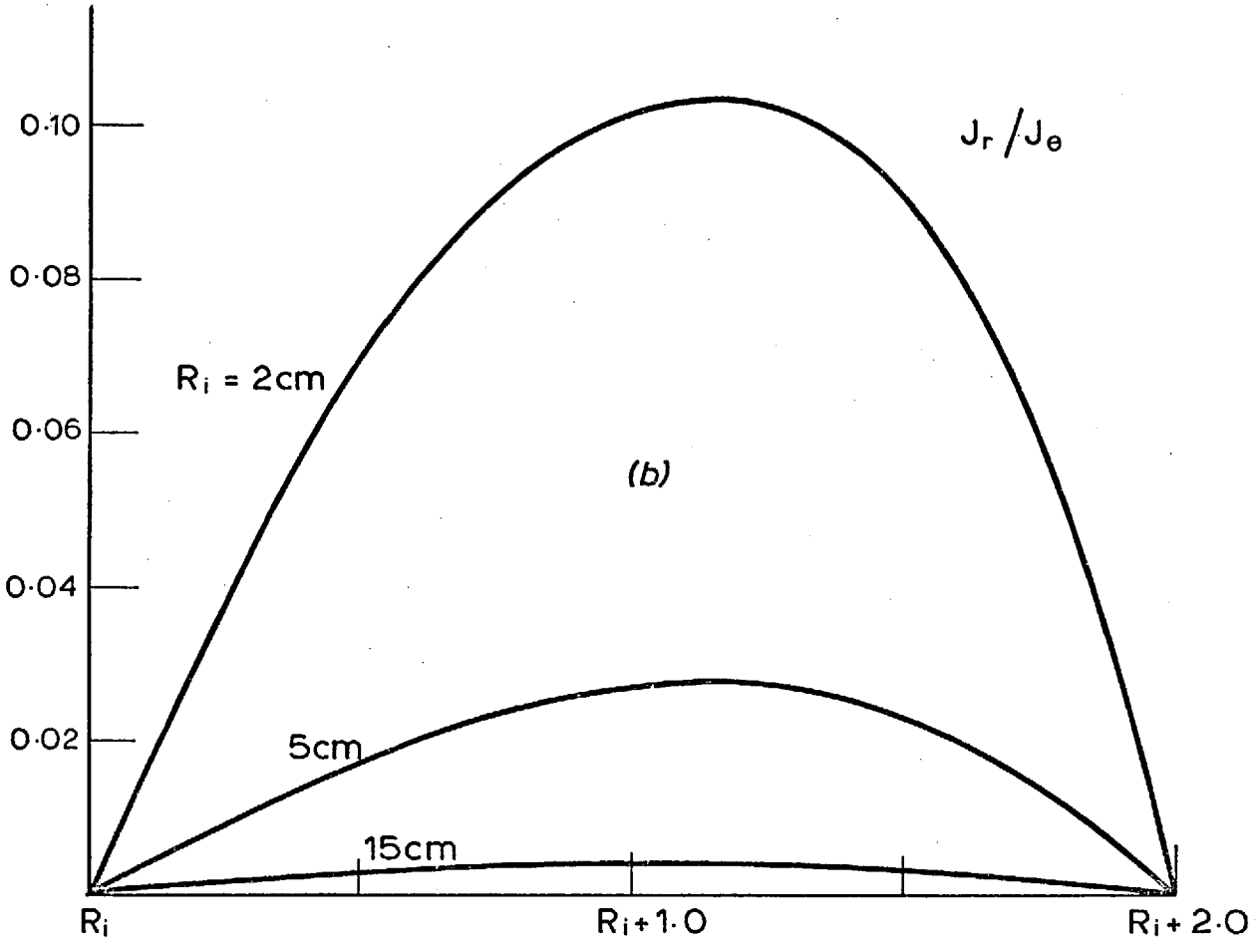


Fig. 2·32 Effect of curvature on the induced radial current density distribution. (a) J_z/J_θ (b) J_r/J_θ

2.15 Conclusions

A general theory for solving the electromagnetic field, which is in general three dimensional, has been developed for a class of induction devices which have an infinitely long, multiregion, circular-cylindrical structure, excited by two-dimensional current sheets. An equivalent circuit, which consists of double transmission lines, has been found to describe the electromagnetic behaviour of this model. These transmission lines are found to be mutually coupled, at their terminals, through complex turns ratio ideal transformers in order to satisfy the electromagnetic boundary conditions at the interfaces between different regions. Some special cases, which arise in machines problems, have been studied and simplified forms of transmission lines couplings have been obtained.

The concept of replacing a continuous transmission line by a large number of elementary circuits has been adopted, in order to eliminate the need for using any form of Bessel function, and the configuration of the so-called 'micro-T' circuits is deduced for each one of the two transmission lines. For the sake of generality, the displacement current has not been ignored, and its effect was found to be represented by capacitor elements in the equivalent circuit.

Close investigation for the special case of conducting and non-conducting regions show that, for the low (power) frequency applications, the 'magnetic' field components at

any point in a non-conducting region, can be fully described in terms of only 'one' of the two transmission lines, while the other is left open circuit. However, if the 'electric' field components are required to be known, this open circuit line can be replaced by another 'transformed' line whose flow quantity (i.e. current) is some function of the limiting value of the ratio between the curl of $\bar{H}$ vector and the permittivity as $\varepsilon \to 0$.

For the special case when the conducting region is bounded by two non-conducting regions, it has been found that the equivalent double transmission lines can be reduced to one four-terminal network.

An experimental model has been tested, the two-dimensional current sheet has been provided by a three-phase helical winding. A very good agreement has been obtained between the experimental and theoretically calculated flux density radial distribution curves.

It has been found that the equivalent networks already derived in the literature for either circumferential or axial excitation current sheets situations are special cases of the general network obtained in this chapter. Throughout the analysis, it has been assumed that both the electric and magnetic field posses three components, and none was assumed zero. As a result, the currents induced in any conducting

region, was found to be three dimensional, although the exciting current has only two components, a fact, to the author's belief, that has not been appreciated before this study.

The effect of motion has not been discussed in detail in this chapter. However, the network model developed can represent this effect by replacing the frequency (ω) by its value as measured in a reference frame fixed in the conducting regions. This is true provided that there is no relative motion between the different conducting regions of the mathematical model.

It is believed that this study is quite general, for the form of excitation function assumed in the early begining , and it may highlight some new concepts in solving electrical machine problems.

Chapter 3

Three-dimensional electromagnetic field analysis of a multilayer planar model excited by a two dimensional surface current sheet

3.1 Introduction

In chapter 2, the field solution has been obtained for a multiregion cylindrical structure excited by a 2-D current sheet. The double T.L. model developed has been obtained under the restriction that there is no relative motion between different conducting regions whether they are in electrical contact or not. However, the effect of motion under this restriction can be introduced by substituting for the angular frequency ω by the slip frequency $s\omega$. That is the field solution will be referred to a reference frame which is stationary w.r.t. all the conducting regions.

In this chapter, the problem will be taken a step further. A multi-layer planar model will be considered. Each conducting layer can have a different velocity. To have a completely general model, the assumption of zero 'normal current density' at the interfaces of the layers will not be adopted. Thus the model can represent the general case of two adjacent conducting regions travelling at different speeds.

Practically, this multilayer planar model can be used to represent all the cylindrical model applicatons discussed in chapter 2 if the effect of curvature is to be neglected. Perhaps, the most important field of application is the linear induction devices, and in particular the 'linear induction motor'. A brief survey of this subject may be considered as a useful literature review for the mathematical model which will be considered in this chapter.

3.2 Linear Induction Motor - Historical Review

Since the invention of the induction motor in 1888 by Nikola Tesla[3.1] in U.S., the research and development were mainly directed towards the rotary induction motor. The story of its evolution, whereby a 100 hp motor of today occupies the same space as a 7.5 hp machine in 1897, is a remarkable example of engineering advancement.

Little concern, or almost negligence, had been paid to the linear version of the induction motor. The early traces of a linear induction machine (LIM) may go back to 1895[3.2] when the idea of propelling the shuttle of waeving looms by a contact free electrical or mechanical means was considered. Some, but rather isolated, attempts had been considered to utilize the linear induction motor in different applications. Among these applications was its

use as a propulsion unit in a transportation system[3.3-3.8]. The most important event of all was the use of LIM as an aircraft launcher known as the 'Electropult' in the late 1940's.

Starting in the mid 1940's, Laithwaite built his first linear induction motor by 1948, mostly during his lunch hours[3.10], in order to test the feasibility of using linear motors to drive the shuttles of weaving machines. He then started a series of publications in 1955[3.11-3.18] reviving the interest of using the linear induction machines in many applications and in particular for high speed ground transportation.

Since then, many different research institutions in the U.S., Japan, Germany, France and U.K. started an extensive study of LIMs. The research includes theoretical studies, constructing experimental test rigs and even full size vehicles propelled by linear induction machines[3.19].

The linear induction machine, as an electromagnetic problem is, no doubt, more complex than its rotary version. This is generally due to its larger air-gap and its open magnetic circuit. However, the treatment of this problem has been tackled by many authors at different levels of complexity.

The early theoretical treatments of the LIM as a field problem made much use of the publication in the area of Magnetohydrodynamic (MDH) induction machines, mainly due to Russian authors, used as pumps for transferring liquid metals. This MHD machines involved liquid metal, rather than solid, secondaries and hence the problem is basically an interconnection between an electromagnetic process and a hydraulic phenomenon. However, the concurrent solution of the electromagnetic field and the hydrodynamic equations is not an easy task. Therefore, in practice the two phenomena were examined separately. In the electromagnetic side of the problem, the liquid metal is regarded as a 'solid body' which moves at a velocity equal to the average speed of the liquid[3.20].

The schematic diagram of the linear induction motor (known as the longitudinal flux LIM to differentiate it from the lately invented transverse flux linear motor[3.21]) is shown below in Fig. (3.1).

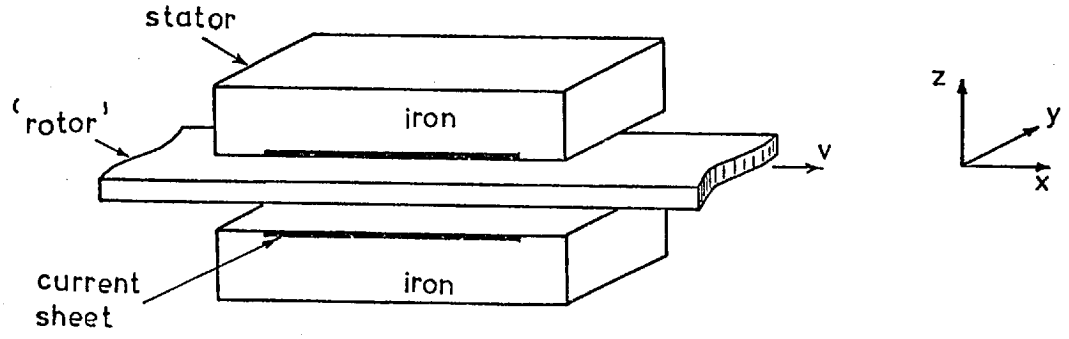


Fig.(3.1) Schematic diagram of LIM.

Each specific region of the physical model has a finite thickness, width and length, except the secondary region which is usually assumed to be an infinitely long region. The scientific literature is rich in a wide variety of different methods of analysing these special induction devices. A principal difficulty in the analysis is due to the edge effects. These edge effects arise from two sources: the discontinuous nature of the excitation primary current and the discontinuous ferromagnetic stator (primary) structure.

A comprehensive review of all the published literature in the field of linear induction motor analysis is beyond the capacity of a single chapter. However, the salient analytical methods are briefly listed in the next few sections.

3.3 One-Dimensional Analysis

Only 'one' finite dimension effect is considered at a time.

3.3.1 Finite thickness model

In which the excitation current sheet has only a y-component. The mathematical model extends to infinity in both the x- and y- directions, i.e. the discontinuity

of the magnetic circuit and the excitation function in the longitudinal and transverse directions is neglected. The analysis of this model is very similar to the analysis of rotary induction machines when the effect of curvature is neglected. Typical examples are the analysis reported by Blake[3.22], Blachford[3.23], West and Hesmondhalgh[3.24], Verze and Ulmanis[3.25], Nonaka and Yoshida [3.26, 3.27], Ooi and White[3.28], Wang[3.29] and Freeman[3.30]. Freeman's analysis is the most generalised of the treatments. He solved the problem for any number of multilayer planar regions. Slotting effects can be approximately introduced by considering both electrically and magnetically anisotropic layers. The allowance for finite thickness helps in calculating the air-gap flux density x- and z- components, hence,'normal forces' in a single sided LIM can be automatically calculated from the Maxwell stress tensor.

3.3.2 Finite width model

The machine is assumed to be infinitely long. The air-gap leakage flux is negelcted, i.e. the flux density crosses the air-gap normally (z-component only) with constant magnitude. The skin effect in the secondary sheet is neglected and both primary and secondary currents are replaced by equivalent, infinitesimally thin, current sheets. Russell and Norsworthy[3.31] considered this model to analyse screened rotor induction motors. The air-gap

is usually very small in these machines, hence they assumed that the flux density is uniform across the machine width. Bolton[3.32] assumed this model to study the transverse edge effect in LIMs. He allowed flux density variation in the x-direction. To simulate the finite iron width, Bolton assumed that the magnetic field is absent outside the iron edges.

3.3.3 Finite length model

In this model, the finite length effect is considered only. The machine is assumed infinitely wide in the transverse direction, and the flux is assumed to cross the air-gap normally. The primary and secondary currents are replaced by one-dimensional current sheets. Yamamura et al[3.33] solved the problem as if there were no edge effects, then they introduced the finite length effect by applying the boundary condition: " the integration of the flux density along the machine length is zero ". Effectively, in their solution, no allowance has been made for the fringe edges. However, their solution gives an explanation in a very simple way, of the phenomenon of having forces at the synchronous speed. Ooi[3.34] introduced the effect of iron saliency in the longitudinal direction in a rather different way. He used a similar model but assumed the air-gap permeance to be space dependent or, equivalently a space dependent permeability $\mu(x)$.

Alwash and Eastham[3.35] modelled the finite iron length in this type of one-dimensional analysis, by introducing the concept of a stepped air-gap. The air-gap of the machine is suddenly enlarged outside the stator iron. This effect is introduced mathematically by representing the air-gap permeance by a Fourier series. It should be noted that this method, which could be referred to as the permeance-harmonic approach, requires the assumption that the flux crosses the air-gap normally.

3.4 Two-Dimensional Analysis

In this analysis, two effects are considered at the same time. This analysis can be divided into two main methods according to whether the finite iron extension in the longitudinal direction is introduced or not.

3.4.1 Finite excitation models

In which the primary excitation current discontinuity is taken into consideration, while the stator iron discontinuity is neglected. Again, these models can be sub-divided into three groups according to which two (out of the three) finite effects are going to be considered, as follows:

(i) Finite thickness and width model

The mathematical model assumes a large number of infinitely long machines laid parallel to each other which

are excited with alternate polarity. The actual discontinuity in the material, in the transverse direction, is ignored and the hypothetical assumption of this array of the machines permits the representation of the excitation two-dimensional current sheet by a Fourier series in the transverse direction. A typical analysis of this model is due to Preston and Reece[3.36]. Similar models were considered by Wood and Concordia[3.37], Angst[3.38], Okhremenko[3.39 - 3.41], Veske[3.42], Parts[3.43] and Vilnitis[3.44]. Freeman and Lowther[3.45, 3.46], in order to generalise this treatment, considered a multilayer version of this model and gave the solution in terms of surface wave impedances. Alden and Nolan[3.47], independently, considered the same multilayer model but they formulated the solution in a transfer matrix form. It is worth mentioning that Lowther[3.48] formulated his multilayer solution in transfer matrix form but he did not publish it.

(ii) Finite thickness and length model

The mathematical model assumes that the material extends to infinity in the x-y plane, while the air-gap region and the secondary conductors each possess a finite thickness. The current sheet is one dimensional having an x-directed component only and there is no variation w.r.t. y. However, the finite distribution of the excitation current along the x-direction is considered. The solution of this field problem is formulated in terms of a Fourier transform. Typical examples are the analysis of Sudan[3.49],

Valdmanis[3.50], Yamamura et al[3.51, 3.52]. The analysis determines the solution of the field components in the Fourier space, then using the residue theorem, the field components can be recovered by an inverse transform process. However, Iwamoto and Yamamura[3.53] show that, for the force and input power calculation, the transformed magnetic field and exciting current components can be used directly without doing the inverse transform process. The problem reduces to merely a simple numerical integration process. Engelen and Peschka[3.54] pointed out that this mathematical model could be tackled either by Fourier transform (as indicated in the above references) or by two-sided Laplace transform. They used the latter mathod in their analysis arguing that it offers the advantage of representing a complex analytical function in the image space. Moreover, it is possible to obtain the characteristics of the machine in the image space, which implies a large simplification of the mathematical treatment. It is interesting to note that, Engelen and Peschka gave the primary current locus, for constant supply voltage, for different values of slip.

Nonaka and Yoshida[3.55] solved a similar mathematical model. They replaced the primary current sheet by a Fourier series, rather than a Fourier integral, taking the finite excitation extension into consideration. Effectively their model is equivalent to an infinite repetition of machines along the longitudinal direction (x). These machines are infinitely wide in the transverse direction (y).

(iii) Finite length and width model

Schieber[3.56], in order to study the finite length and width of LIMs considered an idealised model of an infinitely long, infinitesimally thin conducting sheet having a finite width and moving with a constant speed in the air-gap of a finite width and length electromagnet. He introduced the discontinuity of primary iron by assuming that the primary currents produce a primary magnetic field which has a constant value under the area covered by the stator iron, and zero value outside this region. Mathematically he represented this primary field by a superposition of continuous wavenumbers in the longitudinal direction and discrete odd wavenumbers in the transverse direction. In fact this is equivalent to the assumption of an infinite repetition of machines in the transverse direction, while in the longitudinal direction only one isolated machine with finite excitation length is assumed.

Schieber solved this electromagnetic field problem using the 'Fitzgerald vector superpotential' which has the advantage of being unidirectional (in the z-direction in this case) for the considered case of planar current flow.

3.4.2 Finite excitation and finite stator iron length model

The methods developed to study both the finite length and thickness effects assume an infinite length of the stator

iron. This is a common assumption usually made for reasons of mathematical simplicity. While it may be expected that this assumption is not too serious near the entry end of the motor, it might be expected that substantial effects occur at the exit end where rotor currents are carried out of the stator.

Dukowicz[3.57], in order to simulate the finite iron length, postulated appropriate two current sheets located ahead of the entry edge and behind the exit edge respectively. The approach to solve this field problem is based on a Fourier transform technique.

3.5 'Three'Dimensional Analysis

There is no doubt that the increasing interest in the linear machine as one of the possible means for high speed ground transportation has clearly demanded more rigorous design techniques and in particular the necessary mathematical tools of analysis with which design can be more effectively carried out. Since the power consumption of such high-speed trains at speeds of 400 to 500 Kph is approximately 10 to 20 MVA, a three-dimensional analysis of such motors is of great practical importance. This analysis can be divided into different methods according to whether the finite iron length is taken into consideration or not.

Note:

Strictly speaking, a '3-D' analysis should allow for the finite length and width of both the iron and the excitation current, as well as the finite width of the secondary sheet. Accordingly, the author supports the idea that a more proper classification of this section would be under the heading of '2½-D' rather than 3-D analysis. However, the heading has been quoted as 3-D analysis since it is widely accepted by many researchers in this field.

3.5.1 Finite excitation model

This model is usually referred to as Oberretl[3.58] model since he was the one who first published it. The model does not intorduce the iron discontinuity, and it consists of a two-dimensional matrix of excitation windings which lie in the xy-plane. Along the longitudinal direction (y) each exciting winding extends a distance which is equal to the primary length, and separated form the next winding with sufficient distance to ensure no mutual effect between fluxes of different machines. In the transverse direction, the excitation windings are infinitely repeated with alternative polarity. The two-dimensional excitation current sheet is then represented by a double Fourier series. Recently, Yamamura and Ito[3.59] derived a three-dimensional analysis of a slightly different model. Instead of having an infinite repetition of excitation winding along the

longitudinal direction, they considered an isolated winding. But still the assumption of having an array of machines along the transverse direction has been adopted. Again they used a Fourier transform in the longitudinal direction, and Fourier series in the transverse direction and they took account of both the normal and tangential fluxes in the air-gap.

Williamson[3.60] considered a multi-layer version of the Oberretl model, and solved the field problem allowing for magnetic and conducting anisotropy for each layer. In deriving his solution, Williamson assumed the normal current, at the interfaces of each layer, to be zero. A reasonable assumption when there are no conducting regions in electrical contact.

3.5.2 Finite excitation and finite iron length model

In order to introduce the finite extension of the stator iron in the direction of motion, North[3.61] adapted and extended the Energy Storage/Lagrangian methods to account for both the excitation and ferromagnetic effects. The mathematical model assumed a two-dimensional excitation current sheet given in terms of double Fourier series.

The secondary induced space harmonic currents are

transformed, in a similar way to the so-called d-q transformations, and referred to a fixed stator frame of reference. Ordinarily, the orthogonal property of the space harmonic current distributions would prevent mutual coupling between the different harmonic rotor currents. However, North found that the presence of the iron discontinuity perturbs this orthogonality and this in turn results in extra terms in the force expression. He referred to these forces as created due to discontinuity in the ferromagnetic stator structure. It is worth mentioning that although North developed his treatment in a very general way, he applied it to the special case when the iron discontinuity is neglected. Before giving any assessment to the practicality of this analysis, it should be checked against the experimental results with the introduction of iron discontinuity.

3.6 Numerical Methods

The problem of solving for the magnetic field and calculating forces, power and efficiency of linear induction machines has been tackled numerically by many authors. For instance, Holley, Nasar and del Cid[3.62] presented a finite difference method for solving the fields in a double sided linear induction motor. The finite length effects of the primary iron were considered, however, the excitation currents were assumed one dimensional and in the transverse direction,

i.e. transverse edge effects were neglected. The iron core was assumed magnetically linear. Foggia, Sabonnadiere and Silvester[3.36] used the finite element method for solving for the vector potential of a single sided LIM. In their model, the speed term is introduced explicitly, and the magnetic non-linearity of iron is assumed. The finite length effect is considered, while the transverse edge effect is neglected.

Some other numerical methods are also found in the literature. For example, Elliot[3.64] devised what is known as the 'Mesh/Matrix method'. The idea behind this method is that the secondary is represented by a ladder mesh of individual conductors, hence the voltage equations for the mesh can be obtained. The magnetic field created by the winding (primary) and mesh (secondary) currents is calculated in terms of the unknown currents using the actual iron shape with slots. Then the matrix is inverted to obtain the currents, and the field and powers are determined from the currents. The finite length is introduced by extending the mesh far enough from the ends of the iron. The finite width, however, is introduced in a less accurate way by increasing the resistance of the side bars in the matrix equation and by the use of the Bolton correction factor.

More details about numerical methods and available computer programs for solving the field problem of linear induction devices may be found in reference (3.65).

3.7 Mathematical Model

The mathematical model consists of an arbitrary number of stratified regions (N) arranged in a form of multilayer planar structure as shown in Fig. (3.2). Each region is assumed homogeneous, isotropic and magnetically linear. σ_M, μ_M and s_M are respectively the conductivity, relative permeability and slip of a general region M. The whole structure is assumed infinitely long in both x and y directions (as defined in figure 3.2), i.e. this model neglects the finite iron extension. However, each region has a finite thickness in the z direction, except both the upper and lower boundary regions which are assumed to extend to infinity in the positive and negative z-directions. The excitation winding is modelled by an infinitesimally thin two-dimensional current sheet which has finite extension in both the x and y direction. The current sheet lies between any two layers.

Generally, the excitation current sheet can be expressed in terms of double 'complex' Fourier series in order to model its finite extension in the x and y direction. Mathematically, its components are given by:

$$\begin{Bmatrix} K_x \\ K_y \end{Bmatrix} = \sum_m \sum_n \begin{Bmatrix} \hat{K}_x \\ \hat{K}_y \end{Bmatrix}_{m,n} \exp\{j(\omega t - \beta_m x + \alpha_n y)\} \qquad (3.1)$$

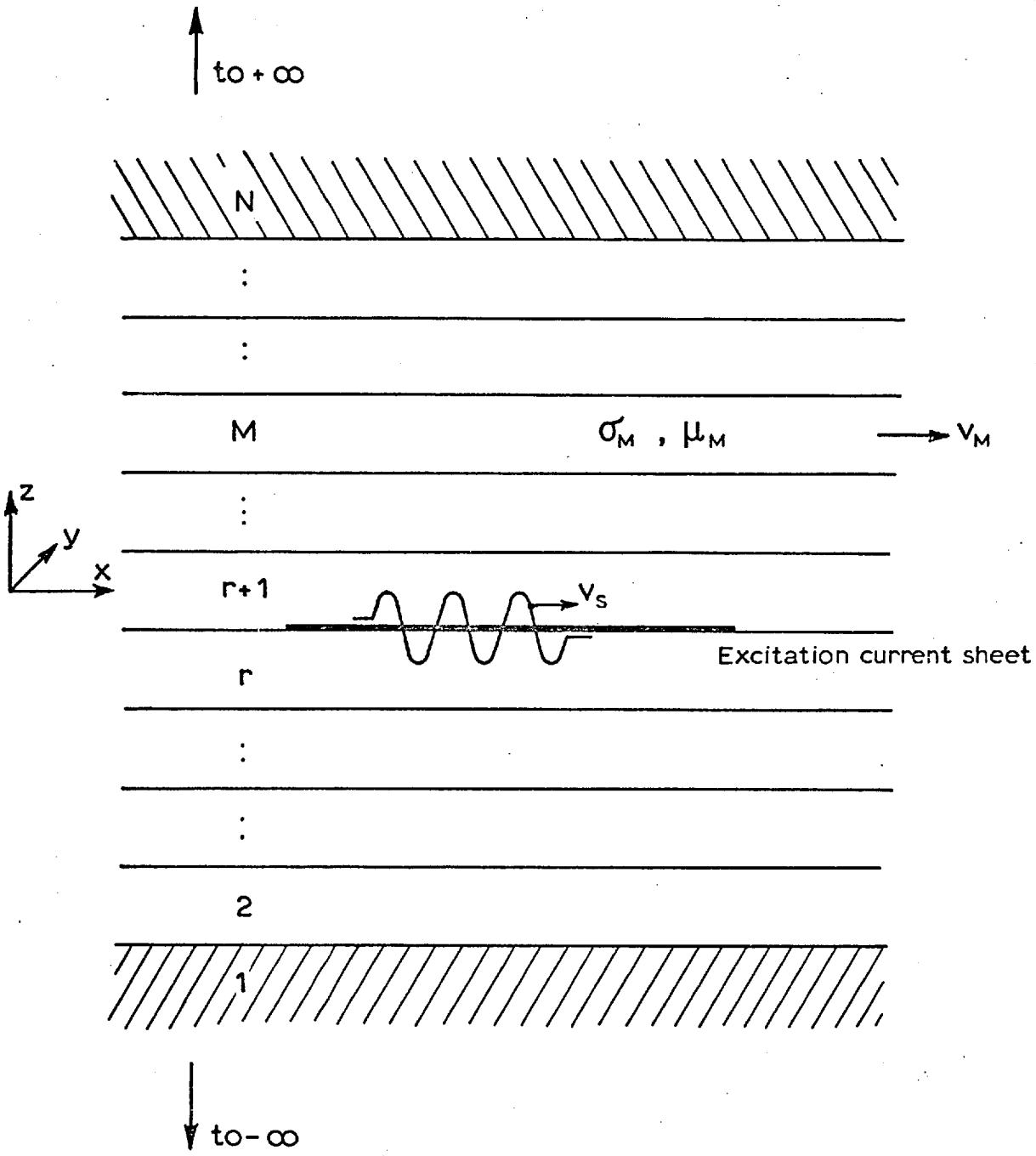


Fig. 3.2 Multilayer planar model

The relation between the (m,n) wave numbers of the x- and y-components of the current sheet can be established from $\nabla . \bar{K} = 0$,

$$\text{i.e.} \quad (\hat{K}_x/\hat{K}_y)_{m,n} = \alpha_n/\beta_m \tag{3.2}$$

The exact expressions of $(\hat{K}_x)_{m,n}$ and $(\hat{K}_y)_{m,n}$ for different values of m and n can be obtained from the actual distribution of the excitation current by a standard Fourier series (or integral) methods[3.58]. In the rest of this report, we will consider 'one' travelling wave, derive the solution for it, then by superposition the complete solution for the whole excitation spectrum can be evaluated. The subscripts m and n will be omitted for brevity.

3.8 Theory

3.8.1 Maxwell equations

Consider a 'stationary reference frame', for a general region (M), Maxwell equations could be written in the form:

$$\begin{aligned} \nabla \times \bar{E} &= -\frac{\delta \bar{B}}{\delta t} \\ \nabla \times \bar{H} &= \sigma_M(\bar{E} + \bar{v}_M \times \bar{B}) \end{aligned} \tag{3.3}$$

For a sinusoidal time variation, $\delta/\delta t$ could be substituted

by $(j\omega)$. Again, the subscript M will be omitted for brevity.

Taking the divergence of the second curl equation of (3.3), and substituting for $\bar{v} = v_x \bar{i}$ we get:

$$\nabla . \bar{E} = \mu\sigma v_x E_x \tag{3.4}$$

i.e. the divergence of the electric field measured in a stationary reference frame in presence of moving conducting media is not zero generally. $\nabla.\bar{E}$ is equal to zero in the following cases:

i) $E_x = 0$, i.e. case of one-dimensional current sheet.

ii) $\sigma = 0$, for non-conducting regions.

iii) $v_x = 0$, i.e. stationary region w.r.t. the frame of reference.

3.8.2. H-field governing equation

Assuming a travelling wave solution in the x-direction of the form: $\exp\{j(\omega t - \beta x)\}$, hence $\delta/\delta x$ could be replaced by $(-j\beta)$. Taking the curl of the 2nd Maxwell curl equation we get:

$$\begin{aligned} \nabla \times (\nabla \times \bar{H}) &= \sigma \nabla \times \bar{E} + \sigma \nabla \times (\bar{v} \times \bar{B}) \\ &= -j\omega\mu\sigma\bar{H} + \mu\sigma \nabla \times (\bar{v} \times \bar{H}) \end{aligned} \tag{3.5}$$

Consider the term $\nabla \times (\bar{v} \times \bar{H})$;

$$\nabla \times (\bar{v} \times \bar{H}) = \bar{v}\,(\nabla.\bar{H}) - \bar{H}(\nabla.\bar{v}) + (\bar{H}.\nabla)\bar{v} - (\bar{v}.\nabla)\bar{H} \tag{3.6}$$

Since $\nabla.\bar{H} = 0$ (assuming magnetic linearity) and since $\bar{v}$ is 'independent' of the space coordinates, hence euqation (3.6) reduces to:

$$\nabla \times (\bar{v} \times \bar{H}) = -(\bar{v}.\nabla)\bar{H} \tag{3.7}$$

Substituting for $\bar{v}$ and $\delta/\delta x$ as indicated before, equation (3.7) reduces to:

$$\nabla \times (\bar{v} \times \bar{H}) = j\beta\, v_x\, \bar{H} \tag{3.8}$$

The L.H.S. of equation (3.5) can be written in the form:

$$\begin{aligned} \nabla \times (\nabla \times \bar{H}) &= \nabla(\nabla.\bar{H}) - \nabla^2\bar{H} \\ &= - \nabla^2\bar{H} \end{aligned} \tag{3.9}$$

Substituting from (3.8) and (3.9) into equation (3.5) we get:

$$\nabla^2\bar{H} = j\omega\mu\sigma\bar{H} - j\beta\mu\sigma v_x\, \bar{H} \tag{3.10}$$

Defining the slip of the region as:

$$s = \frac{v_s - v_x}{v_s} \tag{3.11}$$

Where

v_s = linear synchronous speed

= ω/β

and substituting into (3.10) we get:

$$\nabla^2 \bar{H} = j\omega\mu\sigma s \bar{H} \tag{3.12}$$

3.8.3 E-field governing equation

Taking the curl of the first Maxwell curl equation and after some algebraic manipulations we get:

$$\nabla^2 \bar{E} = \mu\sigma \frac{\delta \bar{E}}{\delta t} + \nabla(\nabla.\bar{E}) - \mu\sigma\, \bar{v} \times \nabla \times \bar{E} \tag{3.13}$$

Assuming constant linear velocity in the x-direction, and substituting for $(\nabla.\bar{E})$ from equation (3.4), equation (3.13) reduces to:

$$\nabla^2 \bar{E} = \mu\sigma \frac{\delta \bar{E}}{\delta t} + \mu\sigma\, v_x \nabla E_x + \mu\sigma v_x \{(\frac{\delta}{\delta x} E_y - \frac{\delta}{\delta y} E_x)\, \bar{j} - (\frac{\delta}{\delta z} E_x - \frac{\delta}{\delta x} E_z)\, \bar{k}\} \tag{3.14}$$

Again, substituting for v_x from equation (3.11) it can be easily shown that the components of equation (3.14) satisfy the vector Helmholtz equation given by:

$$\nabla^2 \bar{E} = j\omega\mu\sigma s \bar{E} \tag{3.15}$$

3.9 Transmission Line Modelling

It has been shown that both the electric and the magnetic field vectors satisfy the vector Helmholtz equation. For further simplification, substituting for:

$$\delta^2/\delta x^2 = -\beta^2$$
$$\delta^2/\delta y^2 = -\alpha^2$$

we get:

$$\{\frac{\delta^2}{\delta z^2} - \gamma^2\} \cdot \begin{bmatrix} \bar{E} \\ \bar{H} \end{bmatrix} = 0 \qquad (3.16)$$

where

$$\gamma^2 = \beta^2 + \alpha^2 + j\omega\mu\sigma s$$

Similarly, as has been shown in chapter 2, the solution of this field problem can be obtained using a T.L. electromagnetic equivalent network. First we have to derive the expressions of the 'transverse' field components (i.e. y- and z-components) in terms of the 'axial' field components (i.e. x-components). This can be achieved by solving the two Maxwell equations simultaneously. The results are given directly by the following equations:

$$E_y = (1/\gamma_o^2) \cdot \{(j\beta + \sigma\mu v_x) \frac{\delta}{\delta y} E_x + j\omega\mu \frac{\delta}{\delta z} H_x\} \qquad (3.17)$$

$$E_z = (1/\gamma_o^2) \cdot \{(j\beta + \sigma\mu v_x) \frac{\delta}{\delta z} E_x - j\omega\mu \frac{\delta}{\delta y} H_x\}$$

$$H_y = (1/\gamma_o^2) \cdot \{j\beta \frac{\delta}{\delta y} H_x - \sigma \frac{\delta}{\delta z} E_x\}$$
$$H_z = (1/\gamma_o^2) \cdot \{j\beta \frac{\delta}{\delta z} H_x + \sigma \frac{\delta}{\delta y} E_x\} \qquad (3.17)$$

Where

$$\gamma_o^2 = \beta^2 + j\omega\mu\sigma s$$

i.e.

$$\gamma^2 = \gamma_o^2 + \alpha^2$$

It should be noted here that the main difference between this formulation and that reported in chapter 2 is the presence of the terms which are proportional to the relative speed between the moving medium and the reference frame. These terms can be thought of as injected voltage or current dependent sources in the equivalent network as will be shown later

3.9.1 Equivalent circuit with voltage sources

The electromagnetic field tangential components E_x, E_y, H_x and H_y are the only ones required to deduce the interface coupling circuit. The expressions of E_y and H_y can be rewritten from equations (3.17) in the form:

$$E_y = (1/\gamma_o^2) \cdot \{j\beta \frac{\delta}{\delta y} E_x + j\omega\mu \frac{\delta}{\delta z} H_x\} + (\sigma\mu\, v_x/\gamma_o^2) \cdot \frac{\delta}{\delta y} E_x \qquad (3.18a)$$

$$H_y = (1/\gamma_o^2) \cdot \{j\beta \frac{\delta}{\delta y} H_x - \sigma \frac{\delta}{\delta z} E_x\} \qquad (3.18b)$$

In order to derive the equivalent circuit parameters let us write the expressions of the field components in terms of the flow and potential quantities of the double T.L. equivalent circuit.

If V'(z) and V"(z), I"(z) and I"(z) are the voltages and currents of the E- and H-lines respectively, the field components can be written generally in the form:

$$
\begin{aligned}
E_x &= V'(z)\, e'_x + 0 \\
H_x &= 0 + I''(z)\, h''_x \\
E_y &= V'(z)\, e'_y + V''(z)\, e''_y + e \\
H_y &= I'(z)\, h'_y + I''(z)\, h''_y + i
\end{aligned}
\qquad (3.19)
$$

The terms (e) and (i) in the R.H.S. of the E_y and H_y equations represent voltage and current sources. The other e's and h's in equation (3.19) are known in mirco-wave theory as the 'form functions'.

Comparing the corresponding terms in equations (3.18) and (3.19), and keeping in mind the equivalent T.L. equations given by:

$$
\begin{aligned}
\frac{dV'}{dz} &= -Z'\, I' \\
\frac{dI''}{dz} &= -Y''\, V''
\end{aligned}
\qquad (3.20)
$$

such that $Z' Y' = Z'' Y'' = \gamma^2$, by virtue of equation (3.16)

It can be simply shown that:

$$
\begin{aligned}
e'_y &= -(\alpha\beta/\gamma_o^2)\, e'_x \\
h''_y &= -(\alpha\beta/\gamma_o^2)\, h''_x \\
Z' &= (\gamma_o^2/\sigma) \cdot (h'_y/e'_x) \\
Y'' &= (\gamma_o^2/j\omega\mu) \cdot (-e''_y/h''_x) \\
e &= (\alpha\beta/\gamma_o^2) \cdot (j\omega\mu\sigma/\beta^2) \cdot (1 - s)\, V'\, e'_x \\
i &= 0
\end{aligned}
\tag{3.21}
$$

For a general case when a two-dimensional current sheet exists between two adjacent layers M and M+1, travelling with two different linear speeds, the continuity relations can be satisfied as follows:

(i) Continuity of E_x:

$$
\{V'\, e'_x\}_M = \{V'\, e'_x\}_{M+1} \tag{3.22}
$$

ii) Continuity of H_x: (allowing for K_y)

$$\{I''\ h''_x\}_{M+1} = \{I''\ h''_x\}_M + K_y \qquad (3.23)$$

iii) Continuity of H_y: (allowing for K_x)

$$\{I'\ h'_y\}_{M+1} = \{I'\ h'_y\}_M + \{(-\alpha\beta/\gamma_o^2) I''\ h''_x\}_M - \{(-\alpha\beta/\gamma_o^2)\ I''\ h''_x\}_{M+1} - K_x \qquad (3.24)$$

iv) Continuity of E_y:

$$\{-V''\ e''_y\}_{M+1} = \{-V''\ e''_y\}_M - \{(-\alpha\beta/\gamma_o^2)\ V'\ e'_x\}_M + \{(-\alpha\beta/\gamma_o^2)\ V'\ e'_x\}_{M+1} + e_M - e_{M+1} \qquad (3.25)$$

The general equivalent circuit which satisfies the interface coupling conditions (3.22 - 3.25) is shown in Fig. (3.3).

The voltage sources appearing in the above equivalent circuit are of 'terminal dependent type', i.e. their values are directly proportional to the interface voltage of the E-line.

There are some circuit analysis packages which can model 'branch dependent current sources' rather than these

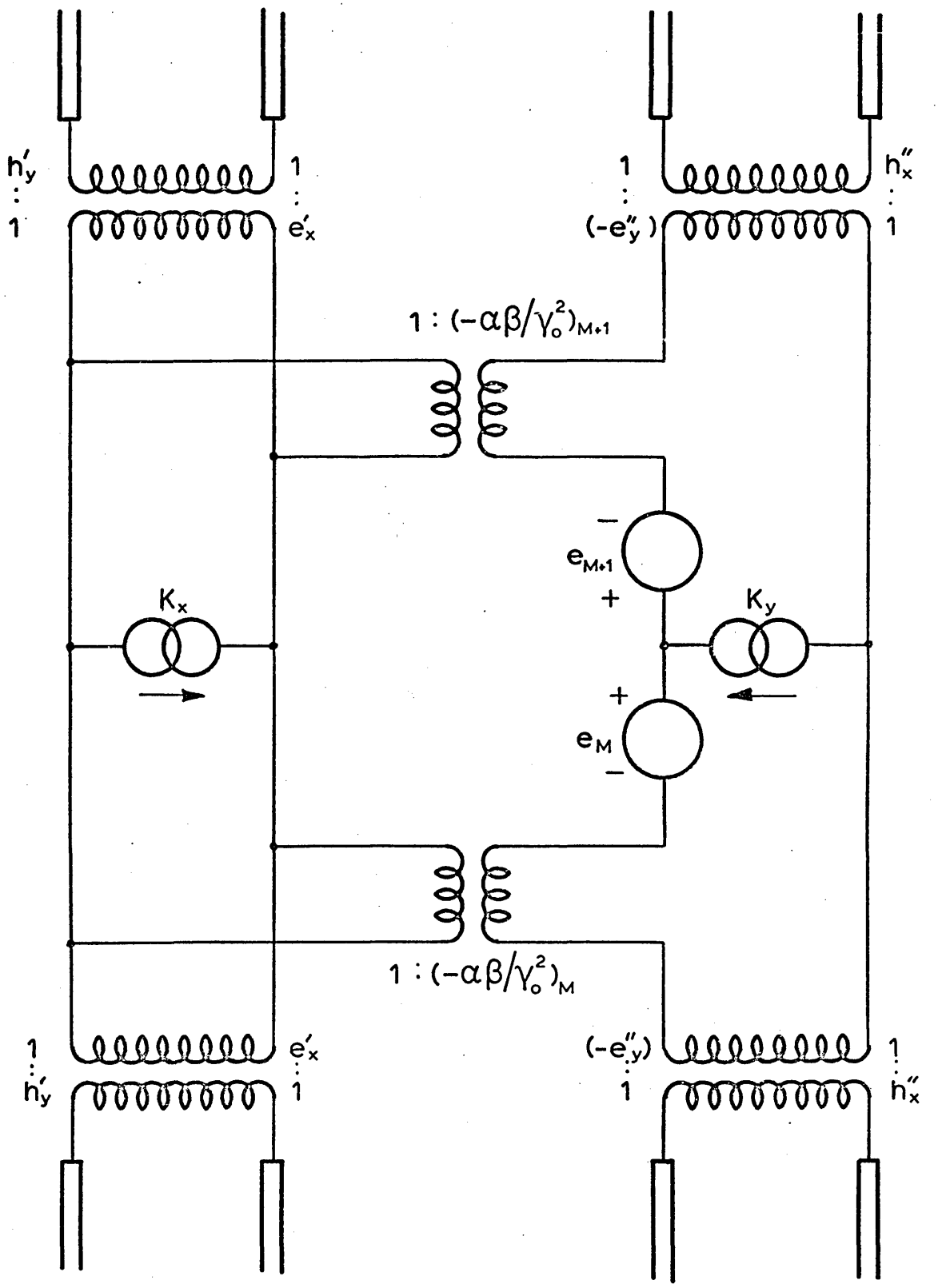


Fig. 3·3 Interface general coupling circuit with voltage sources.

'terminal dependent voltage sources'. In order to make use of such packages, another equivalent circuit will be developed in the following section, in which the effect of motion will be introduced by inserting current instead of voltage sources.

3.9.2 Equivalent circuit with current sources

This circuit can be obtained by rearranging the expressions of E_y and H_y, given by equation (3.17), as follows:

$$E_y = (1/\gamma_o^2) \cdot \{(j\beta + \sigma\mu\, v_x) \frac{\delta}{\delta y} E_x + j\omega\mu \frac{\delta}{\delta z} H_x\} \qquad (3.26a)$$

$$H_y = (1/\gamma_o^2) \cdot \{(j\beta + \sigma\mu\, v_x) \frac{\delta}{\delta y} H_x - \frac{\delta}{\delta z} E_x\} - (\sigma\mu\, v_x/\gamma_o^2) \frac{\delta}{\delta y} H_x \qquad (3.26b)$$

Similarly, comparing equations (3.26) and (3.19) we get the following relations:

$$\begin{aligned} e'_y &= (\alpha/\beta) \cdot \{j\omega\mu\sigma/\gamma_o^2 - 1\}\, e'_x \\ h''_y &= (\alpha/\beta) \cdot \{j\omega\mu\sigma/\gamma_o^2 - 1\}\, h''_x \\ Z' &= (\gamma_o^2/\sigma) \cdot (h'_y/e'_x) \\ Y'' &= (\gamma_o^2/j\omega\mu) \cdot (-e''_y/h''_x) \end{aligned} \qquad (3.27)$$

$$i = (-\alpha\beta/\gamma_o^2) \cdot (j\omega\mu\sigma/\beta^2) \cdot (1 - s) \cdot I'' h_x''$$

$$e = 0 \qquad (3.27)$$

And the interface coupling circuit can be derived from the continuity relations. In this case, the continuity of E_x and H_x (allowing for K_y if any) yields the same equations as (3.22) and (3.23) respectively.

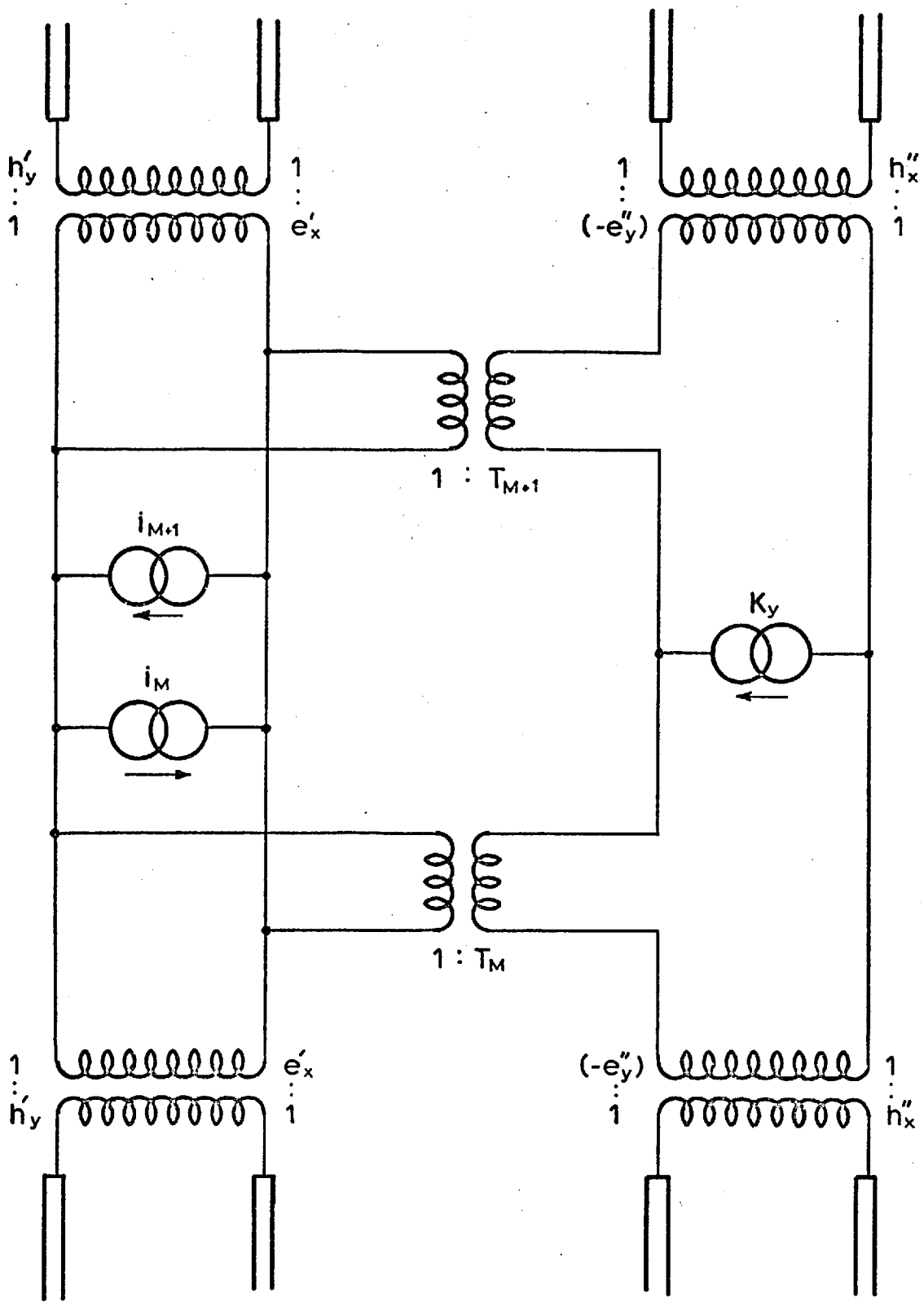
The continuity of H_y can be satisfied as follows:

$$\{I' h_y'\}_{M+1} = \{I' h_y'\}_M + \{(\alpha\beta/\gamma_o^2) \cdot (j\omega\mu\sigma/\beta^2) I'' h_x''\}_M$$
$$-\{(\alpha\beta/\gamma_o^2) \cdot (j\omega\mu\sigma/\beta^2) I'' h_x''\}_{M+1} + i_M - i_{M+1}$$
$$-[(\alpha/\beta) \cdot \{(I'' h_x'')_M - (I'' h_x'')_{M+1}\} + K_x] \qquad (3.28)$$

And the continuity of E_y can be satisfied by the following equation:

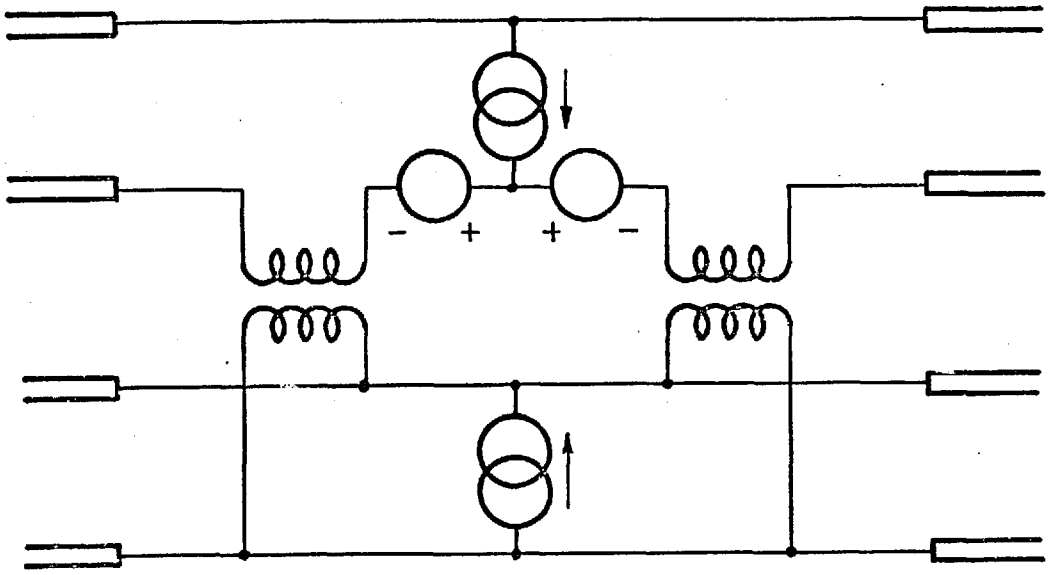
$$\{-V'' e_y''\}_{M+1} = \{-V'' e_y''\}_M - \{(\alpha\beta/\gamma_o^2) \cdot (j\omega\mu\sigma/\beta^2) V' e_x'\}_M$$
$$+\{(\alpha\beta/\gamma_o^2) \cdot (j\omega\mu\sigma/\beta^2) V' e_x'\}_{M+1}$$
$$+ (\alpha/\beta)\{(V' e_x')_M - (V' e_x')_{M+1}\} \qquad (3.29)$$

The last term in the R.H.S. of equation (3.28) is equal to zero by virtue of equations (3.2) and (3.23). Also the last term in the R.H.S. of equations (3.29) is equal to zero

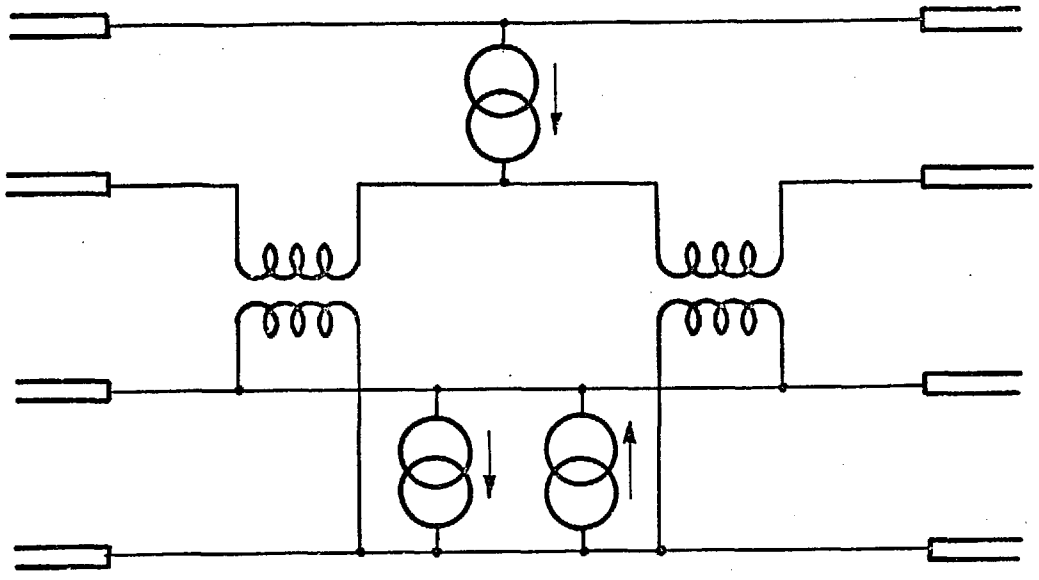


$$T = -(\alpha\beta/\gamma_o^2) \cdot (j\omega\mu\sigma/\beta^2)$$

Fig. 3·4 Interface general coupling circuit with current sources.



(a)



(b)

Fig. 3·5 Simplified interface coupling circuit.

(a) with voltage sources

(b) with current sources

by virtue of equation (3.22). Thus, the equivalent circuit which satisfies the equations (3.22), (3.23), (3.28) and (3.29) will be as shown in Fig. (3.4).

In order to reduce the number of coupling transformers in the interface equivalent circuit, we can choose:

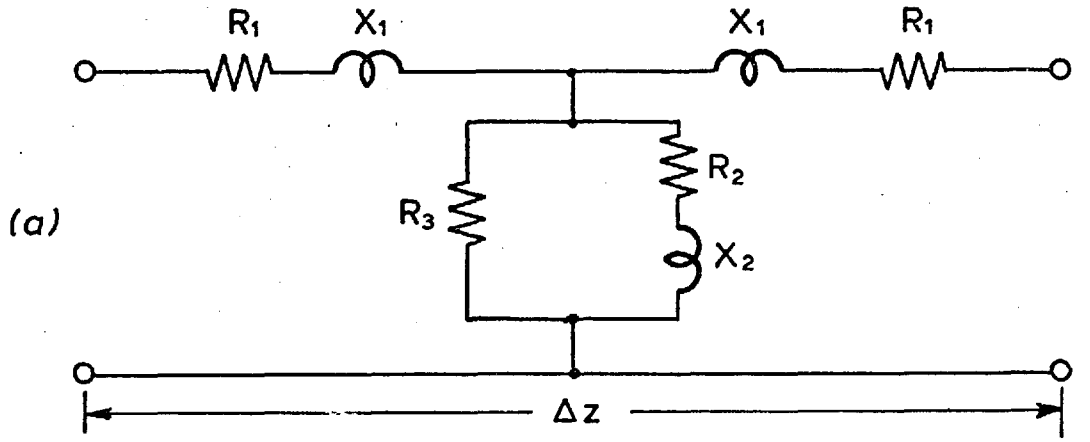
$$h''_x = 1, \qquad \text{therefore} \quad e''_y = -1$$
$$e'_x = 1, \qquad \text{therefore} \quad h'_y = 1 \tag{3.30}$$

And the equivalent circuits reduce to those shown in Fig. (3.5).

3.9.3 The micro-T circuits of E-and H-lines

Having established the interface coupling circuit for this multi-layer mathematical model, the treatment would be exactly similar to the procedure discussed earlier in chapter two for the multi-region cylindrical model.

The micro-T circuits of both the E- and H- lines can be derived from equations (3.21) or (3.27) together with (3.20) and (3.30). These circuits are shown in Fig. (3.6). The effect of displacement current is neglected, however it can be introduced, if required, in similar way to that shown in the analysis of chapter 2.

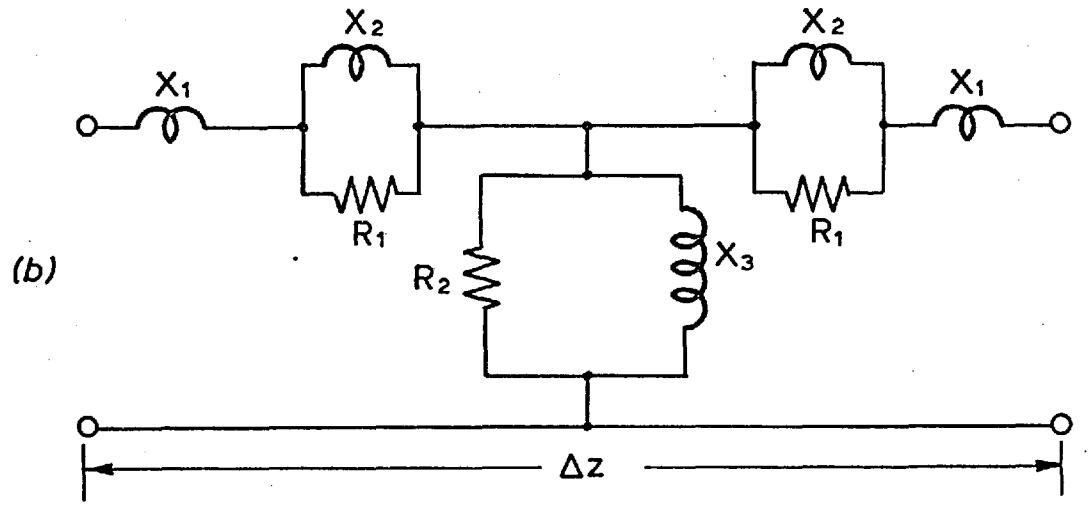


(a)

$R_1 = \beta^2/2\sigma \cdot \Delta z$ $\qquad X_1 = \omega\mu s/2 \cdot \Delta z$

$R_2 = \beta^2/\sigma\alpha^2 \cdot 1/\Delta z$ $\qquad X_2 = \omega\mu s/\alpha^2 \cdot 1/\Delta z$

$R_3 = 1/\sigma \cdot 1/\Delta z$



(b)

$R_1 = \alpha^2/2\sigma s \cdot \Delta z$ $\qquad X_1 = \omega\mu/2 \cdot \Delta z$

$R_2 = 1/\sigma s \cdot 1/\Delta z$ $\qquad X_2 = \omega\mu\alpha^2/2\beta^2 \cdot \Delta z$

$X_3 = \omega\mu/\beta^2 \cdot 1/\Delta z$

Fig. 3·6 The micro-T circuits of planar model

(a) E-line (b) H-line

(displacement current is neglected)

Again the E-line of a non-conducting region is an open circuit.

It is worth mentioning that the main difficulty of having non-uniform transmission lines, which appear in cylindrical models, does not exist for the planar model. So it could be simpler to use transfer matrices to relate the voltages and currents at both sides of any one transmission line in the network, instead of discretizing the continuous line into large number of micro-T circuits. The elements of the transfer matrices will be given in general in terms of hyperbolic functions which are straightforward to calculate.

3.10 Some Special Cases

3.10.1 The coupling circuit between two adjacent non-conducting regions:

Consider first the equivalent circuit with current sources. The conductivity is zero, hence both i_M and i_{M+1} are zero. Also the turns ratios of the coupling transformers become zero, i.e. there will be no coupling between the two lines. The equivalent circuit reduces to that shown in Fig. (3.7).

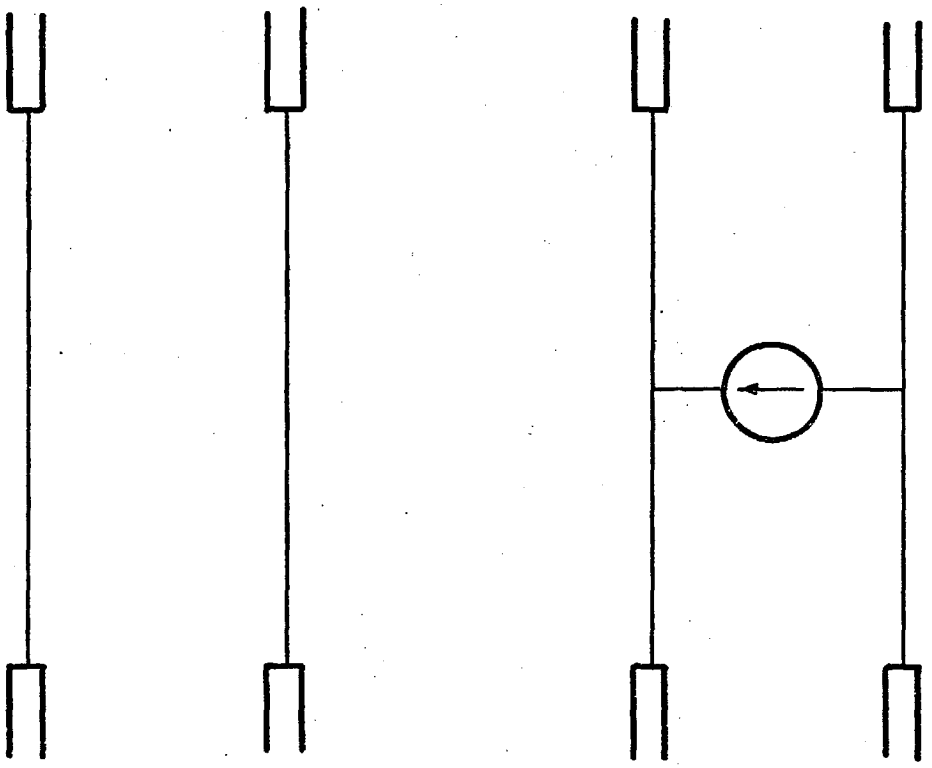


Fig. 3·7 Interface coupling circuit of two adjacent non-conducting regions.

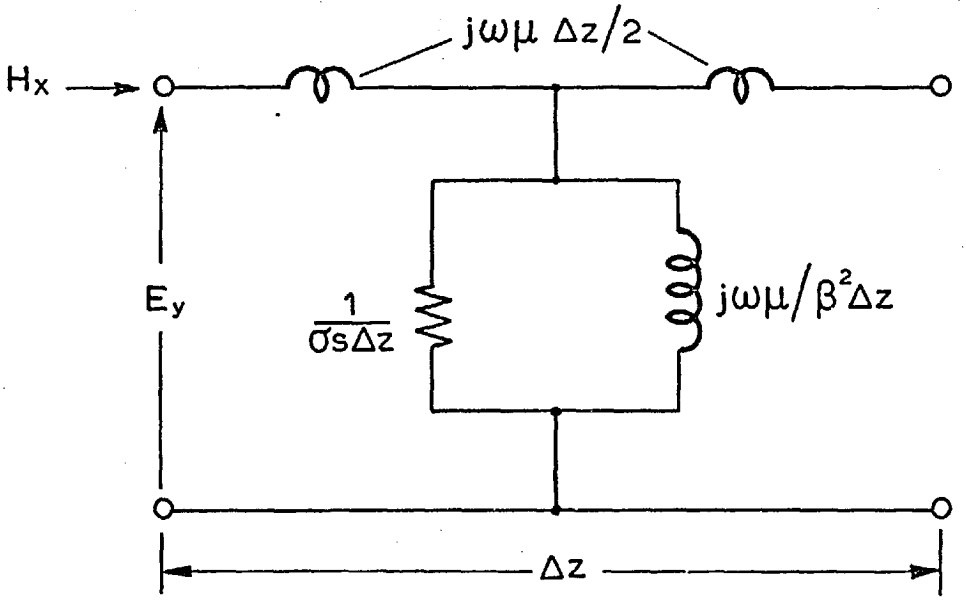


Fig. 3·8 The micro-T circuit of 1-D planar model

On the other hand, if we consider the equivalent circuit which contains voltage sources, e_M and e_{M+1} will be short circuited (proportional to the conductivity σ). The turns ratio of the two coupling transformers will be equal to $(-\alpha/\beta)$. And since they both have equal voltages at the E-line side, hence their H-line side voltages will be equal. Furthermore, they are in phase opposition, hence the net voltage injected in the H-line due to these two transformers is zero. While the total current injected by these transformers in the E-line is euqal to;

$$(-\alpha/\beta).\{(I'')_{M+1} - (I'')_M\}$$

$$= -(\alpha/\beta)\ K_y = -K_x$$

This current together with the current source K_x will inject 'zero' current in the E-line. Consequently, the equivalent circuit reduces to that shown in Fig. (3.7).

3.10.2 One-dimensional excitation

If $K_x = 0$, and only K_y exists, the problem reduces to the mathematical model considered by Freeman[3.30]. This model can be deduced from the above general model by allowing (α) to tend to zero.

As $\alpha \to 0$ the coupling between the two lines disappears for either the conducting or non-conducting regions. Since

$K_x = 0$, there will be no excitation to the E-line. The double T.L. equivalent network reduces then to only 'one' T.L., which is the H-line. Moreover, the voltage sources, which might be present in the network, will be short circuited, since they are proportional to (α).

As a result, the whole equivalent circuit becomes a cascade connection of a number of T.L.s. The circuit parameters of any one of these lines are given by:

$$Y'' = (\beta^2 + j\omega\mu\sigma s)/j\omega\mu$$

and since $\gamma^2 = \gamma_o^2$ in this case ($\alpha = 0$)

therefore

$$Z'' = j\omega\mu$$

The micro-T circuit which represent this line will be as shown in Fig. (3.8).

The circuit is exactly similar to that derived by Freeman[3.66] in his 1-D theory.

3.10.3 The equivalent four-terminal network of a conducting region stationary in the frame of reference and bounded by two infinitesimally thin non-conducting layers

Since the conducting region is stationary in the reference frame, the relative slip (s) and the angular frequency ω, which appear in the previous equations, should be substituted for by unity and $\omega' = s\omega$ respectively. ω' is the angular frequency measured in a reference frame fixed in the region under consideration. The current (or voltage) dependent sources of the deduced equivalent circuit, will be open (or short) circuited.

On the other hand, since the conducting region is bounded by two non-conducting regions, the coupling transformers at both sides of the equivalent T.L. network representing this region both will have same turns ratio T.

Bearing in mind the above mentioned substitutions, the turns ratio T will be given by:

$$T = -(\alpha\beta/\gamma_o^2)(j\omega\mu\sigma s/\beta^2)$$

where

$$\gamma_o^2 = \beta^2 + j\omega\mu s$$

The equivalent network will be as shown in Fig. (3.9) below.

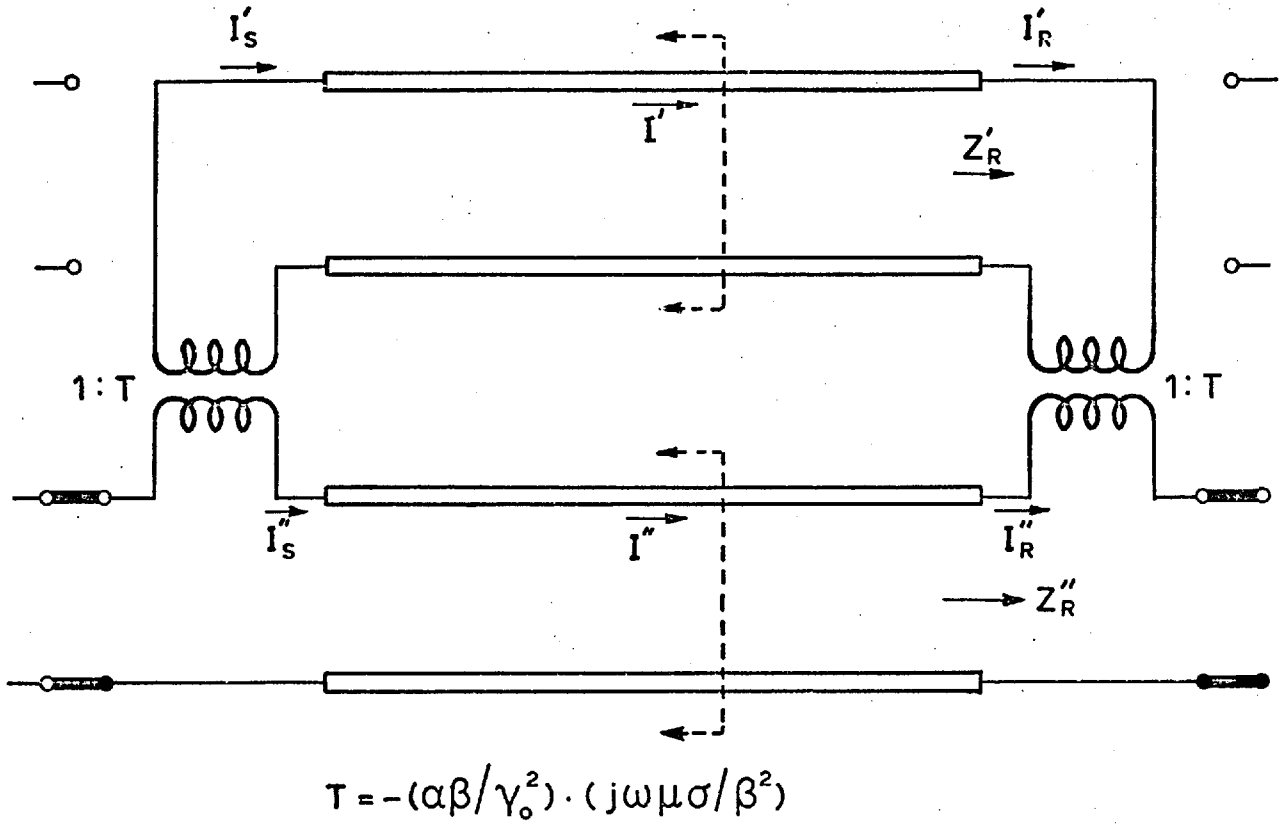


Fig. 3·9 Equivalent network of a stationary conducting layer bounded by two non-conducting layers.

Since E_z in this case is measured in a reference frame fixed in the conducting region, the expression of the induced current density component normal to the excitation surface can be obtained by multiplying the E_z expression, given by equation (3.17), by the conductivity σ. For this case, J_z will be given by:

$$J_z = (\sigma s \omega \mu \alpha / \gamma_o^2) \cdot \{I'' - I'/T\} \qquad (3.31)$$

From the T.L. theory, we can write directly,

$$I_r/I_s = 1 /\{\cosh(\gamma L) + (Z_r/Z_o) \cdot \sinh(\gamma L)\} \qquad (3.32)$$

Where Z_r and Z_o are the receiving end and the characteristic impedances of the T.L. length L. I_r and I_s are the receiving and sending end currents respectively.

Equation (3.32) can be written for each of the two lines. Bearing in mind that:

$$I_s'/I_s'' = I_r'/I_r'' = T$$

together with equation (3.32), it can be easily shown that:

$$(Z_r/Z_o)' = (Z_r/Z_o)'' \qquad (3.33)$$

Again, using the result obtained from equation (3.33) together with the expression of the current at any section in the T.L., it can be easily shown that: I' = TI" always. Substituting for this in equation (3.31), the induced eddy current in a direction normal to the excitation surface is equal to zero.

In fact, this result has been usually assumed in the analysis of similar mathematical models (see Preston and Reece[3.36]).

Similarly, as has been shown in section (2.13), the equivalent network shown in Fig. (3.9) can be reduced to only one T.L.

Before referring the E-line quantities to the H-line side, let us use the following per unit system:

For the H-line:

Base voltage = Q

Base current = 1.0

therefore,

Base impedance = Q

therefore

$$Z''_o = (js\omega\mu/Q).(\gamma/\gamma_o^2) \quad \text{p.u.}$$

For the E-line:

Base voltage = 1.0

Base current = Q

therefore,

Base impedance = 1.0/Q

Therefore, $Z'_o = (Q/\sigma).(\gamma_o^2/\gamma)$ p.u.

And to satisfy the boundary conditons (coupling circuit), the turns ratio T should be changed to (T/Q).

Let $Q = (1 + \frac{\alpha^2}{\beta^2})$

According to equation (2.71), the double T.L. can be reduced to 'one' equivalent T.L. whose characteristic impedance Z_o is given by:

$$Z_o = Z''_o + T^2 Z'_o \qquad (3.34)$$

Its propagation constant is γ. Substituting for the different parameters of the R.H.S. of equation (3.34) we get:

$$\begin{aligned} Z_o &= (js\omega\mu\gamma/Q\gamma_o^2) + \{(1/Q).js\omega\mu\sigma\alpha/\beta\gamma_o^2\}^2.\{Q\gamma_o^2/\sigma\gamma\} \\ &= js\omega\mu/\gamma \qquad \text{p.u.} \end{aligned} \qquad (3.35)$$

The current flowing in this T.L. is I", which is equivalent to the magnetic field component H_x.

The series impedance and parallel admittance per unit length of this T.L. are given by:

$$Z = js\omega\mu \qquad \text{p.u.}$$

$$Y = \gamma^2/js\omega\mu \qquad \text{p.u.}$$

The single equivalent T.L. developed in this section is identical with that reported by Freeman and Lowther[3.45].

It should be noted that the treatment in this section is constrained by the assumption that the conducting region is stationary in the reference frame. The angular frequency ($\omega' = s\omega$) used in this section represents the frequency

measured by an observer in this reference frame.

Similar single T.L. representation can be found for the situation where more than 'one' conducting region is considered, provided that 'all' the conducting regions are relatively at rest. In such a case the frame of reference should be chosen fixed with respect to these conducting layers. However, if there are two or more conducting regions in the model travelling at different speeds, the equivalent circuit developed in this section will be invalid, and we should resort to the general double T.L. with injected sources.

It has been found that there will be no normal component of the induced eddy current in an electrically isolated planar conducting region . If there exist two adjacent conducting regions having different conductivity and they are not electrically isolated, then a normal current component is likely to circulate. Again the general double T.L. equivalent circuit should be used to predict the performance of the mathematical model.

Finally, it is worth mentioning that the Freeman and Lowther's two-dimensional model is only valid for cases when there is one conducting region or more than one such that they are all relatively at rest and electrically isolated from each other.

Also, the transfer matrix treatment by Alden and Nolan[3.47]

is only valid for the above mentioned model. It is incorrect to claim that it is general for any number of regions having different speeds as they mentioned in their paper.

3.11 Conclusions

The problem of calculating the electromagnetic field components of a multilayer planar induction device excited by a two-dimensional current sheet has been considered. An equivalent network of the double T.L. has been found to represent the mathematical model.

The effect of speed has been found to include current (or voltage) sources in the equivalent network. The magnitudes of these sources are in general proportional to the relative speed between the conducting region under consideration and the reference frame.

Simple special cases have been considered. The most interesting of them is the reduction of the double T.L. to only a single line exactly similar to that derived by Freeman and Lowther some years ago. It has been shown that the two-dimensional analysis by Freeman and Lowther and also by Alden and Nolan is limited to those models having only 'one' conducting region, or if there are more, then all the conducting regions should be relatively at rest and electrically isolated from each other.

It is believed that the equivalent network developed in this chapter is very general. To the author's belief no one else has yet derived a method to calculate the 'normal' circulating current between different conducting media in electric contact and sliding on each other (a situation likely to happen in liquid metal MHD pumps). The equivalent network derived in this chapter provides the means by which this current could be calculated.

CHAPTER 4

Induction Devices having Circumferentially directed Excitation Current - The Infinitely Long Model

4.1 Introduction

In the multiregion induction devices discussed earlier it was shown that each region can be represented by an equivalent circuit in transmission line form. The circuit elements of such transmission lines are, in general, functions of the region parameters; such as its conductivity, permeability and permittivity. They might also be functions of some other factors defined by the exciting (or source) function such as wave number or wave length.

An accurate knowledge of the region parameters is essential to calculate the distribution of the electric and magnetic fields in it. This in turn will permit the calculation of forces exerted on the region in force or torque production devices (e.g. electrical machines), or will determine the effectiveness of a certain region to shield or screen magnetic or electric fields.

In the case of non-magnetic conducting regions, the parameter that must be known precisely is the conductivity. In fact all the conducting materials used are in general alloys and not pure elements, so the conductivity will

depend mainly on the chemical composition. In the case of copper, for instance, the presence of 0.005% phosphorus will decrease the conductivity by about 4%. Many other impurities, in addition to variations in alloy composition, also affect the conductivity, although in most cases the effect is smaller. Porosity changes the effective conductivity of a piece of metal by concentrating currents into a smaller volume. Currents cannot pass across the microscopic voids and in being diverted around them they raise the current density in the surrounding metal and thereby the effective resistance seen by any observer outside. Variation in grain size and hardness, and the presence of internal stresses also have slight effects on the conductivity. Usually the manufacturers supply tables which give the average properties of their products. Typical conductivity values are given in a range where the extreme values may differ by 10% or more. Since the experimental work reported in this thesis has the sole objective of proving the validity of the equivalent circuit derived, any uncertainty, however slight it is, is required to be eliminated whenever possible. Hence it is clear that the conductivity of the conducting region used much be determined, and not just taken from the manufacturers' tables.

Following the major theme in this thesis, it was thought that if the conductivity of the cylindrical conducitng region could be obtained adopting a field technique, this will high-

light and emphasize the practical importance and the effectivness of using the equivalent circuit derived from the field equations. This can be done by using the actual conducting cylinder, the resistivity of which is required, as a region in a simple induction device. The field components are then to be measured and calculated. Comparison between the experimental results and a family of curves obtained from the theoretical treatment drawn for different conductivities will lead to more accurate results than those supplied by the manufacturers.

In all tests for the helical winding excitation, the conducting region was always either a tube or a solid rod of an aluminium alloy. The tests were done for different conducting region dimensions, where the flux density distribution and/or the screening ratio were the results of interest.

The simplest field problem arises when the excitation function, i.e. the exciting current, has only one component, which of course must vary with time sinusoidally, in order to produce eddy currents in the conducting region, but it has a constant spatial distribution in one direction. So it was suggested that an exciting current in either the θ-direction or z-direction would be possible for this purpose. A θ-direction exciting current was preferred because it can be realised practically more easily than the z-directed exciting current. There will be no problem of end effects such as

when the conductors are laid parallel to the cylinder axis.

Adopting a θ-directed exciting current as an energizing function, the excitation coil will be simply solenoidal. It may be wound directly on the cylinder leaving a small air-gap between them, or it can be wound round a former, then the conducting region can be inserted to form a conducting, non-magnetic core to it.

A search through the literature shows that, the solution of the field equations for this particular geometrical configuration is not an original one. There are many papers[4.1-4.6] which deal with the calculation of the impedance of an infinitely long solenoidal coil encircling conducting tube or solid cylinder .

In fact, Förster[4.1] during the early 1950's, applied the technique of eddy-current non-destructive testing to the detection of faults such as cracks in metallic tubing. In this test, the tube in passed through a pair of short solenoidal coils. The coils are energised with alternating current so producing, by induction, eddy currents which will flow circumferentially in the tube wall. These two coils are connected in a circuit, where they are balanced by other coils which contain a uniform tube free from faults. An unbalanced condition arises when a fault appears inside one of the coils and the resulting out-of-balance voltage can be used to trigger an automatic rejecting mechanism.

This practical problem is usually tackled theoretically by calculating the input impedance of a long solenoid which has a conducting non-magnetic core. In principle, there is no difference between the two models, the one devised for studying the eddy current non-destructive test problem, and the other which will be dealt with in this work. However, the main difference lies in the technique of theoretical treatment, as will be shown later.

4.2 Review of Previous Work

In reviewing the previous work, one can see that this problem has been investigated by many researchers since the early 1950's, for instance, Förster[4.1], Hochshild[4.2], bareham[4.3], Blitz and Rowse[4.4], Lloyd[4.5] and recently Freeman and Bland[4.6].

Förster[4.1] calculated the input impedance of an infinitely long solenoid coil encircling an infinitely long conducting tube or solid rod, which may be fully or partially filling the excitation coil core. The results were usually given in the form of normalised impedance diagrams.

Hochshild[4.2], presented a comprehensive mathematical study of the same problem where he developed his analysis to calculate the circumferential eddy current/radial distribution for a solid circular bar. Then he extended his theory to the more general case of three concentric cylinders which could be used

to calculate the impedance of air-cored tubular conductors.

Bareham[4.3], following the others solved the Maxwell field equations and calculated the current distribution in an air-cored hollow conducting tube.

Blitz and Rowse[4.4] used the theoretical curves reported by Forster and developed an experimental method to define the magnitude and position of a defect in hollow conducting tube to a high degree of precision.

Lloyd[4.5] solved the same problem and gave his results of impedance calculation in the form of a table, each value corresponding to two variables which are the tube outer to inner diameter ratio and the outer diameter to skin depth ratio.

Freeman and Bland[4.6], making use of the analogy between the equations governing the electric and magnetic field penetration in the field problem and those which govern the voltage and current waves propagation along a transmission line, derived the equivalent transmission line model. Each region is then replaced by the corresponding transfer matrix which related the field quantities at both its boundaries. This technique makes the solution much easier especially if a large number of concentric regions is to be considered. The boundary conditions in such a case will be satisfied automatically by simply connecting the transmission lines in cascade. Thus there will be no need at all for lengthy algebraic manipulation to

determine the separation constants.

The mathematical expressions developed were invariably extremely cumbersome since they involved the use of modified Bessel functions having arguments lying on the 45^{o} ray in the complex plane. The somewhat simpler transfer matrices for a conducting region, used by Freeman, also involve modified Bessel functions.

The analysis which will be developed here will take the transmission line modelling a step further by representing each region by a string of a sufficient number of what we can call micro-T or -π circuits. A criterion for the choice of this number will be discussed.

The main advantage of such a technique lies in avoiding the necessity of using Bessel functions, simplifying programming and saving in computation time.

4.3 Mathematical Model and Fields of Application

4.3.1 The mathematical model

Consider a set of N infinitely long concentric cylindrical regions as shown in Fig. (4.1) with the excitation being a circumferential current sheet which lies at the outer boundary

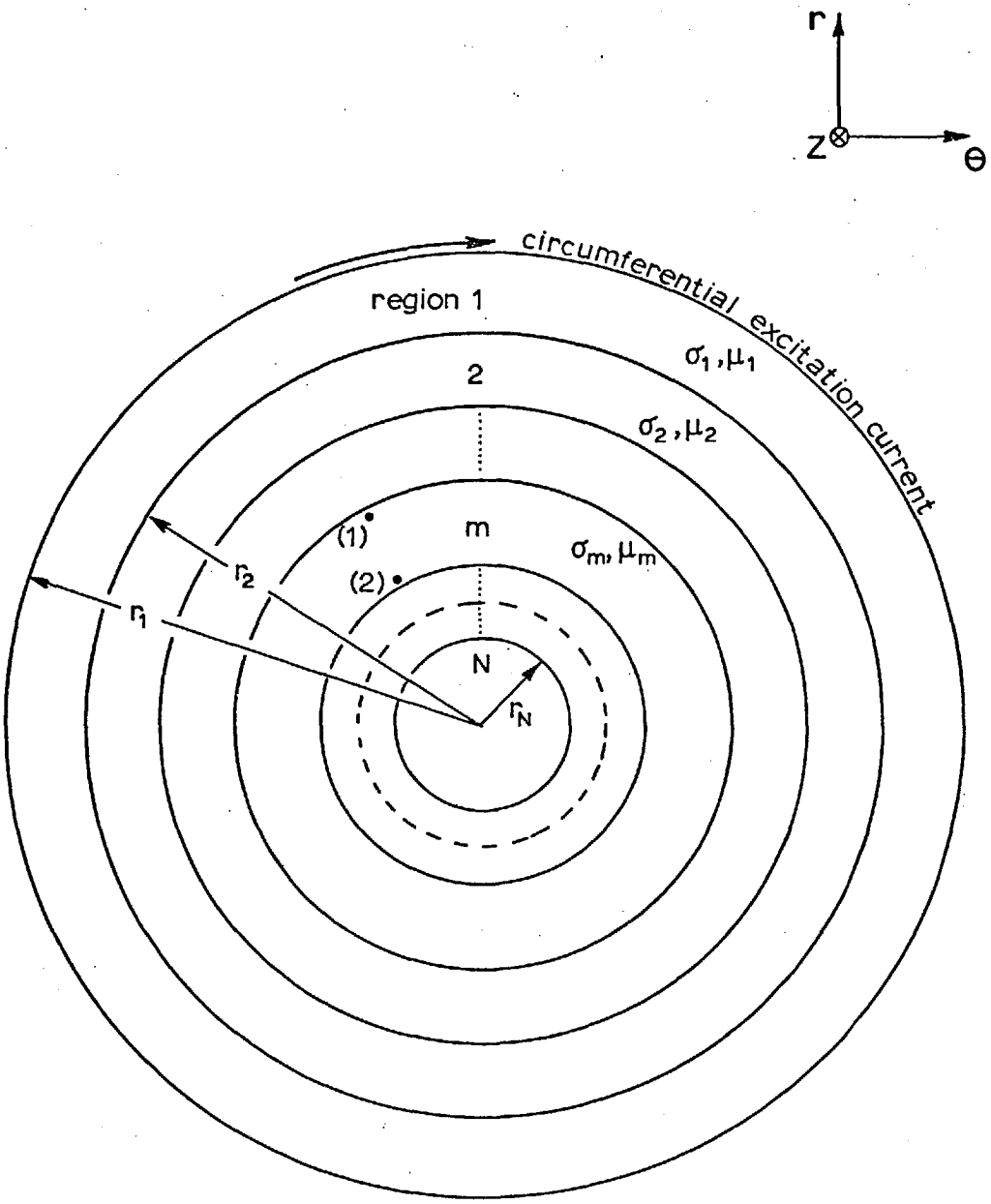


Fig. 4·1 Section through the mathematical model.

surface of the outermost region. Each region is assumed isotopic, homogeneous and linear with single valued parameters. The model excludes the possibility of having one or more of its regions magnetically non-linear. However, regions with permeability different from μ_o can be introduced.

4.3.2 Fields of application

This mathematical model is suitable to represent, for the purpose of theoretical treatment, the following practical applications which involve solid bars, tubes or coated cylinders as conducting regions:

1. Eddy-current induction heating or surface heat treatment.

2. Non-destructive detection of flaws such as cracks, seams, inclusions, dimensional defects, impurities, porosity.

3. Quality control for difference in dimensions or determining the inner and outer diameters and thickness of different samples.

4. Determining physical properties such as conductivity, permeability, grain size, preferred crystal orientation.

5. Determining mechanical properties of the specimen such as hardness, tensile strength, internal stresses and strains.

6. Determining the impedance of infinitely long inductors encircling one or more conducting layers or screened by conducting shields and calculating the associated losses in each conducting region.

4.4 Field Equations

4.4.1 Assumptions and formulation

- Since the excitation current flows in the θ-direction only, the electric field vector $\bar{E}$ has only a θ-component.

- No variation of the field quantities in either θ- or z-directions.

$$\text{i.e. } \frac{\delta}{\delta\theta} = 0$$

$$\text{and } \frac{\delta}{\delta z} = 0$$

- All field components vary with time as $e^{j\omega t}$ thus the differential time operator can be replaced by a simple multiplier ($j\omega$).

- Displacement currents are neglected.

The general Maxwell field equations are:

$$\nabla \times \bar{E} = -\frac{\delta \bar{B}}{\delta t} \tag{4.1}$$

$$\nabla \times \bar{H} = \bar{J} = \sigma \bar{E} \tag{4.2}$$

Expanding the first vector equation in circular cylindrical coordinates, substituting for $\bar{B} = \mu_o \bar{H}$ and $\frac{\delta}{\delta\theta} = \frac{\delta}{\delta t} = E_r = E_z = 0$

then $$\frac{\delta}{\delta r}(rE_\theta) = -j\omega\mu_o r H_z \tag{4.3}$$

Similarly, vector equation (4.2) reduces to:

$$\frac{\delta}{\delta r}(H_z) = -\sigma E_\theta \tag{4.4}$$

Since we have only E_θ, H_z and J_θ components, the subscripts will be omitted without ambiguity.

Eliminating E from (4.3) and (4.4) we get;

$$\frac{\delta^2 H}{\delta r} + \frac{1}{r}\frac{\delta H}{\delta r} - j\omega\mu\sigma H = 0 \tag{4.5}$$

and eliminating H from (4.3) and (4.4) we get;

$$\frac{\delta^2 E}{\delta r^2} + \frac{1}{r}\frac{\delta E}{\delta r} - \{\frac{1}{r} + j\omega\mu\sigma\}E = 0 \tag{4.6}$$

4.4.2 Methods of solution

Equations (4.5) and (4.6) are the modified Bessel differential equations. The solutions are standard and are given in the form:

$$H(r) = A\, I_o(j^{\frac{1}{2}}r/d) + B\, K_o(j^{\frac{1}{2}}r/d) \qquad (4.7)$$

$$E(r) = C\, I_1(j^{\frac{1}{2}}r/d) + D\, K_1(j^{\frac{1}{2}}r/d) \qquad (4.8)$$

From equations (4.4), (4.7) and (4.8) the relations between A, B, C and D can be determined. The result is:

$$C = -A\sqrt{j\omega\mu/\sigma}$$

$$D = B\sqrt{j\omega\mu/\sigma}$$

Where: A, B are constants which can be determined from the boundary conditions at the interfaces between regions.

I_o and K_o are modified Bessel functions of zero order.

I_1 and K_1 are modified Bessel functions of the first order.

Equations (4.7) and (4.8) represent the general solution for the magnetic and electric fields inside any one region. A complete solution for a general N region model requires the application of boundary conditions.

This solution can be obtained by any one of the following methods:

(i) Purely algebraic manipulation.

(ii) Transfer matrix surface impedance method.

(iii) Micro-T circuit method.

In the following sections, the above methods will be discussed in more detail.

4.5 Purely Algebraic Manipulation Method

This has been employed by many authors[4.1 - 4.5], but it is limited to a relatively small number of regions. A three-region model as shown in Fig. (4.2) was the largest to be solved by this method. This permits calculation of the impedance of infinitely long solenoid encircling a hollow tube (or solid cylinder as a special case), allowing for an air-gap between the excitation coil and the conducting tube.

Applying the appropriate boundary conditions, the magnetic field at any radius (r) within the wall of the conducting tube shown in Fig. (4.2), is given as a function of the magnetic field at the outer surface of the tube (H_s) by[4.3]:

$$H(r) = H_s\left\{\frac{G\ I_o(\gamma) + F\ K_o(\gamma)}{G\ I_o(\beta) + F\ K_o(\beta)}\right\} \qquad (4.9)$$

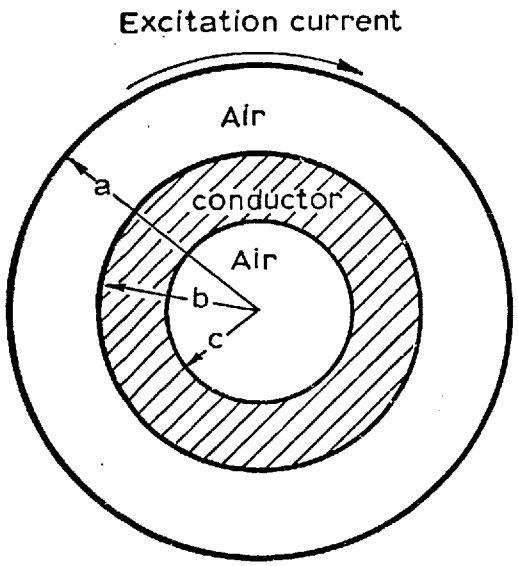


Fig. 4·2 Three-region model

And the current density at any point in the tube wall is given in terms of the current density at the outer surface by[4.3]:

$$J(r) = J_s \left\{ \frac{G\ I_1(\gamma) - F\ K_1(\gamma)}{G\ I_1(\beta) - F\ K_1(\beta)} \right\} \qquad (4.10)$$

Hence the normalised solenoid impedance is given by[4.5]:

$$\frac{Z}{\omega L_o} = \frac{2d\sqrt{j}}{b} \left\{ \frac{G\ I_1(\beta) - F\ K_1(\beta)}{G\ I_o(\beta) + F\ K_o(\beta)} \right\} \eta^2 + j(1 - \eta^2) \qquad (4.11)$$

Where:

$$\alpha = \frac{c}{d}\sqrt{j}$$

$$\beta = \frac{b}{d}\sqrt{j}$$

$$\gamma = \frac{r}{d}\sqrt{j} \qquad c<r<b$$

$$G = K_1(\alpha) + \frac{1}{2}\alpha K_o(\alpha)$$

$$F = I_1(\alpha) - \frac{1}{2}\alpha I_o(\alpha)$$

L_o = the inductance of the solenoidal coil in the absence of the conducting tube.

$$L_o = \frac{1}{2}\mu_o a^2$$

It is quite obvious that the equations (4.9), (4.10) and (4.11) are cumbersome and need standard transformation for its numerical computation.

4.6 Transfer Matrix Surface Impedance Method

Freeman in a series of papers[4.7 - 4.9], showed that the problem of multiregion induction devices can be simplified, especially for large number of regions, by using a transfer matrix technique. Briefly, the field equations are to be solved by using the method of separation of variables and the arbitrary constants to be eliminated to leave the boundary E and H

quantities as unknown variables. The E and H quantities at the region surfaces are then related by a transfer matrix. As an example, the E and H quantities at the points (1) and (2) of the general region m shown in Fig. (4.1) can be related by:

$$\begin{bmatrix} E \\ H \end{bmatrix}_2 = \begin{bmatrix} a_m & b_m \\ c_m & e_m \end{bmatrix}_m \begin{bmatrix} E \\ H \end{bmatrix}_1 \qquad (4.12)$$

Each region may be represented by an equation having the same form as equation (4.12). By'matching' E and H quantities at the boundaries, a chain of transfer matrices can be set up. Hence by introducing a known value of E or H at a point in the chain, all the E and H values may be found.

Applying Freeman's method to the model shown in Fig.(4.1) we get[4.6]:

$$\begin{bmatrix} E_1 \\ H_1 \end{bmatrix} = \begin{bmatrix} T_1 \end{bmatrix} \begin{bmatrix} T_2 \end{bmatrix} \cdots\cdots \begin{bmatrix} T_{N-1} \end{bmatrix} \begin{bmatrix} E_N \\ H_N \end{bmatrix} \qquad (4.18)$$

Where E_m and H_m are the values of E_θ and H_z at radius r_m, respectively.

The elements of the transfer matrix of the general region m are given by:

(i) For non-conducting regions:

$$a_m = \frac{r_{m+1}}{r_m}$$

$$b_m = (j\omega\mu_m/2\ r_m)\ .\ \{r_m^2 - r_{m+1}^2\} \qquad (4.14)$$

$$c_m = 0.0$$

$$e_m = 1.0$$

(ii) For conducting regions:

$$a_m = \gamma_{m+1}\{ I_1(\gamma_m)\ K_o(\gamma_{m+1}) + I_o(\gamma_{m+1})\ K_1(\gamma_m)\}$$

$$b_m = j\omega\mu_m\ r_{m+1}\{ I_1(\gamma_{m+1})\ K_1(\gamma_m) - I_1(\gamma_m)\ K_1(\gamma_{m+1})\}$$

$$c_m = \sigma_m\ r_{m+1}\{ I_o(\gamma_{m+1})\ K_o(\gamma_m) - I_o(\gamma_m)\ K_o(\gamma_{m+1})\}$$

$$e_m = \gamma_{m+1}\{ I_o(\gamma_m)\ K_1(\gamma_{m+1}) + I_1(\gamma_{m+1})\ K_o(\gamma_m)\}$$

Where:

$$\gamma_m = j^{\frac{1}{2}}\ r_m/d_m$$

$$\gamma_{m+1} = j^{\frac{1}{2}}\ r_{m+1}/d_m$$

$$d_m = (1/\omega\mu_m\sigma_m)^{\frac{1}{2}}$$

Attention should be drawn here to the typographical error which appears in equation (15) of reference (4.6). Using the same symbols of this reference, this equation should read:

$$C_n = [j\gamma_n^2 r_{n-1}/\omega\mu_n]\{I_o(\alpha_n) K_o(\alpha_{n-1}) - K_o(\alpha_n) I_o(\alpha_{n-1})\}$$

(iii) The innermost region:

At the innermost region, the relation between E_N and H_N is given by:

$$E_N/H_N = (j\omega\mu/\sigma_N)^{\frac{1}{2}} \cdot I_1(\gamma_N)/I_o(\gamma_N) \qquad (4.16)$$

for a conducting region.

And

$$E_N/H_N = \frac{1}{2} j\omega\mu_N r_N \qquad (4.17)$$

for a non-conducting region.

The distinction of this method lies in its ability to deal with a large number of concentric regions in a systematic way.

4.7 Micro-T Circuit Method

This method, which will be used for the calculation of the resistivity, is an extension to the previously mentioned transfer matrix method.

4.7.1 Theory

Equations (4.3) and (4.4) can be rewritten in the form

$$\frac{\delta}{\delta r}(rE) = -j\omega\mu_o r H \qquad (4.3)$$

$$\frac{\delta}{\delta r}(H) = -\frac{\sigma}{r} rE \qquad (4.4)$$

Comparing these equations with the standard transmission line equations which are:

$$\frac{\delta V}{\delta r} = - Z I \qquad (4.18)$$

$$\frac{\delta I}{\delta r} = - Y V \qquad (4.19)$$

where Z and Y represent respectively the series impedance and the shunt admittance per unit length of the transmission line whose voltage V and current I are related by the equations (4.18) and (4.19).

The similarity between the field equations and the transmission line equations suggests the construction of an equivalent T.L. whose circuit parameters are related to the electromagnetic field quantities as follows:

$$\begin{aligned} V &= rE \\ I &= H \\ Z &= j\omega\mu_o r \\ Y &= \frac{\sigma}{r} \end{aligned} \qquad (4.20)$$

An elementary section of the equivalent T.L. which satisfies equation (4.20) is shown in Fig. (4.3)a. This section will be called a micro-T circuit, a string of these will represent the whole region as shown in Fig.(4.5). It should be noted that an equivalent π instead of T can represent the elementary section Δr as it is already well appreciated from T.L. literature.

4.7.2 Non-conducting region equivalent circuit

For the special case of a non-conducting region, the conductivity is zero, and the shunt resistance of the micro-T circuit will be infinite. The T-circuit then reduces to that shown in Fig. (4.3)b.

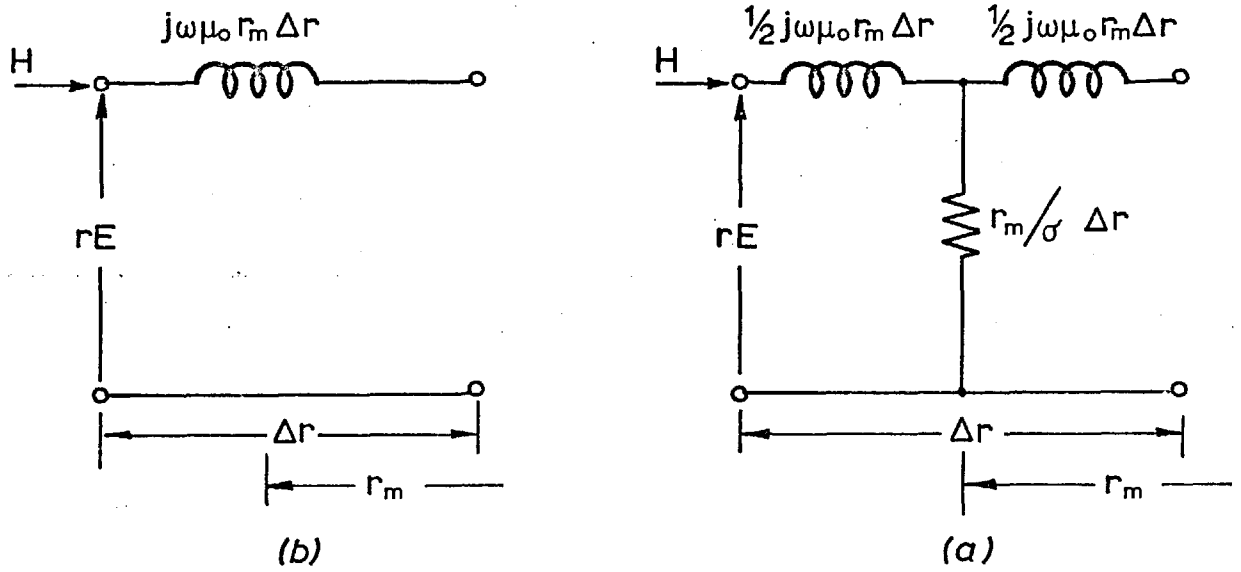


Fig. 4·3 Micro circuit of an elementary subregion
(a) Conducting (b) Air gap

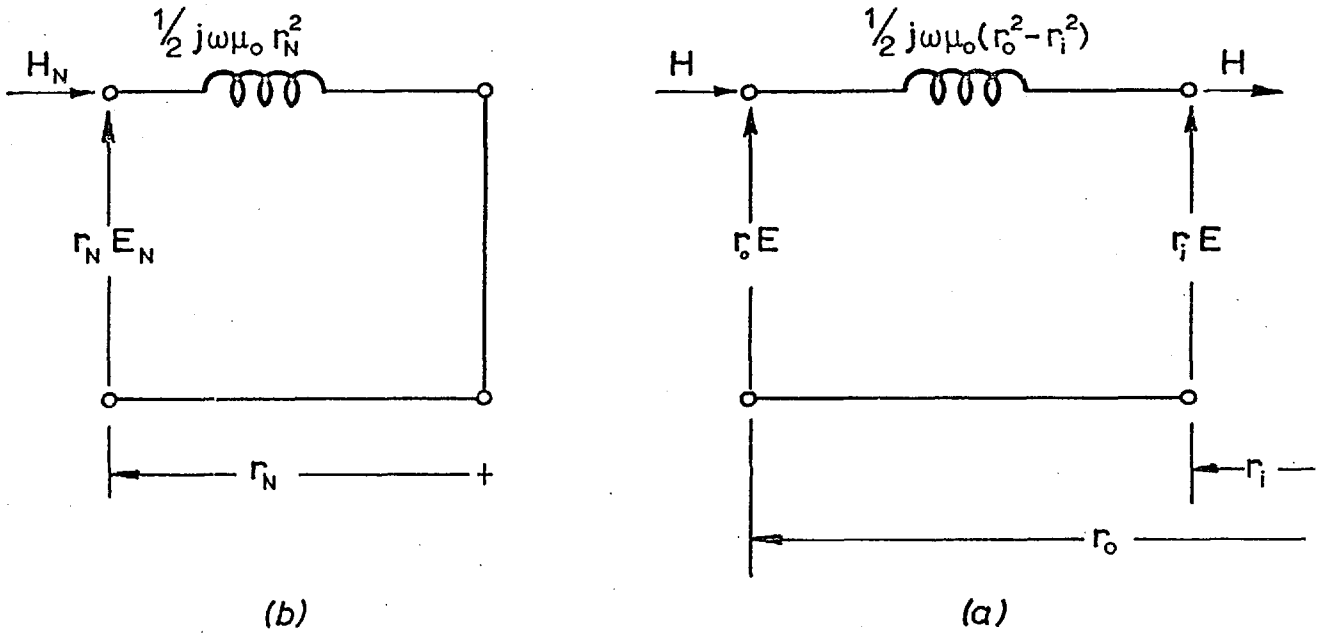


Fig. 4·4 Equivalent circuit of an air-gap region
(a) Air-gap region of r_o /r_i radii
(b) Innermost air-gap region

Now, if the non-conducting region has r_i and r_o as its inner and outer radii respectively, the total reactance which represents the region is given by:

$$X_T = \sum_{\text{over } r_i \to r_o} \omega\mu_o r \, \Delta r \qquad (4.21)$$

And in the limit as $\Delta r \to 0$, the summation can be replaced by an integration as follows:

$$X_T = \int_{r_i}^{r_o} \omega\mu_o \, r \, dr$$

$$= \frac{1}{2}\omega\mu_o \, (r_o^2 - r_i^2)$$

Thus, each air-gap region will be simply replaced by a simple inductive element which depends on the inner and outer radii of the region as shown in Fig. (4.4)a, and is given by:

$$X_{gap} = \frac{1}{2} \omega\mu_o (r_o^2 - r_i^2) \qquad (4.22)$$

Where:

r_i = inner radius of the non-conducting region.

r_o = outer radius of the non-conducting region.

For an air-cored hollow conducting tube, the inner most region - region No. N - is simply air. It can be represented by the inductive reactance X_N as shown in Fig. (4.4)b, and is given by:

$$X_N = \frac{1}{2}\omega\mu_o r_N^2 \qquad (4.23)$$

Hence the ratio between the electric and magnetic fields is given by:

$$r_N E_N/H_N = j X_N$$
$$= \frac{1}{2} j\omega\mu_o r_N^2$$

OR $$E_N/H_N = \frac{1}{2} j\omega\mu_o r_N$$

Which is the same expression as given by equations (4.17) of the transfer matrix method.

4.7.3 Conducting region equivalent circuit

The micro-T circuit of a conducting region will be exactly the same as shown in Fig. (4.3)a. The conducting region will be divided into a large number of elementary sub-regions, each will be represented by one micro-T circuit. Increasing the number of subregions will give a more accurate representation, theoretically an infinite number of such sub-regions will give exact representation. A suitable practical number of sub-regions is the one which requires least computation, and yields a good accuracy.

Fig. (4.5) represents the equivalent T.L. circuit of a conducting region subdivided into h elementary sections each representing a thickness Δr.

$$R_i = (1/\sigma\,\Delta r)\, r_i$$

$$X_i = (1/2\,\omega\mu_o \Delta r)\, r_i$$

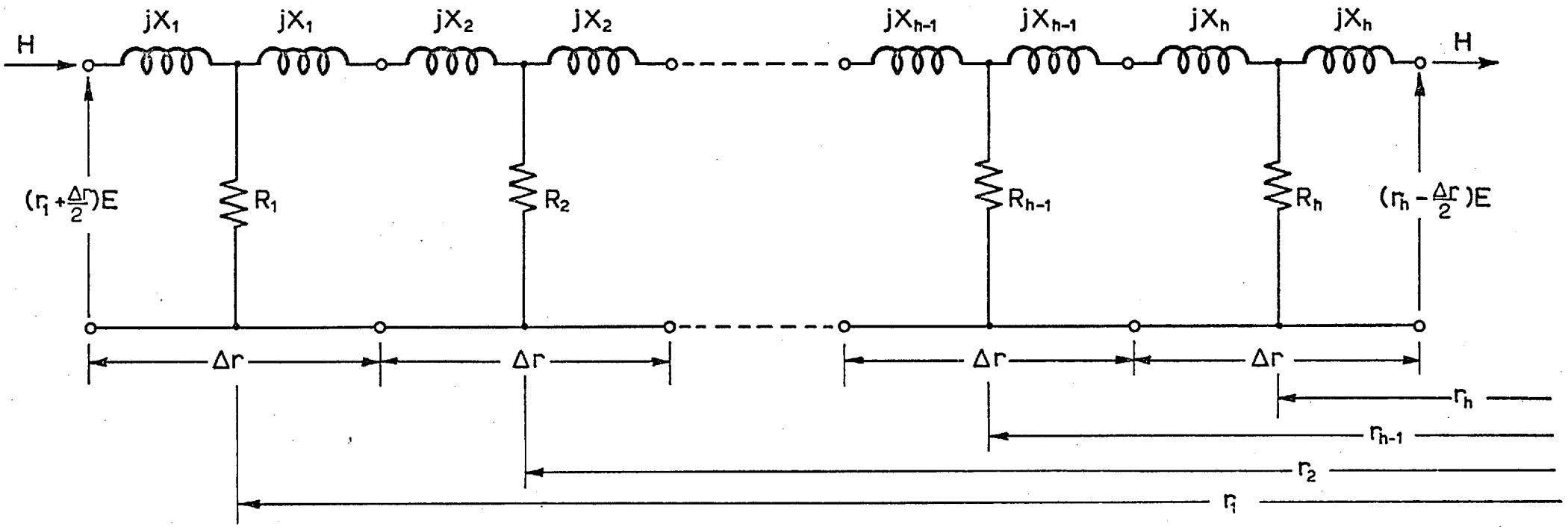


Fig. 4·5 Equivalent circuit of a conducting region divided into (h) subregions

4.8 Criteria for the Choice of the Thickness of the Sub-regions in a Conducting Region

Let us assume that the conducting region is divided into a large number of sub-regions each having a thickness Δr. It is required to estimate the total error obtained in the calculation of the region transfer matrix due to the finite number of subregions.

The micro-T circuit which represents the subregion of thickness Δr is shown in Fig. (4.6)a. Since Δr is usually very small w.r.t. the radius (r), we can assume (r) constant all over the thickness r and equal to the mean radius r_m. The elements of the equivalent circuit are then given by:

$$Z_s = j\omega\mu_o r_m \quad \text{per unit length}$$

$$Z_p = r_m/\sigma \quad \text{per unit length.}$$

Assume now that the same thickness Δr is replaced by a continuous T.L. instead of only one T-circuit, as shown in Fig. (4.6)b. The elements of this transmission line are also calculated at constant radius r_m.

The transfer matrix of one T-circuit shown in Fig. (4.6)a can be written in the form[4.10]:

$$A = \begin{bmatrix} 1 + \tfrac{1}{2} j(\Delta r/d)^2 & j\omega\mu r_m \Delta r\{1 + j(\Delta r/2d)^2\} \\ \sigma\Delta r/r_m & 1 + \tfrac{1}{2} j(\Delta r/d)^2 \end{bmatrix} \quad (4.24)$$

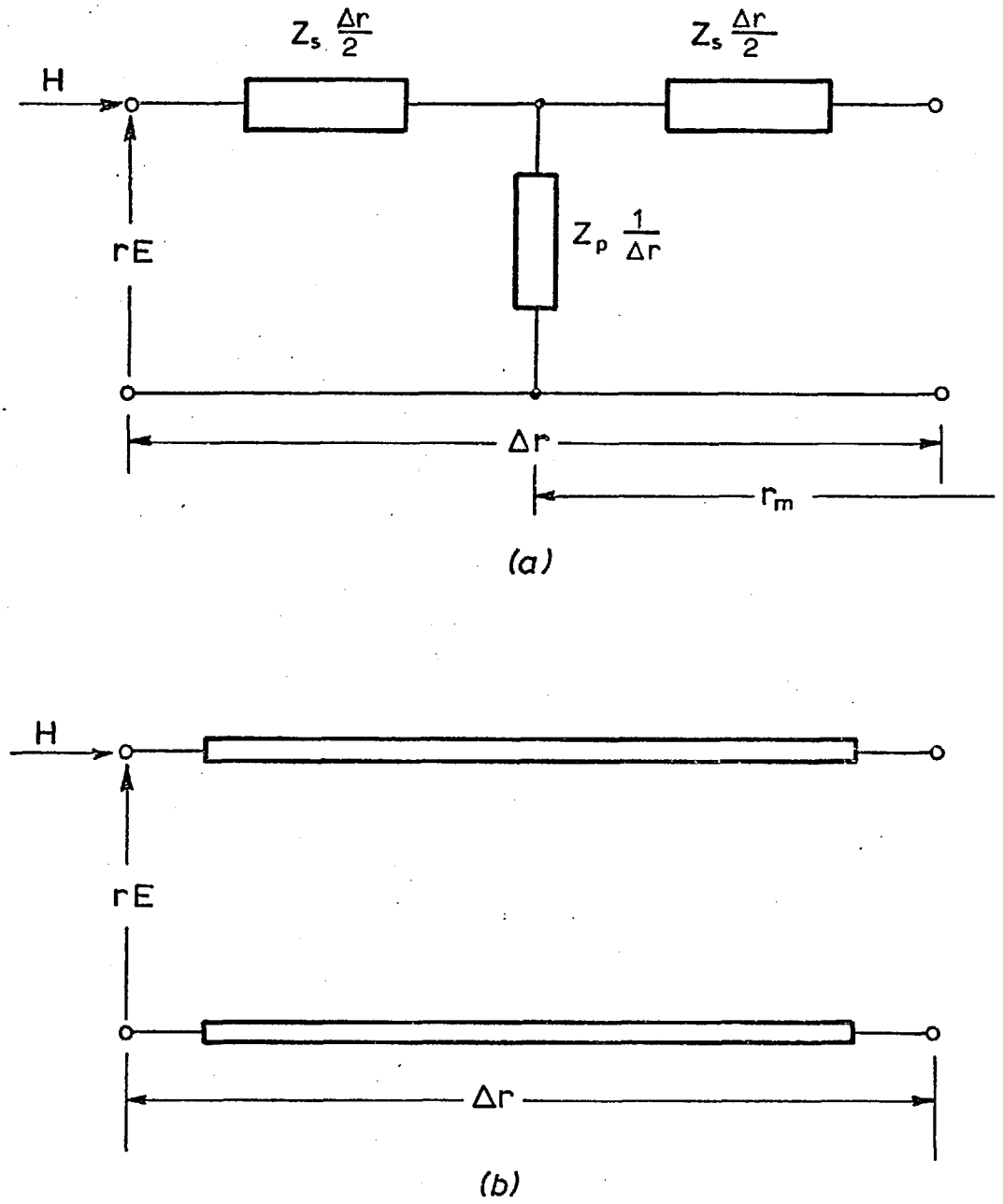


Fig. 4.6 *Equivalent circuit of a subregion thickness Δr of a conducting region.*
(a) One micro-T circuit.
(b) Continuous transmission line.

And the transfer matrix for the T.L. which represents the same thickness Δr is given by[4.10]:

$$A' = \begin{bmatrix} \cosh(\gamma\Delta r) & Z_o \sinh(\gamma\Delta r) \\ 1/Z_o . \sinh(\gamma\Delta r) & \cosh(\gamma\Delta r) \end{bmatrix} \qquad (4.25)$$

Where:

$Z_o = (j\omega\mu/\sigma)^{\frac{1}{2}}$ = ch. impedance

$\gamma = \sqrt{j}/d$ = propogation const.

$d = (\omega\mu\sigma)^{-\frac{1}{2}}$

The hyperbolic functions can be replaced by series expansions which are given by[4.11]:

$$\cosh z = 1 + \frac{z^2}{2!} + \frac{z^4}{4!} + \frac{z^6}{6!} + \ldots\ldots$$

$$\sinh z = z + \frac{z^3}{3!} + \frac{z^5}{5!} + \frac{z^7}{7!} + \ldots\ldots$$

The matrix A' can be rewritten in the form:

$$A' = \begin{bmatrix} a_{11} & a_{12} \\ a_{21} & a_{22} \end{bmatrix}$$

Where: $a_{11} = 1 + \frac{1}{2} j(\frac{\Delta r}{d})^2 + \frac{1}{4!} j^2(\frac{\Delta r}{d})^4 + \frac{1}{6!} j^3(\frac{\Delta r}{d})^6 + \ldots$

$$a_{12} = j\omega\mu r_m \Delta r \{1 + \frac{1}{3!} j(\frac{\Delta r}{d})^2 + \frac{1}{5!} j^2(\frac{\Delta r}{d})^4 + \ldots\}$$

$$a_{21} = \frac{\sigma}{r_m}\Delta r\left\{1 + \frac{1}{3!}\, j\left(\frac{\Delta r}{d}\right)^2 + \frac{1}{5!}\, j^2\left(\frac{\Delta r}{d}\right)^4 + ..\right\}$$

$$a_{22} = 1 + \frac{1}{2}\, j\left(\frac{\Delta r}{d}\right)^2 + \frac{1}{4!}\, j^2\left(\frac{\Delta r}{d}\right)^4 + \ldots$$

Since $\Delta r << d$, terms in $\left(\frac{\Delta r}{d}\right)^4$ and higher order can be neglected, and the matrix A' reduces to:

$$A' = \begin{bmatrix} 1 + \frac{1}{2}\, j\left(\frac{\Delta r}{d}\right)^2 & j\omega\mu r_m \Delta r\left\{1 + \frac{1}{3!}\, j\left(\frac{\Delta r}{d}\right)^2\right\} \\ \frac{\sigma}{r_m}\Delta r\left\{1 + \frac{1}{3!}\, j\left(\frac{\Delta r}{d}\right)^2\right\} & 1 + \frac{1}{2}\, j\left(\frac{\Delta r}{d}\right)^2 \end{bmatrix} \quad (4.26)$$

Let us now define an error matrix (ε) whose elements are the per unit difference of the corresponding elements of the two matrices A and A' . Thus (ε) is given by:

$$(\varepsilon) = \begin{bmatrix} 0\left(\frac{\Delta r}{d}\right)^4 & -\frac{1}{12}\, j\left(\frac{\Delta r}{d}\right)^2 + 0\left(\frac{\Delta r}{d}\right)^4 \\ \frac{1}{6}\, j\left(\frac{\Delta r}{d}\right)^2 + 0\left(\frac{\Delta r}{d}\right)^4 & 0\left(\frac{\Delta r}{d}\right)^4 \end{bmatrix} \quad (4.27)$$

Where:

$0\left(\frac{\Delta r}{d}\right)^4$ represents a series of order $\left(\frac{\Delta r}{d}\right)^4$ and higher powers.

The max. error which occurs in the calculations obtained when the subregion thickness is represented with one T-circuit instead of a continuous transmission line, will be of the order $\frac{1}{6}\left(\frac{\Delta r}{d}\right)^2$.

i.e. ε = per unit error due to each T-circuit.

$$\simeq \frac{1}{6}\left(\frac{\Delta r}{d}\right)^2 \qquad (4.28)$$

If (h) is the number of the subregions which represent a conducting region of thickness (ℓ), the thickness of each subregion is given by:

$$\Delta r = \frac{\ell}{h}$$

The total accumulative error ε_t of this region is given by

$$\varepsilon_t < \varepsilon + \varepsilon(1 + \varepsilon) + \varepsilon(1 + \varepsilon + \varepsilon^2) + \ldots\ldots$$

$$\ldots\ldots\ldots (1 + \varepsilon + \varepsilon^2 + \ldots \varepsilon^{h-1})$$

$$\simeq h\varepsilon + (h - 1)\varepsilon^2 + (h - 2)\varepsilon^3 + \ldots + \varepsilon^h$$

If ε is small enough, all higher powers of ε can be neglected w.r.t. ε

Therefore Total error = $\frac{\ell}{\Delta r} \cdot \frac{1}{6}\left(\frac{\Delta r}{d}\right)^2$

The subregion thickness Δr can be determined according to the degree of accuracy required from the expression:

$$\Delta r < 3.\varepsilon_t.\ \delta.\ \frac{1}{(\ell/\delta)} \qquad (4.29)$$

Where ℓ/δ = the region thickness in skin depths.

δ = the eddy current skin depth ($\delta = (2/\omega\mu\sigma)^{\frac{1}{2}}$)

ε_t = total per unit accumulative error in representing the length (ℓ/δ) by micro-T circuits instead of continuous T.L.

Usually the field components attenuate as they penetrate into the conducting region. If the total accumulative error for the first skin depth into the conducting region is limited to 1%, the relation between the subregion thickness and the skin depth will be: Δr = 3% of skin depth. However, in practice, it is often possible to work with Δr = 5 - 10% of skin depth without undue loss of accuracy.

4.9 Boundary Conditions

The boundary conditions in a quasi-static magnetic field system and in the absence of relative motion between the adjacent regions, can be represented by the two equations[4.12]:

$$\begin{aligned} \bar{n} \times (\bar{H}^a - \bar{H}^b) &= \bar{K} \\ \bar{n} \times (\bar{E}^a - \bar{E}^b) &= 0 \end{aligned} \qquad (4.30)$$

Where:

$\bar{n}$ is the normal to the boundary surface

$\bar{E}^a$, $\bar{E}^b$ the electric field vectors at both sides of the boundary surface

$\bar{H}^a$, $\bar{H}^b$ the magnetic field vectors at both sides of the boundary surface.

$\bar{K}$ = the free surface current density (or current sheet) in amperes per metre, which flow on the boundary surface.

Applying equations (4.30) in our case, when no current sheet lies on the boundary:

$\bar{H}_t$ and $\bar{E}_t$ are continuous

i.e. H_z and E_θ are continuous

For the transmission line modelling, this means that the two lines which represent two regions, adjacent to each other with no current sheet at the interfaces, are to be connected in cascade as shown in Fig. (4.7)a.

When there is any current sheet at the boundary surface, the discontinuity of tangential - $\bar{H}$ component can be represented by inserting a current source as shown in Fig. (4.7)b, whose magnitude is equal to the current sheet amplitude.

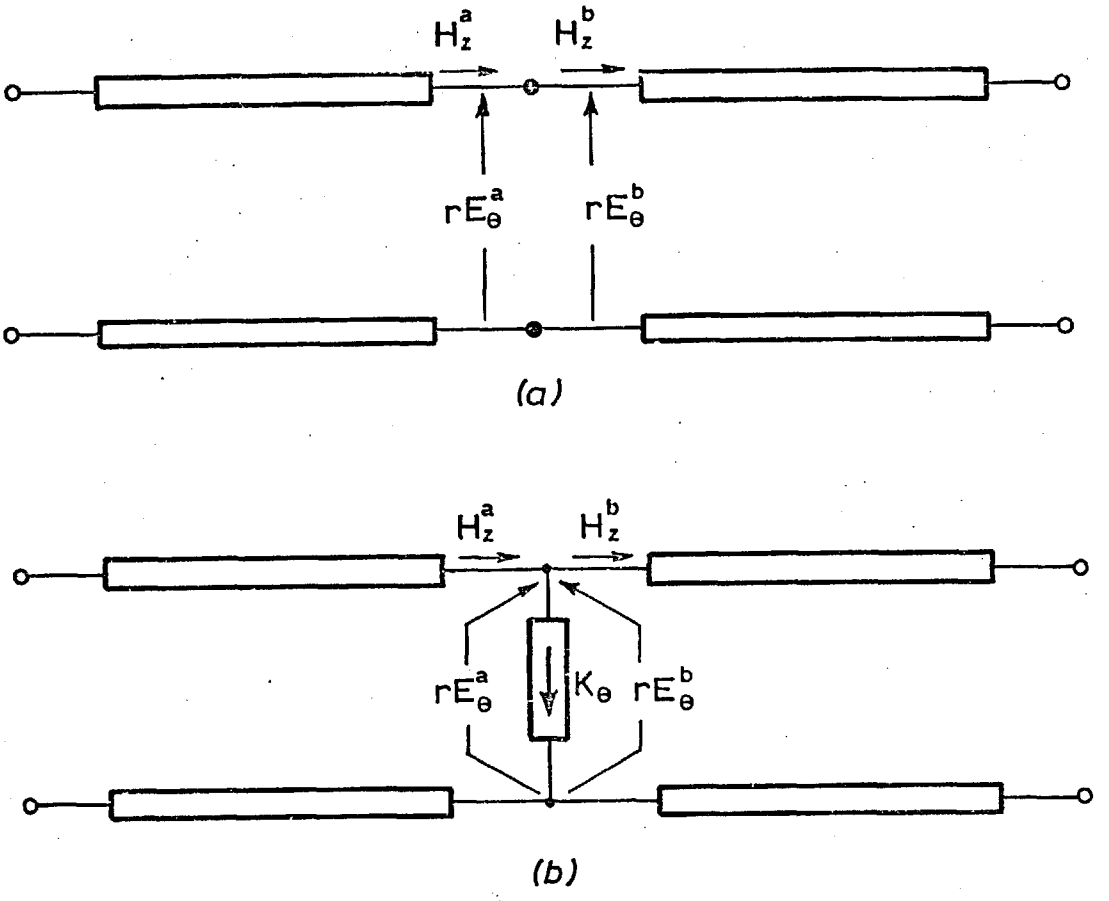


Fig. 4.7 The boundary conditions

(a) No current sheet at the boundary

(b) In presence of current sheet

4.10 Calculation of the Terminal Impedance from the Surface Wave Impedance

The input impedance measured between any two points in the equivalent network gives the ratio between the potential function and the flow function at these points. These two functions, or quantities, are (rE) and (H) respectively.

In the literature, the ratio between E and H is given the name "surface wave impedance". Kron indicated that the

θ-component of the electric field vector $\bar{E}$ is given as a tensor variable $E'_{(\theta)}$ which is equal to rE . Thus, let us define the "tensorial surface wave impedance" as the ratio (rE/H_z). Consequently, any impedance measured from the T.L. model is merely a tensorial wave impedance.

The terminal impedance of the excitation coil can then be calculated from the tensorial surface wave impedance by relating the field quantities E and H to the terminal quantities as follows[4.6]:

$$V = 2\pi aTE$$

and $$I = \frac{\ell}{T} H$$

where T= number of turns.

Therefore $$Z_t = \frac{V}{I} \frac{2\pi T^2}{\ell} \cdot \frac{aE}{H}$$

$$\doteq \frac{2\pi T^2}{\ell} \cdot Z_s(a) \qquad (4.31)$$

Where: $Z_s(a)$ = The tensorial surface wave impedance measured at the excitation mean radius.

It should be noted here that the terminal impedance calculated from equation (4.31) does not include the a.c. resistance of the solenoid winding. In fact the voltage V which appears in this equation can be measured at the terminals of a shadow winding which has the same number of turns as the excitation winding.

4.11 Conductivity Measurement

In section (4.7), the theoretical treatment of calculating the impedance of an infinitely long solenoidal coil encircling an infinitely long conducting tube was developed. The associated equivalent circuit shows that the conductivity of the core material is one of the major factors which affects the impedance value.

The objective of this section is to show how the conductivity of a cylindrical smaple can be obtained reasonably accurately from a knowledge of the input impedance of a solenoidal coil which encircles the sample.

The procedure can be summarized in the following steps:

(i) The input impedance of the solenoidal coil which encircles the conducting sample is to be measured experimentally for different values of the supply frequency. The range of test frequencies can be determined according to the test specimen dimensions as well as its average value of conductivity, as will be shown later in section (4.11.3).

(ii) For different values of assumed conductivity, which lies within the conductivity range supplied by the manufacturers, the input impedance frequency response is to be computed numerically. The frequency

range for the computed results, could be the same used for the experiment.

(iii) Plot both, the experimental results, and a family of numerically computed impedance curves on the same graph. The conductivity of the cylindrical sample, will then be the one which corresponds to the theoretically calculated curve which matches the experimental points.

It is to be noted that, the previous procedure assumes a knowledge of the approximate value of the conductivity of the cylindrical sample. However, if the conductivity is not known at all, an experimental step must precede the previous steps in order to estimate its value.

This can be done as follows:

(i) According to the sample dimensions, a value of (b/d) which corresponds to maximum value of (R/ω) can be estimated from curve shown in Fig. (4.10).

(ii) The frequency f_m which corresponds to $(R/\omega)_{max}$ is to be determined experimentally.

The average value of conductivity σ, can then be estimated from the equation:

$$\sigma_{av} = \frac{b^2}{2\pi\mu f_m}\left(\frac{d}{b}\right)^2 \qquad (4.32)$$

Where:

b outer diameter of the sample.

This average value, σ_{av}, can be used as a starting point, and the whole process reported earlier in this section is to be followed to obtain the value of the conductivity σ to an estimated accuracy of 1%.

4.11.1 Experimental set up

Four aluminium alloy specimens with different dimensions as indicated in the Table below, were tested.

Specimen	Inner radius (m)	Outer radius (m)	Thickness/outer radius
Solid bar	0.0	0.0254	1.0
Tube 1	0.019	0.038	0.5
Tube 2	0.0221	0.0254	0.13
Tube 3	0.0664	0.0757	0.123

For the first three samples, the excitation winding was a single layer solenoid, 1.155 m in length and of radius 0.0485 m. For the fourth sample, the excitation coil was wound directly on the conducting tube, separated from it by a thin layer of insulation.

In all the cases, the excitation winding was supplied from a variable frequency motor/alternator set. The frequency was monitored using an oscilloscope and a calibrated oscillator.

The electric field E near the outer radius of the conductor, was measured by means of an E-search coil. The E-coil consists of 200 turns of very thin wire wound round the conducting tube. The magnetic field H was calculated from the relation :

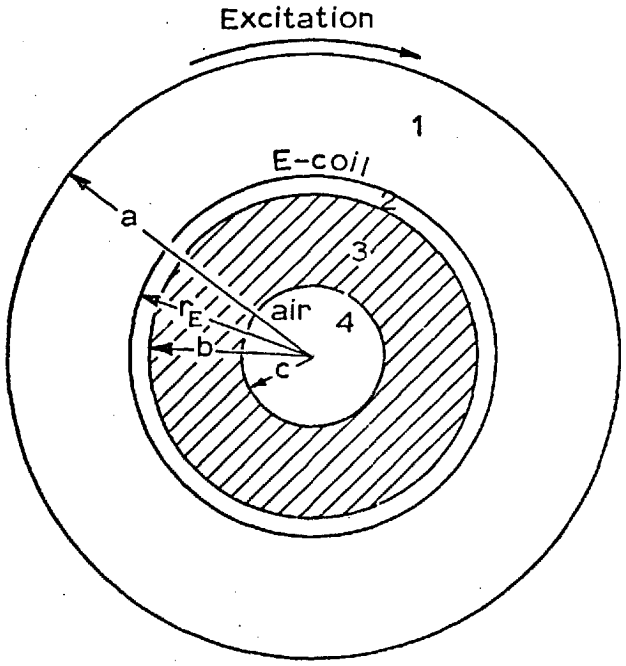
$$H = \frac{T}{\ell} I \qquad \text{amperes/m}$$

As a check, a small H coil was inserted in the gap between the solenoidal coil and the conducting cylinder. The H values, so obtained, agreed very closely.

The phase angle between E and H was measured using a phase angle meter.

4.11.2 Equivalent circuit and method of computation

The equivalent circuit which represents the experimental model is shown in Fig. (4.8)b. The locations of the E-search coil and the excitation coil are shown in Fig. (4.8)a. The position of the E-coil was chosen to be immediately round



(a)

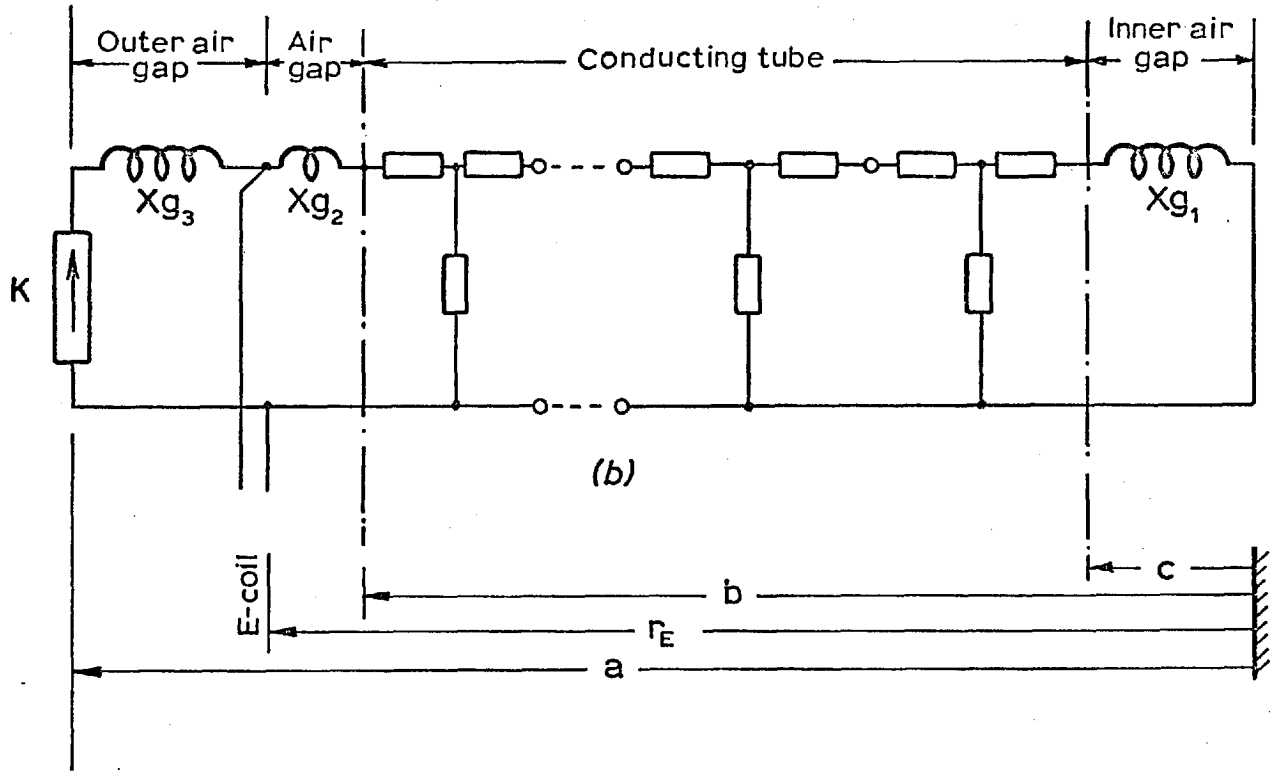


Fig. 4·8 Experimental model
(a) Schematic diagram
(b) Equivalent circuit

the cylindrical sample to ensure a very small air gap, which represents the insulation layer, in order to facilitate the measurement of the phase angle with reasonable accuracy. On the other hand, if the E-coil was placed at the excitation radius, the input surface wave impedance would be highly 'inductive', which would result in poor accuracy when calculating its 'resistive' component.

Based on the equivalent circuit shown in Fig. (4.8)b, the tensorial surface wave impedance seen at the E-coil mean radius could be calculated systematically as follows:

(i) Calculate the inductive reactance of the inner-most air-gap region (if any) X_{g_1} from equation (4.23).

(ii) Specify the maximum tolerance error ε_t, then calculate the thickness and the number of the required micro-T circuits to represent the conducting region.

Equation (4.29) suggests that a subregion thickness of about 5% of the depth of penetration ($d^2 = 1/\omega\mu\sigma$) will limit the error to less than 1%.

(iii) Generate the elements of the individual micro-T circuits, assuming that for each T-circuit the radius is constant all over the thickness Δr and equal to its mean value.

Add the elements of the conducting region equivalent transmission line in series and in parallel, according to the circuit confirguration, starting from the inductive reactance X_{g_1} and working towards X_{g_2}.

(iv) The impedance calculated after adding X_{g_2}, represents the tensorial surface wave impedance as seen at the mean radius of the E-search coil. X_{g_2} could be calculated from the expression given in equation (4.22).

The tensorial surface wave impedance at the excitation radius could be computed by adding jX_{g_3} to the value calculated from the last step.

Note: Usually the air-gap between the E-search coil and the outer radius of the conducting region is very small. Its effect on the calculation of the input impedance is negligible at low frequencies. At high frequency, the skin depth being so small, the flux trapped in this air region may be comparable with the flux penetrating into the conducting region. This would result in certain inaccuracy. A discussion of this problem is fully reported by Freeman in reference (4.6).

4.11.3 Choice of the test frequency

The method which was described in section (4.11) for accurate determination of the conductivity of a cylindrical sample required testing the experimental model for different frequencies.

The choice of the test frequencies is not quite arbitrary, since the relation between impedance and frequency is not generally linear.

The impedance of an infinitely long solenoid closely encircling an infinitely long conducting solid cyclinder can be conveniently normalised to its corresponding value when it is air-cored. The normalised impedance diagrams are then plotted as shown in Fig. (4.9). Examining these normalised impedance diagrams shows that the corresponding change in the real and imaginary components of $(\frac{Z}{\omega L_o})$ with frequency depends mainly on two factors:

i The frequency itself and the conductivity of the core material. Their effect is been introduced by a single quantity (b/d).

ii The per unit thickness of the tube wall referred to the outer diameter of the sample.

Generally, for small values of (b/d), the real component of $(z/\omega L_o)$ increases very quickly, almost linearly, with increase

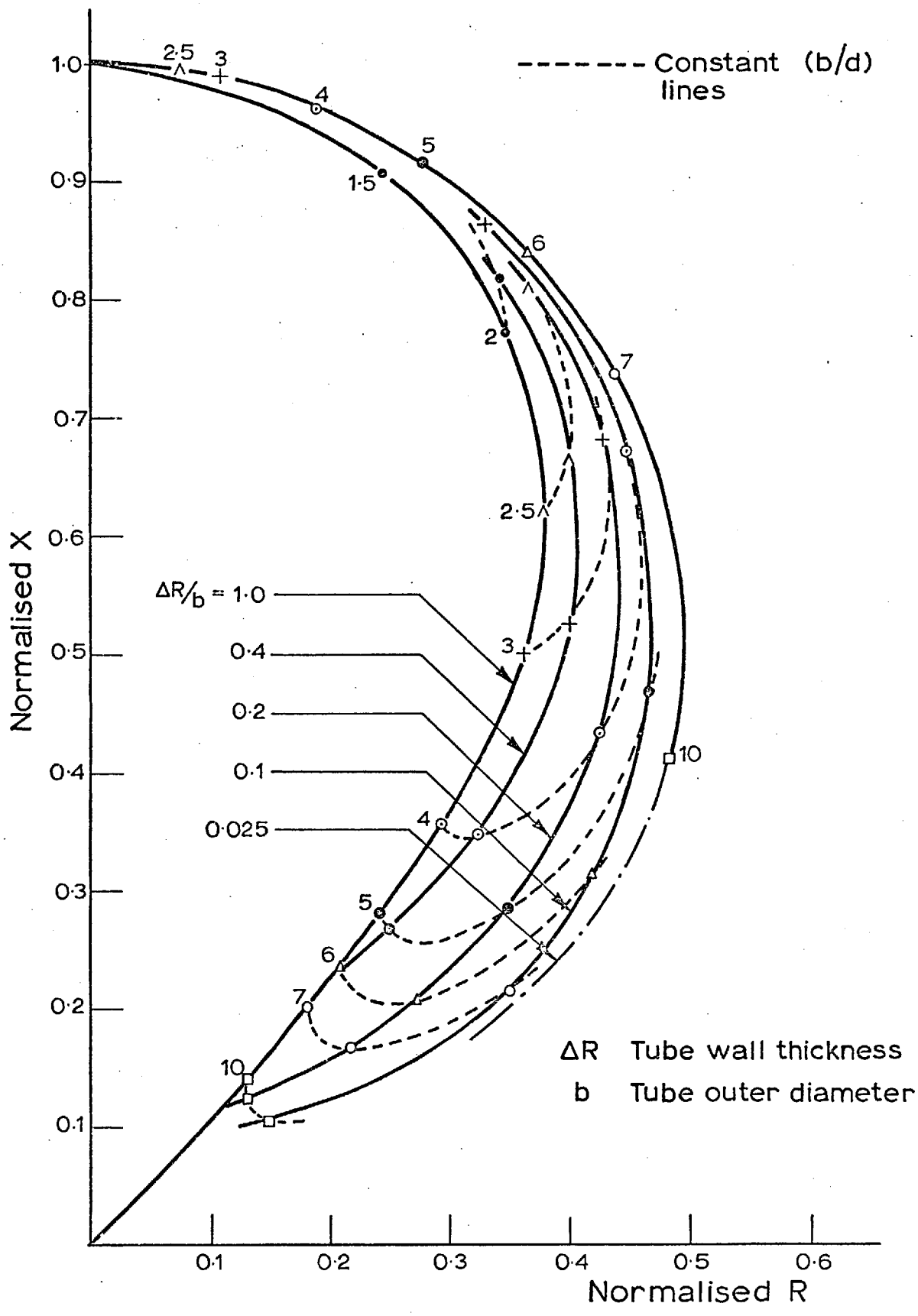


Fig. 4·9 Normalised impedance diagrams for infinitely long solenoid encircling conducting tubes having different wall thickness.

in b/d value. While the corresponding imaginary component drops but not as fast as the change in (R/ω). For very large values of (b/d), the percentage change in both real and imaginary parts of $(Z/\omega L_o)$ is almost the same. However, the rate of this change with increase in b/d is much less than for small values of b/d. Moreover, the points on the impedance diagram which correspond to different high values of (b/d) are crowded and so close that the resolution is very poor. Keeping all these things in mind, it was thought that an adequate range of test frequencies could be chosen such that the frequency which corresponds to the maximum value of $(R/\omega L_o)$ is included in the range. The lower and upper limits of this frequency range are then below and above this frequency, such that $(R/\omega L_o)$ reaches 60-70% of its maximum value at the both ends of the frequency range.

For this reason, a curve was plotted in Fig. (4.10) in order to estimate the appropriate working range of (b/d) for different values of the tube wall thickness. It should be noted that for a very thin tubes, it is inevitable to work with large values of (b/d). Consequently, the small air-gap between the tube outer diameter and the E-search coil, will affect the imaginary part of $(Z/\omega L_o)$ specially near the upper limit of the frequency range. In such a case it is advisable to push the lower frequency limit down, and to rely on the real part of $(Z/\omega L_o)$ curves specially near the upper limit of the frequency range.

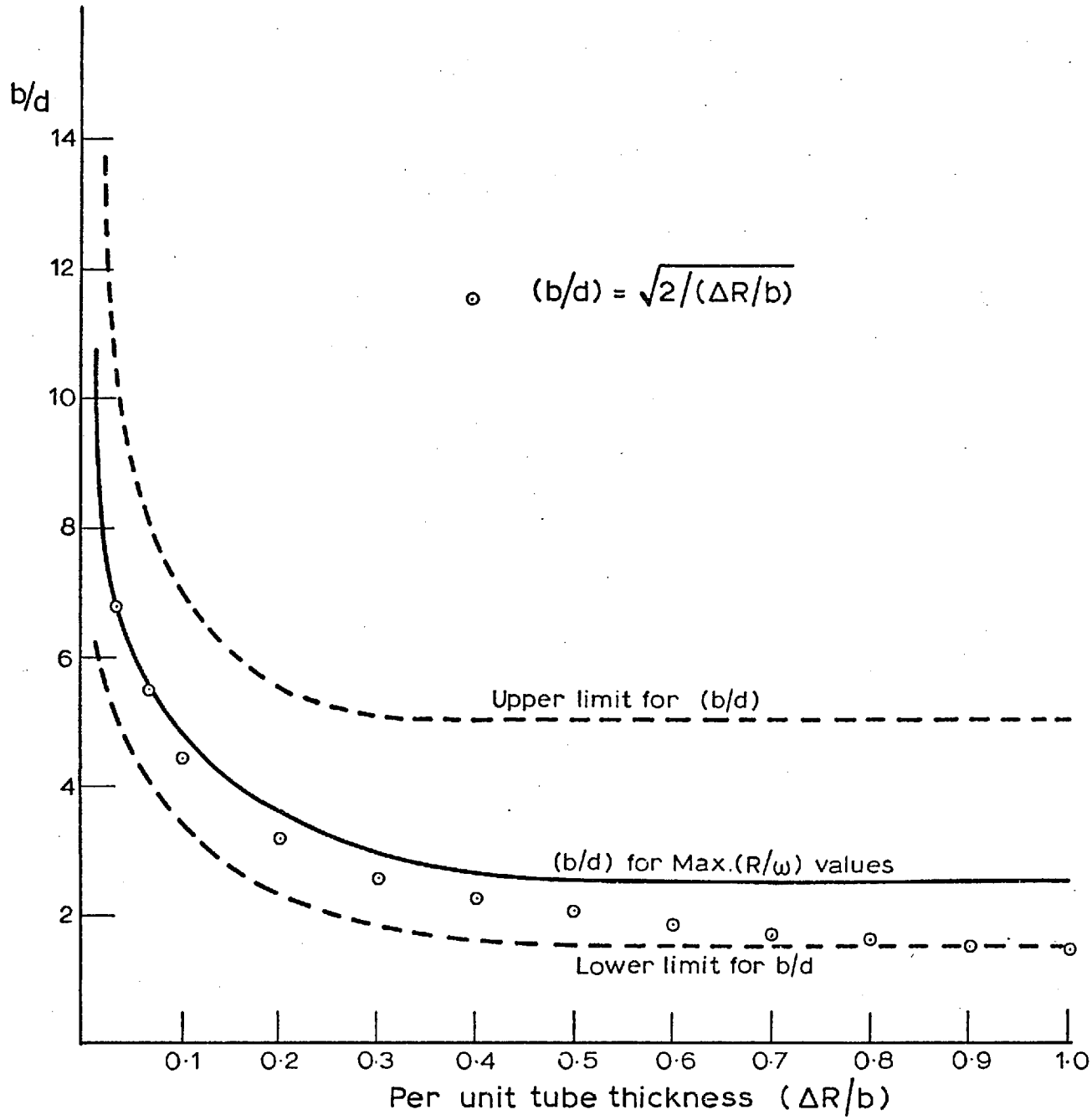


Fig. 4·10 Range of (b/d) values for maximum resolution.

The dotted lines which appear in Fig. (4.10) are drawn for a constant value of $(R/\omega L_o)$ which corresponds to approximately 60% of its maximum value.

4.11.4 Approximate representation of very thin conducting tubes

If a very thin conducting tube is considered, i.e. if $R \ll b$, the conducting region can be represented by only 'one' micro-T circuit, thickness Δr. Furthermore, the two inductive elements which appear in the series branches of the micro-T circuit could be neglected w.r.t. the large inductive element which represents the air core of the tube. The equivalent circuit reduces to:

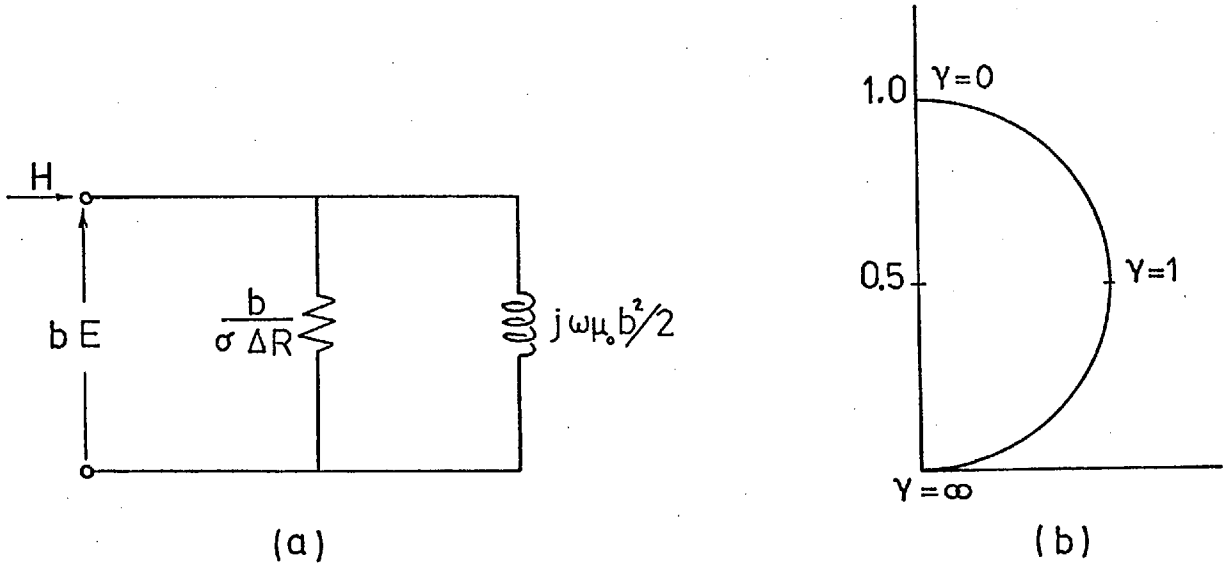


Fig. 4.11: Very thin conducting tube

(a) Equivalent circuit. (b) Normalised impedance locus.

The normalised input impedance as calculated from the above circuit is given by:

$$(Z/\omega L_o) = j/\{1.0 + j\gamma\} \qquad (4.33)$$

Where

$$\gamma = 0.5\ (b/d)\ (\Delta R/d)$$

The locus described by $Z/\omega L_o$ is a circle whose radius is 0.5 and centre (0.0, j0.5) as shown in Fig. (4.11)b.

The point which corresponds to the max. $(R/\omega L_o)$ value is now defined by $\gamma = 1$. That is, (b/d) which corresponds to max. $(R/\omega L_o)$ can be obtained from the following relation:

$$(b/d) = \sqrt{2.0/(\Delta R/b)} \qquad (4.34)$$

The values of (b/d) as obtained from equation (4.34) are plotted for different values of $(\Delta R/b)$ in Fig. (4.10).

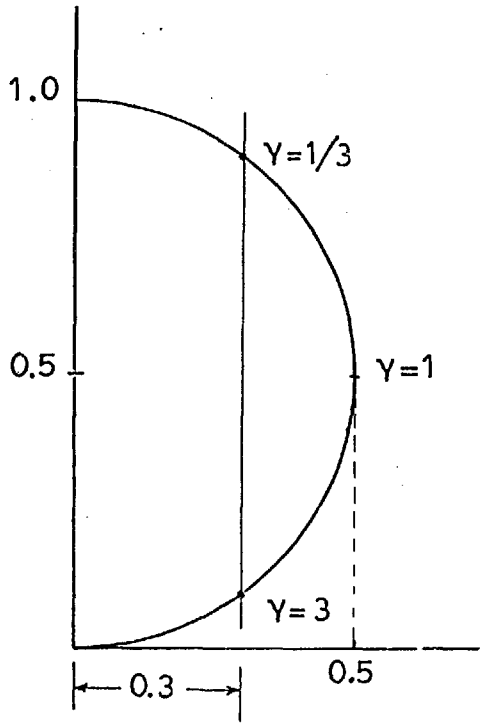
Examining Fig. (4.10), one can conclude that for values of $(\Delta R/b) < 0.07$, the value of (b/d) for max $(R/\omega L_o)$ could be obtained directly from equation (4.34). For other values of $(\Delta R/b)$, we can use the graph of Fig. (4.10) to estimate (b/d). However, as a rule of thumb we can take:

$$b/d = 2.5 \quad \text{for} \quad \Delta R/b > 0.4$$

$= \sqrt{2.0/(\Delta R/b)}$ for $\Delta R/b > 0.4$

Similarly, the upper and lower limits of (b/d) which correspond to 60% of $(R/\omega L_o)_{max}$ are given for very thin tubes by:

$\gamma=3$ and $\frac{1}{3}$ respectively.



Again, as a rule of thumb,

for $R/b > 0.4$: $1.5 < (b/d) < 5.0$

$R/b < 0.4$: $(1/\sqrt{3})\sqrt{2/(\Delta R/b)} < (b/d) < \sqrt{3}\sqrt{2/(\Delta R/b)}$

4.12 Test Results: Diagrams and Discussions

The materials of the test specimens were aluminium alloys whose conductivity, as obtained from the manufacturers data, varied between 2.55 - 2.95 x 10^7 mho/metre. Calculations were performed for nine different values of conductivity, lying in this range, starting from 2.55 x 10^7 with steps of 0.05 x 10^7, i.e. a step which corresponded to an approximate change of 2% in the conductivity value.

Typical test results for only one specimen (0.0254/0.0221m tube) are shown in Figures (4.12) to (4.15).

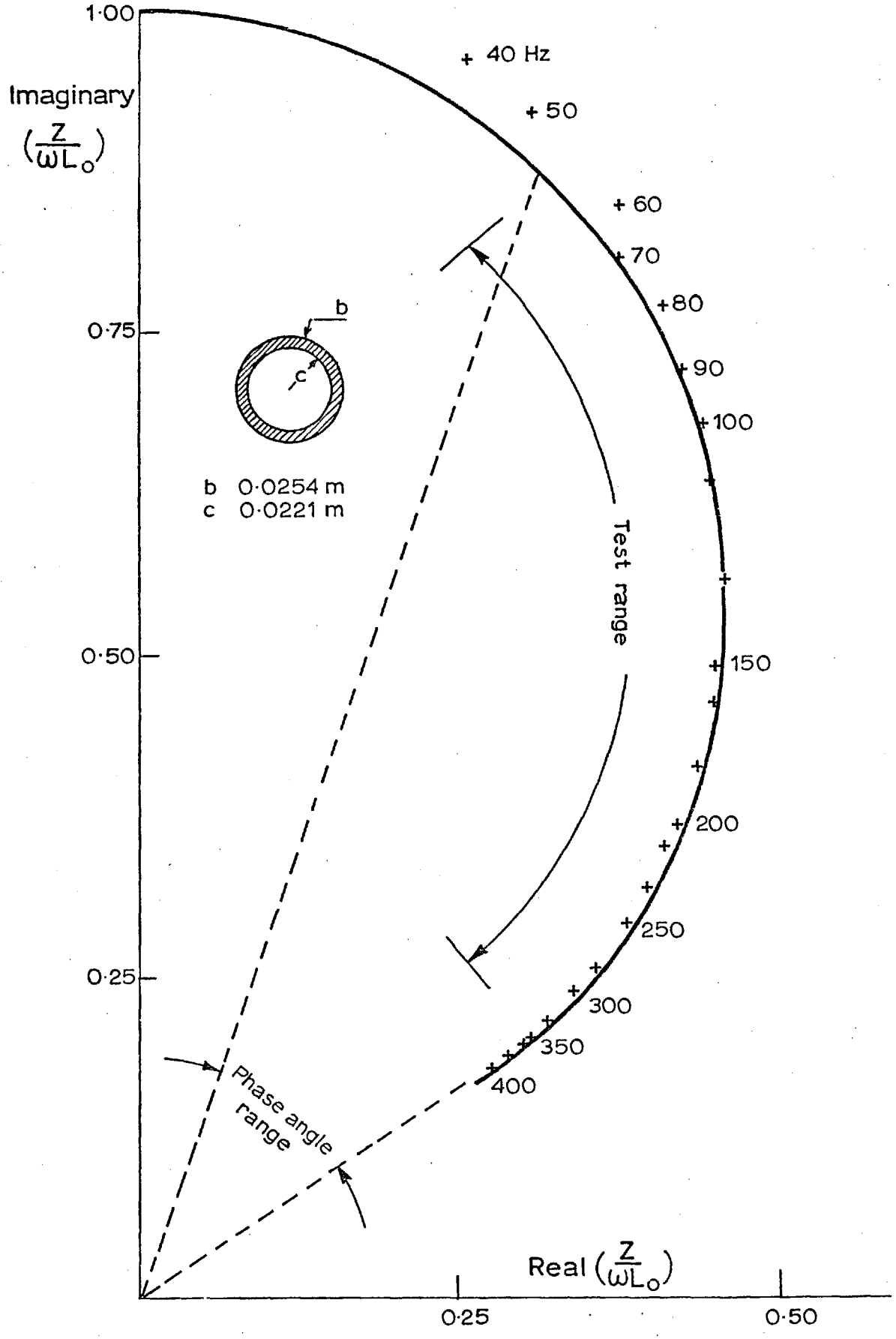


Fig. 4·12 Normalised impedance diagram

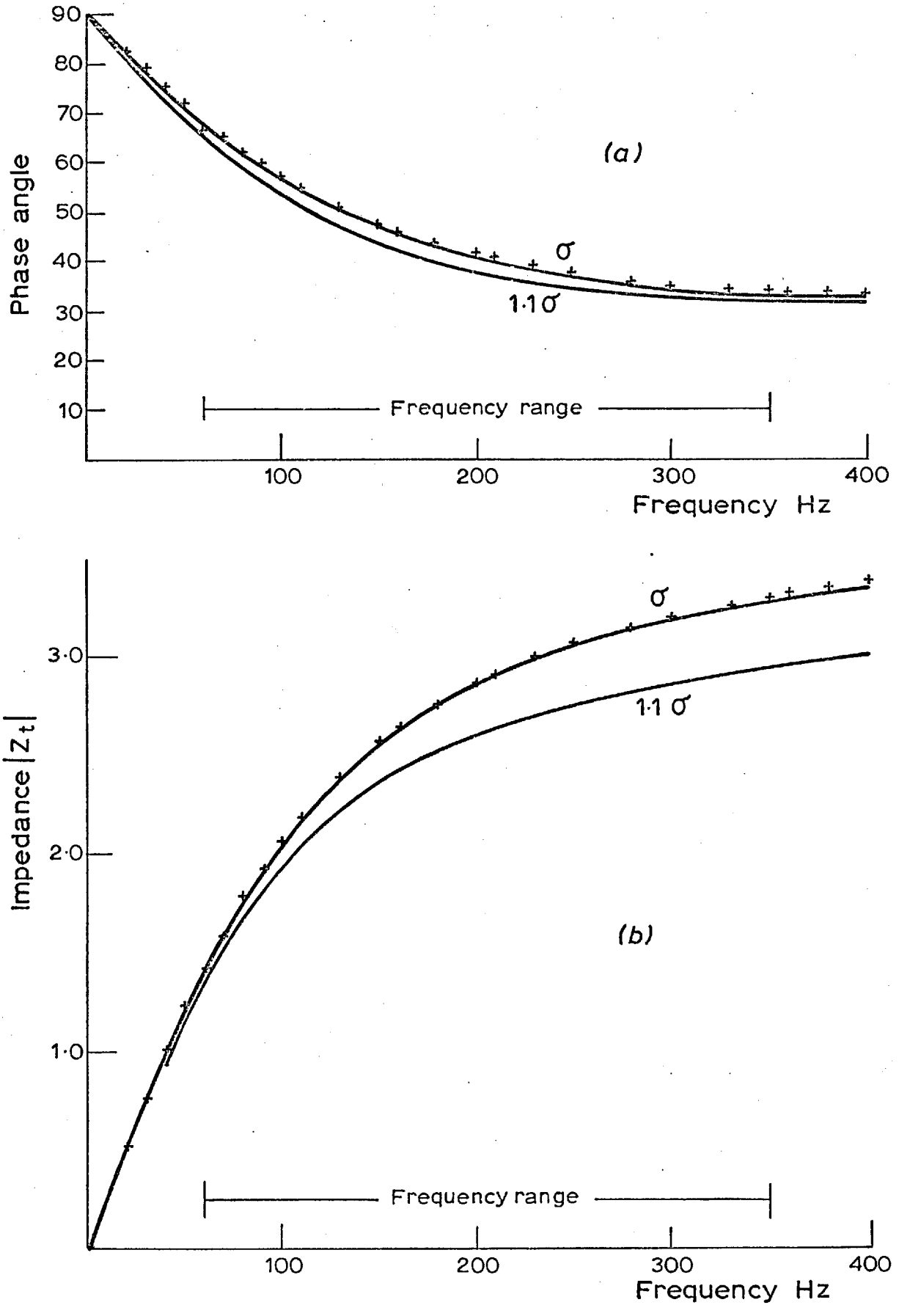


Fig. 4·13 Impedance variation with frequency
(a) Phase angle (b) Amplitude

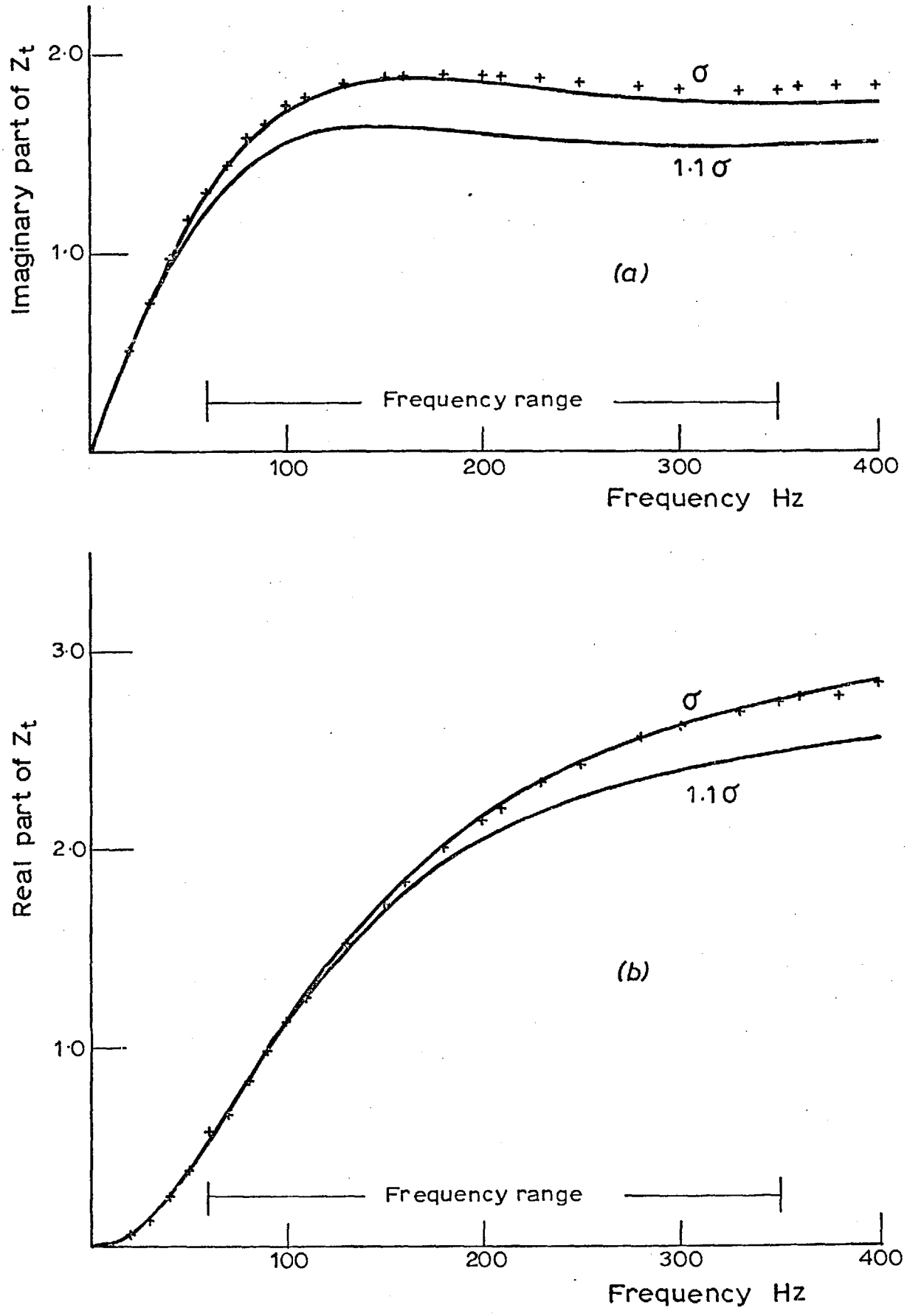


Fig. 4·14 Resistance and reactance variation with frequency
(a) Reactance (b) Resistance

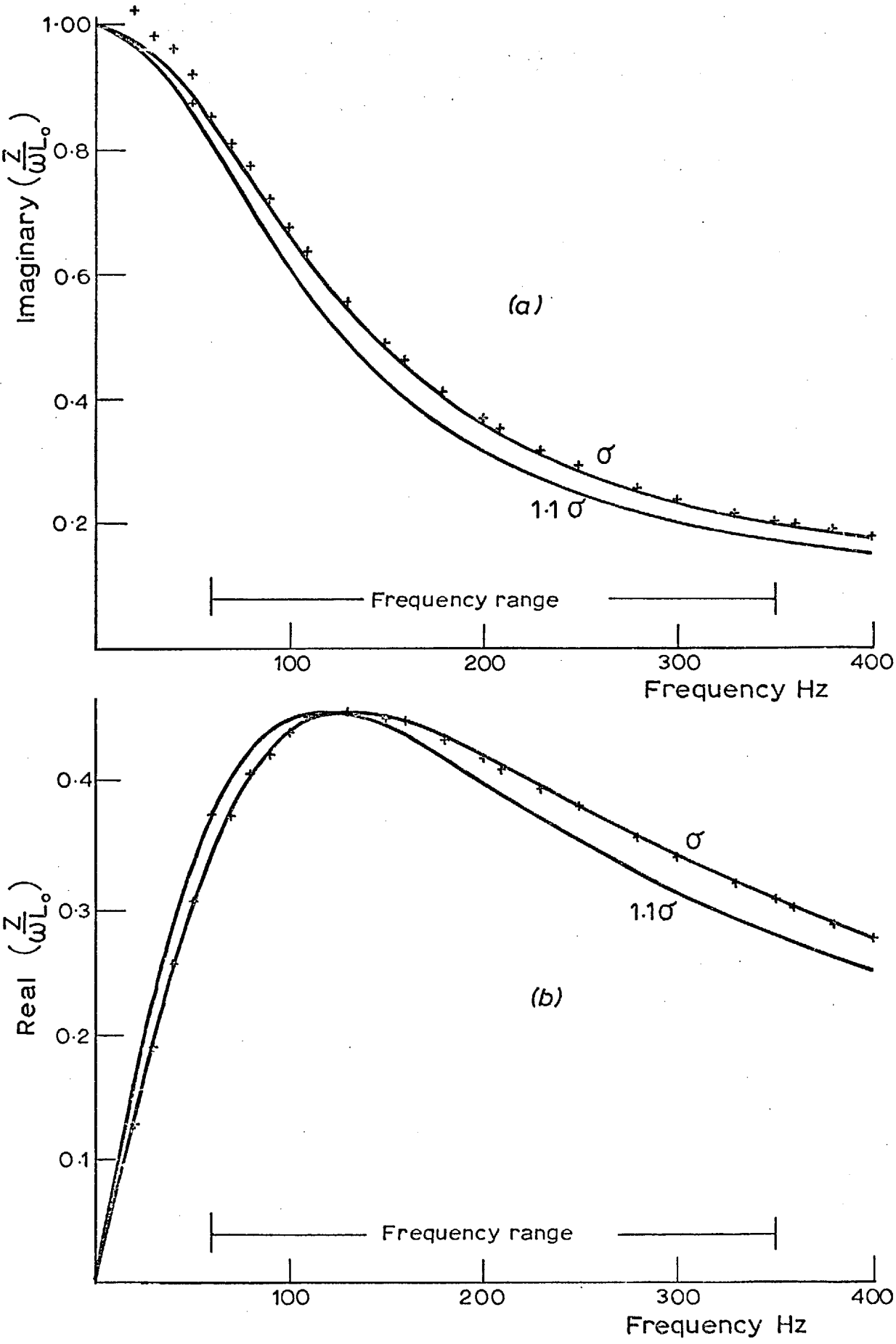


Fig. 4·15 Normalised impedance variation with frequency
(a) Reactance (b) Resistance

Instead of plotting all the computed curves, only those which match the experimental points are shown. In addition, to show the effect of varying the conductivity value, the relevant computer results for an increase of 10% in σ are shown as well.

Examining the graphs shown in Figures (4.12) to (4.15), one can conclude the following points:

- In the first portion of the frequency response curves, the impedance, its real and its imaginary components, increase almost linearly with increase in the frequency. However, the change of these quantities with conductivity is too small to make sensible deductions. As the frequency increases towards its upper limit, the corresponding impedance plots for different values of conductivity separate slightly allowing a good judgement of which theoretically computed curve fits the experimental results.

  The diagrams clearly show that the conductivity could be easily obtained from the comparison of the theoretical and experimental points to an accuracy of about 1 or 2%.

- As far as the phase angle plots are concerned, the diagram shown in Fig. (4.13)a indicates that the angle changes by about 10% according to change of 10% in σ. The maximum change occurs within the chosen range of test frequencies.

- The normalised real component of the terminal impedance exhibits a steep rise as the frequency increases from zero. This rise becomes steeper as the conductivity increases. The normalised R then reaches a maximum value, after which it starts to decrease. The rate of decrease is much less than the rate of rise. This indicates that at low frequencies any error or uncertainty in measuring the test frequency would have a far greater effect than it could have near the upper frequency limit.

- The normalised reactance curves decrease smoothly with increase in the frequency, specially within the test frequency range allowing good resolution all over the range.

In general, it appears that the resolution of the different frequency response curves becomes better near the higher limit of the frequency range.

4.13 Conclusions

The problem of solving the electromagnetic field equations of an infinitely long mathematical model which consists of multilayer concentric cylinders with circumferentially directed excitation currents has been discussed. It was

shown that although the problem itself is not new, the method adopted in this chapter was not used before to solve such a problem.

The method of modelling the physical problem is called the 'micro-T circuit' approach. It extends the previously published transfer matrix surface wave impedance technique, with the advantage of eliminating the necessity of using Bessel functions. This in turn makes the solution simpler and even within the capacity of some available programmable calculators.

It was shown that the method is quite general, and is capable of solving problems involving any large number of concentric cylinders with the possibility of having more than one circumferential excitation current sheet acting at different radii.

A literature review indicates the practical importance of the special case of three or four region models. For example, this model is usually employed for the theoretical treatment of non-destructive eddy-current testing of cylindrical specimens or for the calculation of the impedance of long solenoid encircling either a solid cylinder or a hollow tube, which may be fully or partially filling the solenoid.

The method described in this chapter utilizes the idea of replacing each region with an equivalent 'transmission line".

The non-conducting regions, such as air-gaps, were found to be simply represented by an inductive reactance whose magnitude depends on the inner and outer radii of the region. The conducting regions on the other hand, were found to be replaced by 'non-uniform' or 'tapered' transmission lines. The micro-T circuit technique discretizes this continuous lines to a number of T-circuits in cascade. Each T-circuit will then represent an elementary sub-region. The number of the elementary subregions in any one region, i.e. the number of the micro-T circuits representing one T.L. was found to be such that the sub-region thickness is approximately 5% of the 'depth of penetration'. This will confine the error in the calculation to about 1% or less.

A method was suggested for determining the conductivity of conducting solid cylinders or hollow tubes whose order of conductivity is approximately known. An electromagnetic equivalent circuit was developed. Four cylindrical samples, with different geometrical dimensions, were tested for experimental confirmation of the theoretical analysis.

It was shown that the frequency range required for the frequency response tests is approximately defined by:

(i) $1.5<(b/d)<5$ for thick tubes of 40% wall thickness or larger.

(ii) $\sqrt{(2/3)/(\Delta R/b)} < (b/d) < \sqrt{6/(\Delta R/b)}$ for thin tubes of less than 40% wall thickness, i.e. $(\Delta R/b) < 0.4$.

For very thin tubes, care must be given to the seemingly small gap between the specimen and the E-search coil, especially at high frequencies.

CHAPTER 5

Induction Devices having Circumferentially Directed Excitation Currents - Finite Length Model

1 Introduction

The analysis reported in Chapter 4 assumes that both the conductor and the excitation current distribution extends to infinity in the axial direction. The close agreement between the experimental and computed results suggests that the assumption is reasonable if the ratio between the axial length of the excitation and its radius is very large. In some applications, however, this ratio is not large enough and the finite length effects of the excitation must be taken into consideration. This includes all the applications mentioned in section (4.3.2) above, when the axial length of the excitation coil is of the order of, or less than, its radius. Among the first who introduced the finite length effect in calculating the inductance of a 'current sheet', air-cored solenoidal coil, was Nagaoka[5.1]. Making use of elliptic integrals, Nagaoka developed an expression for the self inductance of the finite length coil as a fraction of the self inductance per unit length of an infinitely long solenoid. This fraction has since become known as the 'Nagaoka factor'.

Moullin[5.2], in 1949, solved the same problem of finding the self inductance of finite length coil, by a 'new' means. He solved the problem in terms of Bessel functions instead of elliptic integrals. His method of solution was based on finding the magnetic field vector $\bar{H}$ due to an infinite succession of uniform sheets on a common axis, each of a length equal to the coil length, and separated from one another with a pitch (g). The current in any particular sheet is in anti-phase to the current in its two immediate neighbours. To find the inductance of an isolated solenoid, Moullin permitted the pitch (g) to be large compared with both the length and the radius of the solenoid that the mutual inductance between the solenoid and its two immediate neighbours should become negligible.

The work by Moullin, prompted Phillips[5.3] to calculate the change of inductance when a single-layer solenoid is placed coaxially inside a cylindrical screening can. In his analysis, Phillips assumed the screen to be a perfect conductor, where the electro-magnetic field at radii greater than the screen mean radius was zero everywhere. In such a way, the screen as well as the coil itself were replaced by two current sheets, each acting at its corresponding mean radius. Because the screen was assumed a perfect conductor, the expression for the inductance was found to be independent

of the operating frequency, the thickness of the screen or the conductivity of the screen material. Comparing his results with those obtained experimentally by Bogle[5.4], who obtained a simple formula for the fractional change of inductance of a coil when it is screened, Phillips found a close agreement over a wide range of (coil length/coil radius) ratios.

In a series of papers, Butterworth[5.5 - 5.7] calculated the high-frequency resistance of an isolated single layer solenoid. He did not replace the excitation winding by an equivalent current sheet, on the contrary, he considered each turn and calculated the eddy current losses in it due to the passage of alternating current. Due to the fact that the coil winding is composed of certain number of turns, each turn will be immersed in the magnetic field due to the current in the other turns. The alteration of this field will produce an eddy-current system, which contributes to an increase in the winding losses. This additional loss is usually referred to in the literature as 'proximity effect'. Butterworth calculated this extra loss and added it directly to the losses in the conductor due to its own field. Throughout his analyses, Butterworth resorted to the use of elliptic integrals. Phillips[5.8] following Butterworth, calculated the extra losses if the finite length solenoid coil is shielded with a screening can. He studied the influence of screening on the expressions of losses

due to proximity effect. Again he replaced the screen by an equivalent current sheet, and considered the screen currents to be uniformly distributed over the skin depth. The solution was given always in terms of Bessel functions. The formula obtained by Phillips[5.8], for the screen losses, was found to agree very well with that empirically obtained by Bogle[5.4] provided that the coil is not too short.

In conclusion, as far as the screening of finite length coil is concerned in the work reviewed above, the high frequency situation was considered only, i.e. where the skin depth of the conducting screen is very small with respect to its thickness. This permitted the replacement of the screen by a current sheet, and the assumption of constant current distribution over the skin depth.

In the later part in the last decade, Onoe[5.9] presented a useful review of some Japanese papers which dealt with more or less similar problems. Then he presented a more general treatment where he used Green's function to analyse three different cases:

case 1 An infinitely long cylindrical conductor placed concentrically inside a solenoid coil.

case 2 A solenoid coil placed concentrically inside an infinitely long hollow cylindrical conductor.

case 3 A coil placed perpendicularly to a semi infinite plane conductor.

Onoe pointed out that these mathematical models cover the theoretical analysis of some practical problems, such as delay lines and magnetostriction transducers which are used for mechanical filters. This of course is in addition to the calculation of the impedance of finite length coils which encircle conducting cores or are shielded from outside by conducting screens.

Although Onoe's derived equations are general, they are so complicated that recently a paper by Yamamato and Baba[5.10] was solely devoted to calculate the impedance of a finite solenoid coil encircling an infinitely long conducting solid rod using Onoe's equations. The results were tabulated for certain specific geometrical ratios and for certain specific radius/skin depth ratios.

Onoe was mainly concerned with the calculation of the input impedance to his mathematical model. It is not obvious how his treatment could be extended, without further complications, to calculate the radial distribution of the eddy current and/or the magnetic

field inside the conducting region, or along its axial direction. Such distributions are very important for the calculation of the electromagnetic stress on the conducting region or for determining the frequency[4.3] suitable for eddy current testing.

The tables reported by Yamamato and Baba[5.10], although they cover a quite wide range of practical cases, do not represent for instance, the case where the conducting solid rod is replaced by a hollow cylinder whose thickness is comparable with the skin depth at the working frequency. Also they do not cover the class of problems where the cyclindrical conductor is concentrically placed outside the solenoidal coil or in general when there is more than one conducting region.

Apart from the class of practical problems which are concerned with the calculation of the impedance of finite length coils, the production of continuously cast shapes using electromagnetic forming[5.11 - 5.14] is one of the important practical applications where the finite length of the excitation current must be introduced. A word or two here about this method, it involves the shaping of the liquid metal solely by an electromagnetic field, producing cast products of different shapes with a very high surface quality and good microstructure combined with a substantial reduction

in cost[5.13]. A general arrangement of the process is shown in Fig. (5.1). An inductor ring is used to induce an alternating magnetic field which in turn generates the electromagnetic forces in the liquid metal. The forces arise from the interaction of the axial component of the magnetic field with the induced circumferential eddy currents.

These forces exert an electromagnetic pressure on the liquid metal surface squeezing it in a radial direction. The metal so compressed forms a column, the shape of which depends upon the cross section of the inductor and the dimensions upon the intensity of the magnetic field. It has been reported[5.13] that this method of electromagnetic casting is widely used in the U.S.S.R. for casting round bars of various aluminium alloys with a diameter up to 50 cm, and for a rectangular slabs with a cross section of 30 x 150 cm in lengths of up to 6 metres. The average consumption of electric power for casting 1 ton of molten metal varies from 20 to 40 kWh. In all the available Russian papers nothing is reported about the theoretical treatment concerning the problems of calculating the magnetic field of the inductor, the induced eddy currents in the conducting metal and the generated forces.

If as a first approximation the problem is mathematically modelled as an infinitely long conductor

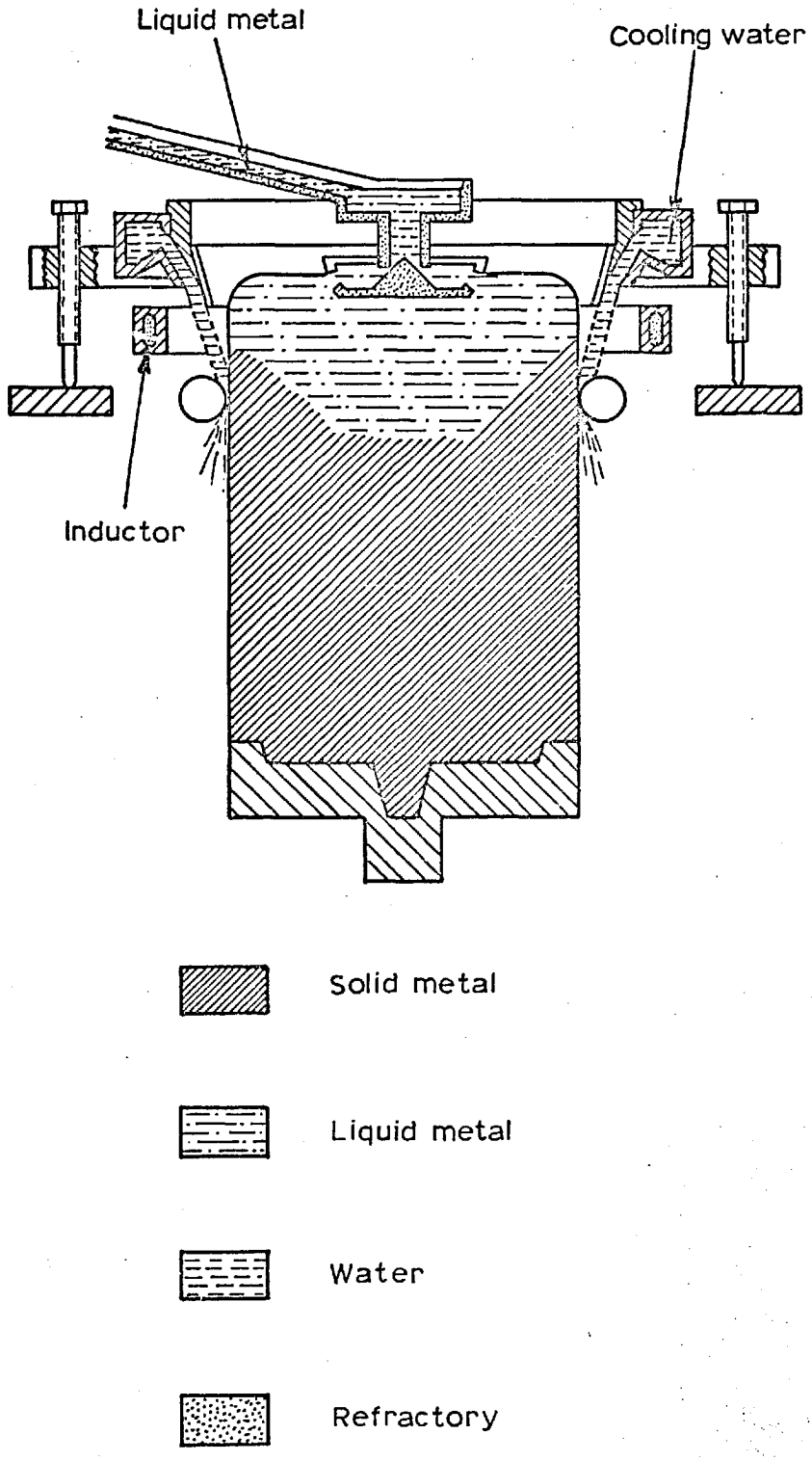


Fig. 5·1 *Electromagnetic metal forming, the casting equipment.*

surrounded by a solenoidal coil of finite axial length, a search through the literature shows that Fluerasu and Galan[5.15] solved a similar problem. They calculated the distribution of the induced eddy current along the axial direction of a very long cylindrical conductor placed in an a.c. circular coil of finite length, as well as the associated power loss. Their results were calculated for the case of strong skin effects, i.e. when the thickness of the conducting bar is several times the skin depth at the working frequency.

The expression for the current density distribution without any approximation is reported in their paper in a form of an infinite integration of some complex function of Bessel functions with complex arguments which do not lie on the 45^{o} line of the complex plane. The integration is difficult to calculate, and simplifications were needed. This limited the results obtained by Fluerasu and Galan to the cases of strong skin effects.

Dodd[5.16] solved a similar problem numerically using the relaxation technique with finite difference approximations.

In this chapter, it will be shown that the transmission line modelling technique can be extended to solve the multi-region cylindrical problem taking into consideration the finite axial length effect of the

the circumferentially directed excitation current. The representation,as will be shown later, will be general to cover any number of concentric conducting or nonconducting regions, inside or outside the excitation current surface. A method will be developed to calculate the input impedance, the axial and the radial distribution of the induced eddy current in the conducting regions. The validity of this method will be checked against published material. The excitation finite length effects on the radial distribution of the induced eddy currents in a conducting cylinder will be examined by comparing the published curves for the infinitely long model with those based on the method developed in this Chapter.

5.2 Theory

5.2.1 Mathematical model

The mathematical model consists of any number of infinitely long concentric cylindrical regions. Each region may be conducting, nonconducting or magnetic provided that it is isotropic, homogenous and linear with single valued parameters. The excitation is provided by a 'current sheet solenoid' which has a finite axial length 2τ as shown in Fig.(5.2). The excitation current, being restricted to a circumferential direction,

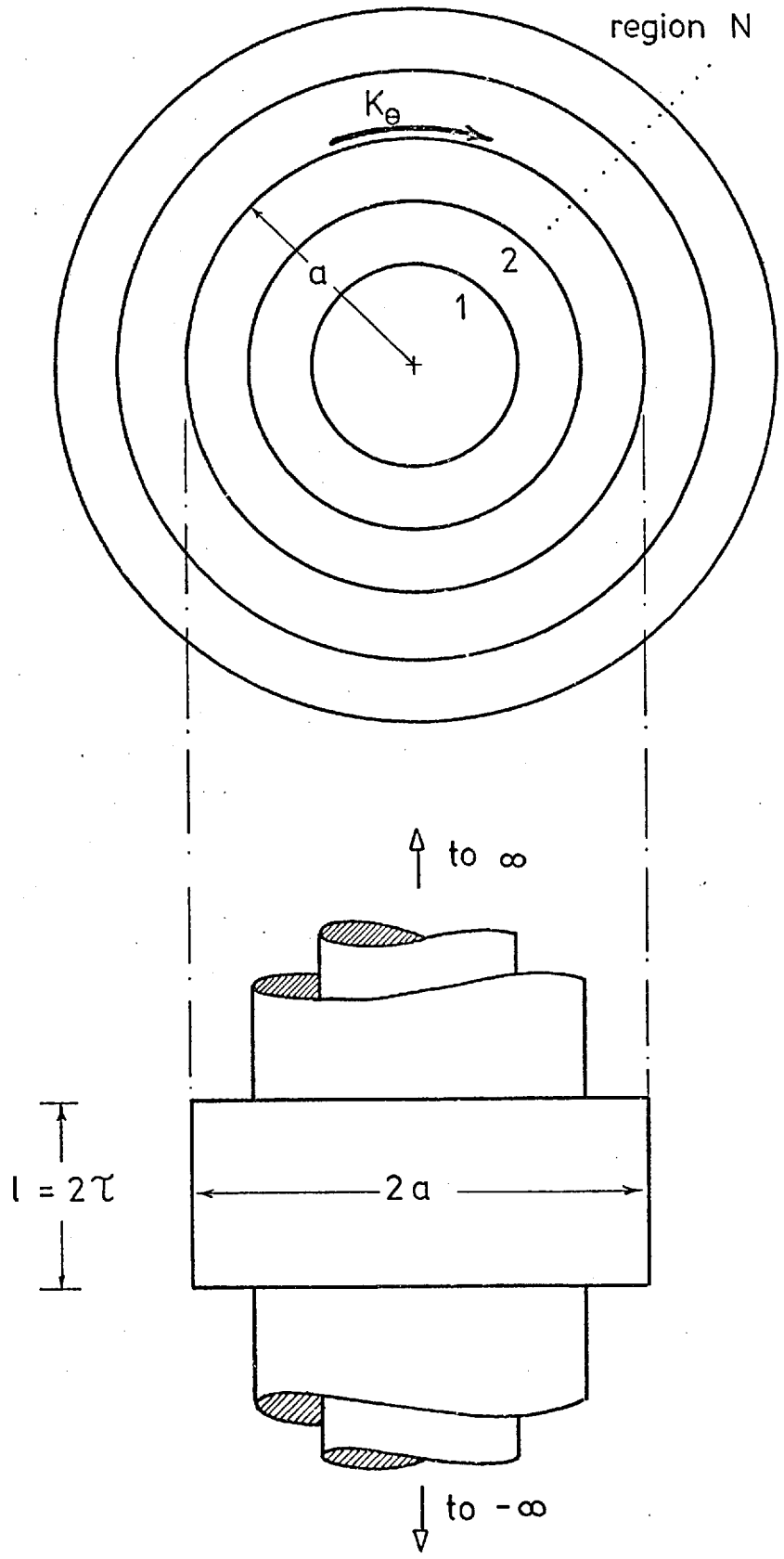


Fig.(5.2) The Mathematical Model

has θ-component only and lies at the boundary surface between any two adjacent regions.

This model differs from the model considered in Chapter 4 in restricting the circumferential excitation to a finite length in the axial direction.

5.2.2 Excitation current expression

Consider an infinite succession of uniform current sheets on a common axis, each of length equals the solenoid 2τ, and separated from one another with a pitch $2T$. It should be noted that it will not matter whether the adjacent current sheets have anti-phase currents or not, since in the analysis T will be allowed to increase without limit in order to simulate the isolated finite length solenoid.

Consequently, the distribution of the excitation current density in the z-direction will be as shown in Fig. (5.3).

Let the current in the N turns solenoid be:

$$i = \hat{I} \cos(\omega t) \qquad (5.1)$$

Then the spatial distribution of the current density can be represented in terms of the complex

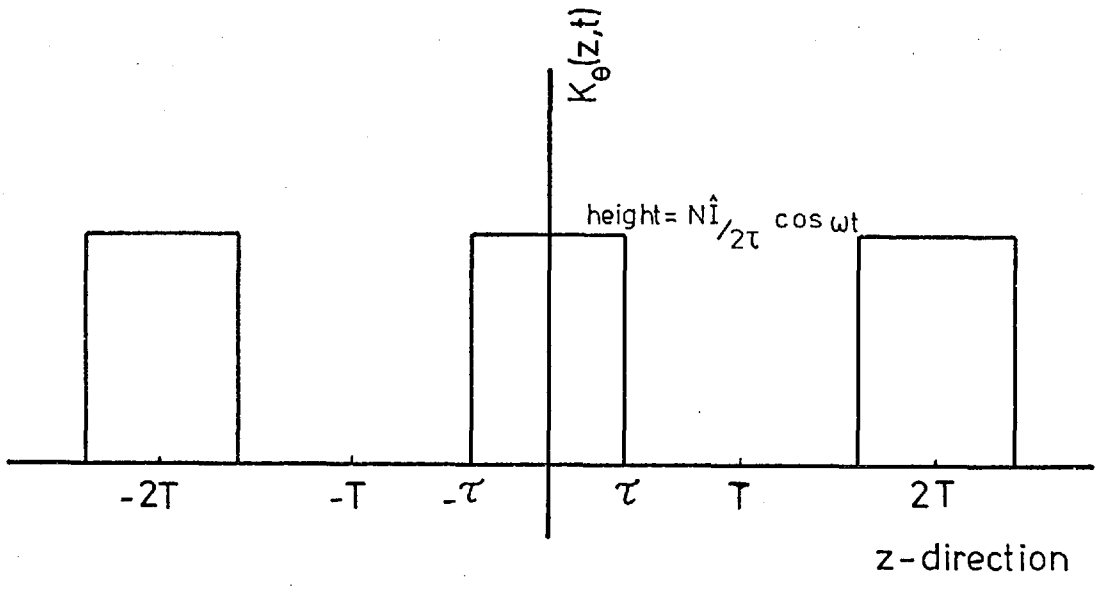


Fig.(5.3) Excitation current density distribution

Fourier series:

$$K_\theta(z,t) = (N\hat{I}/2\tau).\cos\omega t.\sum_{n=-\infty}^{\infty}(A_n/\Delta\Omega)\ \exp(jn\ \Delta\Omega\ z)\ \Delta\Omega \qquad (5.2)$$

Where $\Delta\Omega$ is given by:

$$\Delta\Omega = \pi/T$$

From the theory of Fourier series, the coefficient A_n can be calculated from the expression:

$$A_n = (1/2\pi) \int_{-\pi}^{\pi} f(z) . \exp(-jn\ \Delta\Omega\ z)\ d(\Delta\Omega\ z)$$

And from Fig. (5.3) the function f(z) can be represented mathematically by:

$$f(z) = 1.0 \qquad -\tau < z < \tau$$

$$= 0.0 \qquad \text{elsewhere in the period } (-T) \text{ to } (+T)$$

Substituting for f(z) in equation (5.3) we get:

$$(A_n/\Delta\Omega) = (\tau/\pi) . \sin(\Omega_n\tau)/(\Omega_n\tau) \qquad (5.4)$$

Where:

$$\Omega_n = n.\Delta\Omega$$

Equation (5.4) indicates that as $\Delta\Omega$ decreases to zero (when $T\to\infty$), A_n will tend to zero as well, but the quantity $(A_n/\Delta\Omega)$ will not tend to zero. Because of this, the expression of current density K_θ given by equation (5.2) is in terms of $(A_n/\Delta\Omega)$ and not A_n directly.

The linear current density expression (equation (5.2)) becomes:

$$K_\theta(z,t) = (N\hat{I}/2\tau) \cos\omega t \sum_{n=-\infty}^{\infty} (\tau/\pi) \{\sin(\Omega_n\tau)/(\Omega_n\tau)\} \exp(j\Omega_n z)\Delta\Omega \qquad (5.5)$$

The term $\sin(\Omega_n\tau)/(\Omega_n\tau)$ is known in the literature as 'Fourier kernel', it goes to unity as $(\Omega_n\tau)$ goes to zero, and it is an even function as shown in Fig.(5.6a). It should be noted that $\exp(j\Omega_n z)$ is not an even function. Bearing this in mind, in an attempt to get the expression of K_θ in terms of travelling wave, equation (5.5) can be written in the form:

$$K_\theta(z,t) = (N\hat{I}/2\pi)\ \Delta\Omega \sum_{n=0}^{\infty} Kr_n \cdot 2\cos(\Omega_n z)\cos\omega t$$

Where:

$$Kr_n = \sin(\Omega_n\tau)/(\Omega_n\tau)$$

Thus the expression of the linear current density is finally given by:

$$K_\theta(z,t) = (N\hat{I}/2\pi)\ \mathrm{Re} \sum_{n=-\infty}^{\infty} Kr_n \exp\{j(\omega t + \Omega_n t)\ \Delta\Omega \qquad (5.6)$$

Now, if T is allowed to increase without limit, i.e. $T \to \infty$

$\Delta\Omega \to d\Omega$

$\Omega_n \to \Omega$

And the summation sign of equation (5.6) will be replaced by an integration sign.

Then the current density expression of an isolated uniform current sheet extending over the axial length (2τ), will be given by:

$$K_\theta(z,t) = (N\hat{I}/2\pi) \int_{-\infty}^{\infty} Kr_n \cdot \exp\{j(\omega t + \Omega z)\}\, d\Omega \qquad (5.7)$$

Equation (5.7) represents the actual current density distribution without repetition as shown in Fig. (5.3). The sign standing for 'Real Part' is removed from the expression but it is to be kept in mind if the instantaneous values are required.

5.2.3 Transmission line modelling and equivalent circuit

Consider the nth spatial harmonic component K_n of the linear current density expression given by equation (5.6) to be acting alone at the excitation radius. K_n is then given by:

$$K_n = (N\hat{I}/2\pi) \cdot Kr_n \cdot \Delta\Omega \cdot \exp\{j(\omega t + \Omega_n t)\} \qquad (5.8)$$

With the excitation current having only a θ-directed component, E_r, E_z and H_θ are all zero, and the field equations reduce to:

$$\left.\begin{aligned} (-1/r)\ \frac{\delta}{\delta z}\ (rE_\theta) &= -j\omega\mu\ H_r \\ (1/r)\ \frac{\delta}{\delta r}\ (rE_\theta) &= -j\omega\mu\ H_z \\ \frac{\delta}{\delta z}\ H_r - \frac{\delta}{\delta r}\ H_z &= \sigma E_\theta \end{aligned}\right\} \qquad (5.9)$$

The use of the separation of variables techniques for solving the electromagnetic field equations (5.9) imposes the condition that the term $\exp\{j(\omega t + \Omega_n z)\}$, which appears in the current expression of equation (5.8), should appear in all the field components. Consequently, the following substitutions can be made:

$$\frac{\delta}{\delta t} = j\omega$$

$$\frac{\delta^2}{\delta z^2} = -\Omega_n^2 \qquad (5.10)$$

The field equations which relate E_θ and H_z will then reduce to:

$$\frac{\delta}{\delta r}(rE_\theta) = -j\omega\mu\, H_z$$

$$\frac{\delta}{\delta r}(H_z) = -\{\sigma/r + \Omega_n^2/j\omega\mu r\}\, rE_\theta \qquad (5.11)$$

Which when compared with the transmission line equations (4.18) and (4.19) yield the following relationships:

$$\begin{aligned} rE_\theta &\rightarrow V \\ H_z &\rightarrow I \\ j\omega\mu r &\rightarrow z \\ \sigma/r + \Omega_n^2/j\omega\mu r &\rightarrow y \end{aligned}$$

The elementary T-section, whose length is Δr, which represents the equivalent T.L. is shown in Fig. (5.4), where H_n and E_n represent the axial magnetic and the circumferential electric fields components respectively as a result of the nth spatial harmonic component of the excitation current density.

As shown before, section (4.7), each region can be represented by a string of micro-T circuits in cascade.

The continuity of the electric field component E_θ and the magnetic field component H_z (when there is no current sheet at the interface between the two regions) at a boundary surface will be satisfied automatically by connecting the equivalent transmission lines in series. The discontinuity of H_z at any surface where the current sheet exists, will be represented by connecting a current source between the two terminals which correspond to this surface.

Fig. (5.5a) shows the complete equivalent circuit of the nth spatial harmonic, where each region is replaced by an equivalent transmission line. In fact each one of these transmission lines is composed of a number of the micro-T circuits, shown in Fig. (5.4),

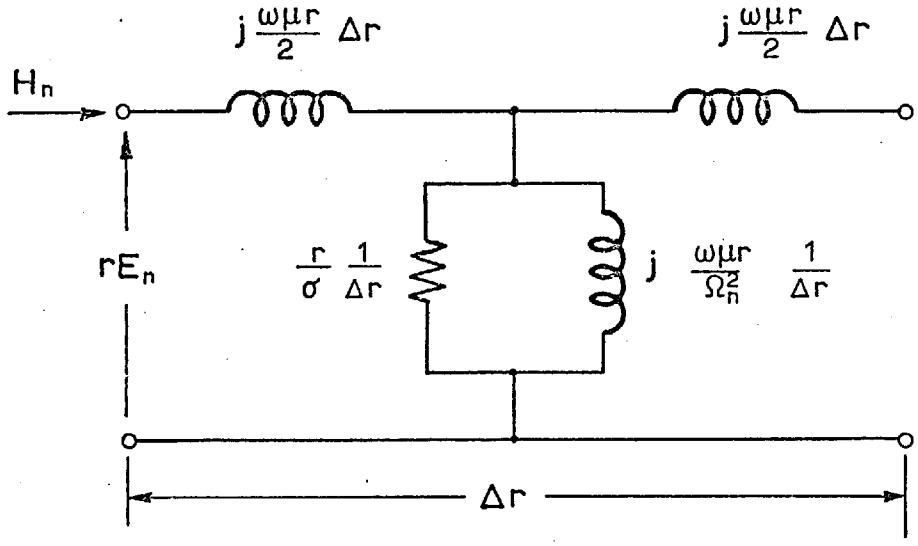


Fig. 5·4 n^{th} spatial harmonic equivalent micro-T circuit.

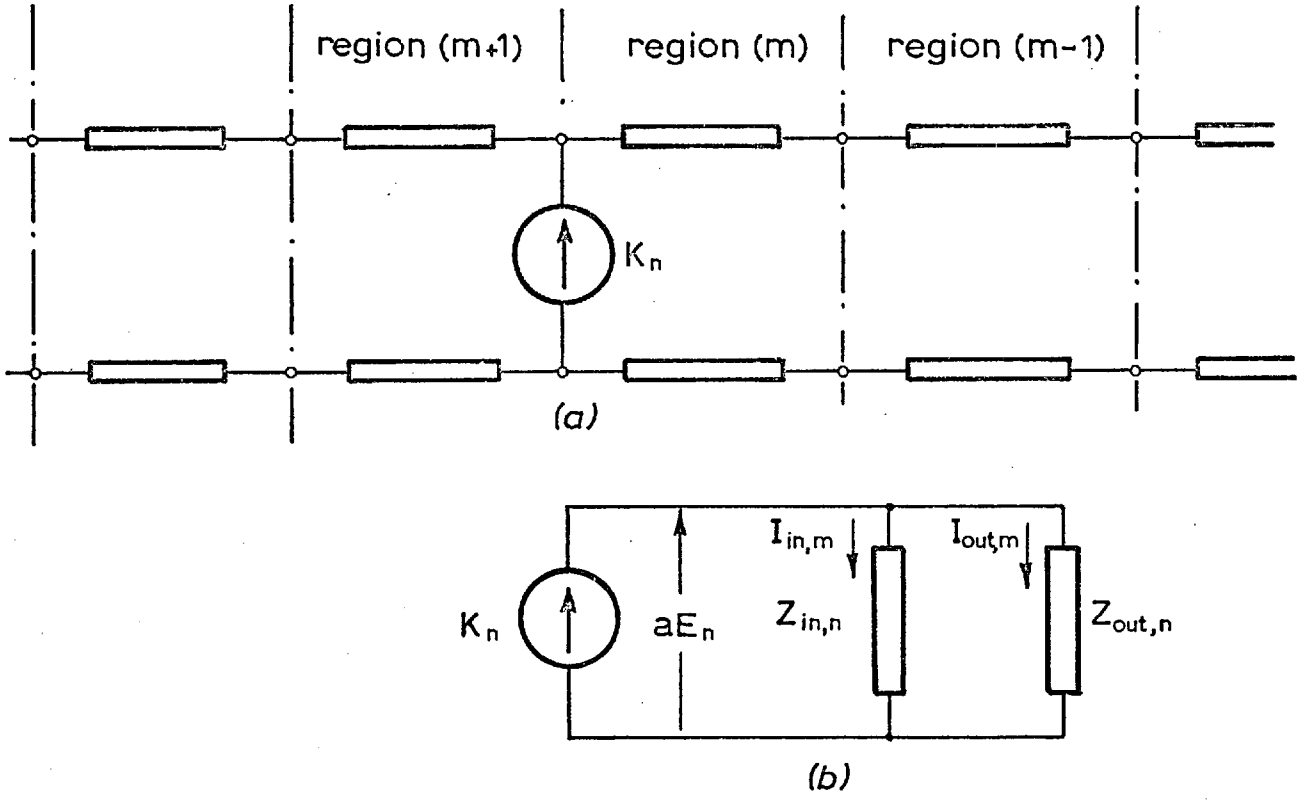


Fig. 5·5 Equivalent circuit of the n^{th} spatial harmonic

whose elements correspond to the constants of the region. Because of the fact that the length Δr is very small, the elements of each micro-T circuit are assumed constant over this length, and calculated for the mean value of r.

5.3 Calculation of the Terminal Input Impedance of the Excitation Coil:

The resultant inner and outer input tensorial surface wave impedances of the nth spatial harmonic, $Z_{in,n}$ and $Z_{out,n}$ shown in Fig. (5.5b) can be calculated starting from the far end of the equivalent transmission line, adding the impedances of the micro-T circuits in series and in parallel as appropriate, according to the circuit configuration, till reaching the terminals which correspond to the excitation.

From circuit theory,

$$a\, E_n = K_n\, Z_{T,n} \qquad (5.12)$$

Where:

$Z_{T,n}$ is the parallel combination of the tensorial surface wave impedances seen looking inwards and outwards at the excitation radius (a), and is given by:

$$Z_{T,n} = Z_{in,n} \cdot Z_{out,n} / (Z_{in,n} + Z_{out,n}) \qquad (5.13)$$

And the expression for aE_θ can be written directly by adding all the terms which correspond to the different spatial harmonic components of the excitation current.

$$\text{i.e.} \quad aE_\theta(z,t) = \sum_{n=-\infty}^{\infty} aE_n \tag{5.14}$$

Substituting for $(a\,E_n)$ from equations (5.12) and (5.6), we get:

$$aE_\theta(z,t) = (N\hat{I}/2\pi) \sum_{-\infty}^{\infty} Kr_n \cdot Z_{Tn} \cdot \exp\{j(\omega t + \Omega_n z)\} \cdot \Delta\Omega \tag{5.15}$$

Thus the amplitude of the electric field phasor is given by:

$$a\hat{E}_\theta = (N\hat{I}/2\pi) \sum_{-\infty}^{\infty} Kr_n \cdot Z_{Tn} \cdot \exp(j\Omega_n z) \cdot \Delta\Omega \tag{5.16}$$

The peak terminal voltage $\hat{V}$ can be related to the electric field $\hat{E}_\theta(z)$ by the equation:

$$\hat{V} = 2\pi aN(\hat{E}_{\theta,av}) \tag{5.17}$$

where $\hat{E}_{\theta,av}$ = average value of $\hat{E}_\theta(z)$ over the length of the coil, and is given by:

$$a\,\hat{E}_{\theta,av} = (1/2\tau) \int_{-\tau}^{\tau} a\,\hat{E}_\theta(z)\,dz \tag{5.18}$$

Applying the integration of equation (5.18) term by term to equation (5.16) we get:

$$a\hat{E}_{\theta,av} = (N\hat{I}/2\pi) \sum_{-\infty}^{\infty} \{Kr_n\}^2 \cdot Z_{Tn} \cdot \Delta\Omega \qquad (5.19)$$

If $Z = \hat{V}/\hat{I}$

= terminal input impedance

Combining (5.17) and (5.19), and rearranging, the terminal input impedance is given by:

$$Z = N^2 \sum_{-\infty}^{\infty} \{Kr_n\}^2 \cdot Z_{Tn} \cdot \Delta\Omega \qquad (5.20)$$

If the finite length effects are ignored, the the inductance of the air-cored solenoid coil would be L_o where:

$$L_o = \mu_o \pi a^2 N^2/2\tau \qquad (5.21)$$

It is common to use a normalised values for the impedance of a finite length coil as: $Z/\omega L_o$, thus:

$$Z/\omega L_o = (2\tau/\pi\mu_o\omega a^2) \sum_{-\infty}^{\infty} \{Kr_n\}^2 \cdot Z_{Tn} \cdot \Delta\Omega \qquad (5.22)$$

For an isolated finite length solenoidal coil, the normalised input terminal impedance can be obtained from (5.22) by permitting T to increase without limit.

Consequently, $\Delta\Omega \rightarrow d\Omega$, so the summation sign can be replaced by an integration operator, thus:

$$Z/\omega L_o = (2/\pi\ \mu_o\ \omega\ a^2) \int_{-\infty}^{\infty} \{Kr\}^2 \cdot Z_{Tn} \cdot d(\Omega\tau) \qquad (5.23)$$

The integration kernel $\{Kr\}^2 = \{\sin(\Omega\tau)/(\Omega\tau)\}^2$ is an even function. Similarly, $Z_T(\Omega)$ is dependent on Ω_n^2, hence its value for both +ve and -ve values of Ω(or n) is the same. This allows changing the limits of integration of equation (5.23) and multiplying by a factor of 2 as follows:

$$Z/\omega L_o = (4/\pi\ \mu_o\ \omega\ a^2) \int_{-\infty}^{\infty} \{\sin(\Omega\tau)/(\Omega\tau)\}^2 \cdot Z_{Tn}\ d(\Omega\tau) \qquad (5.24)$$

The integration is straight forward to perform numerically. The kernel $(\sin(x)/x)^2$ decreases rapidly with (x) as shown in Fig. (5.6b). The upper integration limit of equation (5.24) can often be as low as 4π. For all values of $x>4\pi$, the kernel will be less than 0.6% of its value at x = 0.0, and it will still be decaying very fast. The method of calculation can be briefly summarized in the following steps:

(i) Calculate $Z_{in}(\Omega)$, $Z_{out}(\Omega)$ and $Z_T(\Omega)$ for a range of values of $\Omega\tau$ from zero to 4π. Examine the variation of Z_T, it might be necessary to increase the upper limit or to decrease the sampling interval of $\Omega\tau$,

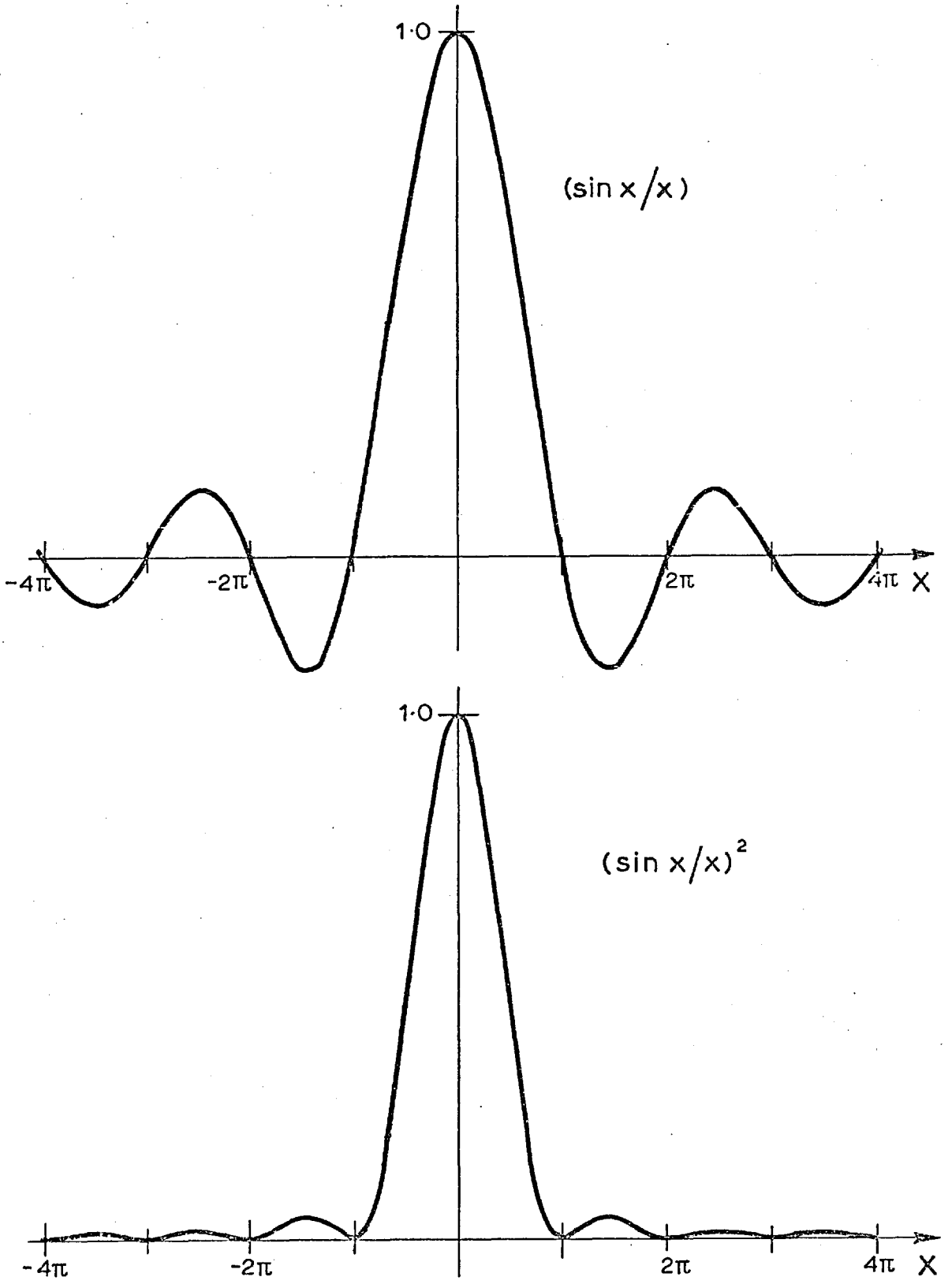


Fig. 5·6 Integration kernels

(ii) Multiply corresponding values of $(\sin(\Omega\tau)/\Omega\tau))^2$ and $Z_T(\Omega)$ then integrate using, for example, Simpson's rule.

The calculated impedance so obtained does not include the resistance of the exciting coil conductor. This can be simply added to the calculated impedance.

5.4 Current Density Distribution

In a conducting region, the induced eddy current is related to the electric field component by:

$$J_\theta = \sigma E_\theta \qquad (5.25)$$

The distribution of the induced eddy currents can be calculated by computing the distribution of (E_θ) along the equivalent transmission line which corresponds to the conducting region. This can be effected systematically as will be shown later.

The spatial nth harmonic component of the excitation current sheet is given above by equation (5.8). Working in terms of per unit values, the per unit electric field $\epsilon(r)$, at any radius (r), will be calculated for unit input current.

The actual electric field component can then be obtained by referring the input current to its value K_n given by equation (5.8). The method of calculating J_θ distribution as a function of the axial coordinate z, at a certain radius r' can be summarised as follows:

For a certain value of spatial harmonic frequency (Ω),

(i) Calculate $Z_{in,n}$, $Z_{out,n}$ and Z_{Tn} as shown above in section (5.3).

(ii) Calculate the per unit electric field tensor component $a\varepsilon$ at the excitation radius, and the input currents I_{in}, I_{out} from the relations:

$$\begin{aligned} a\varepsilon &= 1.0\ Z_{Tn} \\ I_{in} &= Z_{out,n}/Z_{Tn} \\ I_{out} &= Z_{in,n}/Z_{Tn} \end{aligned} \qquad (5.26)$$

(iii) Calculate the electric field $r'\varepsilon(r')$ at any desired radius r', starting from the excitation radius and proceeding towards r'. This can be achieved by replacing each T.L. with a suitable number of micro-T circuits in cascade. The input voltage and current of the first T-circuit are known, i.e. $a\varepsilon$ and I_{in} or I_{out}. Thus the corresponding values at r' can be obtained by applying

the fcllowing equation, which relates the quantities on both sides of a T-circuit, as many times as the number of the T-sections from the excitation radius till (r') is reached.

$$\begin{bmatrix} V_o \\ \\ I_o \end{bmatrix} = \begin{bmatrix} (1 + Z_s/2Z_p) & -(Z_s + Z_s^2/4Z_p) \\ \\ -1/z_p & (1 + Z_s/2Z_p) \end{bmatrix} \cdot \begin{bmatrix} V_i \\ \\ I_i \end{bmatrix} \qquad (5.27)$$

Where $Z_s = j\,\mu r_m\,\Delta r$

$Z_p = 1.0/(\sigma/r_m + \Omega^2/j\,\mu r_m)\,\Delta r$

r_m = mean radius

V_o, I_o = output quantities

V_i, I_i = input quantities

The steps from (i) to (iii) are then to be repeated for different values of Ω starting from zero. It should be noted that, only positive values of Ω need to be used, since Z_{Tn} is an even function of Ω.

The actual value of the electric field component at the radius r' can then be given by:

$$E_\theta(z,t,r') = (N\hat{I}/2\pi)\ \mathrm{Re}\ \exp(j\omega t) \sum_{-\infty}^{\infty} Kr_n . \varepsilon(\Omega_n, r') . \exp(j\Omega_n z) .\ \Delta\Omega \qquad (5.28)$$

Where:

$$\varepsilon(\Omega_n, r') = \varepsilon(-\Omega_n, r')$$

And in the limit as $\Delta\Omega \to d\Omega$, the amplitude of the induced eddy current at any radius (r'), can be obtained from equations (5.25) and (5.28),

$$\hat{J}_\theta(z,r') = (N\hat{I}/2\pi)\ \sigma \int_{-\infty}^{\infty} Kr \cdot \varepsilon(\Omega,r') \cdot \exp(j\Omega z) \cdot d\Omega \qquad (5.29)$$

Note that this integration is simply the inverse Fourier transform of the function:

$$Kr \cdot \varepsilon(\Omega,r')$$

which can be easily performed numerically or by using standard computer library programs for this purpose.

It should be noted that, since both $Kr = \sin(\Omega\tau)/\Omega\tau$ and $\varepsilon(\Omega,r')$ are even functions, the equation (5.29) can be written in the form:

$$\hat{J}_\theta(z,r') = (N\hat{I}/\pi) \cdot \sigma \cdot \int_0^{\infty} \{\sin(\Omega\tau)/\Omega\tau\} \cdot \varepsilon(\Omega,r') \cdot \cos(\Omega z) \cdot d\Omega \qquad (5.30)$$

Remark:

The magnetic field as a function of r' and z can be obtained similarly from the expression:

$$\hat{H}(z,r) = (N\hat{I}/\pi) \int_o^{\infty} \{\sin(\Omega\tau)/\Omega\tau\} \cdot I(\Omega,r') \cdot \cos(\Omega z) \cdot d\Omega$$

Where:

$I(\Omega,r')$ is the flow function (i.e. equivalent current) of the T.L. equivalent circuit. It is calculated simultaneously with $\epsilon(\Omega,r')$.

A comparison between using the direct integration method or using the fast Fourier transform technique, in order to calculate $J_\theta(z,r)$ will be discussed later in section (5.6.2).

5.5 Normalised Terminal Impedance of Finite Length, Air-Cored Solenoidal Coil

The objective of this section is to check the analysis developed in this chapter against the well known expressions given by Nagaoka[5.1]. Nagoaka solved this problem by making use of elliptic integrals. In what follows, the analysis will be completely based on the 'surface wave impedance approach'.

5.5.1 Simple expressions for the input wave impedance of non-conducting innermost and outermost regions

For a non-conducting region, it can easily be shown that E_θ satisfies the equation:

$$\left[\frac{\delta^2}{\delta r^2} - \frac{1}{r} \frac{\delta}{\delta r} - \Omega_n^2 \right] . \; rE_\theta = 0$$

Its solution is given directly in the form[5.17]:

$$rE_\theta = r\{A \; I_1(\Omega_n r) + B \; K_1(\Omega_n r)\} \qquad (5.31)$$

Where I_1 and K_1 are modified Bessel functions.

If the non-conducting region is the innermost one, to have E_θ bounded as (r) tends to zero, equation (5.31) reduces to:

$$rE_\theta = r \; A \; I_1(\Omega_n r)$$

Consequently, H_z will be given by:

$$H_z = -(\Omega_n / j\omega\mu) \; A \; I_o(\Omega_n r)$$

If Z_i is the 'input' tensorial surface wave impedance looking 'into' the innermost region, then

$$Z_i = r_i \; E_\theta / (-H_z)$$
$$= j(\omega\mu_o \; r_i / \Omega_n) . \; I_1(\Omega_n \; r_i) / I_o(\Omega_n \; r_i) \qquad (5.32)$$

On the other hand, if the non-conducting region is the outermost one, the bounded solution for E_θ and H_z

as (r) tends to infinity, is given by:

$$rE_\theta = r\ B\ K_1(\Omega_n r)$$

$$H_z = (\Omega_n/j\omega\mu_o)\ B\ K_o(\Omega_n r)$$

Consequently, the 'input' tensorial surface wave impedance Z_o, looking 'into' the outermost region is given by:

$$Z_o = r_o\ E_\theta/H_z$$

$$= j(\omega\ \mu_o\ r_o/\Omega_n)\ .\ K_1(\Omega_n r_o)/K_o(\Omega_n r_o) \qquad (5.33)$$

5.5.2 Expression for the Nagaoka factor derived from the surface wave impedance

Consider the mathematical model indicated in Fig. (5.7). The inner and outer tensorial surface wave impedances seen at the excitation radius (a) will be given by equations (5.32) and (5.33).

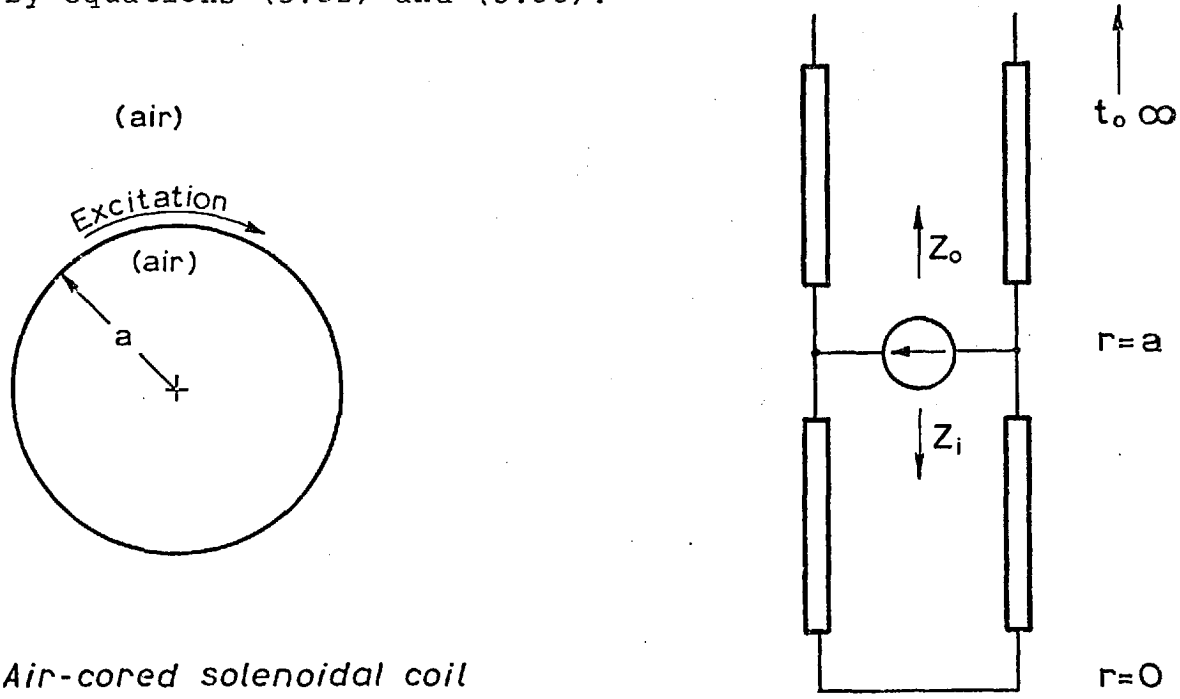


Fig. 5·7 Air-cored solenoidal coil

(a) Mathematical model (b) Equivalent circuit

Thus the resultant input tensorial surface wave impedance $Z_T(\Omega)$, which appears in equation (5.13), is given by:

$$Z_T(\Omega) = j \frac{\omega\mu_o a}{\Omega} \frac{(I_1/I_o) \cdot (K_1/K_o)}{(I_1/I_o) + (K_i/K_o)} \qquad (5.34)$$

Where I_i, I_o, K_i and K_o are all modified Bessel functions whose arguments are all equal to (Ωa). Since the Wronskian $W(K_n(y), I_n(y))$ is given by[5.18]:

$$W(K_n(y), I_n(y)) = I_n(y) \cdot K_{n+1}(y) + I_{n+1}(y) \cdot K_n(y)$$
$$= 1/y$$

Thus the wave impedance $Z_T(\Omega)$ expression reduces to:

$$Z_T(\Omega) = j\,\omega\mu_o\, a^2\, I_1(\Omega a) \cdot K_1(\Omega a) \qquad (5.35)$$

But the normalised terminal input impedance of the solenoidal coil $Z/\omega L_o$ is given by equation (5.24), hence substituting for $Z_T(\Omega)$ from (5.35) we get:

$$Z/\omega L_o = j4/\pi\tau \cdot \int_0^\infty \{\sin(\Omega\tau)/\Omega\}^2 \cdot I_1(\Omega a) \cdot K_1(\Omega a)\, d\Omega$$

Changing the integration variable to be (Ωa), rearranging the terms and substituting for:

$$\tau = 1/2 \quad , \quad \Omega a = \chi$$

we get:

$$Z/j\omega L_o = \nu = (8a/\pi l) \cdot \int_0^\infty \{\sin(\chi l/2a)/\chi\}^2 \cdot I_1(\chi) \cdot K_1(\chi) \cdot d\chi$$

Which is the same expression for Nagaoka's factor obtained elsewhere[5.9]

5.3.3 Nagaoka factor in terms of complete elliptic integrals

The expression of Nagaoka's factor in terms of elliptic integrals, as reported in Nagaoka's paper, is as follows:

$$\nu = (4/3\pi k') \{(k'/k)^2 \cdot \{K(k) - E(k)\} + E(k) - k\} \qquad (5.37)$$

Where:

$k'^2 = l^2/(4a^2 + l^2)$

$k^2 = 4a^2/(4a^2 + l^2)$

$K(k)$ and $E(k)$ are complete elliptic integrals of the first and second kinds respectively, and are given by:

$$K(k) = \int_0^{\pi/2} (1 - k^2 \sin^2\theta)^{-\frac{1}{2}} \, d\theta$$

$$E(k) = \int_0^{\pi/2} (1 - k^2 \sin^2\theta)^{\frac{1}{2}} \, d\theta$$

Rearranging equation (5.37), one can get:

$$\nu = (8a/3\pi lk^3)\{(2k^2 - 1)E + (1 - k^2)K - k^3\} \qquad (5.38)$$

It is worth noting that equation (46) in Onoe's paper (both the original and the translated one) is wrong. The final '-1' should read '$-k^3$' as indicated in equation (5.38). The complete elliptic integrals K(k) and E(k) are usually tabulated for different values of (k). However, they can be evaluated numerically in a very simple manner with the aid of ordinary hand calculator. Freeman[5.19] presented the algorithm for this calculation, and it will be quoted here very briefly just for reference.

The elliptic integrals K and E can be calculated numerically as follows:

$$K(k) = \pi/2a_n \qquad (5.39)$$

$$E(k) = K(k)(1 - \tfrac{1}{2}\{c_o^2 + 2c_1^2 + \ldots + 2^n c_n^2\})$$

Where the values of a_n, c_o, c_1, ... c_n can be obtained from an 'arithmetico-geometrical' scale formed as follows:

$$\begin{array}{lll} a_o = 1 & b_o = \sqrt{1 - k} & c_o = k \\ a_1 = \tfrac{1}{2}(a_o + b_o) & b_1 = \sqrt{(a_o\, b_o)} & c_1 = \tfrac{1}{2}(a_o - b_o) \\ \vdots & \vdots & \vdots \\ a_n = \tfrac{1}{2}(a_{n-1} + b_{n-1}) & b_n = \sqrt{(a_{n-1} b_{n-1})} & c_n = \tfrac{1}{2}(a_{n-1} - b_{n-1}) \end{array}$$

The above table of values is continued until c_n is insignificant, usually limited by the number of places the calculator can carry. The scale converges very rapidly, for example, with k = 0.999999, the value of n is 6 for $c_n < 10^{-8}$.

In section (5.6.1) some values of the Nagaoka's factor will be calculated, for different axial/excitation mean radius ratios, using the transmission line technique, and then these will be compared with those reported[5.10] and those obtained, using a hand calculator, from equations (5.38) and (5.39).

5.6 Computations and Comparison with the Published Material:

5.6.1 Nagaoka' factor and terminal impedance

Nagaok[5.1] developed an expression for the impedance of an air-core short solenoid coil in terms of the impedance per unit length of an infinitely long solenoid times a factor. This factor has been known in the literature since then as Nagaoka's factor. He tabulated this factor for different values of axial length/radius ratio of the coil. Similarly, Yamamoto and Baba[5.10] published a set of tables, based on equations originally given by Onoe[5.9], from which the

impedance of short coil surrounding an infiniely long solid conductor may be determined.

In order to judge the correctness, the limitations and the accuracy of the transmission line modelling method developed in this chapter, the normalised impedance of some finite length solenoidal coils, air-cored or encircling infinitely long solid conductors having different geometrical ratios will be calculated. The results then will be compared with those obtained by Nagaoka and Yamamoto and Baba.

The calculation of the normalised impedance for different values of l/a ratio is based on numerically integrating equation (5.24). $Z_T(\Omega)$ will be numerically obtained as mentioned before in section (5.3). As argued before, the integration Kernel $(\sin x/x)^2$ decays rapidly as (x) increases, and this will allow limiting the integration upper limit to a relatively small value.

The numerical integration process, using Simpson's rule for example, requires sampling the integrand of equation (5.24) at equal intervals.

The sampling rate as well as the integration upper limit are chosen according to the spatial frequency response of the integrand of equation (5.24). The kernel is plotted in Fig. (5.6b), while the wave

impedance/spatial frequency response curves are plotted in Fig. (5.8) for an air-cored colenoid, and in Figs. (5.9) and (5.10) for a solenoid encircling a long conducting solid cylinder.

For all the results reported in the following section, the integration upper limit was taken $\Omega\tau = 4\pi$. The sampling rate of $Z_T(\Omega)$ was taken as:

$$\Delta\Omega \cdot \tau = \pi/6$$

and it was assumed that both the real and imaginary components of $Z_T(\Omega)$ varied linearly between each two adjacent samples.

Typical calculation results are given in tables (5.1) and (5.2) below.

The normalised impedance values of table (5.2) are calculated for different values of coil length/coil radius, l/a, and for different values of $(a/d)^2$.

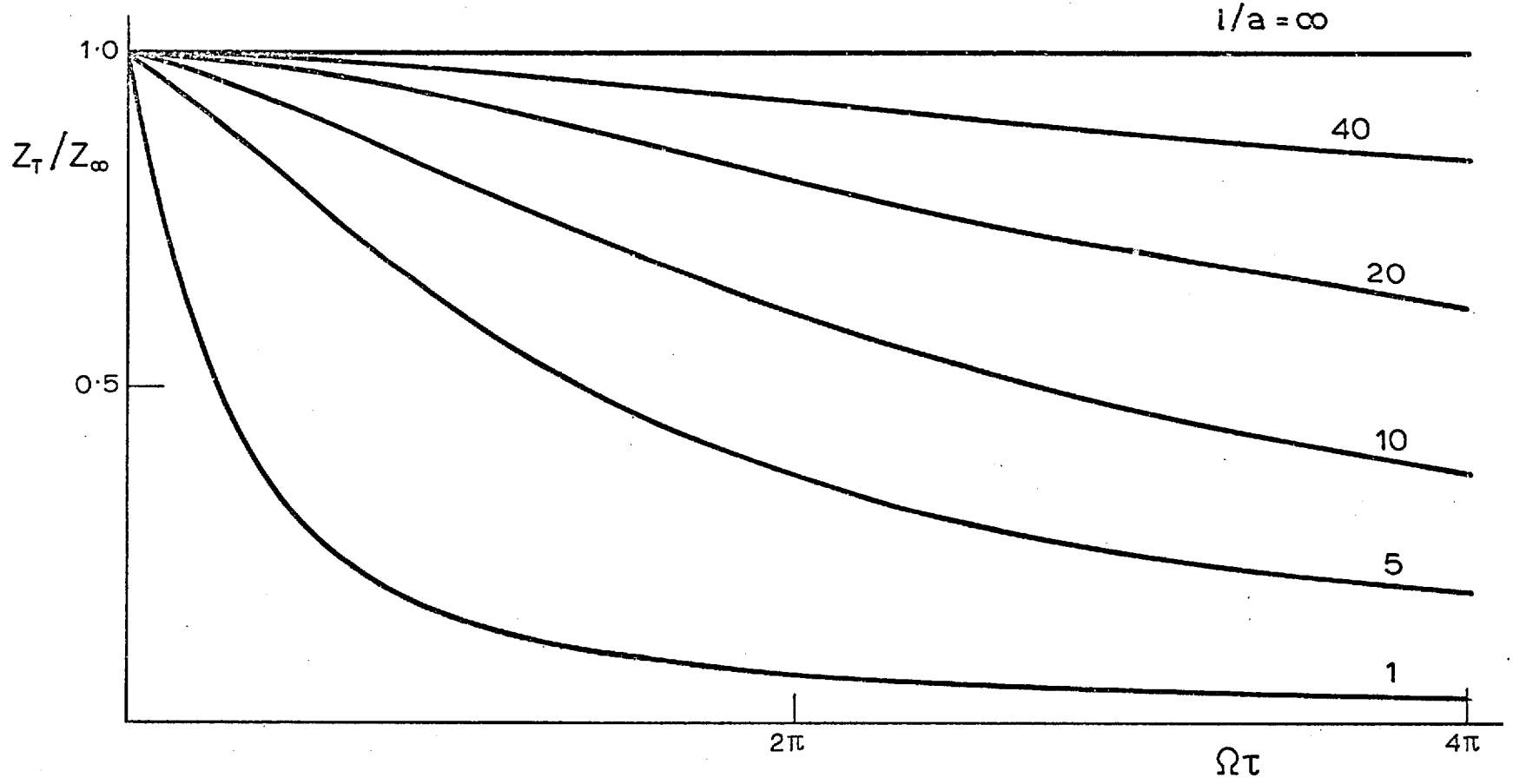


Fig. 5·8 The normalised surface wave impedance of an air-cored solenoid

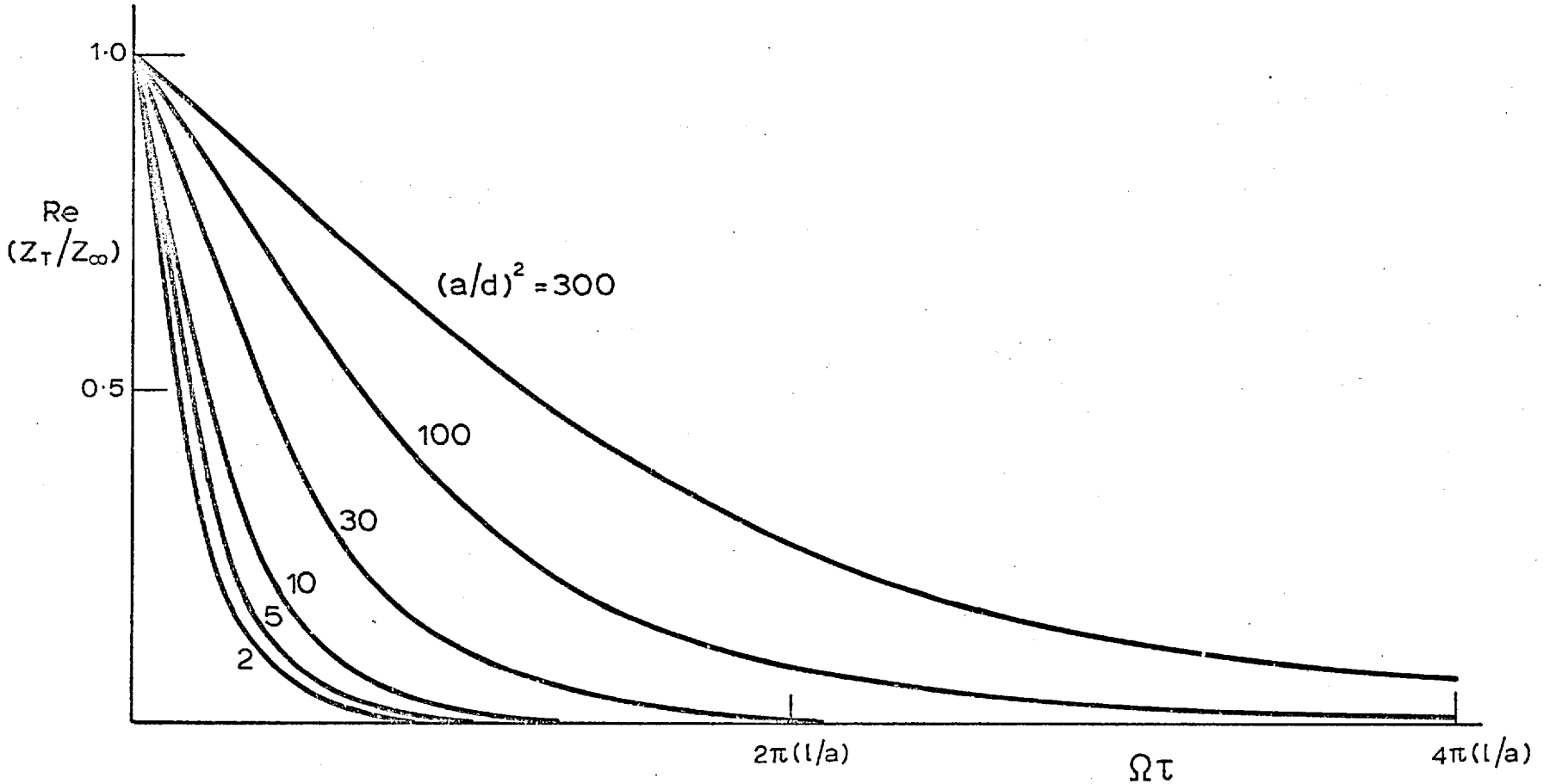


Fig. 5·9 The real part of the normalised surface wave impedance of a conductor-cored solenoid

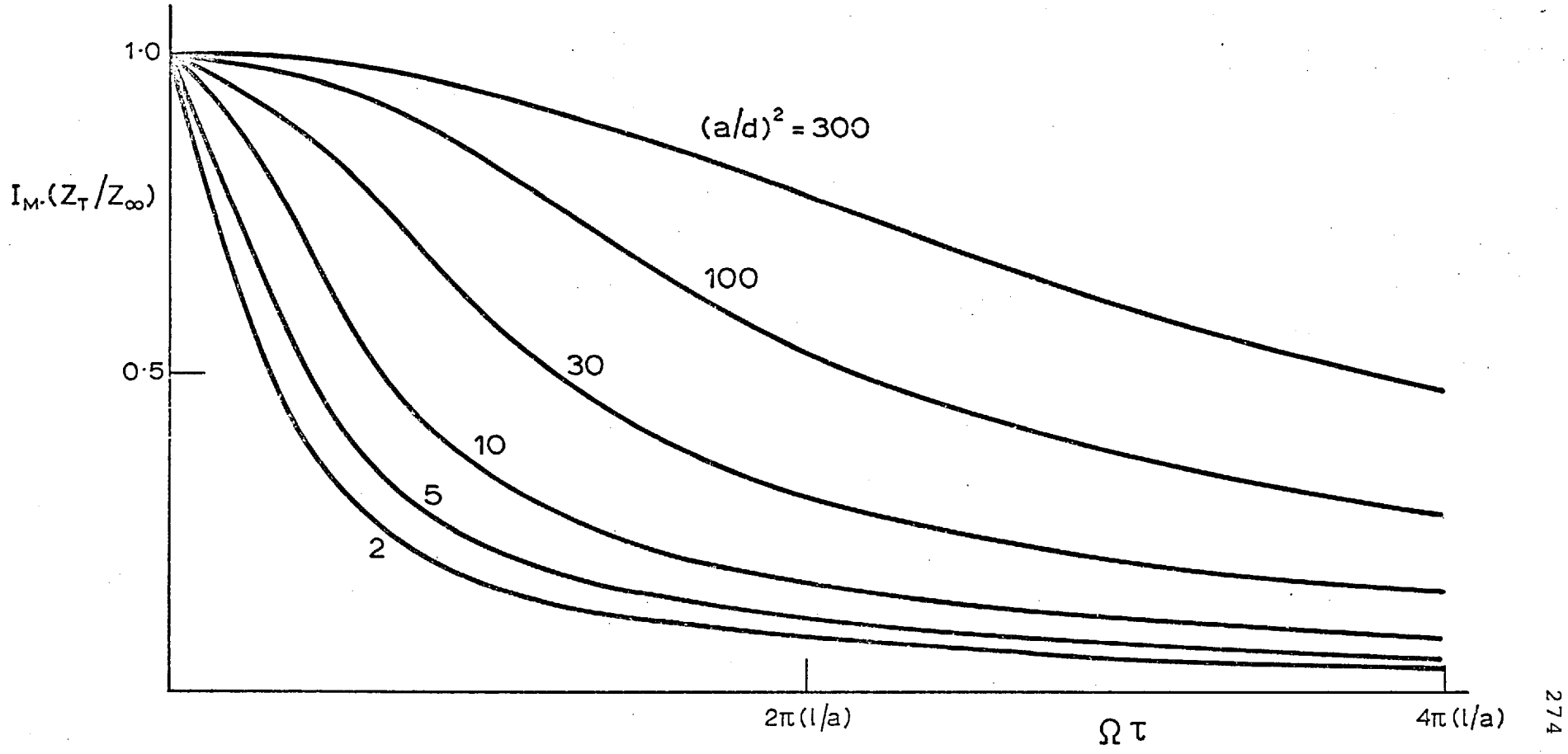


Fig. 5·10 The imaginary part of the normalised surface wave impedance of a conductor-cored solenoid

Table 5.1: Nagaoka's factor ν

1/a	ν	ν'	ν''
1.0	0.526	0.52637	0.525510
5.0	0.850	0.84570	0.849856
10.0	0.920	0.91447	0.920093
20.0	0.959	0.94982	0.958807
40.0	0.979	0.96554	0.979092

ν = Nagaoka's factor from reference (5.10)

ν' = Nagaoka's factor calculated from T.L. modelling technique.

ν'' = Nagaoka's factor calculated from the elliptic integrals expression of equations (5.38) and (5.39)

Table 5.2: Normalised impedance of short solenoid encircling long conducting solid cylinder

$(\frac{a}{d})^2$	l/a = 1.0		l/a = 5.0		l/a = 10.0		l/a = 20.0	
	Re	Im	Re	Im	Re	Im	Re	Im
2	0.0742	0.05069	0.170	0.7978	0.195	0.8577	0.209	0.891
	0.0758	0.05067	0.1698	0.7973	0.1949	0.8522	0.2087	0.882
5	0.139	0.4409	0.293	0.631	0.329	0.664	0.348	0.682
	0.1407	0.4388	0.2924	0.6276	0.3277	0.6589	0.3463	0.6743
10	0.162	0.35	0.295	0.441	0.321	0.454	0.335	0.461
	0.1622	0.3473	0.294	0.4382	0.3196	0.4492	0.3322	0.4534
15	0.158	0.29	0.261	0.354	0.279	0.362	0.290	0.366
	0.1572	0.2956	0.260	0.3513	0.2782	0.3572	0.2869	0.3592
30	0.138	0.224	0.201	0.252	0.212	0.255	0.218	0.258
	0.1376	0.2229	0.2005	0.2493	0.2106	0.2516	0.2151	0.2523
100	0.0976	0.132	0.123	0.140	0.127	0.140	0.129	0.141
	0.0974	0.1306	0.1221	0.1374	0.1255	0.1378	0.127	0.1379
300	0.0647	0.079	0.075	0.081	0.0766	0.081	0.0774	0.082
	0.0646	0.0774	0.0743	0.0795	0.0755	0.0796	0.0760	0.0796

The first line corresponding to each $(a/d)^2$ is the published values in ref. (5.10), while the second line is the calculated value from T.L. modelling method.

One can expect that the main sources of difference between the computed results from T.L. modelling and those obtained by numerical calculation of Onoe's integrals

reported in ref. (5.10), are due to:

(i) Truncation error

This arises because of limiting the integration of equation (5.24) to (4π) instead of infinity.

(ii) Sampling error

Which is the result of sampling the continuous function $Z_T(\Omega)$ at a rate of $\Delta\Omega.\tau = \pi/6$, and assuming linear variation of both its real and imaginary components during the sampling interval.

Comparing the results of the two methods, which appears in tables (5.1) and (5.2), one can conclude:

a) For small values of 1/a (e.g. 1/a = 1.0), the average difference over a wide range of $(a/d)^2 = 2 \rightarrow 100$ was well below 1%.

b) For values of 1/a varying between 1.0 and 40.0, and $(a/d)^2$ varying between 2 and 300, the largest difference was of the order of 2%.

c) The difference in calculating the resistive component of the impedance was in general less than that in the inductive component.

Studying the frequency response curves, Figures (5.8), (5.9) and (5.10) of the different cases suggest that:

(i) In general, better accuracy can be obtained for small values of (1/a) by increasing the sampling rate of the surface wave impedance, since it decays very rapidly with ($\Omega\tau$) as (1/a) decreases. While better accuracy for large values of (1/a) can be achieved by increasing the integration upper limit to 6π or 8π instead of 4π, this is because $Z_T(\Omega)$ decreases slowly in such a case.

(ii) For constant (1/a) values, the surface wave impedance decreases as ($\Omega\tau$) increases. The reduction is larger for small values of $(a/d)^2$ than for large values. So the accuracy can still be improved by; increasing the sampling rate for small values of $(a/d)^2$, and extending the upper limit of integration for large values of $(a/d)^2$.

The normalised impedance values are plotted in Fig. (5.11) for different geometrical ratios. It should be noted that the plotted values correspond to the value of the normalised impedance $Z/\omega L$, divided by the Nagaoka's factor ν calculated for the specific 1/a ratio.

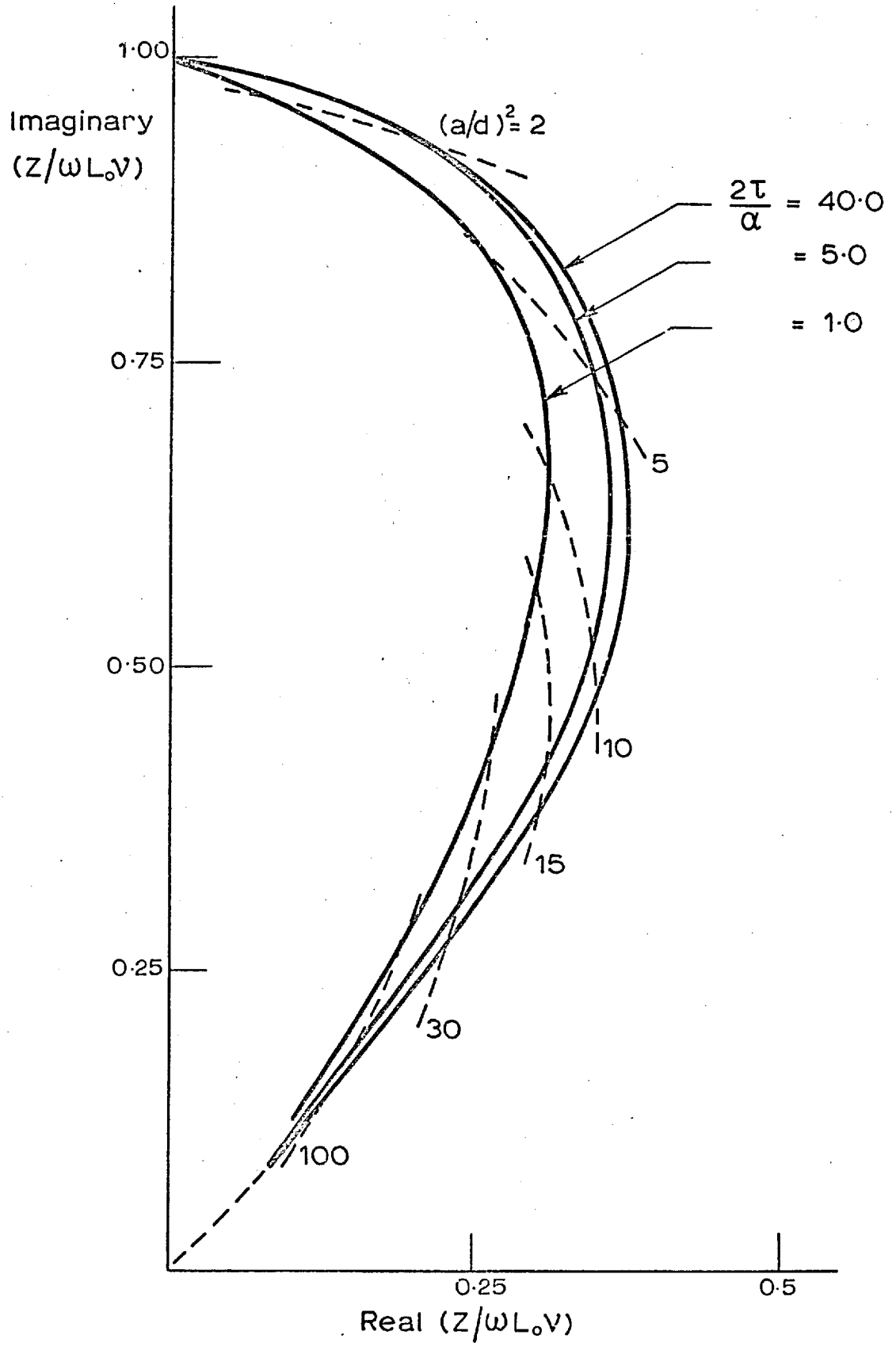


Fig. 5·11 Normalised impedance diagram

5.6.2 Axial distribution of the surface current density

The surface current density distribution in the axial direction shown in Figs. (5.12) and (5.13) could be obtained from equation (5.30), where r' was taken equal to the outer radius of the conducting solid cylinder.

The integration of equation (5.30) was calculated by two different methods:

(i) Direct numerical integration.

(ii) Using a standard 'Fast Fourier Transform' (F.F.T.) computer library program based on the Cooley-Tukey algorithm.

(i) Direct integration method

The integration of equation (5.30) was calculated numerically using Simpson's rule. The sampling rate of $\underline{\varepsilon}(\Omega)$ was taken to be $\Delta\Omega\tau = \pi/6$, and it was assumed that both its real and imaginary components varied linearly between each two adjacent samples. The integration upper limit was taken as $\Omega\tau = 7\pi$ instead of 4π as before. This is because the integration kernel in this case (which is $(\sin \Omega\tau/\Omega\tau)$ does not attenuate as quickly as its 'squared' value.

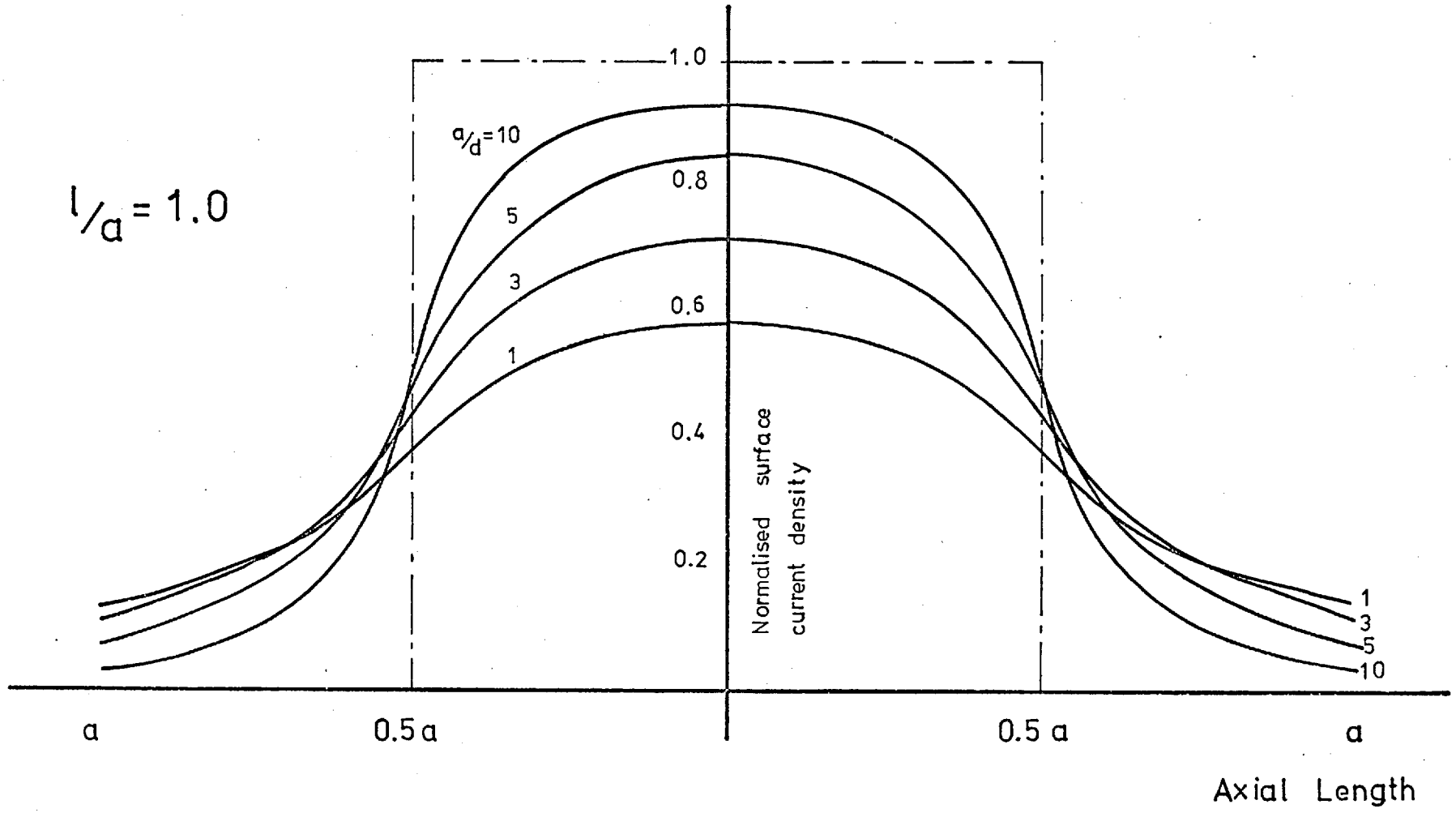


Fig.5.12 Axial distribution of the induced normalised surface current density in the conducting bar. ($l/a = 1.0$)

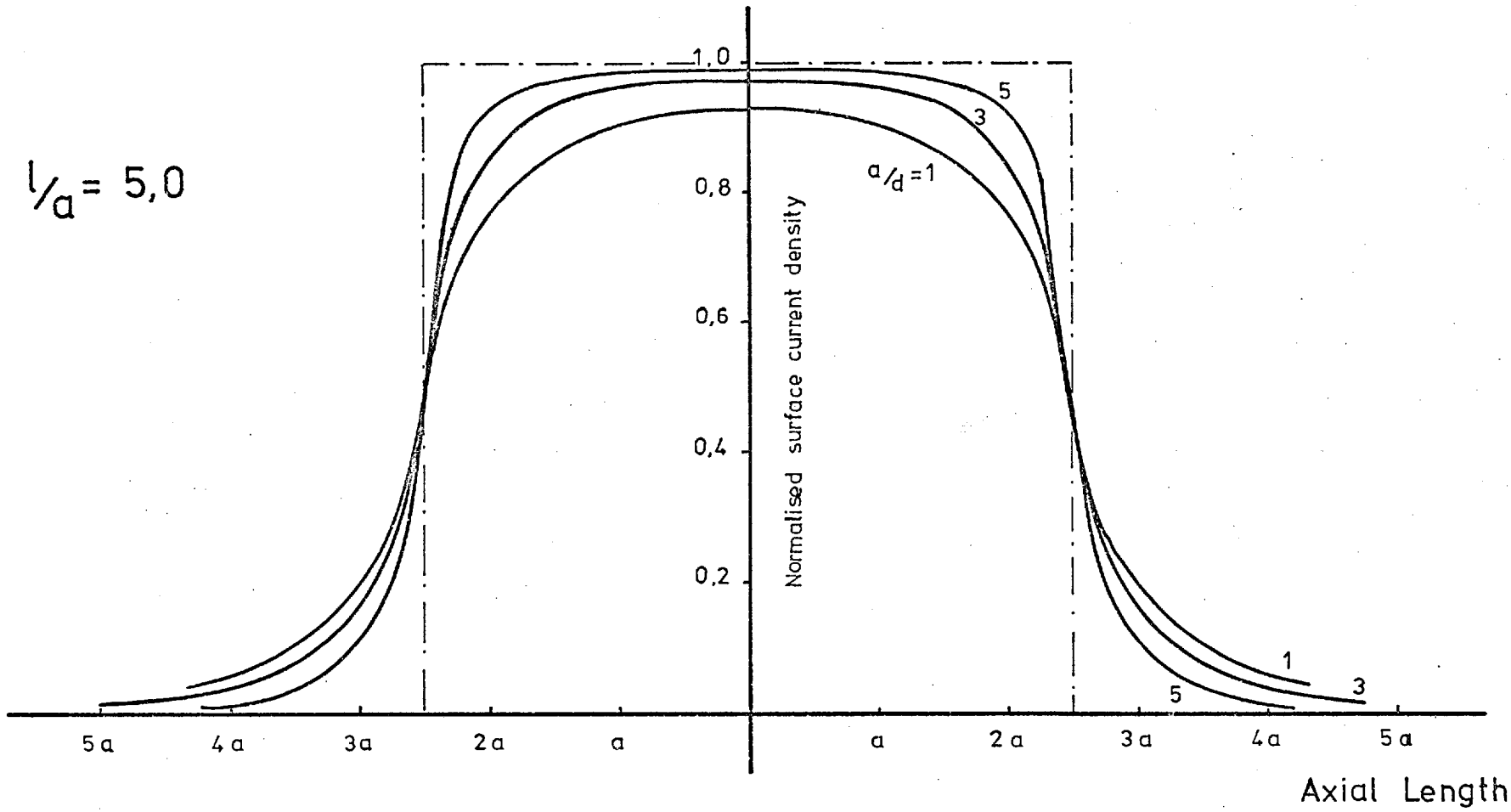


Fig. 5.13 Axial distribution of the induced normalised surface current density in the conducting bar. ($l/a = 5.0$)

It is worth mentioning that, if the integration upper limit was taken as 5π instead of 7π, the difference in the absolute values of the results does not exceed 4%, while the difference in the per unit value is much smaller.

(ii) F.F.T. method

A standard computer library program, based on the Cooley-Tukey algorithm was used to calculate the integral given by equation (5.30).

Since the frequency response characteristics as shown in Fig. (5.9) and (5.10) are well behaved, a relatively small number of samples is required. Sixty four samples were taken, with a sampling rate of $\Delta\Omega\tau = \pi/10$. This permitted the calculation of the variation of the surface current density in the axial direction up to a distance of $z = 6.4\tau$, with an incremental spacing of $\Delta z = 0.1\tau$.

The agreement between the results of calculations by the two methods was very close.

Generally, the F.F.T. method is characterised by its relatively small number of arithmetic operations involved in the calculations as compared with the direct

numerical integration method. The F.F.T. method gives the same number of output points, which correspond to different Z's as the number of input samples. In our case, the variation in the axial direction z is expected to be smooth. The integration then needs to be calculated for a small number of values of z, for instance, z/τ = 0, 0.25, 0.5, 0.75, 1.0, 1.5, 2. Thus the computer time needed for direct integration may be equal to, if it is not less than, that required for FFT method.

The distribution of the surface current density was calculated for the two cases of 1/a = 1.0 and 5.0 and for different values of (a/d), Figs (5.12) and (5.13) respectively.

Each curve which corresponds to a certain value of (a/d) is normalised to the induced surface current density of an infinitely long model for the same (a/d) value. The curves indicate that the induced surface current density becomes more uniform under the excitation coil as the frequency increases even for small values of (1/a). It also shows that the induced current outside the excitation zone decreases as the frequency increases, and it is of course attenuated away from the excitation coil.

5.6.3 Radial distribution of the circumferential current density

Forster, Hochshild and Bareham, all calculated the radial distribution of the induced eddy currents in a conducting solid cylinder or tube, when it is encircled by an infinitely long solenoid.

Nothing was reported about this distribution if the solenoidal coil has finite axial length. However, Bareham[4.3] estimated the errors arising when the theory for infinitely long solenoidal coils is applied to calculate the eddy current distribution in case of short coils, to be unlikely to exceed 30%.

Adopting the T.L. modelling technique, the radial distribution of eddy current induced was easily calculated using equation (5.30) as indicated in section (5.4).

Fig. (5.14) shows the current distribution over a cross-section which lies in the plane $z = 0$, i.e. at the middle of the solenoidal coil. The coil has a ratio $l/a = 1.0$. The amplitude of the current density was plotted for different frequencies, and each curve was normalised to its corresponding surface current density value.

On the same graph, curves obtained by Hochshild

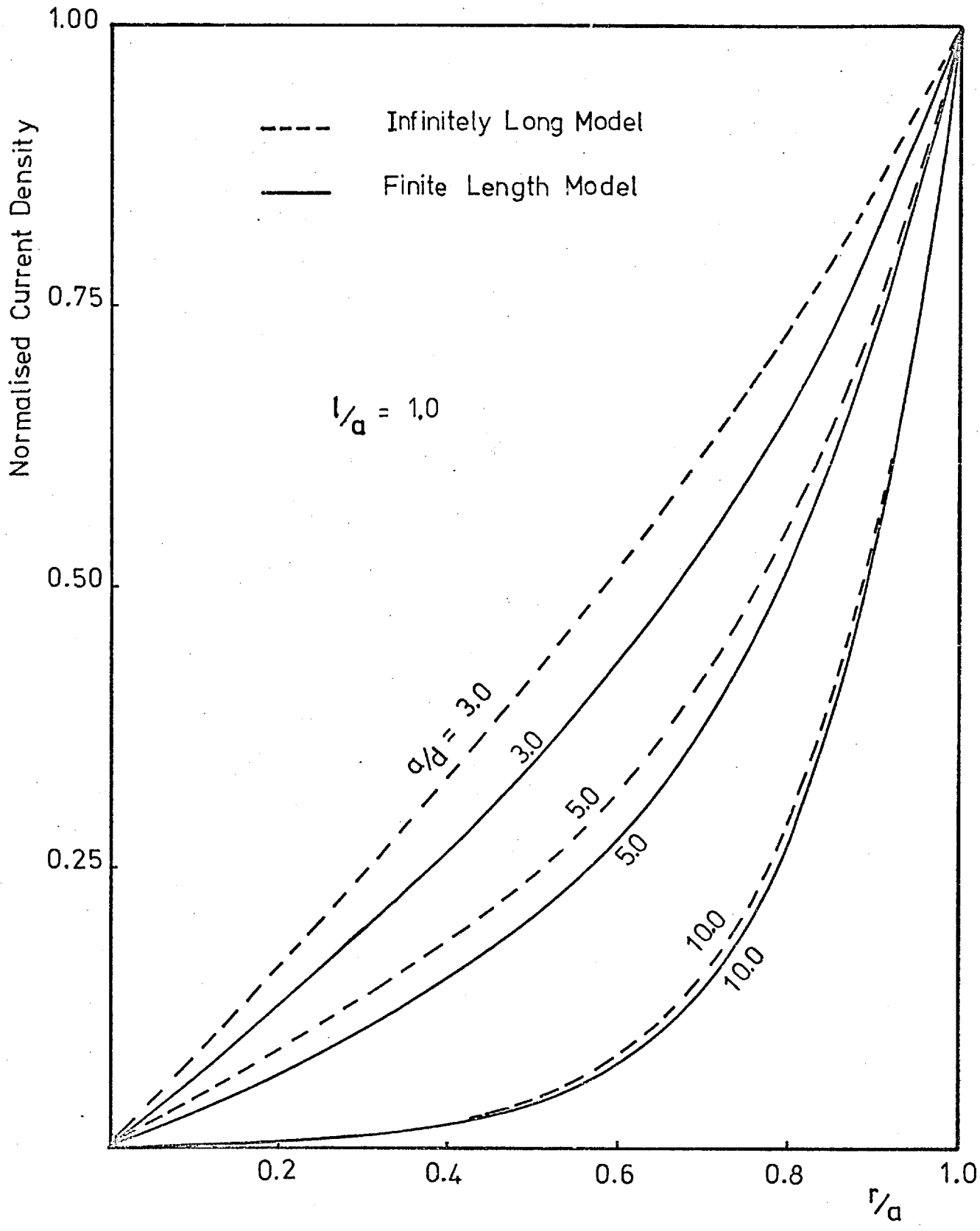


Fig.5.14 Radial distribution of the normalised amplitude of the induced eddy current in a conducting bar.

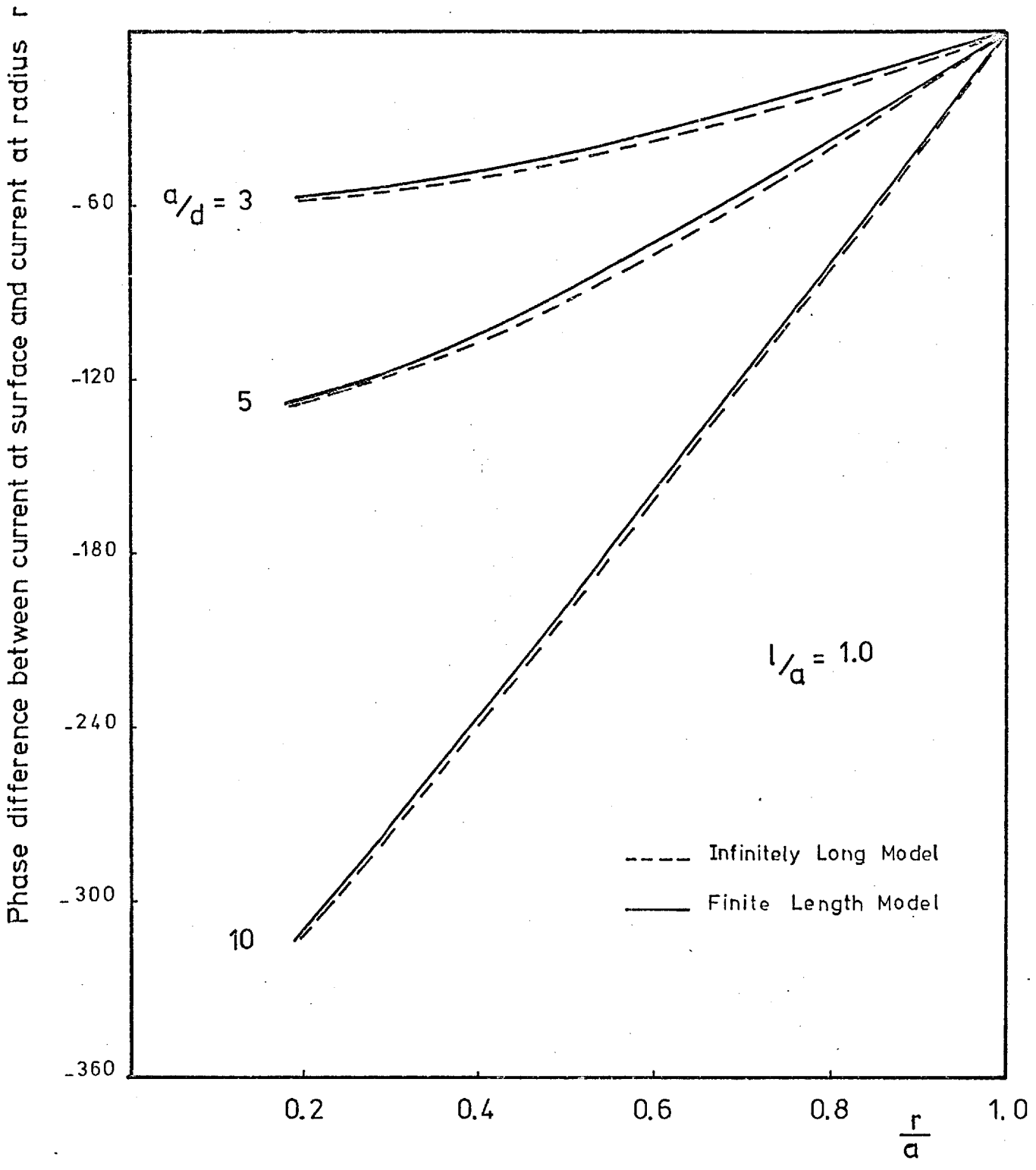


Fig. 5.15 Variation of the phase difference between current at the surface and current at radius r

were plotted for the same case when the excitation coil is infinitely long. Fig. (5.15) shows the phase angle of the induced eddy currents.

From the results of the two cases, it can be seen that, due to the finite length effect, the normalised induced eddy current is smaller in magnitude and is slightly advanced in phase when compared with the results calculated for the infinitely long model. Usually the values of a/d between 1.0 and 5.0 are used for eddy current non-destructive testing of conducting cylindrical specimens. In this range, and for a coil where l/a = 1.0, the normalised value of the induced current at a radius equal to half the conducting cyinder outer radius was found to be about 20% less than the corresponding value of the infinitely long model. As the frequency increases, this difference decreases. However, this 20% drop does not represent the decrease in the actual value of the current. To give some idea of how much the value of the current density will decrease with the introduction of finite length effect, a family of curves, which relate the amplitude of the surface induced current density to its value obtained for an infinitely long model having the same ampere-turns per metre, are plotted in Fig (5.16).

As an example, the amplitude of the induced current, at a radius r = 0.5a, in an infinitely long solid cylinder closely encircled by a solenoidal coil of negligible

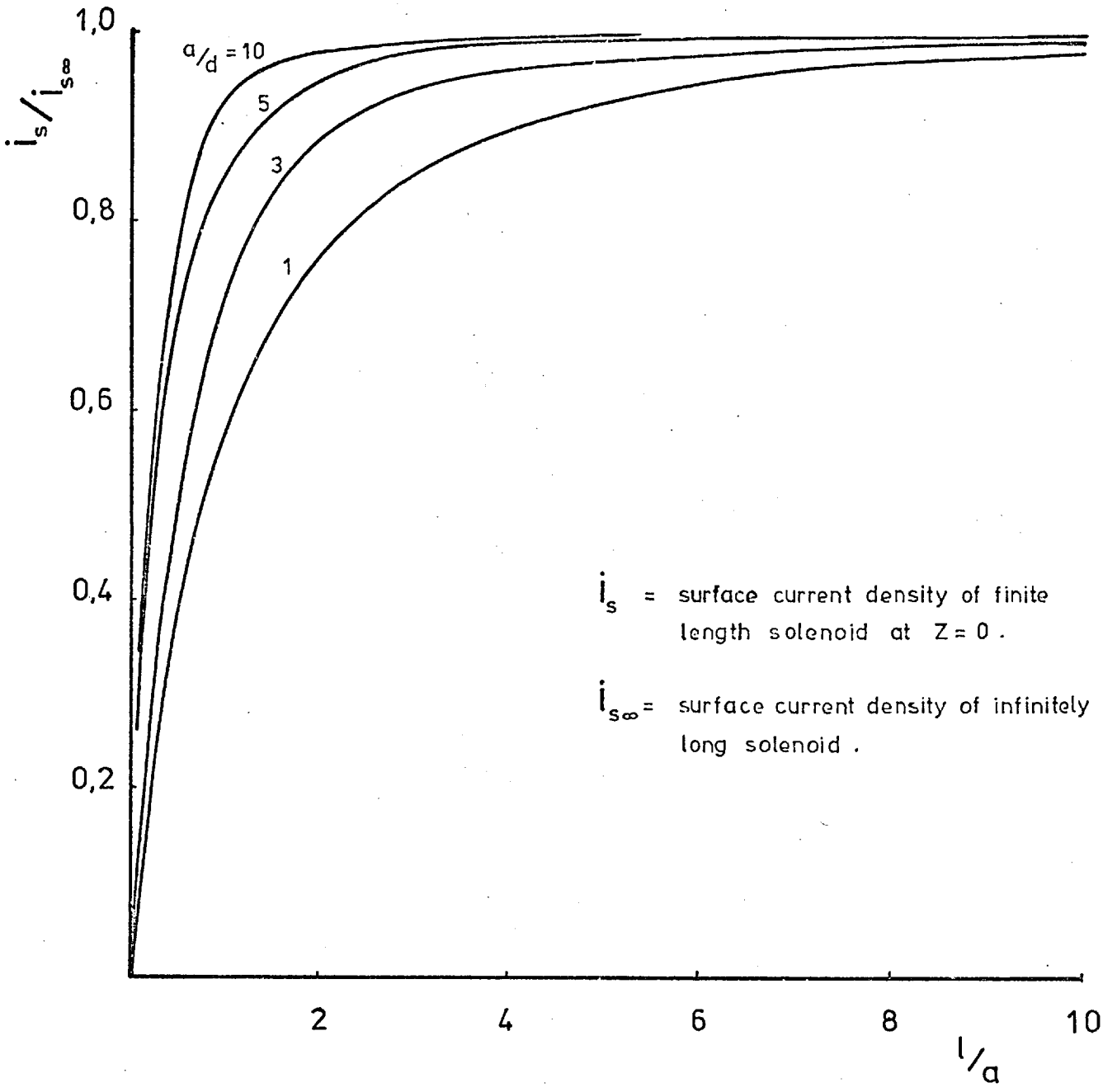


Fig. 5.16 Normalised surface current density curves in the plane z = 0.0

thickness and with a length equal to its radius, when the frequency is such that a/d = 3.0, can be obtained as follows:

From Fig. (5.14) the normalised value of the current at that radius is 19% less than the corresponding value for an infinitely long model. From Fig. (5.16), the amplitude of the induced surface current density is only 72% of the value which corresponds to an infinitely long model. Hence the actual drop in the value of the amplitude of the induced current density due to the introduction of the finite length effect is given by:

$$(1 - 0.81 \times 0.72) \times 100 = 42\%$$

5.7 Conclusions

A new method has been described for the calculation of the impedance of a solenoidal coil of finite length in a multi-region circular cylindrical structure of infinite length.

The method makes use of a transmission line analogy and hence completely avoids all Bessel functions. The method has been checked against published results for the case of a solenoid surrounding a single solid conductor. The results agree tolerably well. The sources

of difference between these results were briefly discussed, and ways of achieving better accuracy were presented.

Simple mathematical expressions for the surface wave impedance of the non-conducting innermost and outermost regions are developed. These expressions, together with the concept of wave impedance are employed to derive an expression for Nagaoka's factor. The obtained expression by the method reported in this chapter is found to be identical to the original expression as derived by Nagaoka. The calculated Nagaoka's factor was found to agree very closely, especially for short coils, with other published values.

For computational purposes, it was indicated that Nagaoka's factor could be obtained, with the aid of a hand calculator, to a high degree of accuracy, (e.g. 9 decimal points), using the expression in terms of elliptic integrals. These elliptic integrals were calculated in a very simple and rapid way, by constructing a rapidly convergent 'arithmetico-geometrical' scale.

The distribution of the induced surface current density in the axial direction is obtained for different values of (l/a) and for different frequencies. The radial distribution of the amplitude of the induced eddy current has been obtained for the value of (l/a)=1

and at different frequencies. The curves show that for the short coils (e.g. $l/a = 1.0$) the magnitude of the induced current drops appreciably as compared with its value obtained for a infinitely long model.

Although the method has only been checked for the simple examples given above, it is claimed to be very general. The current distribution curves in the axial and the radial directions are thought to be original.

CHAPTER 6

Electromagnetic Field Solution of a Concentric Multiple Region Spherical Structure Excited by a One-Dimensional Current Sheet or a Uniform Mangetic Field

6.1 Introduction:

One of the main problems encountered in the process of melting some reactive high melting point metals, is the contamination of the molten metal due to its chemical interaction with the crucible. For instance, titanium when melted in a graphite crucible may contain several tenths to one percent or more of carbon. In an attempt to realise a contamination-free process of melting metals, Okress et. al.[6.1] suggested a method whereby the metal was levitated and melted by electromagnetic induction, using frequencies of the order of 10 kHz. Briefly, the method employs two coaxial coils connected in series across a common capacitor so as to constitute a parallel tuned load to the alternator. The alternating currents in the (generally unequal) coils are in series opposition at all times. The principle of operation of this system is that, the currents in these fixed coils induce in the interposed metal charge, which may for example be a sphere, eddy currents whose interaction with the inducing field gives rise to the necessary supporting and lateral restoring forces. Heating and melting of the levitated sphere will

then depend upon the input power, coupling between the energizing coils and the metal sphere and the frequency in addition to some thermal factors. Okress et. al.[6.1] pointed out that, although the metal sphere could be supported by the electromagnetic field of a single coil energized with alternating current, it drifted laterally from the coil axis and fell out of the influence of the field. This could be eliminated by using two coils instead of one as indicated above.

The basis of the theoretical treatment of this problem, as suggested by the authors[6.1] is stated as follows: "If a homogeneous sphere is set into a magnetic field that is uniform in space and sinusoidally alternating in time at not too high a frequency, then the magnetic field of the eddy currents induced in the sphere is identical with that of a magnetic dipole, alternating in time with the generating field, at a phase and a strength that depend on the generating field strength and frequency, and on the sphere's radius, permeability and resistivity. The net mechanical force which the uniform alternating field exerts upon the dipole, to which the sphere is equivalent, is zero. If now the sphere is put into a non-uniform alternating field, then to a "first approximation" the force may be calculated by replacing the sphere by a dipole that would be produced by a fictitious uniform alternating field having everywhere the value the given non-uniform field has at the centre of the sphere. The actual non-uniform field would exert a force upon this dipole". This method of calculation, as the authors

admitted offers only an approximate solution. However, the agreement between theoretical and experimental results is remarkable. In fact this approximate representation becomes more precise as the sphere is made smaller.

Many of the subsequent papers on electromagnetic levitation of spheres retained the same geometrical configuration suggested by Okress et. al., but differed in their theoretical approach to the problem. For example, Brisely and Thornton[6.2] solved for the vector potential then calculated the magnetic field components, from which the levitation force could be obtained by one of the following methods:

(i) From the force on the eddy currents due to the presence of the field coils.

or (ii) From the force on the coils due to the presence of the field of the eddy currents.

The authors[6.2] calculated the levitation force by the second method.

Smith[6.3] calculated the levitation force for the same problem using another technique. He solved for the magnetic vector potential, from which the magnetic flux density components could be obtained, the force was then obtained as the rate of change of the total stored energy in the magnetic field.

As far as electromagnetic levitation in general is concerned, although somewhat beyond the scope of this chapter, the papers by Boerdijk[6.4] and by Laithwaite[6.5] give an excellent review and list of references.

For all the above references, the problem has been formalized in a spherical coordinate system, the excitation current as well as the induced eddy current in the sphere have been assumed to flow in the ϕ-direction while the magnetic field has been assumed to have both r and θ components but independent of ϕ. These assumptions are usually adopted when solving another different problem. That is the problem of magnetic shield or eddy current screening using a spherical shells. For instance, Popović[6.6] gave a closed form solution for the screening ratio of a magnetic spherical shell situated in an external static uniform magnetic field, provided that the permeability of the shell is assumed constant. Smythe[6.7] solved the same problem for an alternating magnetic field and allowing the spherical shell to have finite conductivity, i.e. he introduced the induced eddy current effects into his calculations.

Apart from the special non-conducting case studied by Popović, the solutions are always given in terms of modified Bessel functions whose arguments involve the radius r.

It has been shown in Chapters 2, 4 and 5 that the modified Bessel functions could be completely avoided if the

problem is formulated in transmission line form. The main objective of this Chapter will be solely devoted to pursue this concept and develop the equivalent transmission line which represents this particular field problem. The electromagnetic field components could then be calculated from this equivalent transmission line. No attempt has been given to study the forces or associated problems, although these could be calculated from a knowledge of field and eddy current distributions. This chapter is strictly concerned with obtaining the electromagnetic equivalent network which helps in calculating the field components as well as the induced eddy currents in the conducting regions. The theoretical results obtained from the transmission line modelling are checked against certain closed forms of solution as well as experimental results.

6.2 Mathematical Model

Consider a set of N concentric spherical regions, as shown in Fig (6.1), each region is characterised by isotropic parameters μ, σ and ε.

The excitation current sheet lies at the boundary surface between any two adjacent regions, it has only a ϕ-component, and it is independent of ϕ.

The time dependence of all vector fields components is of the form: $\exp(j\omega t)$, hence this will permit substituting for the time derivative, whenever it appears in the field equations, by $(j\omega)$.

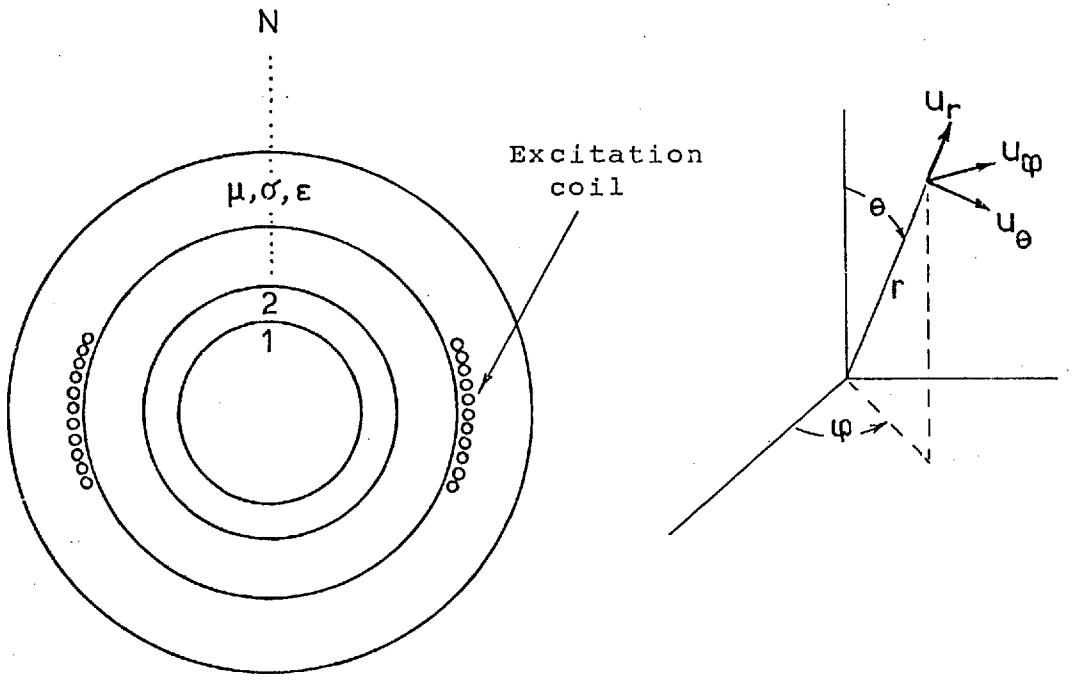


Fig. 6.1: The mathematical model

All field components are assumed independent of ϕ,

$$\text{i.e.} \quad \frac{\delta}{\delta\phi} = \frac{\delta^2}{\delta\phi^2} = 0$$

Because the excitation current has been restricted to flow in the ϕ-direction, the electric field vector at any point will have a ϕ-component only, while the magnetic field vector will have in general components in both the r- and θ-directions.

6.3 Field Equations

Starting from the Maxwell field equations, it can be shown that both $\bar{E}$ and $\bar{H}$ vectors satisfy the vector Helmholtz equation, which is:

$$\nabla^2 \begin{bmatrix} \bar{E} \\ \bar{H} \end{bmatrix} = j\omega\mu\, \sigma_c \begin{bmatrix} \bar{E} \\ \bar{H} \end{bmatrix} \qquad (6.1)$$

Where:

$\sigma_c = \sigma + j\omega\varepsilon$

= complex conductivity

Usually at power frequencies $\sigma_c = \sigma$, i.e. neglecting the displacement current. Throughout the rest of this Chapter, the symbol σ will be used, keeping in mind that it can be complex or purely imaginary if necessary according to the field of application, (intermediate or high frequency).

6.3.1 Formulation

The general expression of the components of the vector Helmholtz equation (6.1) in the spherical polar coordinates are given in reference (6.8).

Since E_r and E_θ are zero, also E_ϕ is independent of ϕ, hence equation (6.1) reduces to:

$$\{\frac{\delta^2}{\delta r^2} + \frac{2}{r}\frac{\delta}{\delta r} - j\omega\mu\sigma\} E_\phi$$

$$+ (1/r^2)\{\frac{\delta^2}{\delta\theta^2} + \cot\theta \frac{\delta}{\delta\theta} - (1/\sin^2\theta)\} E_\phi = 0 \quad (6.2)$$

Where E_ϕ can be written in general in the separable form:

$$E_\phi = \sum_n R_n(r) \cdot \Theta_n(\theta) \exp(j\omega t) \quad (6.3)$$

In fact there is no need to determine the magnetic field vector $\bar{H}$ from its vector Helmholtz equation, as we need to solve for both H_r and H_θ. Since the electric field vector has only a ϕ-directed component, which could be obtained from equation (6.2) the simplest way to obtain the expressions of the magnetic field components is to relate them to the E_ϕ through the curl equation:

$$\nabla X\bar{E} = -j\omega\mu\bar{H} \quad (6.4)$$

Expanding equation (6.4) in the spherical polar coordinates and substituting for $\bar{E}$ by $E_\phi \bar{u}_\phi$ we get:

$$H_\theta = (1/j\omega\mu r) \frac{\delta}{\delta r}(r E_\phi)$$

$$H_r = -(1/j\omega\mu r \sin\theta) \frac{\delta}{\delta\theta}(\sin\theta . E_\phi) \quad (6.5)$$

6.3.2 Solution of the field equations

In order to solve for E_ϕ, substitute from equation (6.3) into (6.2), the surface zonal harmonic $\Theta_n(\theta)$ and the

radial function $R_n(r)$ are then given by[6.7]:

$$\Theta_n(\theta) = A\, P_n^1 (\cos\theta) + C\, Q_n^1 (\cos\theta) \qquad (6.6)$$

and

$$R_n(r) = r^{-\frac{1}{2}} \{A'\, I_{n+\frac{1}{2}} (\gamma r) + C'\, K_{n+\frac{1}{2}} (\gamma r)\} \qquad (6.7)$$

Where:

P_n^1 and Q_n^1 are respectively the first and second kinds of associated Legendre functions of order (n) and degree (1).

$I_{n+\frac{1}{2}}$ and $K_{n+\frac{1}{2}}$ are respectively the first and second kinds of modified Bessel functions of order $(n + \frac{1}{2})$.

A, A', C and C' are constants to be determined by applying the boundary conditions.

$$\gamma^2 = j\omega\mu\sigma$$

The general solution for the electric field vector in any 'one' region of the mathematical model illustrated in section (6.2) can be written in the form:

$$E_\phi(r, \theta, \phi, t) = \sum_n \{ A_n\, P_n^1(\cos\theta) + C_n\, Q_n^1(\cos\theta)\} \cdot r^{-\frac{1}{2}} \{A_n'\, I_{n+\frac{1}{2}}(\gamma r) + C_n'\, K_{n+\frac{1}{2}}(\gamma r)\} \cdot \exp(j\omega t) \qquad (6.8)$$

6.4 Excitation Current Sheet

The solution for the electric field component E_ϕ is given by equation (6.8), while the solution for the magnetic field components H_r and H_θ can be obtained by substituting for E_ϕ in equations (6.5).

It is quite clear from the expression E_ϕ that all the electromagnetic field components have their θ-dependent functions given in terms of the associated Legendre functions. In order to apply the H-tangential continuity relation at the boundary surface where the excitation current sheet exists, the current sheet expressions must be given in terms of the associated Legendre functions as well.

The associated Legendre functions of second kind $Q_n^1(X)$, which appear in the E_ϕ expression, are unbounded at $X = \pm 1$, whereas $P_n^1(X)$ are bounded at $X = \pm 1$ (6.9), which correspond to $\theta = 0, \pi$, and since physically the solution must be bounded at these two values of θ, all the constants C_n which appear in equation (6.8) must be equal to zero.

The excitation current sheet is then required to be expressed in terms of the associated Legendre functions of the first kind only, which are in general $P_n^m(X)$. These functions are orthogonal in the region where X varies between -1, +1, that is to say:

$$\int_{-1}^{+1} P_n^m(X) \cdot P_\ell^m(X)\, dx = 0 \qquad \ell \neq n$$

$$\int_{-1}^{+1} \{P_n^m(X)\}^2 \cdot dx = (n+m)!/\{(n+\tfrac{1}{2}) \cdot (n-m)!\} \tag{6.9}$$

This gives the possibility of expressing any function, which is sectionally continuous in the region (-1,+1), in terms of a series of associated Legendre functions as follows:

$$f(X) = \sum_{n=m}^{\infty} a_n P_n^m(X) \tag{6.10}$$

It should be noted that the summation of this series starts from n = m, since $P_n^m(X) = 0$ for all values where $m > n$.

From equations (6.9) and (6.10), it can be shown that the expression of a_n is given by:

$$a_n = (n+\tfrac{1}{2}) \frac{(n-m)!}{(n+m)!} \int_{-1}^{+1} f(X) \cdot P_n^m(X) \cdot dx \tag{6.11}$$

A schematic diagram of the excitation coil is shown in Fig. (6.2a), its equivalent idealized current sheet spatial distribution is shown in FIg. (6.2b). It is assumed that the excitation current is single phase, sinusoidally variable with time, and its value is given by:

$$i = \sqrt{2}\, I \cos \omega t$$

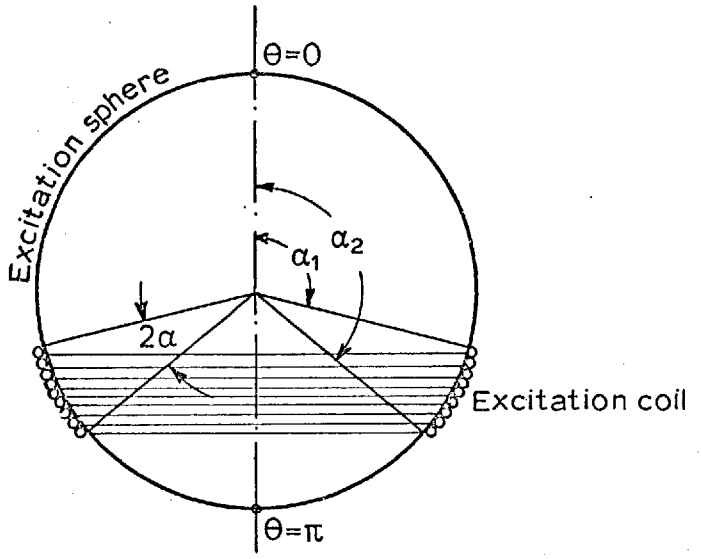


Fig. 6·2a Excitation current distribution

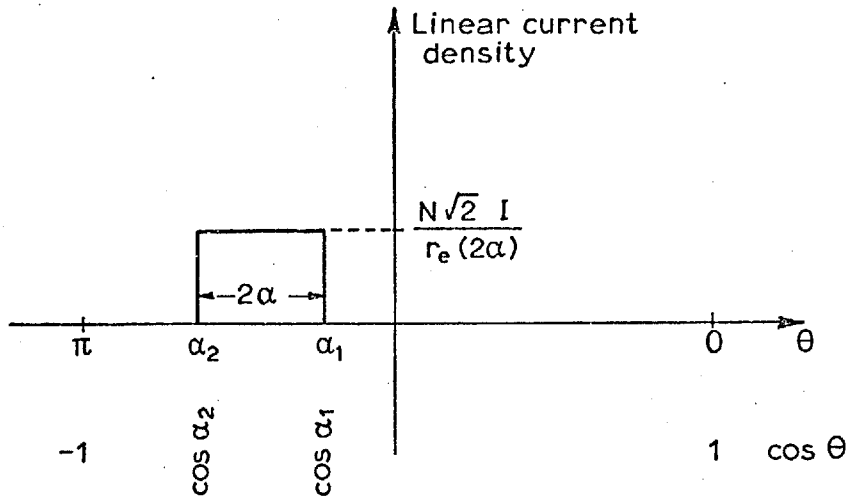


Fig. 6·2b Spatial distribution of excitation current sheet

The amplitude of the excitation current sheet will be then given by:

$$N\sqrt{2}\ I/2\alpha \cdot r_e$$

where:

I = r.m.s. value of excitation current

N = excitation coil number of turns

r_e = radius of the excitation sphere

2α = coil angle in radians, defined as shown in Fig. (6.2).

The excitation current sheet expression accordingly will be given by:

$$K_\phi(\theta, t) = \sum_{n=1}^{\infty} \hat{K}_n P_n^1(\cos\theta) \cdot \mathrm{Re}\ \exp(j\omega t) \qquad (6.12)$$

Where K_n is the amplitude of the current sheet nth surface zonal harmonic, and is given by:

$$\hat{K}_n = \frac{(2n+1)}{2n(n+1)} \int_{\cos\alpha_2}^{\cos\alpha_1} \frac{N\sqrt{2}\ I}{r_e(2\alpha)} \cdot P_n^1(\cos\theta) \cdot d(\cos\theta) \qquad (6.13)$$

For the special case, when:

$$\alpha_1 = \pi/2 - \alpha$$

$$\alpha_2 = \pi/2 + \alpha$$

the first few surface zonal harmonics of the excitation current are given by[6.10]:

$$\hat{K}_1 = \hat{K}\ (3/4)\ \{\sin\alpha.\ \cos\alpha + \alpha\}$$

$$\hat{K}_3 = \hat{K}\ (7/64)\{\ \sin\alpha.\ \cos\alpha(10\ \sin^2\alpha - 9) + \alpha\}$$

$$\hat{K}_5 = \hat{K}\ (11/256)\ \{\sin\alpha\ \cos\alpha\ (56\ \sin^4\alpha - 70\ \sin^2\alpha + 15) + \alpha\}$$

$$\hat{K}_7 = \hat{K}\ (15/32768)\{\ \sin\alpha\ \cos\alpha\ (13728\ \sin^6\alpha - 23408\ \sin^4\alpha + 11060\ \sin^2\alpha - 1330) + 50\alpha\}$$

(6.14)

Where:

$$\hat{K} = NI/\sqrt{2}\alpha r_e$$

The magnitudes of these excitation current sheet harmonics, as a percentage of its fundamental component, are plotted in Fig. (6.3) against the filling factor. The filling factor of this spherical excitation coil is defined as the ratio between the angle covered by the coil and 180^{o}. The curves show that, generally, the harmonic content of the excitation current decreases as either the order of harmonic or the filling factor increases.

6.5 Transmission Line Modelling

In section (6.3.2) it has been found that the functional dependence of the field components on the radius (r) is generally in the form of modified Bessel functions. However,

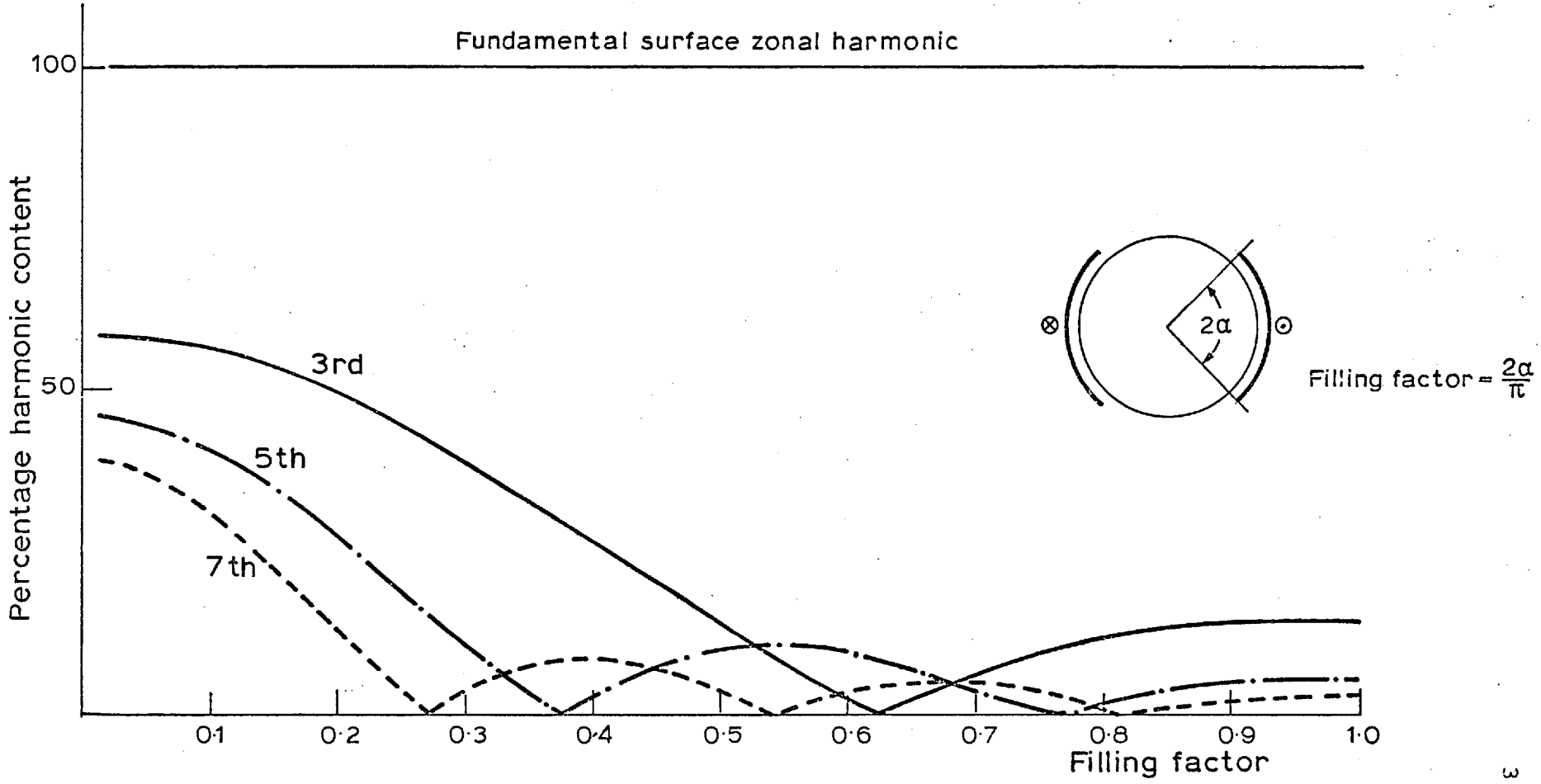


Fig. 6·3 Surface zonal harmonic contents of the excitation current sheet obtained by a symmetrically placed exciting winding.

as it has been shown in the preceding chapters, the need for Bessel functions could be completely avoided by developing a transmission line equivalent network, whose voltage and current distributions along its length are equivalent to the electric and magnetic fields radial distributions across the spherical shell. In this section, an equivalent network will be deduced where the concept of the 'Micro-T' circuit, as been defined before, will be employed.

6.5.1 Micro-T circuit representation

Let the nth zonal harmonic components of the electric and magnetic fields to be written in the form:

$$\begin{aligned} E_{\phi,n} &= E_n(r)\ \ \theta_n(\theta)\ \ \exp(j\omega t) \\ H_{\theta,n} &= H_n(r)\ \ \theta_n'(\theta)\ \ \exp(j\omega t) \end{aligned} \qquad (6.15)$$

Substituting for E and H from equation (6.15) into equations (6.2) and (6.5) we get:

$$\frac{d^2}{dr^2}\{r.E_n(r)\} - \left[\frac{n(n+1)}{r^2} + j\omega\mu\sigma\right].\{r.E_n(r)\} = 0 \qquad (6.16)$$

$$\frac{d}{dr}\{r.E_n(r)\} = j\omega\mu r H_n(r)\ \{\frac{\theta_n'}{\theta_n}\}$$

The generalised transmission line equation is given by:

$$\frac{d^2V(r)}{dr^2} - \frac{1}{Z}\frac{dZ}{dr}\frac{dV(r)}{dr} - ZY\,V(r) = 0 \qquad (6.17)$$

Comparing equations (6.16) and (6.17), term by term, in order to define the elements of the equivalent transmission line, we get:

$$\frac{dZ}{dr} = 0 \qquad (6.18)a$$

$$ZY = \frac{n(n+1)}{r^2} + j\omega\mu\sigma \qquad (6.18)b$$

From equation (6.18a), the series impedance per unit length of the equivalent transmission line must be independent of the radius (r). To satisfy this result as well as equation (6.16), the flow function of this transmission line should be $\{r.H_n(r)\}$ and not $H_n(r)$ only. If (θ_n') is chosen to be equal to (θ_n), the series impedance Z will be given by:

$$Z = j\omega\mu \qquad (6.19)a$$

Hence, the parallel admittance per unit length Y is given by:

$$Y = \sigma + \frac{1}{j\omega\mu}\frac{n(n+1)}{r^2} \qquad (6.19)b$$

And the micro-T circuit of this equivalent transmission line becomes as shown in Fig. (6.4) below.

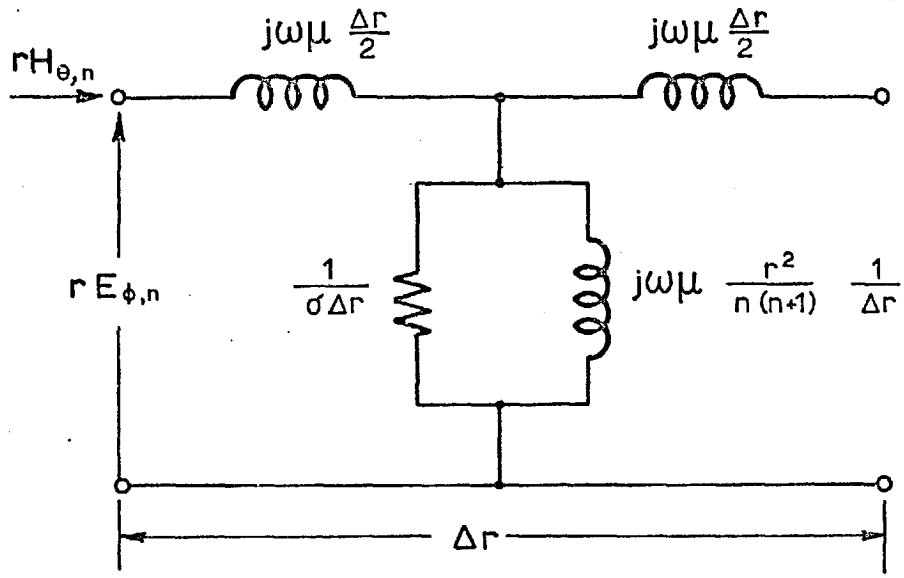


Fig. 6.4 Micro-T circuit of a spherical shell thickness Δr, for the n^{th} harmonic component.

Any single spherical shell region is modelled by joining a number of these micro-T circuits in cascade to form a set. The complete model then consists of a number of these sets, again in cascade. The continuity of $E_n(r)$ and $H_n(r)$ at each region boundary is automatically satisfied. The discontinuity in $H_n(r)$ at the current sheet is modelled by introducing a current source, whose amplitude is $\hat{K}_n$ (as obtained from equation 6.13), at that point in the model.

Notice:

It should be noticed that equation (6.16b) when written in terms of the equivalent transmission line parameters will have the form:

$$\frac{dV}{dr} = ZI$$

where: $V = rE$

$I = rH$

$Z = j\omega\mu$

The -ve sign which usually appears in the standard transmission line equation does not appear in the above equation, which means that the +ve direction of current flowing in the equivalent T.L. of our case is in the direction of the decrease in the distance r.

The micro-T circuit shown in Fig. (6.4) represents in general a conducting, magnetically linear isotropic region. For non-conducting regions, the micro-T circuit is obtained by removing the resistive branch from the circuit.

It is interesting to notice that, the arguments of the modified Bessel functions which appear in the solution of either E_ϕ or H_θ (see for instance equation 6.12), are directly proportional to $\sigma^{\frac{1}{2}}$. Hence, for the case of non-conducting region, when the conductivity is zero, the analytic form of the

solution for E_ϕ will not be in terms of Bessel functions. It will be shown in the next section how the zero conductivity will affect the analytic solution, and how this will lead to modelling the non-conducting region in a transfer matrix form which is, for this special case, simpler than micro-T circuit representation.

6.5.2 Transfer matrix representation of non-conducting spherical shells

Consider a non-conducting spherical shell whose inner and outer radii are (a) and (b) respectively.

The differential equations which describe the electric and magnetic field components in this region can be obtained from equation (6.16) by putting $\sigma = 0$, hence:

$$\left.\begin{aligned} \frac{d^2V}{dr^2} - \frac{n(n+1)}{r^2} V &= 0 \\ \frac{dV}{dr} &= j\omega\mu\, I \end{aligned}\right\} \quad (6.20)$$

Where $V = rE$ and $I = rH$

The solutions for V and I are then given in the form:

$$V(r) = A_n r^{n+1} + B_n r^{-n} \quad (6.21)$$

$$I(r) = (1/j\omega\mu) \cdot \{(n+1)A_n r^n - n B_n r^{-(n+1)}\}$$

A_n and B_n are constants to be determined from the boundary conditions.

Equations (6.21) can be manipulated algebraically in order to eliminate the constants A_n and B_n by relating the voltage and current at both ends of the equivalent T.L. The result can be written in a matrix form as given by equation (6.22) below.

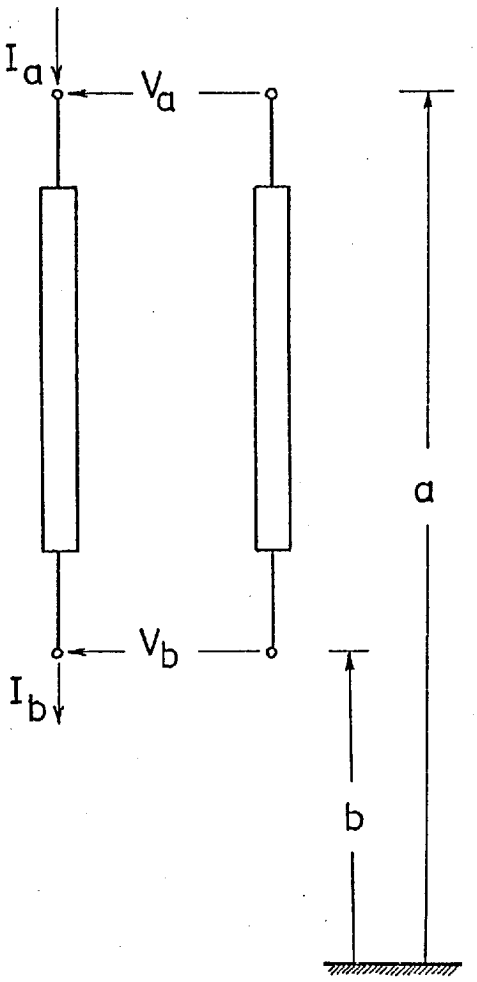


Fig. 6.5: Equivalent T.L. of a non-conducting region.

$$\begin{bmatrix} V_b \\ I_b \end{bmatrix}_n = \frac{1}{(2n+1)} \cdot \begin{bmatrix} C_{1,n} & C_{2,n} \\ C_{3,n} & C_{4,n} \end{bmatrix} \begin{bmatrix} V_a \\ I_a \end{bmatrix}_n \qquad (6.22)$$

Where the transfer matrix elements are given in the form:

$$C_{1,n} = n\,(b/a)^{n+1} + (n+1)\,(a/b)^{n}$$

$$C_{2,n} = -j\omega\mu\,\{a^{n+1}/b^{n} - b^{n+1}/a^{n}\}$$

$$C_{3,n} = (-1/j\omega\mu)\; n(n+1)\,\{a^{n}/b^{n+1} - b^{n}/a^{n+1}\} \qquad (6.23)$$

$$C_{4,n} = (n+1)\,(b/a)^{n} + n(a/b)^{n+1}$$

The sign convention employed in deriving the matrix equation (6.22) assumes input terminals at r = a, and output terminals at r = b, provided that a>b. The positive directions of the current and voltage are as indicated in Fig. (6.5). These directions are consistent with the formulation of equation (6.16b). However, if the positive directions of currents were supposed such that the input terminals are at radius r = b, while output terminals at r = a, where b<a, the matrix equation will still be as given by equation (6.22) but after changing the sign of both $C_{2,n}$ and $C_{3,n}$.

The matrix equation which gives the input quantities V_a and I_a in terms of the output quantities V_b and I_b can be written directly by replacing (a) and (b) and vice versa in equations (6.22) and (6.23).

In conclusion, the matrix equation (6.22) related the electric and magnetic fields components at both inner

and outer surfaces of the non-conducting, magnetically linear spherical shell. The transfer matrix elements are simple functions of the inner and outer radii as well as the permeability of the region. Hence, it is simpler to represent the non-conducting region by its transfer matrix rather than to model it by a set of micro-T circuits in cascade.

6.5.3 Innermost and outermost non-conducting regions: input impedance

If the non-conducting region is either the innermost or outermost regions, the values of (a) or (b) may reach zero or infinity respectively. Then the elements of the transfer matrix, as given by equation (6.22), become infinity. The transfer matrix as it stands now fails to represent these two special cases. A special treatment is needed for these situations, as follows:

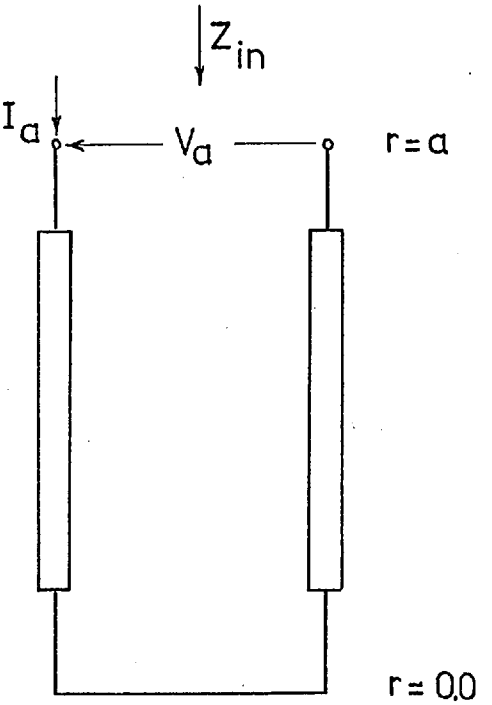
(i) The innermost region is non-conducting, a magnetically linear sphere:

In this case, the solutions for both V and I given by equations (6.21) reduce to:

$$V(r) = A_n r^{n+1} \qquad (6.24)$$

$$I(r) = \frac{1}{j\omega\mu} (n + 1) A_n r^n$$

The direction of the current I is as indicated in the opposite equivalent circuit.



The tensorial surface wave impedance looking 'into' the innermost region is then given by:

$$Z_{in,n} = V(a)/I(a)$$

$$= j\omega\mu a/(n+1) \qquad (6.25)$$

where:

a outer radius of the innermost spherical non-conducting region.

(ii) <u>The outermost region is non-conducting, a magnetically linear spherical shell</u>:

The radial distribution of V(r) and I(r) along the equivalent transmission line in this situation is governed by the equations:

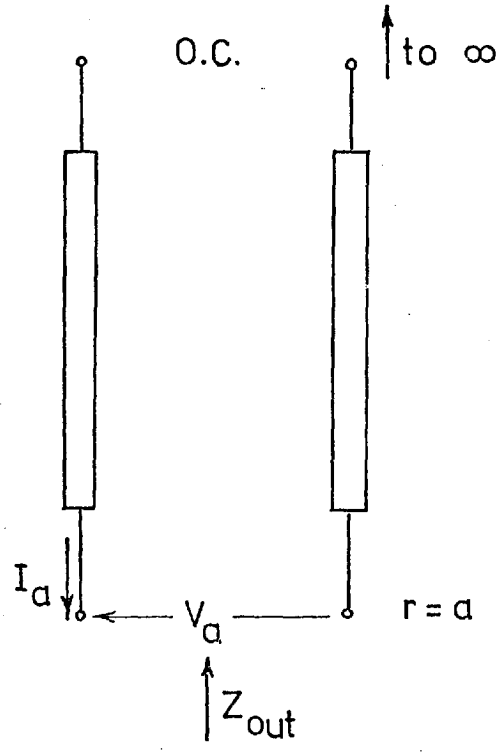
$$V(r) = B_n r^{-n}$$

$$I(r) = \frac{-1}{j\omega\mu} n B_n r^{-(n+1)} \qquad (6.26)$$

If the inner radius of the outermost region is (a), the input impedance $Z_{out,n}$, looking 'into' this region is given by:

$$Z_{out,n} = \frac{V(a)}{-I(a)}$$

$$= \frac{1}{n} j\omega\mu a \qquad (6.27)$$



Summing up the results of section (6.5), the different regions which constitute the multi-shell spherical mathematical model are to be represented as follows:

a) Conducting spherical shell: modelled by a set of micro-T circuits connected in cascade, as obtained in section (6.5.1).

b) Non-conducting spherical shell: represented by its transfer matrix, as described in section (6.5.2).

c) Non-conducting innermost or outermost regions: each can be represented by a single inductive surface wave impedance as derived in section (6.5.3).

It should be noted that if the spatial distribution of the electromagnetic field components is required in a non-conducting region, the easiest way to get it is to represent this non-conducting region by its equivalent transmission line. The transfer matrix helps in relating the field quantities at both the inner and the outer surfaces of the non-conducting region.

6.5.4 Choice of the sub-region thickness Δr:

(i) For a non-conducting region

The equivalent micro-T circuit of the non-conducting region can be deduced from the general circuit shown in Fig. (6.4) by removing the resistive branch from the circuit.

The ratio between the series and the parallel impedances is given by:

$$\frac{Z_s}{Z_p} = \frac{\Delta r^2}{2} \cdot \frac{n(n+1)}{r^2} \qquad (6.28)$$

Consequently the number of the micro-T circuits which represent a non-conducting spherical shell, will be given by:

$$\text{No. of } \mu T \text{ circuits} = \frac{R_o - R_i}{\Delta r}$$

$$= \frac{R_i}{r}\sqrt{\frac{n(n+1)}{2}}\ \sqrt{\frac{Z_p}{Z_s}}\ \left(\frac{R_o}{R_i} - 1\right) \qquad (6.29)$$

Where:

R_i = the inner diameter of the shell

R_o = the outer diameter of the shell

The sub-region thickness Δr is directly proportional to the radius (r), and inversely proportional to the order of harmonic (n), particularly for high values of n. This means that in general, the division of any spherical shell to a number of sub-regions must be increased as the order of harmonic increases. It indicates also that if it is required to keep the series/parallel impedances ratio constant, the subregions should be thinner as the radius decreases. In order to be on the safe side, Δr could be calculated near the inner radius of the region in order to have a certain minimum Z_p/Z_s ratio. As this ratio increases, more accurate results could be obtained, but a larger computation time is required. For the ratio $Z_p/Z_s \simeq 100$ for example, and calculating Δr near the inner radius of the spherical shell, the number of the micro-T circuit will be given by:

$$\text{Number of } \mu T \text{ circuits} \simeq 10\ \sqrt{\frac{n(n+1)}{2}}\ \left(\frac{R_o}{R_i} - 1\right) \qquad (6.30)$$

For the fundamental harmonic (n = 1) equivalent circuit, the above equation reduces to:

$$\text{Number of } \mu T \text{ circuits} \simeq 10\left(\frac{R_o}{R_i} - 1\right)$$

It should be noted that if the ratio R_o/R_i is very large, this number will be unnecessarily large with no actual need since the thin sub-regions are only required for small values of (r), not all over the region. It is suggested that this equation could be used for $R_o/R_i < 2$. If the actual region is thicker, it can be divided to two or more 'major' sub-regions, each has a radii ratio of $R_o/R_i = 2$, then each major sub-region can be divided to a number of micro sub-regions as illustrated earlier.

(ii) For a conducting region:

The micro-T circuit is as shown in Fig. (6.4). The parallel branch is composed of two elements, resistive and inductive. The sub-region thickness, and consequently the number of the micro-T circuits required could be calculated as follows:

- Calculate the number of micro-T circuits as if the inductive element exists alone in the parallel branch.

- Calculate the number of micro-T circuits as if the resistive element exists alone. This situation is similar to that discussed in Chapter 4 in more detail, i.e. $\Delta r \simeq$ 10-20% of the penetration depth.

The number of the micro-T circuits which represents the conducting region will be the sum of the two numbers obtained as above.

This method although semi-empirical, has been found to yield satisfactory results.

6.6 Expression for the Power Flow over a Spherical Surface

The power flowing from the excitation sheet across any spherical surface can be calculated from the Poynting vector, $\bar{S}$, as follows:

$$\bar{S} = \bar{E} \times \bar{H} \qquad w/m^2 \qquad (6.31)a$$

If $\bar{E}$ and $\bar{H}$ are complex values, the vector $\bar{S}$ will be given by:

$$S = \text{Re}\ (\bar{E} \times \bar{H}^*) \quad w/m^2 \qquad (6.31)b$$

Where the asterisk (*) denotes a conjugate value, and both $\bar{E}$ and $\bar{H}$ are expressed as r.m.s. values.

The power input to, or output from, any spherical region is due to the interaction of the E_ϕ and H_θ components at the relevant surface of this region.

To avoid confusion with Legendre functions, let the power symbol be W instead of P.

Therefore, W/unit area = $\mathrm{Re}\ E_\phi\ H_\theta^*$ $\quad W/m^2$

Therefore,

$$W = \mathrm{Re}\ -\int_{\theta=0}^{\theta=\pi} E_\phi\ H_\theta^*\ 2\pi r\ \sin\theta\ r\ d\theta$$

$$= \mathrm{Re}\ 2\pi r^2 \int_0^\pi E_\phi\ H_\theta^*\ (-\sin\theta\ d\theta)$$

$$= \mathrm{Re}\ 2\pi r^2 \int_0^\pi E_\phi\ H_\theta^*\ d(\cos\theta) \qquad (6.32)$$

But

$$E_\phi = \sum P_m^1\ (\cos\theta).V_m(r).\frac{1}{r}$$

$$H_\theta^* = \sum P_n^1\ (\cos\theta)\ I_n^*(r).\frac{1}{r} \qquad (6.33)$$

Therefore,

$$W = \mathrm{Re}\ 2\pi r^2 \int_{\theta=0}^{\pi} \sum \frac{1}{r}\ V_m(r).I_n^*(r).\{P_n^1(\cos\theta).P_m^1(\cos\theta)\}.d(\cos\theta) \qquad (6.34)$$

From the orthogonality of the associated Legendre function equation (6.34) reduces to

$$W = \mathrm{Re}\ 2\pi \sum V_n(r).I_n^*(r)\ \frac{2n(n+1)}{2n+1} \qquad (6.35)$$

Where: $V_n(r)$ and $I_n(r)$ are respectively the voltage and current of the nth zonal harmonic equivalent transmission line, calculated at the radius (r) at which the power flow is required to be calculated.

$I_n(r)$ which appears above should not be confused with the modified Bessel function of the first kind.

6.7 Special Case: Spherical Multiple-Shell Model in a Uniform Magnetic Field

The electromagnetic field problem in a spherical coordinate system has been solved in the previous sections for the case when the source function is produced by a spherical coil which carries current in the azimuthal direction only. In this section, a similar problem will be solved but when the source function becomes a uniform magnetic field. One of the practical aspects of this problem is the shielding of a certain region in space from magnetic fields by enclosing it within a spherical layer of some ferromagnetic or conducting substance. In solving this problem, it will be assumed that the introduction of a spherical model in the region of a uniform magnetic field will only affect the field distribution in the vicinity of this model, but will not affect the field at the distant points.

Referring to Fig. (6.6), let the magnetic field H_o be undirectional and uniform at all points on sphere C. Sphere C concentrically encloses the spherical multiple-shell model, and is situated at a distance from this model, large enough

to justify the uniformity of the field across it.

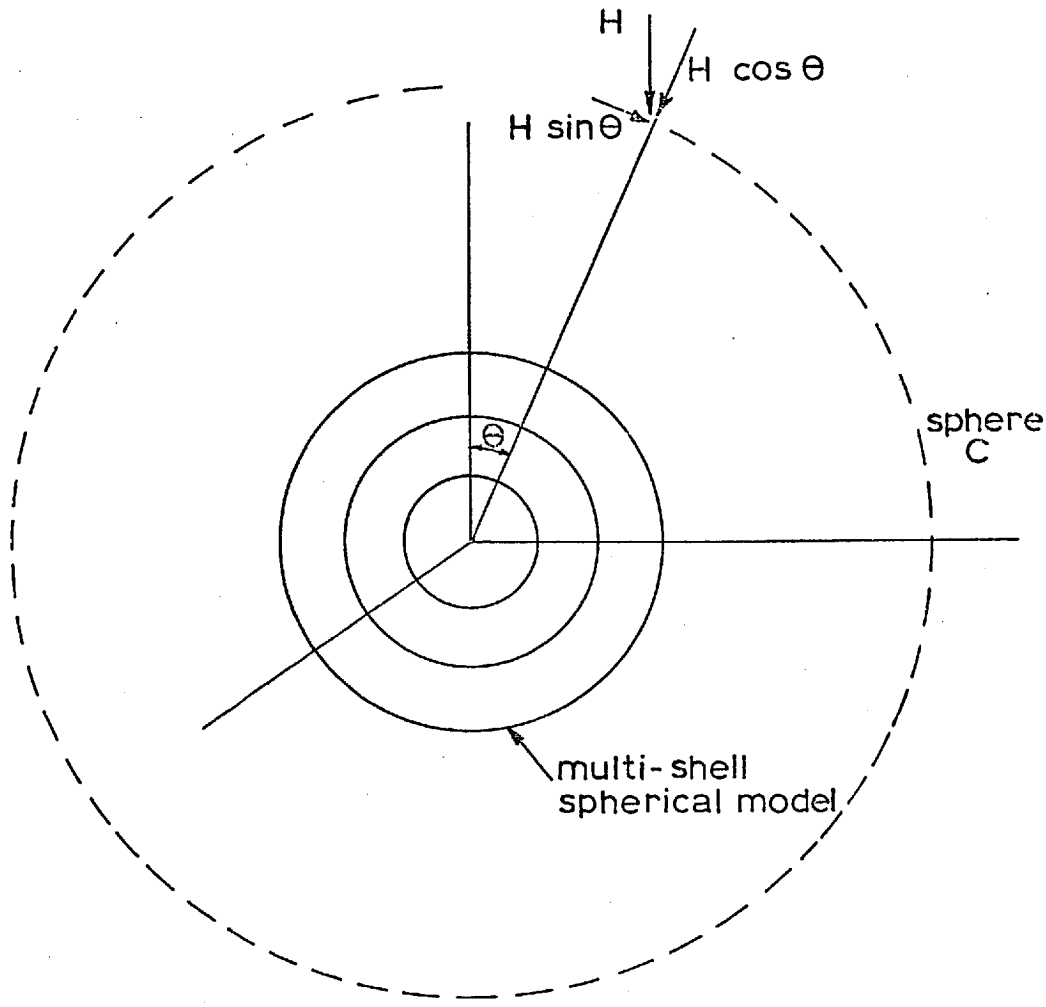


Fig. 6.6 Multi-shell spherical model placed in a uniform magnetic field.

The source magnetic field has two components given by:

$$H_r = -H_o \cos\theta \qquad (6.36)a$$

$$H_\theta = H_o \sin\theta$$

The component H_θ can be written in terms of the associated Legendre functions in the form:

$$H_\theta = H_o P_1^1 (\cos\theta) \qquad (6.36)c$$

This in turn, indicates that the only surface zonal harmonic which will appear in solving this problem is the fundamental harmonic, i.e. harmonic of order n = 1. Equations (6.19) which is written for the harmonic n reduce to:

$$\frac{d^2}{dr^2}\{rE(r)\} - \left[\frac{2}{r^2} + j\omega\mu\sigma\right].\{rE(r)\} = 0$$

$$\frac{d}{dr}\{rE(r)\} = j\omega\mu\, r\, H(r) \qquad (6.37)$$

And for the non-conducting region, equation (6.37a) becomes

$$\frac{d^2}{dr^2}(rE) - \frac{2}{r^2}(rE) = 0$$

The solution of this equation for the innermost region, where r = 0 is a point in the region, is given by:

$$r\, E_i(r) = A\, r^2 \qquad (6.38)a$$

Where A is separation constant.

$E_i(r)$ is the rth dependent function of the electric field in an innermost non-conducting spherical region.

The solution for the magnetic field is then given by:

$$H_i(r) = \frac{2A}{j\omega\mu} \qquad (6.38)b$$

Where $H_i(r)$ is the rth dependent function of the magnetic field in the innermost non-conducting spherical region.

The complete solution for the θ-component of the magnetic field is then given in the form :

$$H_{\theta i} = \frac{2A}{j\omega\mu} \cdot \sin\theta \quad \exp(j\omega t) \qquad (6.39)a$$

The solution for H_{ri} can be determined from both equation (6.39)a and $\nabla.\bar{H} = 0$, the result is:

$$H_{ri} = -\frac{2A}{j\omega\mu} \cos\theta \exp(j\omega t) \qquad (6.39)b$$

$H_{\theta i}$ and H_{ri} are the components of the magnetic field inside the innermost non-conducting spherical region which constitutes the core region of a spherical multiple-shell model placed in a uniform magnetic field. The important conclusion drawn from their expression is that they are independent of the radius (r), also they have similar functional dependence as the components of the exciting field which are given by equation (6.36). Consequently, for the innermost non-conducting region, the magnetic field will be in general uniform, and it will be directed in the same direction as the applied field, but of course there could be a frequency dependent phase shift between these two fields which also depends on the material properties of the physical model,

such as its conductivity and permeability.

The equivalent transmission line representation of the mathematical model illustrated in Fig. (6.6) is shown in Fig. (6.7). The input to this equivalent network is the flow quantity $r_c H_o$, where the radius r_c is the radius of a distant concentric spherical surface. It is assumed that r_c is large enough to ensure that the field produced by the spherical model is negligible with respect to the applied field at that radius.

The transfer matrix which represents any non-conducting region whose inner and outer radii are r_1 and r_2 respectively, written for the fundamental harmonic, is given by:

$$\begin{bmatrix} V_2 \\ I_2 \end{bmatrix}_{\text{at } r_2} = \frac{1}{3} \begin{bmatrix} (r_2/r_1)^2 + 2(r_1/r_2) & j\omega\mu\left[r_2^2/r_1 - r_1^2/r_2\right] \\ 2/j\omega\mu\left[r_2/r_1^2 - r_1/r_2^2\right] & 2(r_2/r_1) + (r_1^2/r_2^2) \end{bmatrix} \begin{bmatrix} V_1 \\ I_1 \end{bmatrix}_{\text{at } r_1} \tag{6.40}$$

The positive directions of I_1 and I_2 are, as indicated in the equivalent network, flowing from the outer radius r_2 towards the inner radius r_1.

Applying equation (6.40) to relate the voltages and currents at both sides of the buffer region transmission line, substituting for r_2 by r_c and for r_1 by r_N which is

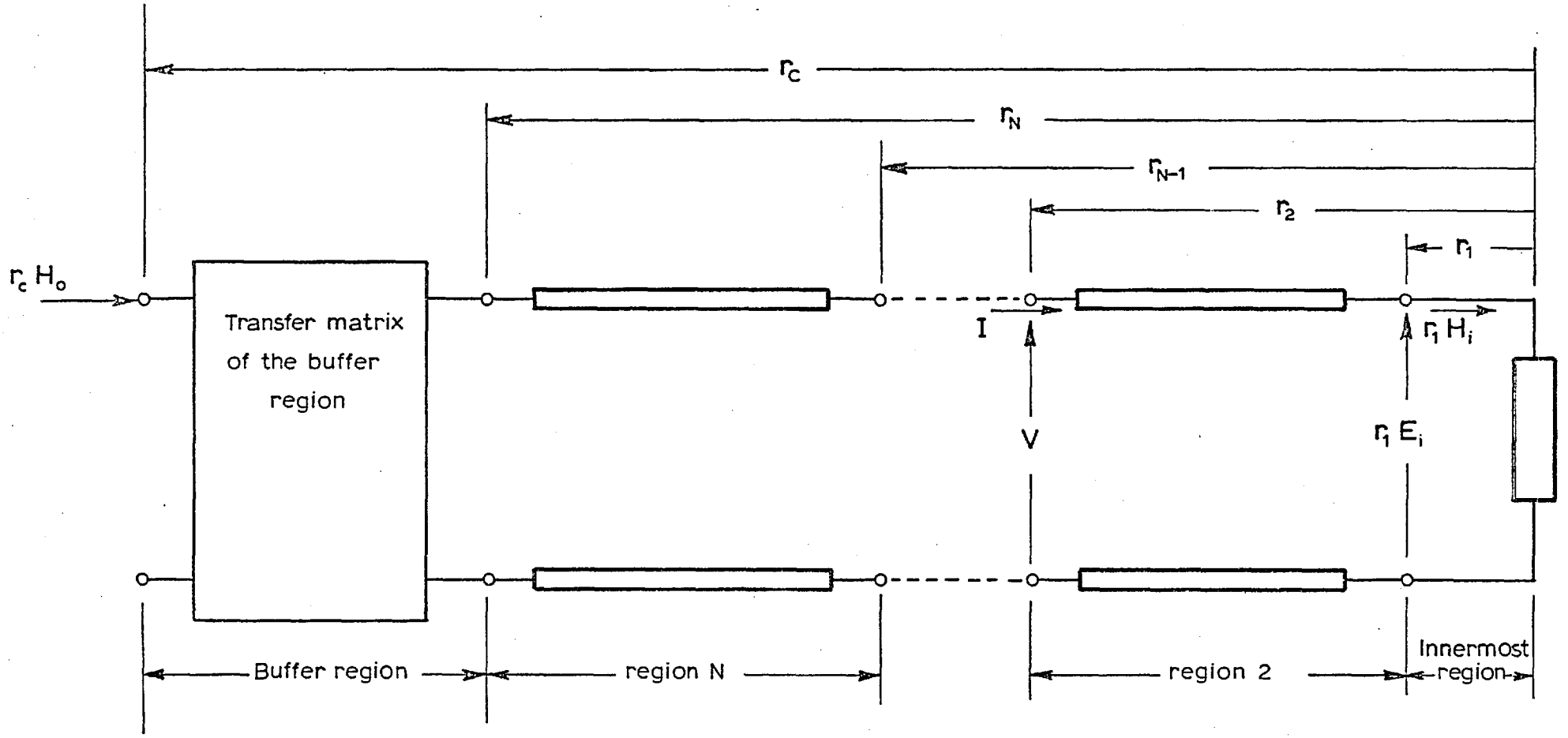


Fig. 6·7 Equivalent transmission line representation of N concentric spherical regions placed in a uniform magnetic field.

the outer radius of the mathematical model and bearing in mind that $I_2 \equiv r_c H_o$ and $I_1 \equiv r_N H_N$, the source field H_o can be related to the field quantities at the radius r_N by:

$$H_o = \frac{1}{3}\left\{ \frac{1}{j\omega\mu_o} \frac{2}{r_N^2}\left[1 - \left(\frac{r_N}{r_c}\right)^3\right]V_N + \left[2 + \left(\frac{r_N}{r_c}\right)^3\right]H_N \right\} \tag{6.41}$$

As r_c increases without limit, the expression for H_o reduces to the form:

$$H_o = \frac{1}{3}\left[\frac{2}{j\omega\mu_o r_N^2} V_N + 2 H_N\right] \tag{6.42}$$

As a check, if all the regions enclosed by the sphere radius r_N are simply air, the relation between V_N and H_N is given by equation (6.28),

$$V_N = \frac{1}{2} j\omega\mu_o r_N \cdot r_N H_N \tag{6.43}$$

Substituting for V_N into equation (6.42) we get:

$H_o = H_N$ which is to be expected.

On the other hand, if all the regions became one solid magnetic non-conducting sphere whose relative permeability is μ_r, the relation between V_N and H_N becomes:

$$V_N = \frac{1}{2} j\omega\mu_o\mu_r r_N^2 H_N \tag{6.44}$$

$$H_o = \left(\frac{\mu_r + 2}{3}\right) H_N \qquad (6.45)$$

which is a well known result, see for instance reference (6.6), page 345.

6.8 Applications

6.8.1 Magnetic shielding

A region in a space can be partially shielded from magnetic fields by enclosing it within a layer of some ferromagnetic substance. For instance, this can be achieved by enclosing this region by a magnetic spherical shell. Popovic'(6.6) solved this problem and calculated the induced magnetic field inside a homogeneously magnetic spherical shell when placed in a uniform static magnetic field. Since the field was static, Popovic' formulated his problem in terms of magnetic scalar potential. Due to the static nature of the applied field, there are no macroscopic currents in the spherical region considered.

The screening ratio as obtained by Popovic' has been reported as follows:

$$\frac{H_{cav}}{H_o} = 9/\{\, 2\mu_r + 5 + (2/\mu_r) - 2(\sqrt{\mu_r} - 1/\sqrt{\mu_r})^2 \; (b/a)^3 \,\} \qquad (6.46)$$

Where: H_o is the applied magnetic field

H_{cav} is the field inside the sphere cavity

a is the outer radius of the spherical shell

b is the inner radius of the spherical chell

μ_r is the relative permeability of the spherical shell

In order to check the validity of the theory developed in this Chapter, the screening ratio as obtained from the closed form solution reported by Popovic will be checked against the same ratio as obtained from the transmission line modelling method.

The transmission line developed in this Chapter assumes an alternating magnetic field, while Popovic gave the solution for a static applied field. The main difference will occur if there is any conducting material involved in the model. In this case the field alternation will induce eddy current which will affect the field solution. However, if all the regions concerned are non-conducting the alternating field has no effect whatsoever on the results. Hence, in order to adapt the network model deduced in this Chapter to represent static problems, even when assuming an alternating and not a static field, the conductivity of all regions will be assumed zero.

A simple computer program has been written in order to calculate the screening ratio (H_{cav}/H_o) of a non-conducting

magnetically homogeneous spherical shell when placed in a uniform field. The algorithm of calculation is based on the equivalent circuit shown in Fig. (6.7), with the number of regions N = 2. The innermost region is an air region where its input surface wave impedance is given by $(j\omega\mu_o b/2)$. The frequency ω could be assumed any value, it has no effect on the calculations as argued before. The radius (b) is the inner radius of the magnetic spherical shell as it appears in the Popovic closed form solution. The method of calculation starts by assigning a value of 1.0 p.u. to the equivalent T.L. current flowing outward from the inner radius of the spherical shell towards the innermost air region, which corresponds to H_{cav}. The voltage at that point can be related to the 1.0 p.u. current through the input surface wave impedance given above.

Once the voltage and current at the 'receiving end' (which is the inner radius) of the spherical shell are known, their corresponding values at the 'sending end' (the outer radius) can be calculated. This can be done either by using the transfer matrix given by equation (6.40), or by calculating the voltages and currents along a string of micro-T circuits in cascade.

The per unit value of the input uniform magnetic field H_o can be obtained from equation (6.42), where V_N and H_N in this case are the voltage and the magnetic field

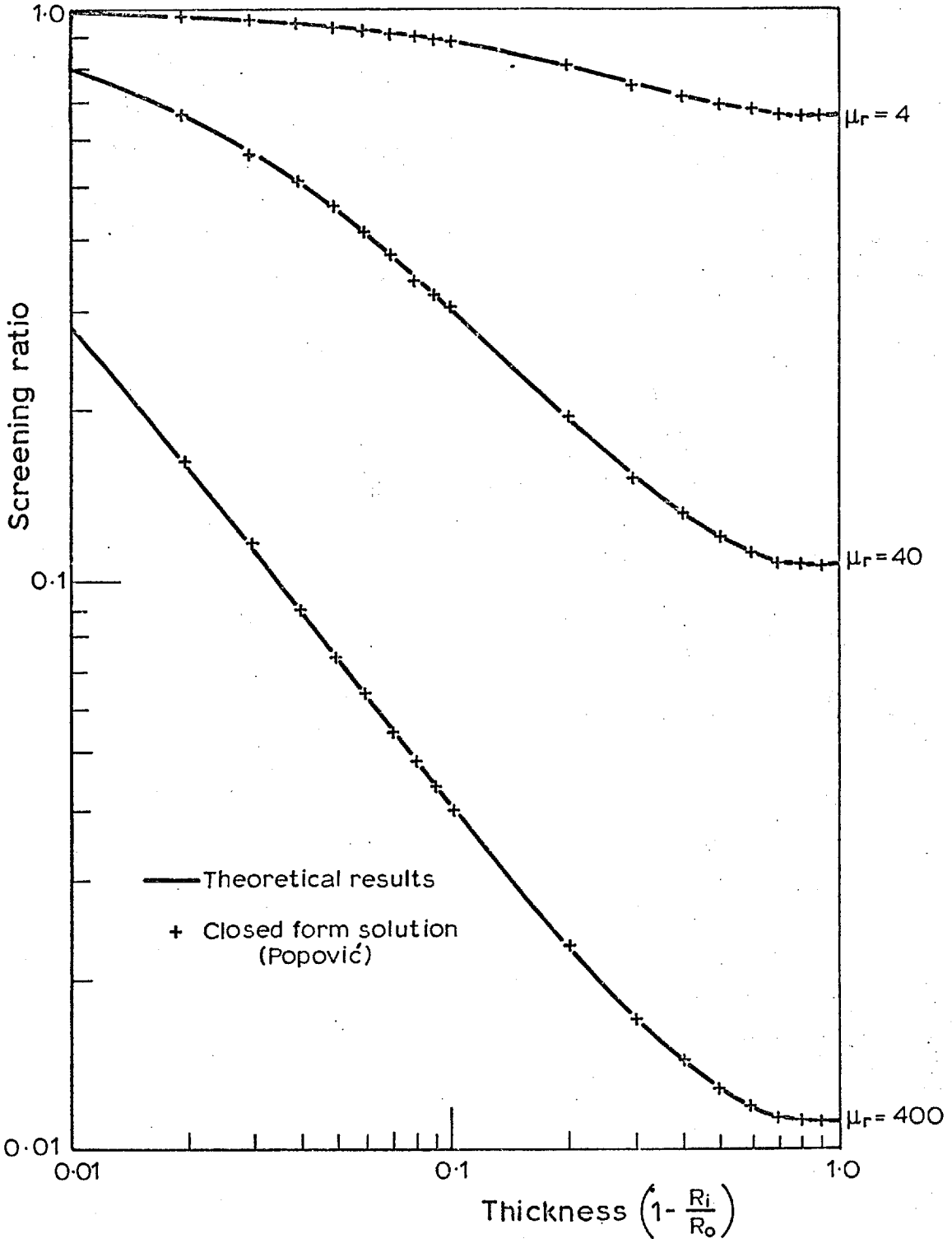


Fig. 6·8 Screening ratio of nonconducting magnetic spherical shell.

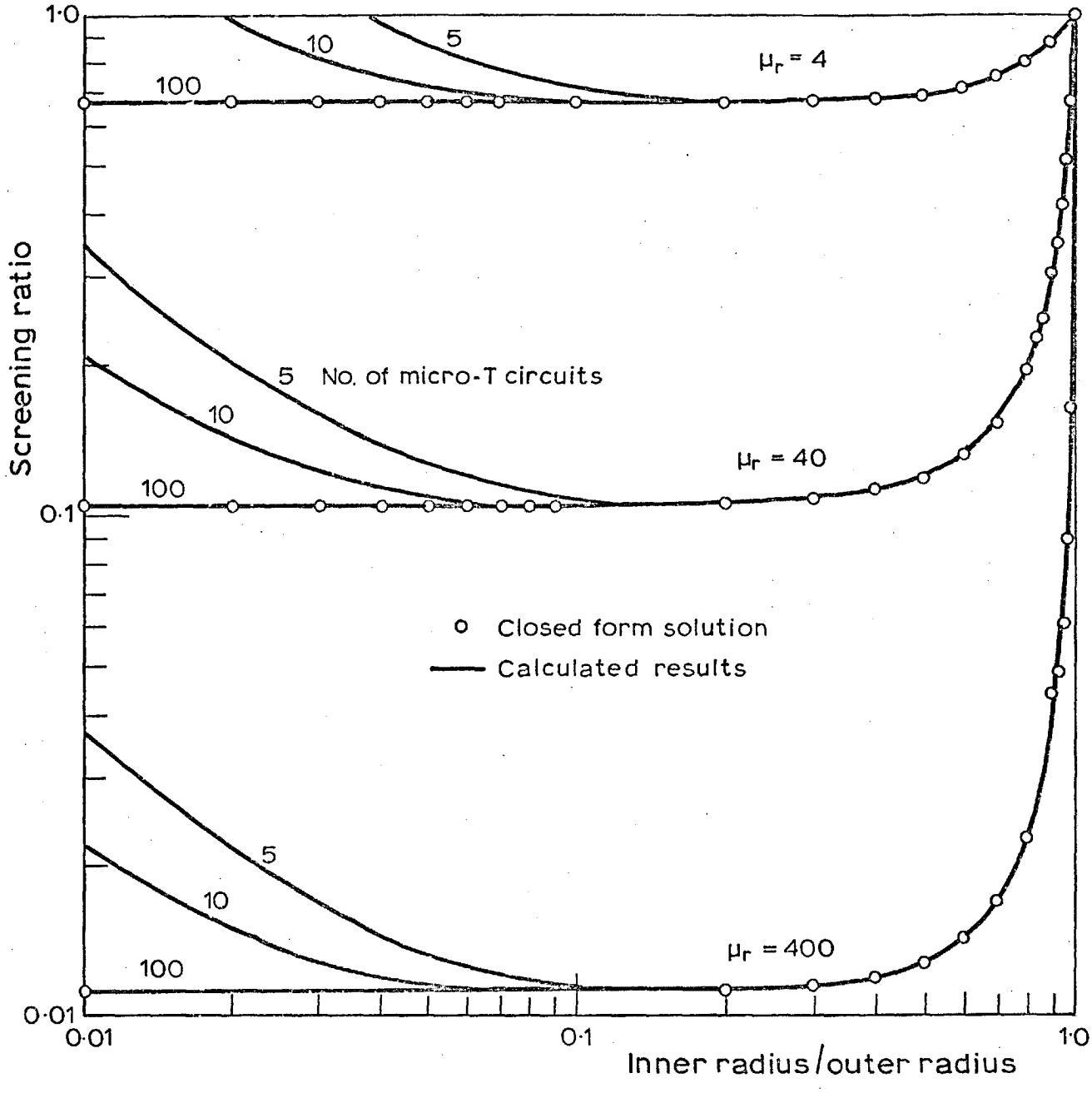


Fig. 6·9 *Effect of choosing the number of micro-T circuits of the magnetic nonconducting spherical shell.*

($H_N = I_N/r_N$) at the 'input terminals' of the spherical shell equivalent T.L. The results of the screening ratio (H_{cav}/H_o) calculated for different spherical shell thicknesses, using the two methods of transmission line modelling and the closed form solution, are plotted in Fig. (6.8). The agreement between the two methods has been found to be within 0.5%.

In order to study the effect of choosing a suitable number of micro-T circuits to represent a spherical shell, the screening ratio has been calculated for different permeabilities $\mu_r = 4$, 40 and 400 for a spherical shell whose outer diameter is equal to 0.1 m while its inner/outer radii ratios varied between 1.0 and 0.01. The magnetic spherical shell has been modelled by a set of micro-T circuits in cascade. The results have been calculated for different numbers of micro-T circuits 5, 10 and 100, and plotted in Fig. (6.9).

The graphs show that a choice of as few as ten micro-T circuits to represent the non-conducting spherical shell gave results almost as accurate as when this number is increased ten times, in a range of inner/outer radii ratios between 1.0 and 0.1.

6.8.2 Eddy current screening

In the previous section (6.8.1) the transmission line modelling technique has been checked for a magnetic but

non-conducting spherical mathematical model. In this section the technique will be checked against an experimental model which involves conducting material. The experimental model consists of an aluminium spherical shell cut into two halves as shown in Fig. (6.10)a. A search coil has been inserted inside the sphere in order to pick up the axial flux density signal. The aim of the test is to determine the screening ratio of the sphere for different excitation frequencies when this excitation has been obtained once from a long solenoid and then from a finite 'length' coil surrounding the sphere. The sphere has been inserted inside the excitation coil such that the induced eddy currents in its wall will flow parallel to the cut in the sphere, to ensure that the discontinuity in the sphere material has virtually no effect on the induced eddy currents in the sphere wall.

The power source used through the test consisted of a motor/alternator set which provided an output of frequency range 50 to 450 Hz.The frequency was determined using a digital frequency counter.

The particulars of the exciting coils are as follows: (The short coil will be referred to as the 'ring coil').

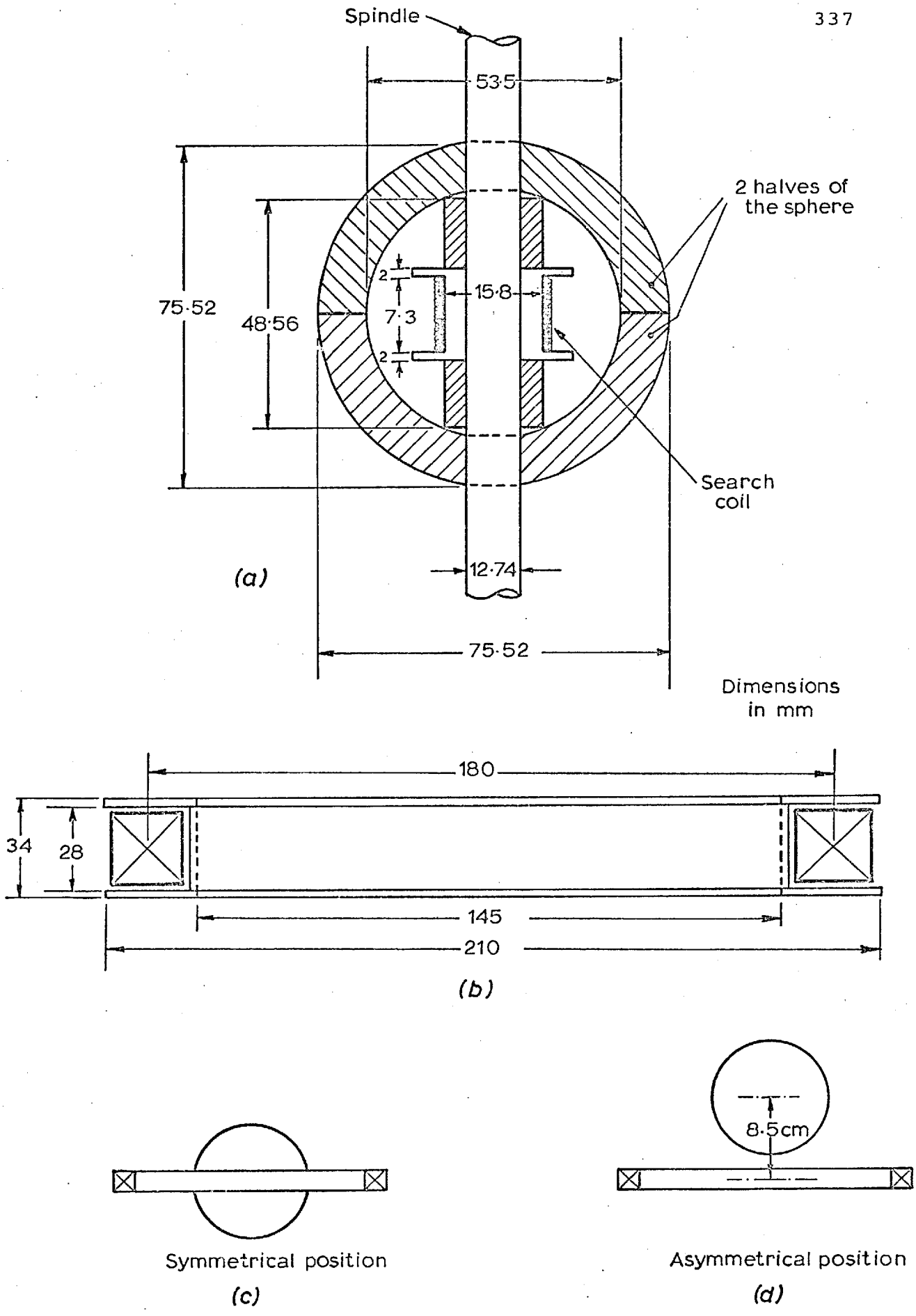


Fig. 6·10 Experimental set-up.

The solenoid

No. of turns = 548 turns

Excitation length = 0.55 m

Inner diameter = 0.98 m

The ring coil

Consists of five separate sections, usually one of them can be used as a shadow coil, while the other four can be connected in series or parallel according to the requirement of the supply available, and they form the excitation coil.

No. of sections = 5

No. of turns/section = 140

Wire diameter = 0.9 mm

The dimensions of the former of this ring coil are shown in Fig (6.10)b.

The conductivity of the spherical shell material has been assumed to be equal to 2.65×10^{7} $\mho$/m.

The test results are plotted in Figs. (6.11) and (6.12), the vertical axis of these two graphs is the ratio between the search coil voltage and the excitation current, i.e. it is proportional to the flux density multiplied by the supply

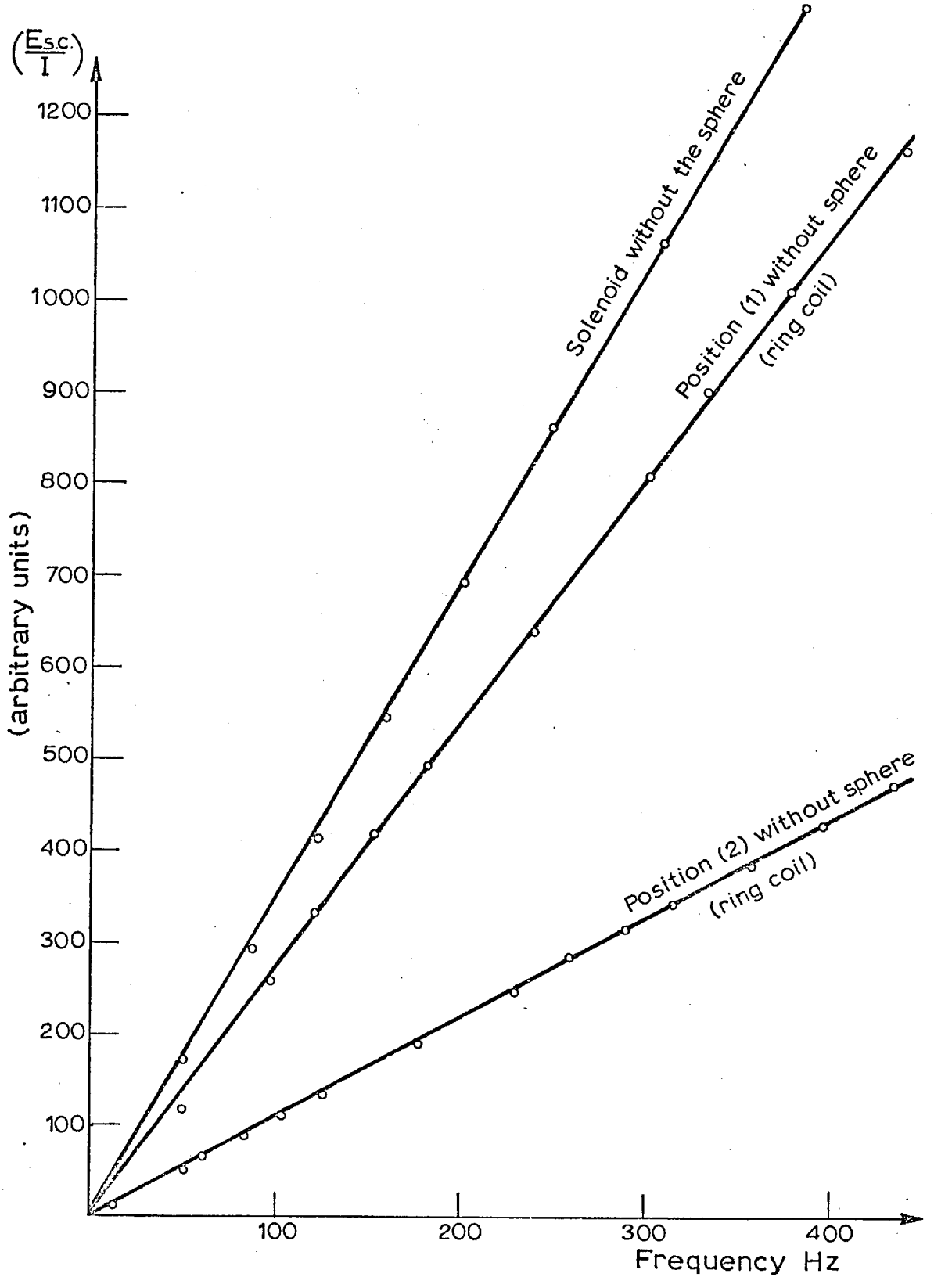


Fig. 6·11 Search coil voltage without the sphere

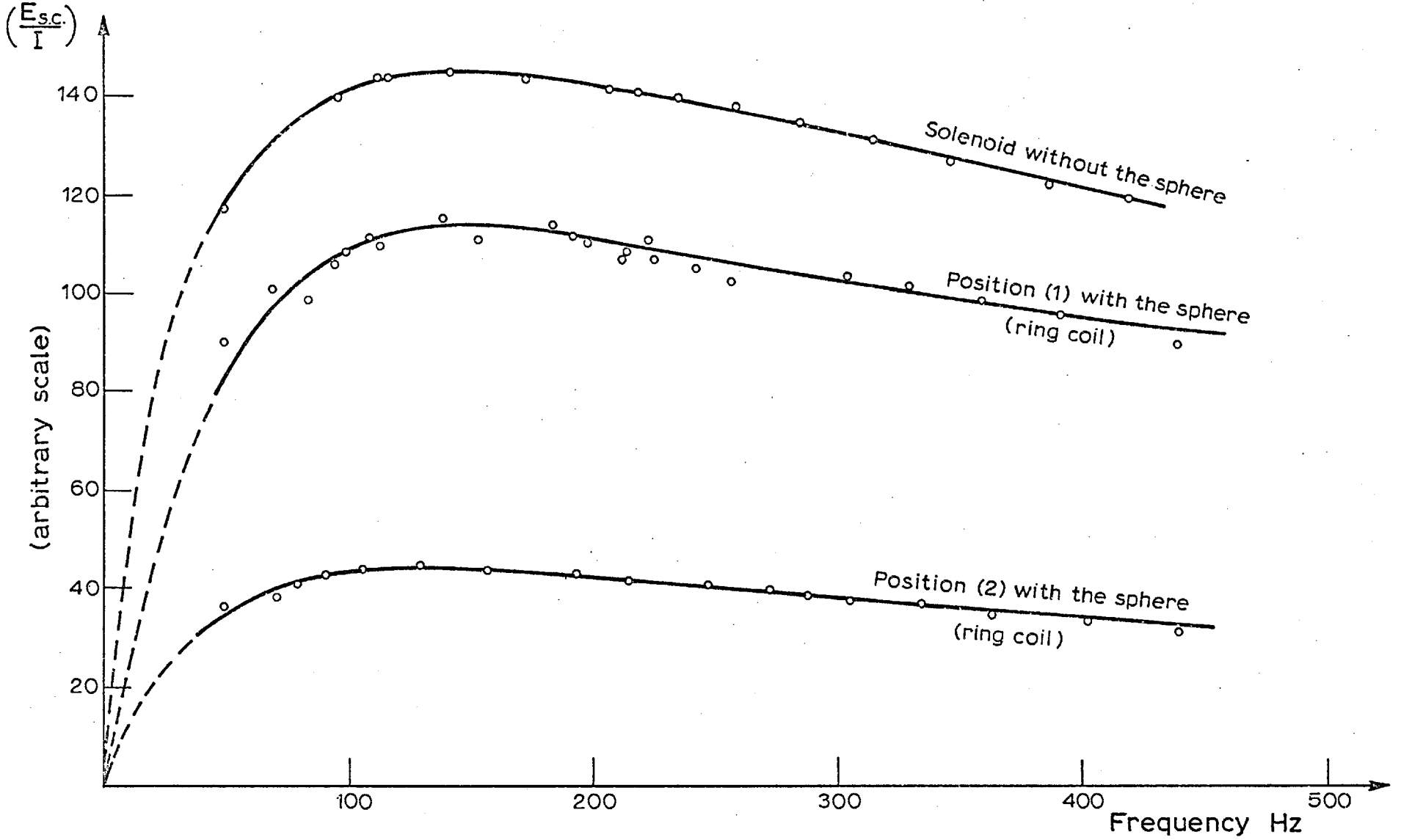


Fig. 6·12 Search coil voltage with the sphere

frequency. When the ring coil has been used as an excitation source, the test has been done twice, once when both the centre of the sphere and the centre of the coil are coincident, then when they are displaced a distance of 8.5 cm in a common axial direction.

The screening ratios for each of these three tests have been calculated by taking the ratio between the corresponding data obtained from curves shown in Fig. (6.11) and (6.12) at the same frequency value. The results are plotted together with the theoretical calculations in Fig. (6.13). The theoretical calculations are based on the fundamental surface zonal harmonic only. The higher harmonics have been neglected. The close agreement between the theoretical and experimental results is remarkable for the three different excitation cases. The agreement between the theoretical and experimental results for the two tests which involve the ring coil excitation was rather surprising, since the actual current sheet spatial distribution is very rich in high order zonal harmonics while the calculation only includes the fundamental. For example, when the sphere is symmetrically placed inside the ring coil, the coil filling factor, as defined in FIg. (6.3), is 0.1. The corresponding harmonic content of this current sheet can be estimated from Fig. (6.3), and is given in the table below:

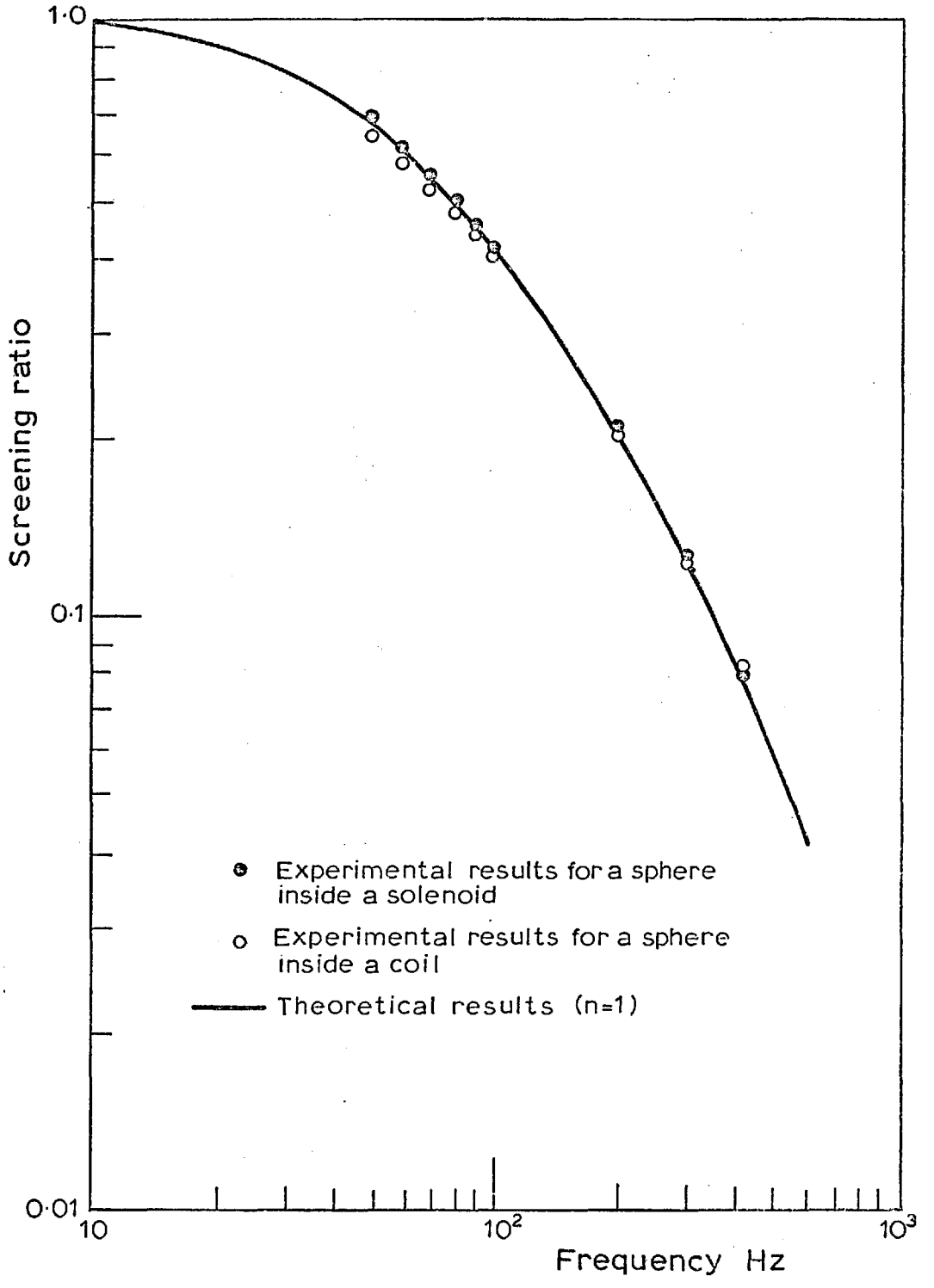


Fig. 6·13 Screening ratio of a conducting sphere.

Order of harmonic n	percentage harmonic content
1	100
3	56
5	40
7	30

In an attempt to find an explanation, two points were required to be investigated:

1. The radial distribution of each zonal harmonic of the magnetic field component H_θ in the absence of the conducting sphere, starting from the excitation radius and proceeding towards the centre where r = 0.

2. The screening effect offered by the conducting sphere for each individual harmonic field component.

As far as the first point is concerned, the solution of the magnetic field equation is straight forward, and is given by equation (2.27), from which we get:

$$\frac{H(r)}{H_{ext}(R)}\Big]_n = \left(\frac{r}{R}\right)^{n-1} \qquad (6.47)$$

Where: $H(r)\big]_n$ and $H_{ext}(R)\big]_n$ are the magnetic field components of harmonic order (n) at radius (r) and excitation radius (R) respectively.

This relation indicates that the magnetic field fundamental component, n = 1, is independent of the radius (r). For any other harmonic order n>1, however, the magnetic field decreases rapidly as we move away from the excitation radius.

This rapid decrease becomes stronger as the order of harmonic increases, as shown in Fig. (6.14).

In order to find the sphere's eddy current screening effect on each harmonic component, the graph of Fig. (6.15) has been calculated as follows:

For the conducting sphere, a per unit magnetic field component, of a general harmonic order n, has been assumed to act at its outer radius, using the transmission line modelling, the corresponding field component at the inner radius could then be calculated. The attenuation factor H_i/H_o is then the ratio between these two field values. This has been done for the different harmonics n = 1, 3, 5 and 7.

It is interesting to notice that, at low frequencies, the attenuation factor curves are almost constant independent of the frequency. This means that the shielding effect provided by the sphere is not mainly due to the induced eddy currents, but it is due to the dependence of the field

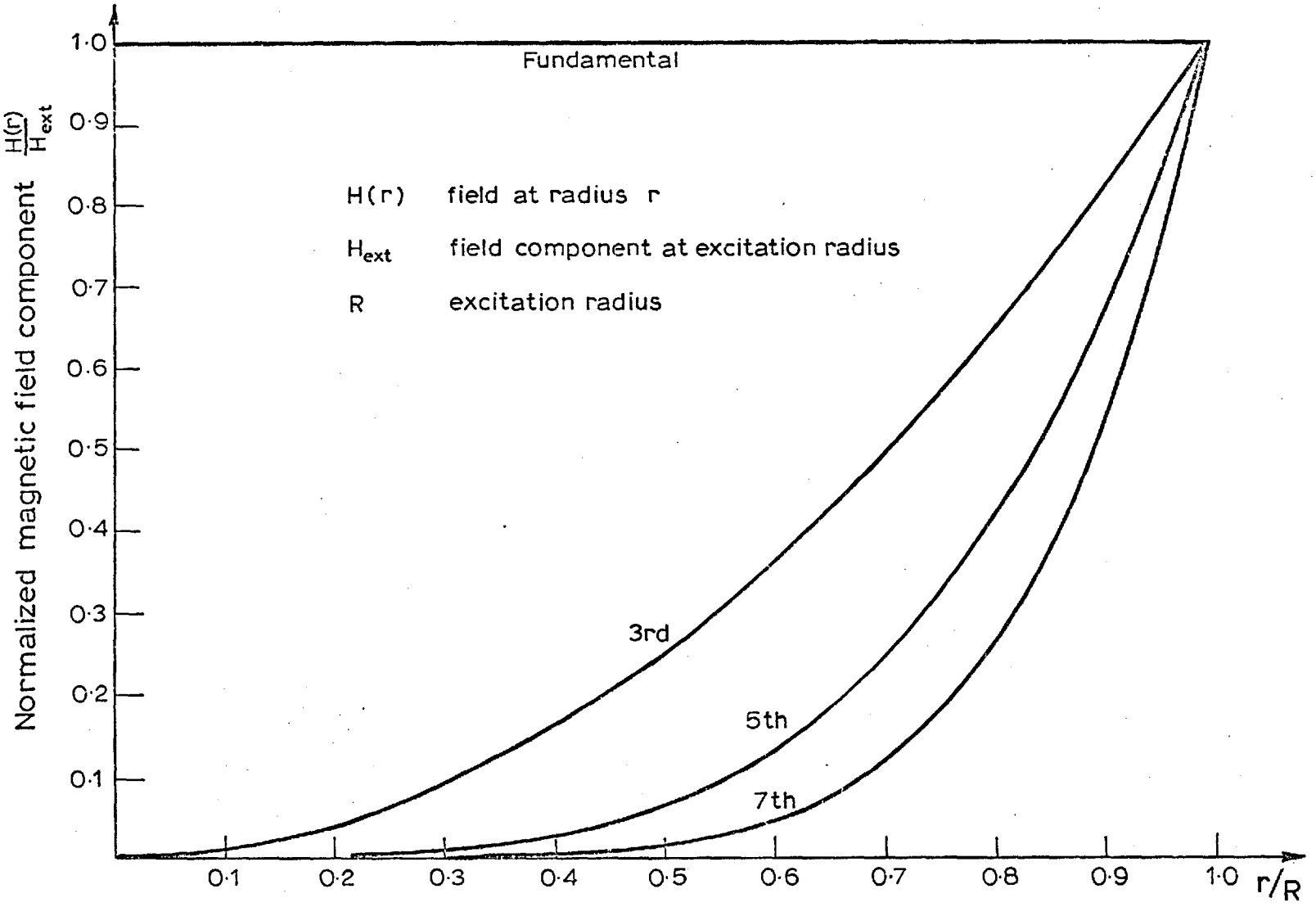


Fig. 6·14 Radial distribution of the magnetic field θ-component for different zonal harmonics.

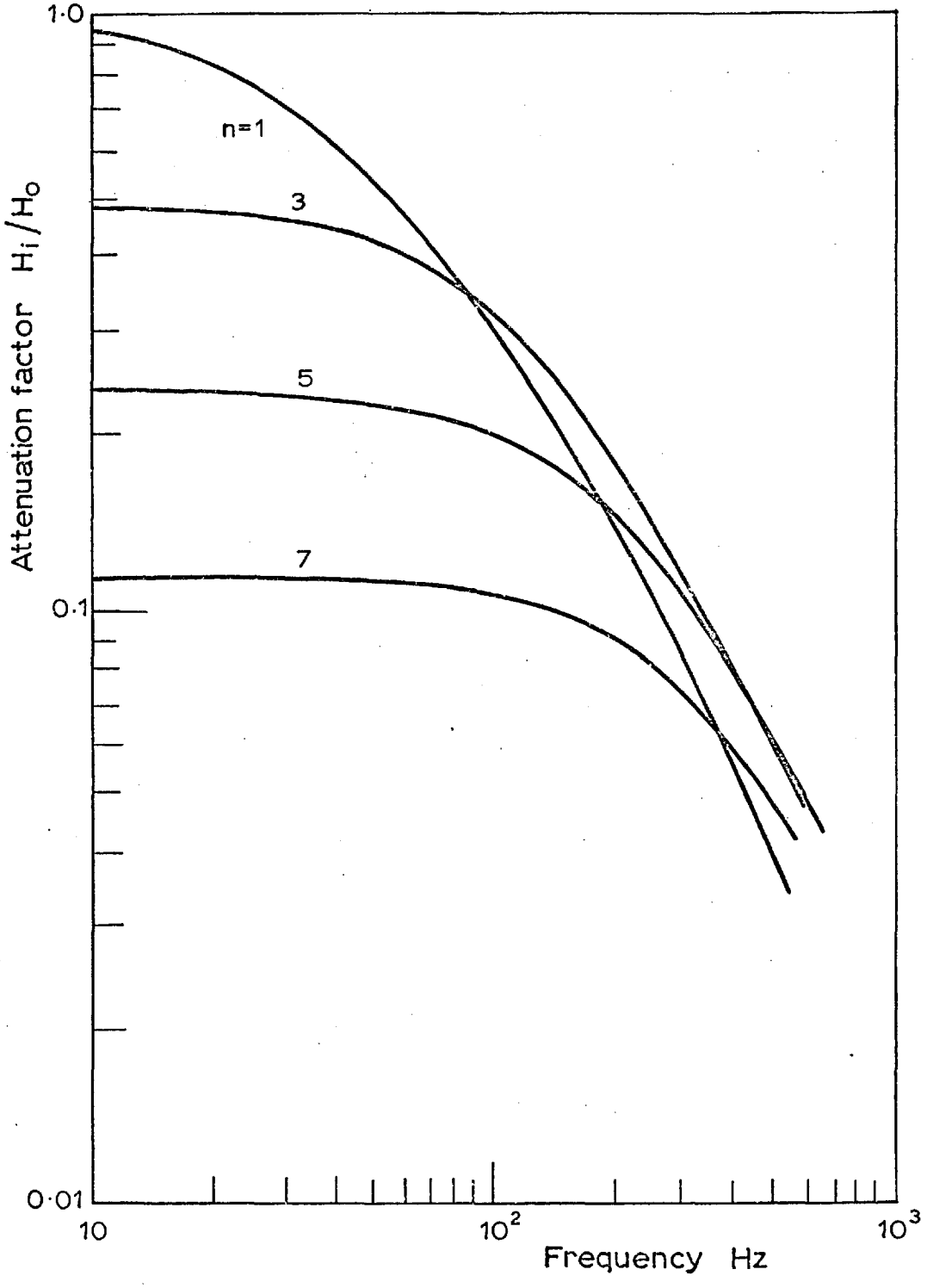


Fig. 6·15 H_i/H_o *ratio curves of the experimental conducting spherical shell for different surface zonal harmonics.*

components on the inner/outer radii ratio. In the limiting case, as the frequency tends to zero, the attenuation factor H_i/H_o will be given by equation (6.47), where r and R become the inner and outer radii respectively. This factor can be also determined from the normalized curves of Fig. (6.14), at the specific radii ratio. The conclusion drawn from the previous discussion is that the attenuation of the magnetic field component as it penetrates in the conducting spherical shell may be attributed to two factors:

1. The screening effect of the induced eddy currents in the spherical shell wall. A similar mechanism to the skin effect phenomenon.

2. The decrease in the field value as it propogates from the excitation source.

The second factor has been discussed separately by considering a non-conducting region. The harmonic field component at any radius (r) has been found to vary with (r) according to the relation: $H(r) \alpha (\frac{r}{R})^{n-1}$ $r<R$, where R is the excitation radius.

The screening effect of the induced eddy current could be 'qualitatively' studied if we succeeded in separating the effect of the 'radius dependence' from the curves of Fig (6.15). This has been done by multiplying the coordinates

of the different curves of Fig. (6.15) by the radii ratio $(R_o/R_i)^{n-1}$ where n is the order of zonal harmonic, R_o and R_i are respectively the outer and inner radii of the conducting spherical shell. The results have been plotted in Fig. (6.16). The drop in the curves as frequency increases becomes slower as the order of harmonic increases. This means that the screening due to the induced eddy currents becomes less effective as the order of harmonic increases. This may be explained as follows; the magnitude of the induced harmonic eddy current becomes smaller as the order of harmonic becomes higher. Consequently, its effect on screening the harmonic magnetic field component becomes weaker.

As far as our experimental model is concerned, and in the light of the above discussion regarding the surface zonal harmonics of the magnetic field component, the agreement between the experimental and theoretical results can be explained as shown below.

As shown in Fig. (6.10)a , the search coil has been placed in order to pick up the average flux density, in the axial direction of the excitation coil, at the centre of the sphere where r = 0. The excitation coil has an average radius of 9.0 cm, while the search coil average radius is 0.79 cm.

The ratio between the search coil and the excitation radii, for the symmetrical position shown in Fig.(6.10)c,

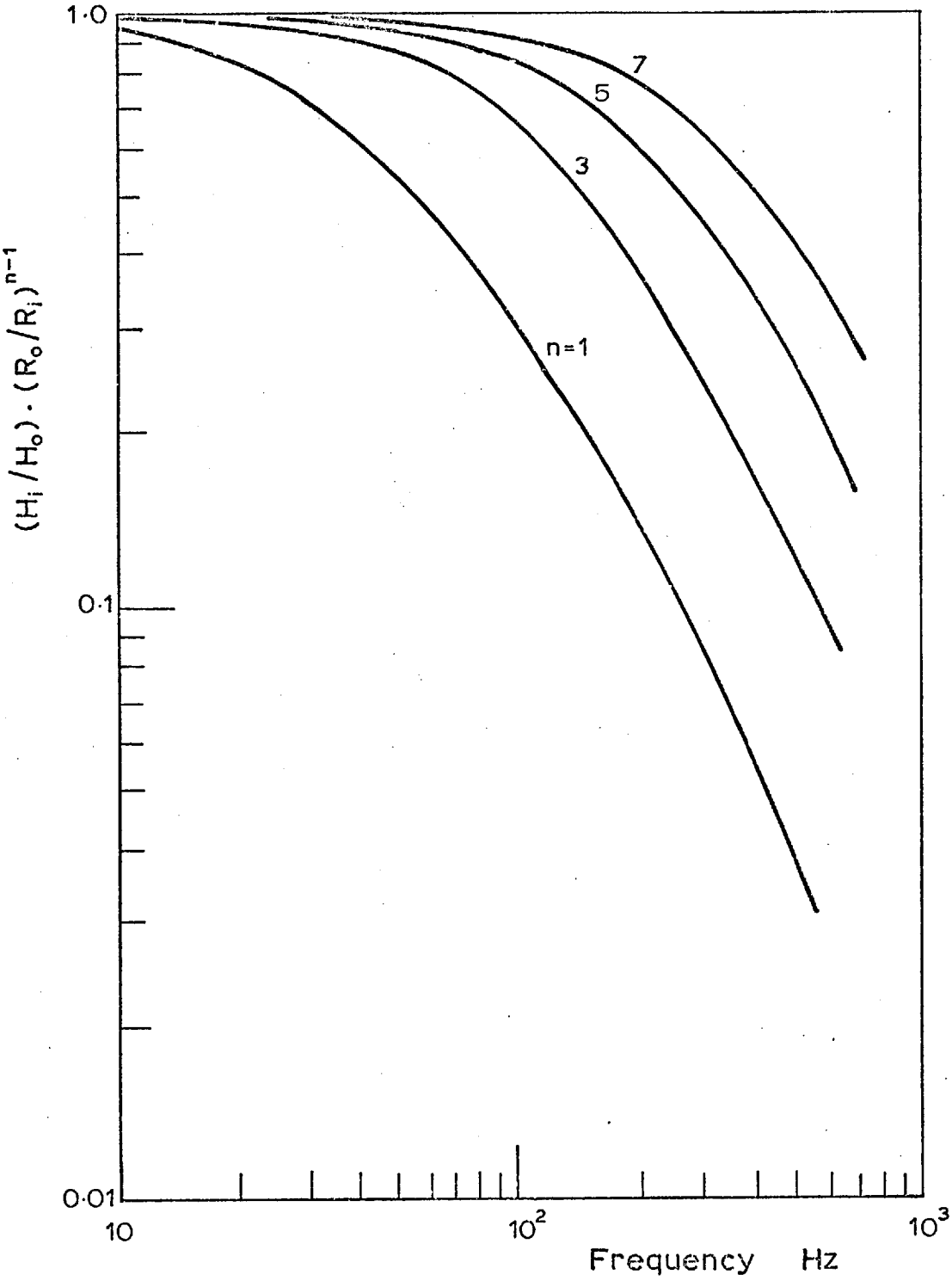


Fig. 6·16 Screening effects of the induced eddy currents of different zonal harmonic orders.

is equal to 0.79/9.0 = 0.0878. For the asymmetrical position, when the sphere is displaced a distance 8.5 cm as indicated in Fig. (6.10)d, the ratio becomes 0.0638. For the first case, even for very low frequencies, the average 3rd harmonic flux density at the search coil will be less than 1% of its value at the excitation radius, while for the second case, it will be less than 0.4%.

In conclusion, as far as the screening problem is concerned, the magnetic field surface zonal harmonics of order higher than the fundamental, attenuate very rapidly with the radius (r). Consequently, modelling the excitation current sheet by its fundamental component only, seems quite adequate for many applications. However, if the field distribution at points near the excitation radius is required, the first few harmonics should be considered, especially if the excitation coil filling factor is very small.

6.9 Conclusions

A new method has been described to solve the electromagnetic field problem of a multi-region spherical model, which consists of any number of concentric spherical shells excited by a spherical one dimensional current sheet. The method has been extended to solve the field problem as if the spherical structure has been placed in a uniform applied magnetic field.

The excitation current sheet expression has been developed as an infinite series of associated Legendre polynomials. The transmission line modelling technique has been adopted in order to avoid the calculation of modified Bessel function of complex arguments.

It has been shown that the conducting region can be modelled by a number of micro-T circuits in cascade. However, it has been proved that, for a non-conducting region, a transfer matrix formulation is the simplest way to relate the electric and magnetic field components at both surfaces of this region. The elments of the non-conducting region transfer matrix have been found as simple functions of the inner and outer radii of this region and its permeability.

If the non-conducting region is either the innermost or the outermost region, a further simplification can be achieved by replacing this region with a single inductive surface wave impedance.

The method has been checked against an analytical solution of a magnetic spherical shell situated in a uniform field. Also it has been checked against experimental results for an aluminium spherical shell placed in a magnetic field firstly produced by a long solenoid, secondly produced by a ring coil. The agreement between the theoretical results and either the closed form analytic solution or the experimental results, is remarkable.

It has been shown that the high order surface zonal harmonics have a very little effect on the value of the screening ratic of a thick conducting or magnetic spherical shell. Even if the excitation current sheet is very rich in surface zonal harmonic contents, in some special applications, such as those considered experimentally in this Chapter, the fundamental component only has been found adequate to represent the current sheet wave-form.

No account of the calculation of forces has been given in this work. It is hoped that the force calculation will be dealt with separately in the future. It is believed that if the spherical shell of air between the excitation and the conducting sphere is small compared with the excitation radius, higher harmonics should be introduced in the force calculation.

The theory derived in this Chapter is believed to be original. Although it has been checked against specific simple cases, it is claimed that the method is general and can solve the field problem for any number of concentric spherical shells provided that the induced eddy current and the impressed excitation current is in the ϕ-direction.

CHAPTER 7

Transients in Layered Structures

7.1 Introduction

Among the number of problems which arise in the area of electrical engineering, the phenomena of the transient diffusion and penetration of the electromagnetic waves in conducting or magnetic media is of special concern specially when the dynamic or transient stability is under consideration.

Historically, the transient problem had a good deal of investigation from the mathematicians who formulated suitable mathematical techniques to solve the various physical problems that arose. A search through the literature shows that the transient problem was initially tackled analytically mainly by using operational calculus methods. Most of the problems considered had extremely simple and idealized configurations, otherwise the algebraic equations obtained were almost intractable and the solutions difficult to interpret. Thus for some years, a good number of problems have been neglected, simply because the classical analytical techniques available could not be effectively implemented.

The advent of digital computers has rendered many of these problems amenable to numerical solutions. Hence design engineers need no longer rely solely on empirical methods

or be forced to avoid problems which are apparently insoluble by traditional methods. The digital computers introduced a new phase in the solution of transient field problems, and there are now many numerical methods which are capable of providing fairly accurate results to transient problems. The only snag is that many of these methods are expensive in computer time and need special training to develop.

The induction devices for which the transient behaviour is required may be divided into two main groups:

(i) Those which can be represented by an equivalent circuit consisting of the lumped circuit elements R, L and C.

(ii) Those in which the mathematical model is considered as a continuum, this necessitates the transient solution of Maxwell's field equations.

In this work, the concern will be devoted to the second class of problems.

But why is a continuum model necessary? The necessity of adopting a continuum model comes from the physical and geometrical nature of the class of devices considered. For instance, in the case of linear induction motors with their large air-gaps or the case of superconducting generators where the windings are surrounded with non-magnetic material. In

both cases, the magnetic coupling between particular current paths is much weaker when compared with conventional machines. Thus, the division of the total flux into a main flux corresponding to a magnetising reactance, and a leakage flux corresponding to a leakage reactance seems to be inadequate.

In fact, the continuum modelling of electric machines, and its treatment directly from Maxwell's field equations can give a generalised form to the problem. The machines will then be in the same category as problems involving radiation from antennas, propagation through waveguides and cavity resonators, eddy currents in conductors, stresses in current carrying structures and many other field problems. This in turn will highlight the possibility of using the techniques commonly used in apparently unrelated topics to solve machine problems.

7.2 Objective of the Present Work

It would be extremely unrealistic to claim that the transient problem of a general (planar, cylindrical or spherical) multilayer induction device could be possibly treated in one chapter. However, the main objective of this chapter is to shed the light on one particular way of solving the transient problem, namely, the transmission line modelling technique.

7.3 Brief Review of Published Material

The solution of the diffusion equation analytically, using operational calculus can be found in many books. For instance, Heaviside[7.1], McLachlan[7.2], Carslaw and Jeager[7.3] and Ku[7.4], solved the problem of suddenly applying a tangential field to a semi-infinite conducting block, or its analogue, a voltage step applied to an infinite transmission lines. A similar problem having a finite thickness air-gap and conducting sheet rotor was examined by Ollendorff[7.5].

Miller[7.6] studied the radial diffusion of transient current in circular conductors when subject to a step tangential magnetic field. Similarly, Vallese[7.7] used Laplace transform theory to study the penetration of the induced eddy current into a semi-infinite conductor excited by either a step or an impulse magnetic field. Grumet[7.8] considered the transient problem of a constant electric field applied abruptly to a homogeneous conductor. Again he used the Laplace transform method and solved the problem when displacement current is introduced, then compared the results when this current is neglected. He showed that the effect of neglecting the displacement current is to introduce error in the induced eddy current distribution for values of time comparable to 0.3×10^{-18} sec. or distance comparable to 10^{-10} metres. In other words, even for very fast transients, displacement currents could invariably be neglected in the low frequency induction devices context. Mocanu[7.9] considered a very similar problem

as Grumet. More recently, Chura[7.10] has examined the single region problem in a paper on homopolar inductor alternators.

Almost all the analytical solutions obtained by the above mentioned authors were restricted to a one region configuration. Two regions models could be analysed analytically, but usually under somewhat restricted conditions.

One of the most important results of solving the transient electromagnetic field propagation problem in layered structures finds an application in the field of geophysical exploration. To date, the major study of quantitative interpretation in transient electromagnetic exploration has been carried out in the Soviet Union. An excellent review of this work is presented by Vanyan[7.11]. In this context, the paper by Morrison, Phillips and O'Brien[7.12] represents a step forward in solving for the two-dimensional electromagnetic field stablished by a circular 'δ-coil' placed parallel to a multi-layered planar model. They employed both a Hankel transform in the radial direction, and a Fourier transform in the axial direction of a circular cylindrical coordinates system. The boundary conditions are matched using the surface wave impedance approach. The time response of the system was calculated numerically with the aid of the Fast Fourier Transform (FFT) algorithm of Cooley and Tukey.

Considering a spherical structure, Hjelt[7.13] solved

the problem of a two-region spherical body subject to a suddently vanishing homogeneous external field. The solution is given as a sum of decaying exponential functions.

Bratoljic[7.14] considered a multilayer cylindrical structure excited by one-dimensional, axially directed, sinusoidally distributed current sheet. This mathematical model has been used to represent superconducting turbo-generators. He used the Laplace transform method, then employed the computer to calculate the inverse transform numerically. More recently, Miller and Lawrenson[7.15] presented an interesting paper where they employed the Fourier transform technique to solve the transient screening problem of superconducting generators. The idea of solving the transient problem by Fourier transform method is by no means new, it is well established in communication theory. However, the major contribution of the above authors is their introduction of this method for low frequency applications. They also presented a most useful discussion of the methods available, including some numerical, for solving transient problems.

Finally, mention should be directed towards the important paper by Baum[7.16]. Baum presented the most important comprehensive review of the methods usually employed in the transient and broad-band analysis and synthesis of antennas and scatterers. Briefly these methods are:

(i) Numerical inverse Fourier transform of frequency domain solutions.

(ii) Analytic s-plane approach.

(iii) Eigenmodes of frequency-domain integral equations.

(iv) Finite-difference time-domain solutions.

(v) Time-domain integral equations.

(vi) Approximate transmission-line models of thin antennas and scatterers.

(vii) Closed form transient solutions for special geometries.

Although the topic of the above mentioned paper is different from the one which is considered in this thesis, the author feels that some of the methods mentioned above (i) to (vii) could be quite fruitful in the context of low frequency induction devices.

7.4 : Transmission-Line Modelling

In chapters 2 to 6, the T.L. modelling technique has been employed to solve the field problem of a number of multi-layer low frequency induction devices. The analysis so far

has been completely devoted to the study of the steady-state under single or polyphase excitation. In this chapter, this technique will be extended to solve some transient problems.

The circuits which have been developed in this thesis can be used directly with FFT to solve transient problem in induction devices. Indeed for double T.L. problems this may be the most convenient method. However, the single T.L. circuits lend themselves to an alternative method in which some form of circuit analysis package can be used. The rest of this chapter will be developed wiht the alternative method in mind.

Many computer installations have in their program library some form of circuit analysis program package, e.g. ECAP[7.17] or SPICE[7.18]. It is simply necessary to generate an equivalent circuit and then specify the applied waveform. This can be of any desired arbitrary waveform shape. The computer then calculates the voltage and the current distributions in the circuit. No knowledge is necessary of the method of analysis employed by the program.

These packages can be useful in analysing the transient problem of some induction devices. This can be achieved as follows:

i - Derive the T.L. analogue of the problem.

ii - Replace the continuous T.L. by a suitable number of micro-T circuits in cascade.

iii - Introduce the elements of the equivalent circuit into ECAP or SPICE.

iv - The output voltage and current of the computer program can then be related to the appropriate components of the field vectors.

It is worth mentioning that this method has been reported by Freeman[7.19], with whom the author was working on this problem for planar models. The only limitation of this method is imposed by the ability of the circuit analysis package to represent the analogue equivalent circuit. For instance, it has been shown in chapters 2 and 3 that a general multilayer cylindrical or planar model might require complex turns ratio transformers in order to satisfy the boundary conditions at the region interfaces. In such cases, ECAP or SPICE cannot be used since they are not capable of modelling the coupling transformers. Instead, the T.L. analogue could be employed to obtain the frequency response of the model. Then the transient response could be obtained, say, by the FFT method[7.15].

7.5 Catalogue of the Micro-T Circuits

The different micro-T circuits which represent one dimensional multilayer planar, spherical or/and cylindrical models are shown in Figs. (7.1) to (7.4).

The key for the different circuits is as follows:

Fig. (7.1): Planar model, 1 - D excitation in the X-direction. Spatial sinusoidal distribution in the y-direction with the wave number β . Motion of individual regions, if any, is restricted in the y-direction.

Fig. (7.2): Spherical model, excited by a unidirectional uniform magnetic field. Induced currents are restricted in the ϕ-direction. (The coordinates of spherical system are defined in Chapter 6).

Fig. (7.3): Cylindrical model, 1 - D excitation in the circumferential θ-direction. Spatial sinusoidal variation in the axial direction with the wave number β. Motion is restricted in the axial direction.

Fig. (7.4): Cylindrical model, 1 - D excitation in the axial z-direction. Spatial sinusoidal variation in the circumferential θ-direction with the wave number α. Motion is restricted in the θ-direction.

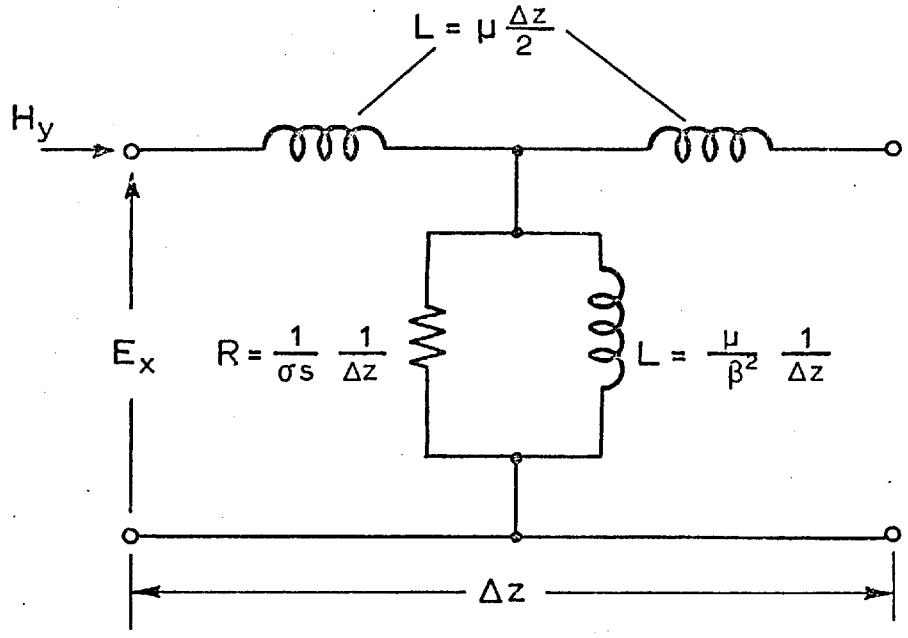


Fig. 7·1 1-D planar model

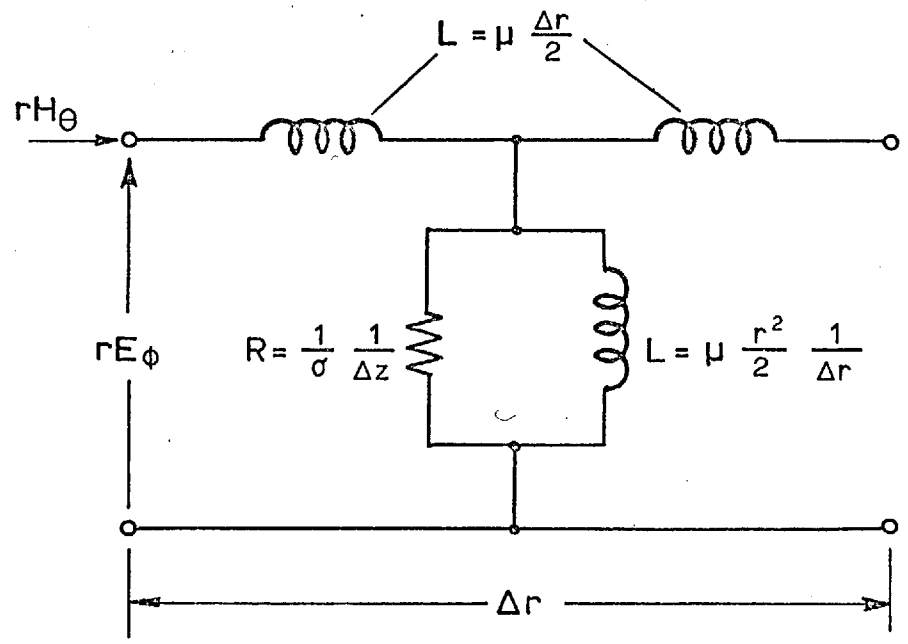


Fig. 7·2 1-D spherical model in a uniform magnetic field.

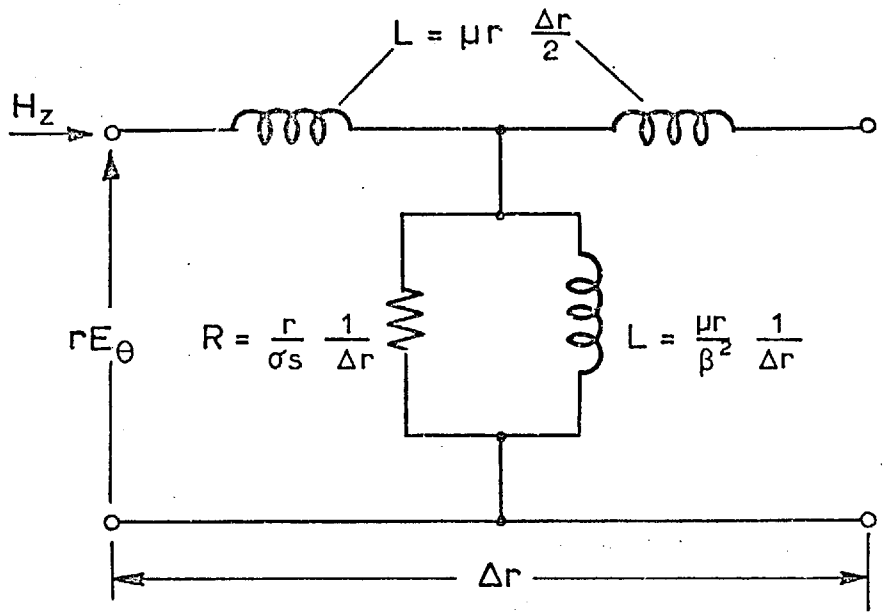


Fig. 7·3 1-D cylindrical model, circumferential excitation.

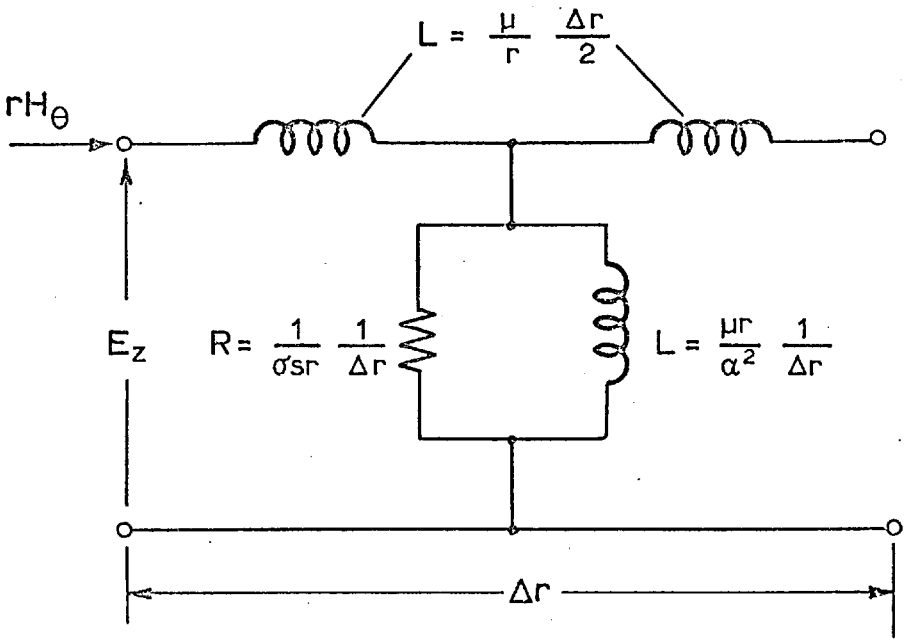


Fig 7·4 1-D cylindrical model, axial excitation only.

The cases of multilayer cylindrical and planar models excited by two-dimensional surface current sheets were not included in the above catalogue. Their equivalent circuits include complex turns ratio transformers, which cannot be modelled by either ECAP or SPICE . If the transient analyses of these models are required, then the FFT approach is recommended, as mentioned above.

Note: The effect of considering the displacement current could be simply introduced by connecting a shunt capacitor across the parallel circuit. The value of the capacitances to be added in circuits of Figs. (7.1) to (7.4) are respectively:

$\varepsilon \Delta z$, $\varepsilon \Delta r$, $(\varepsilon/r)\ \Delta r$ and $\varepsilon r\ \Delta r$.

7.6 Analytical Solutions of Some One-dimensional Planar Models

The main objective of this section is to give the analytical expressions of the electric and magnetic fields transients. Some highly idealised models are considered in order to provide a limited check on the validity of transmission-line modelling for transient problems. However, the derived expressions might give some 'qualitative' physical interpretation to the transient phenomena in some complicated problems.

7.6.1 Micro-T circuits - New concept

Usually, in the T.L. theory, the expressions of the transient distribution of the potential function (voltage) and the flow function (current) are given for infinitely long lines having certain special relations between its parameters. The input function has been invariabley either an impulse or step 'potential'.

So far, the analogy between field and T.L. equations has been established with E analogous to the potential (v) and H analogous to the flow (i). Perhaps this may be due to the similarity between the dimension of (V/i) and (E/H) which is the dimension of impedance.

To make use of the results already reported in the T.L. literature, we propose another way of constructing the analogy. For instance, the potential function (v) will be made analogous to either E or H depending on whether the excitation function of the field problem is either electric or magnetic fields respectively. The equivalent circuit in any one case will be the 'dual network' of the other.

Moreover, the equivalent circuit could be obtained with its flow or potential functions proportional to the rate of change of the field quantity rather than the field component directly.

To illustrate this, consider the simple model of a conducting half space excited by a tangential E- or H-fields as shown in Fig. (7.5). It can be easily shown that the E and H components are related by the following equations:

$$-\frac{\delta E_x}{\delta z} = \mu \frac{\delta H_y}{\delta t} \tag{7.1}$$

$$-\frac{\delta H_y}{\delta z} = \sigma E_x + \frac{\beta^2}{\mu} \int E_x \, dt \tag{7.2}$$

The same equations could be written in the form:

$$-\frac{\delta E_x}{\delta z} = \mu \left(\frac{\delta H_y}{\delta t}\right) \tag{7.3}$$

$$-\frac{\delta}{\delta z}\left(\frac{\delta H_y}{\delta t}\right) = \frac{\beta^2}{\mu} E_x + \sigma \frac{\delta E_x}{\delta t} \tag{7.4}$$

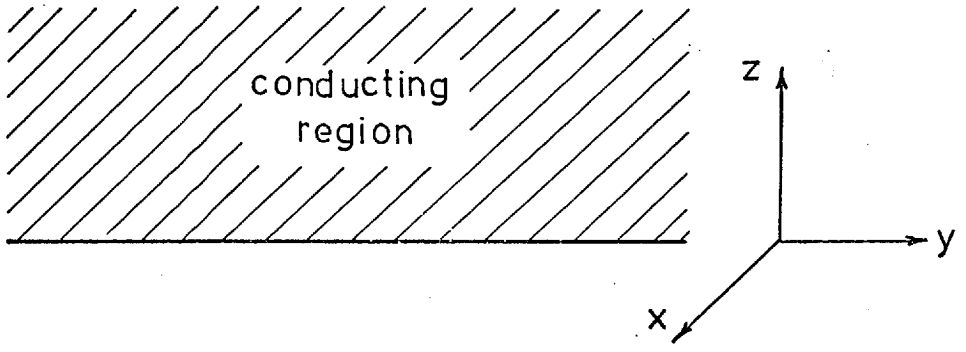


Fig. 7.5: Conducting half space excited by a tangential E or H.

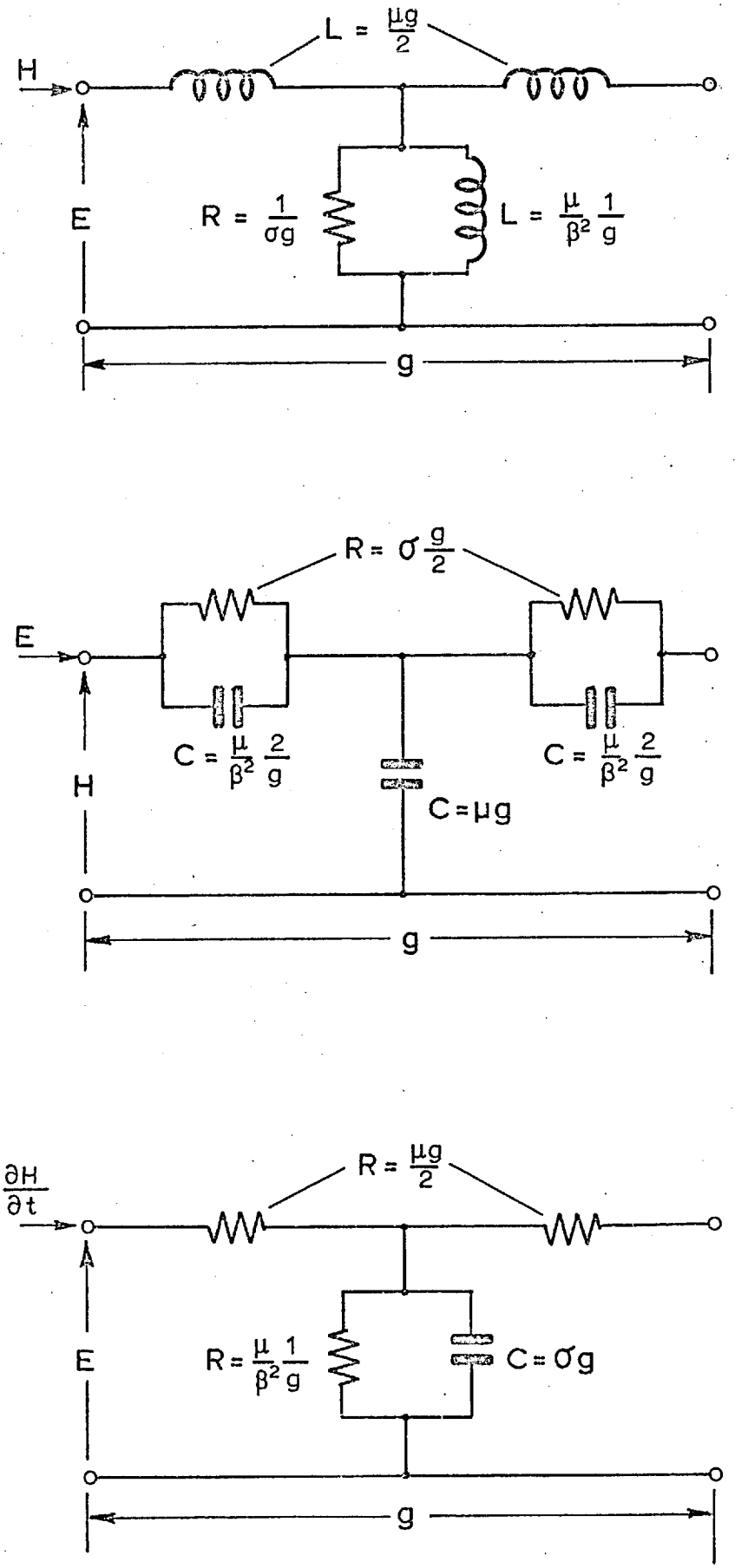


Fig. 7·6 The effect of choosing different flow and potential functions on the elements of the micro-T circuit.

The different micro-T circuits resulting by virtue of choosing different potential and flow functions are shown in Fig. (7.6).

These circuits could be of additional importance if an electric circuit analogue is to be constructed in the laboratory.

7.6.2 Analytical expressions

Consider the mathematical model shown in Fig. (7.5), assuming that the field is independent of y, i.e. $\beta = 0$ in equation (7.1) and (7.2).

The results of solving these differential equations simultaneously for an impulse or unit step input of either H or E fields are quoted below:

I. Input H:

(a) Impulse:

$$H(x, y, 0, t) = H_o\, \delta(t)$$

Therefore

$$H(z,t) = H_o\{0.5\sqrt{\mu\sigma/\pi}.\ (z/t^{3/2}).\ \exp(-\mu\sigma z^2/4t)\} \quad (7.5)$$

and

$$E(z,t) = H_o\{0.5\sqrt{\mu/\sigma\pi}\ (1/t^{3/2}).\ \left[1 - (\mu\sigma z^2/2t)\right].\ \exp(-\mu\sigma z^2/4t)\} \quad (7.6)$$

(b) Step:

$$H(x, y, 0, t) = H_o\, U(t)$$

Therefore

$$H(z, t) = H_o \{1 - \mathrm{erf}(\sqrt{\mu\sigma/t}\ .\ z/2)\} \qquad (7.7)$$

and

$$E(z, t) = H_o \{\sqrt{\mu/\sigma\pi}.\ (1/t^{\frac{1}{2}})\ .\ \exp(-\mu\sigma z^2/4t)\} \qquad (7.8)$$

II. Input E:

(a) Impulse:

$$E(x, y, 0, t) = E_o\, \delta(t)$$

Therefore

$$H(z, t) = E_o \{\sqrt{\sigma/\mu\pi}\ .\ (1/t^{\frac{1}{2}})\ .\ \exp(-\mu\sigma z^2/4t)\} \qquad (7.9)$$

and

$$E(z, t) = E_o\{0.5\sqrt{\mu\sigma/\pi}\ .\ (z/t^{3/2})\ .\ \exp(-\mu\sigma z^2/4t)\} \qquad (7.10)$$

(b) Step

$$E(x, y, 0, t) = E_o\, U(t)$$

Therefore

$$H(z, t) = E_o\{\ 2\sqrt{\sigma t/\mu\pi}\ \exp(-\mu\sigma z^2/4t) - (\sigma z)\ \mathrm{erfc}(\sqrt{\mu\sigma/t}\ .\ z/2)\} \qquad (7.11)$$

and

$$E(z, t) = E_o \left[1 - \mathrm{erf}(\sqrt{\mu\sigma/t}\ .\ z/2)\right] \qquad (7.12)$$

where

$$\mathrm{erf}(x) = 2/\sqrt{\pi} \int_0^x \exp(-u^2)\ du$$

$$\mathrm{erfc}(x) = 1 - \mathrm{erf}(x)$$

It is believed that equations (7.9) and (7.11) of the above listed equations (7.5) to (7.12) have not been reported elsewhere. The other equations can be found in references (7.4) and (7.9) for example.

7.7 Calculations and Experimental Results

7.7.1 Analytical check

A semi-infinite conducting block excited by either a step tangential E- or a step tangential H-fields has been considered. The distribution of the induced electric field inside the conducting block has been calculated for the two excitation cases by two different methods:

(i) Analytically, using equations (7.8) and (7.12).

(ii) Numerically, using the circuit analysis package SPICE.

The SPICE package used can accommodate some 200 nodes, i.e. approximately 100 micro-T circuits. The air-gap regions can be usually replaced in most cases by a single micro-T circuit. The rest could be used to represent the conducting regions. Many problems involve only one conducting region, hence it is possible to use a quite fine sub-division (which is represented by one micro-T cricuit) to model this region.

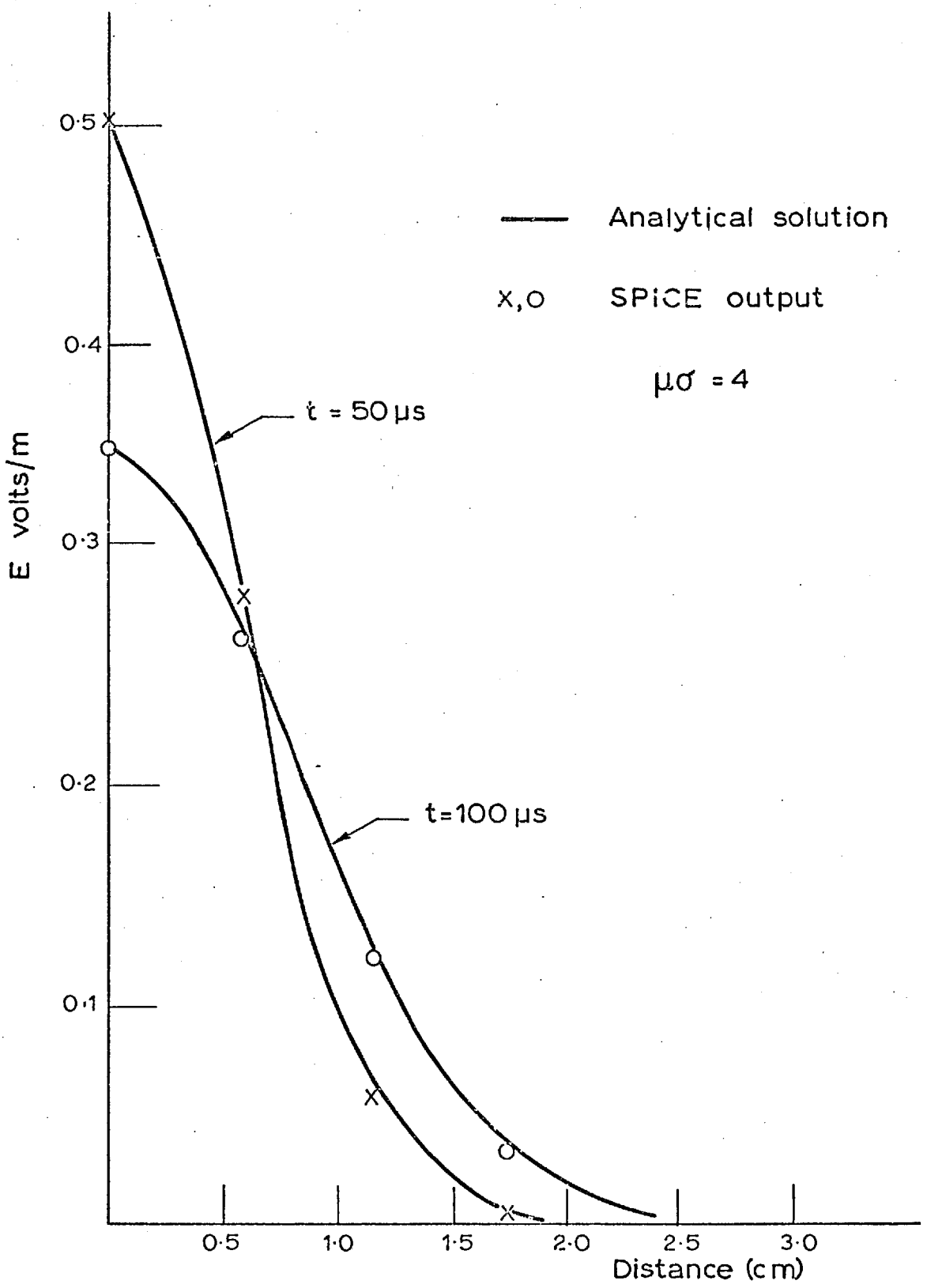


Fig. 7·7 Distribution of the induced E inside a conducting half space due to applied step H at the surface.

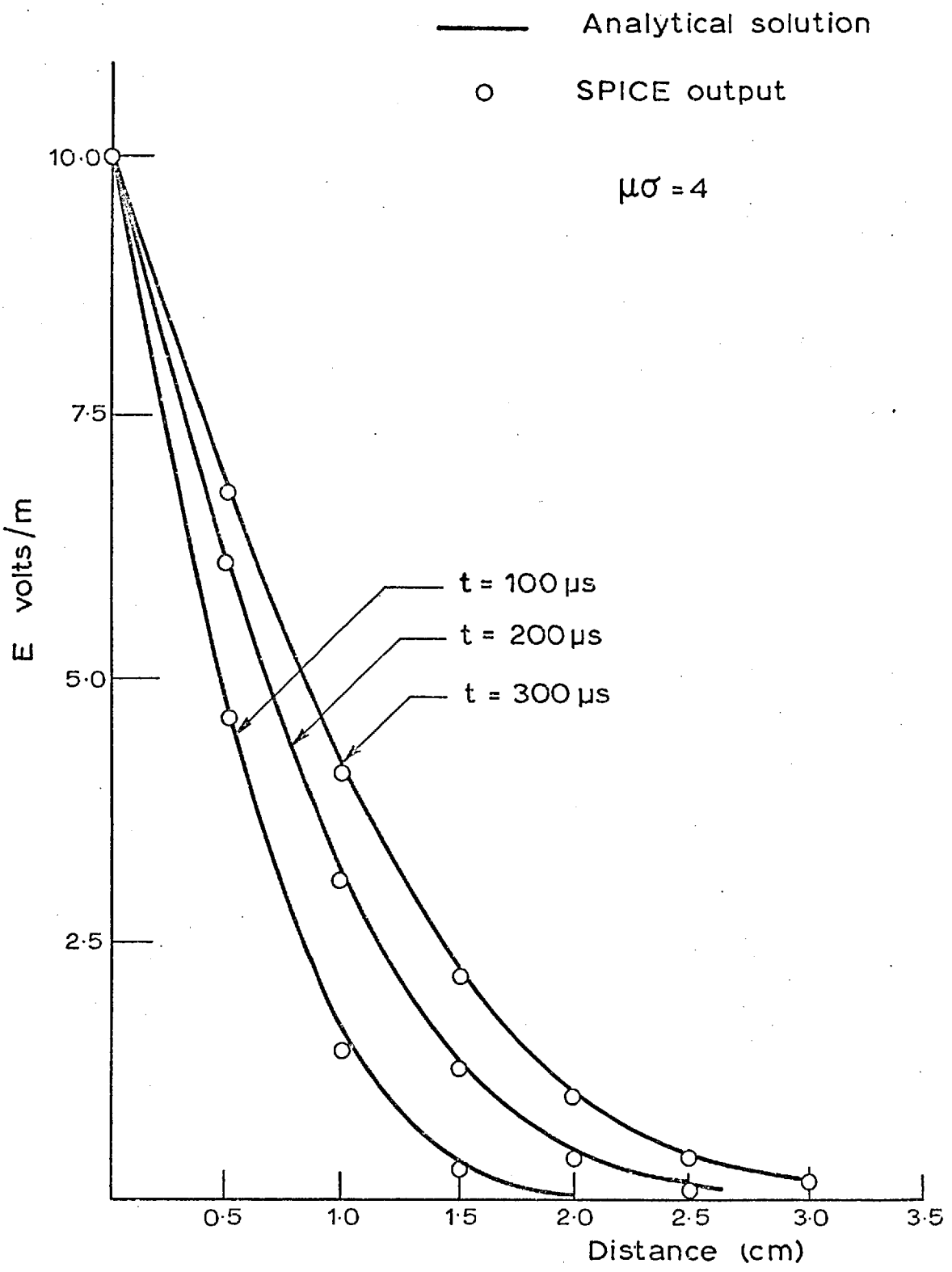


Fig. 7·8 Distribution of the induced E inside conducting half space due to applied step E_o at the surface.

The first 30 mm of the conducting block has been modelled by 30 micro-T circuits. The analytically calculated together with the SPICE output results are plotted in Fig. (7.7) and (7.8) for the two input excitation functions. The agreement between the two methods is good.

7.7.2 Experimental model

A 600 turn solenoidal coil of length 0.6 m and mean radius 0.03775 m was wound round a thick walled aluminium tube of the same length, the inner and outer radii were 0.00953 m and 0.03705 m respectively. A search coil of 200 turns lay between the bar and the excitation winding. A second search coil was placed inside the bar. The set up is shown schematically in Fig. (7.9).

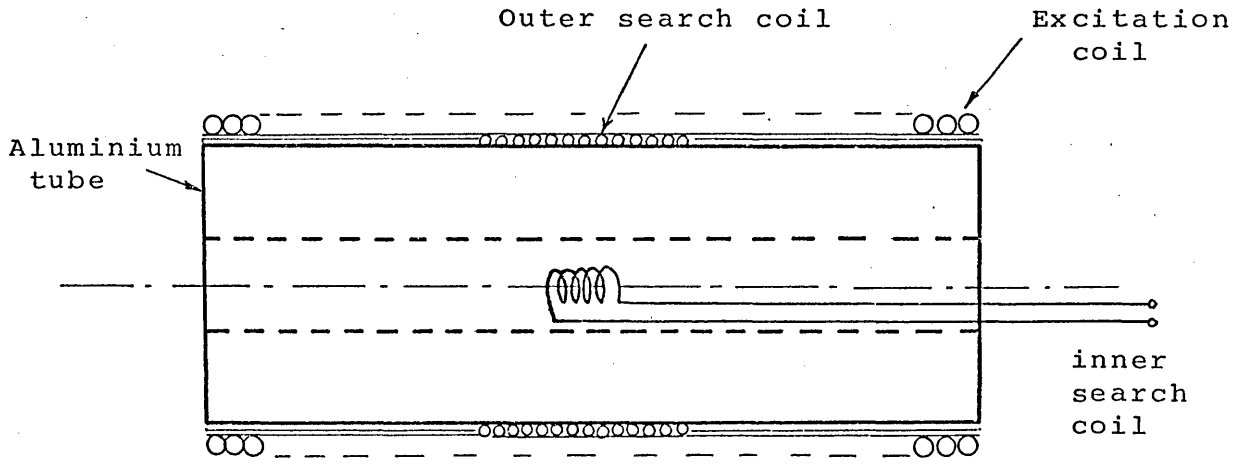


Fig. 7.9: Experimental set up

The input to the solenoid was a step voltage (battery) of 11.78 volts. The steady - state current was 1.5 A. The induced voltages of the inner and the outer search coils were recorded using an ultra-violet recorder. The transient voltage recorded from the outer search coil was too fast, and the speed of the oscillograph paper was not fast enough to give a complete picture of the initial part of the transients. Hence, instead of comparing the induced voltage with the SPICE output, the integrations of the voltage (which is proportional to the flux density) was inspected. The results of the integrated voltage of the outer search coil and the induced voltage of the inner search coil are shown in Fig. (7.10) and (7.11) respectively. The calculated and measured integrated voltage of the outer search coil agreed within 3% for a substantial part of the transient. The final values agreed within 2%. The agreement between the calculated and measured values of the inner search coil voltage was less accurate. However, bearing in mind that the measured voltage was small and an ultra-violet recorder was used, one can say that the agreement is quite close.

It should be mentioned here that the experimental results and the computed curves of Figures (7.7) to (7.11) have been supplied by Mr. H. Lu who was working under the joint supervision of the author and Dr. E. M. Freeman.

For more details about the choice of the sub-region thickness and the time step, refer to reference (7.20).

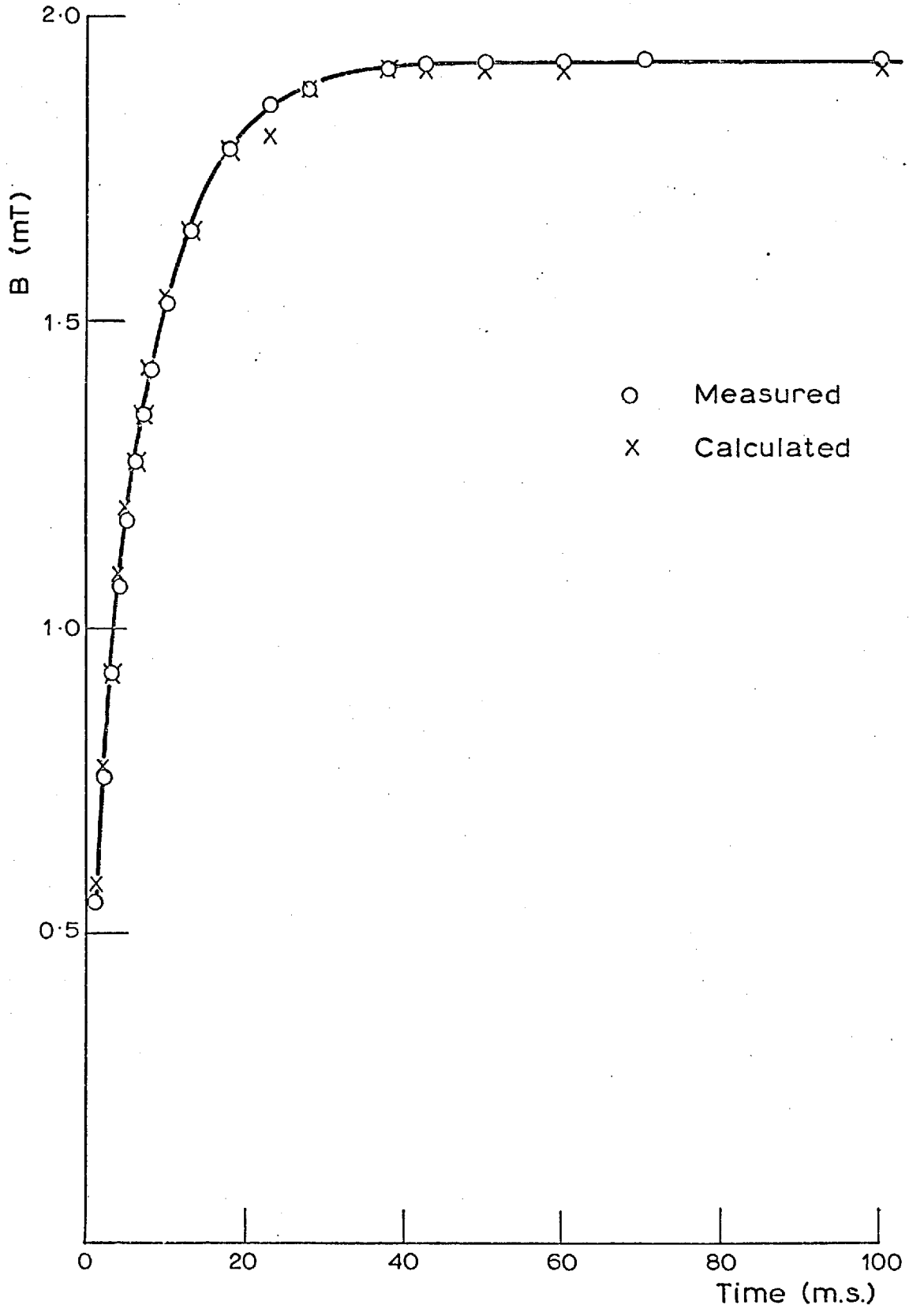


Fig 7·10 *Integrated voltage measured by the outer search coil.*

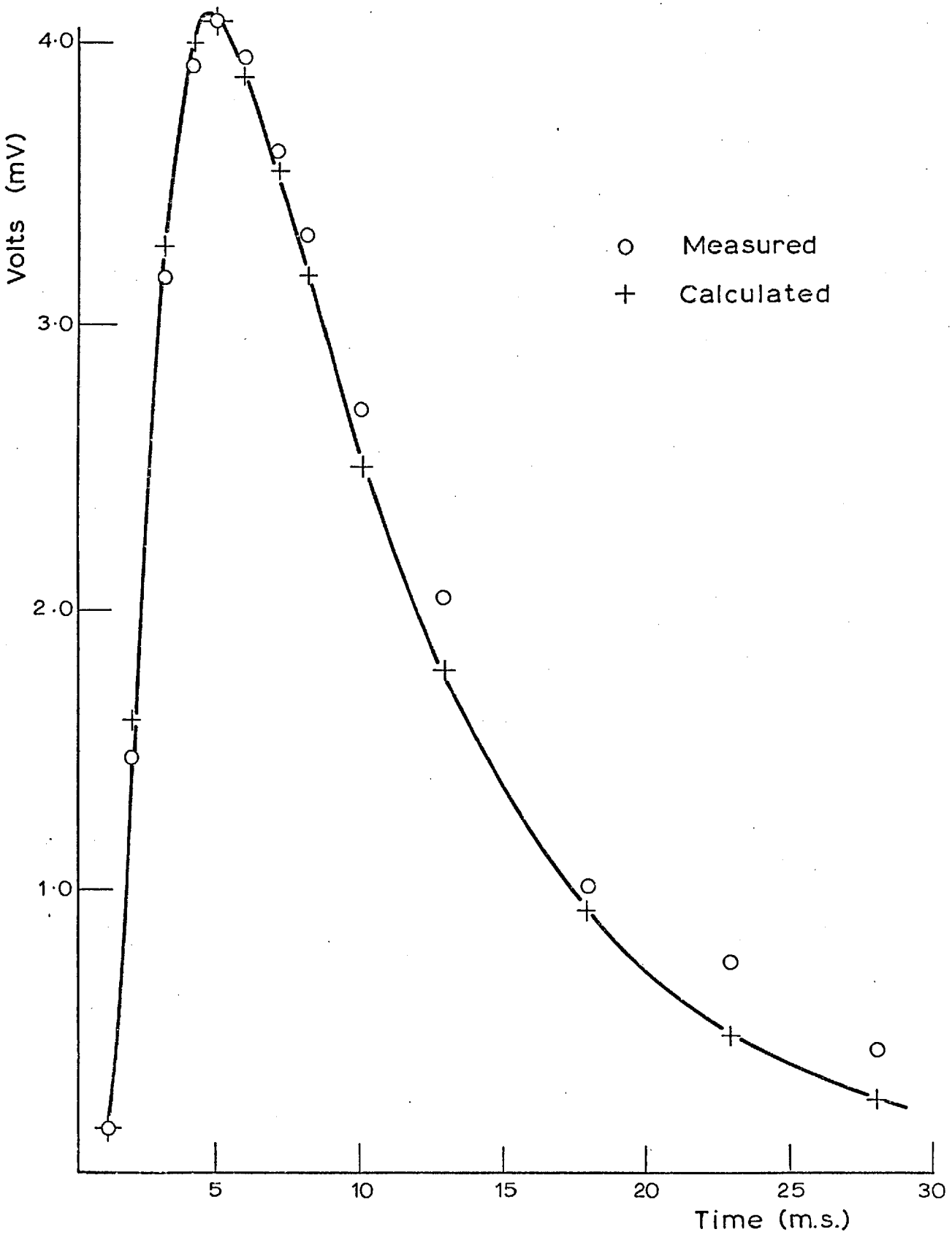


Fig 7·11 Voltage induced in the inner search coil under transient conditions.

7.8 Conclusions

The transient electromagnetic field problem has been considered briefly in this chapter. The transient solution can be obtained algebraically for some highly idealised models, or it can be calculated numerically from the frequency response using Fast Fourier Transform (FFT) method. However, the circuits developed in this thesis lend themselves to another alternative method in which some form of circuit analysis package (such as ECAP or SPICE) is used.

This circuit method has been checked against experimental results and also some closed form of solutions. Both yielded good agreement.

A new concept has been introduced in order to obtain the equivalent micro-T circuit. Accordingly, circuits which include only resistive and capacitive element could represent conducting and non-conducting regions. This has great importance specially when an electrical analogue is required to be built in the laboratory.

Finally, the circuit approach adopted in this work can make use of the already developed, highly efficient methods for calculating transients in power transmission lines as recently described in references 7.21 and 7.22.

Chapter 8

Conclusions and suggestions for future work

The problem of calculating the electromagnetic field components of multi-region cylindrical, multi-layer planar and multiple-shell spherical structures has been generally considered.

Some practical problems such as squirrel cage induction motors, sheet rotor and/or screened rotor induction motors, tubular induction motors, induction pumps for liquid metals and shielding problem of superconducting alternators, can be represented by an idealised multi-region cylindrical structure. In order to study the finite excitation length effects, the excitation winding could be replaced by a travelling wave two-dimensional current sheet. Also, 2-D current sheet is essential to model helical excitation windings which may occur in transverse flux tubular motors, or certain forms of superconducting turbo-alternator.

An equivalent circuit, which consists of non-uniform double transmission lines, has been found to describe the electromagnetic behaviour of this mathematical model. To satisfy the boundary conditions at the adjacent regions interfaces, these double T.L.s are found to be mutually coupled, at their terminals, through complex turns ratio ideal transformers.

The Bessel functions, usually associated with non-uniform lines (and in general with cylindrical structures), have been avoided by replacing any one T.L. by a large number of 'micro-T' circuits in cascade. The configuration of this μ-T circuit has been deduced for each one of these double lines. For the sake of generality, the displacement current has not been ignored, and its effect was found to be represented by capacitor elements in the equivalent circuit.

Close investigation for low frequency applications shows that the 'magnetic' field components at any point in a non-conducting region, can be fully described in terms of only 'one' of the two T.L.s , while the other is left open circuit. However, if the 'electric field components are required to be known, this open line can be replaced by another 'transformed' line.

Also for the special case when any conducting region is bounded by two non-conducting regions, it has been found that the equivalent double transmission lines can be replaced by one four-terminal network.

Throughout the analysis, it has been assumed that both the electric and magnetic fields possess three components, and none was assumed zero. As a result, the currents induced in any conducting region, was found to be three dimensional, although the exciting current has only two

components, a fact, to the author's belief, that had not been fully appreciated before this study. However, this induced current component, normal to the excitation surface, has only an appreciable value at small radii, and decays rapidly as the curvature decreases, i.e. as the radius increases. The effect of motion of the conducting regions of this mathematical model can be implicitly introduced by multiplying the angular frequency ω by the relative slip between the travelling wave and the region under consideration. Having done that, and to still have the same interface coupling circuit as deduced for the stationary case, there should be no relative motion between the different conducting annular layers of the model.

To take the problem of investigating the effect of motion a step further, a multi-layer planar model is considered. Each layer in that model has been assigned an arbitrary linear velocity, in the direction of travelling field. In general this model can represent all the practical applications represented before by the multi-region cylindrical model if the effect of curvature could be neglected. Perhaps the most important field of application is in the linear induction devices, and in particular the linear induction motor and linear induction pumps for liquid metals. In this latter case, the situation of two conducting layers, which are sliding on each other, is likely to occur.

The effect of motion is explicitly introduced in this

multi-layer planar model. Similarly, having decomposed the field into two basic modes, an equivalent double transmission line network has been developed. In this case, the effect of motion has been introduced in the network model through either voltage or current sources. The amplitude of these sources has been found proportional to (1-s) where s is the relative slip between the conducting region and the excitation travelling wave.

For the special case when all the conducting regions, in the multi-layer planar model, are relatively at rest and are such that each of them is bounded by two non-conducting layers, the double transmission line reduces to the single line derived before by Freeman and Lowther. Their T.L. together with the transfer matrix representation reported by Alden and Nolan are limited to the special case mentioned above.

The equivalent metworks already derived in the literature for either the circumferentially or axially excited multi-region cylindrical structure also for the one-dimensionally excited multi-layer planar model have been found to be special cases of the general double transmission line equivalent networks developed in chapters two and three.

Before moving on to another aspect of this work, I would like to emphasize again the distinct feature of Maxwell equations in a generalised cylindrical coordinate system.

That is, the electromagnetic field components in the 'transverse' directions could be completely expressed in terms of its 'axial' components. This in turn allows the decomposition of the main field into two basic modes referred to throughout the text as the E- and H- modes. Such decomposition made it possible to develop the double T.L. equivalent network. This technique is well known in the microwave theory, but it seems that it did not receive much attention for low frequency applications. It has been shown that the finite excitation problem could be analysed using the transmission line modelling technique together with the Fourier integral method. A mathematical model which consists of a multi-region cylindrical structure excited by a circumferential current sheet having finite length in the axial direction, has been considered. This model is of a great practical application in the fields of non-destructive eddy current testing and induction heating when the excitation is provided by a finite length coil. The impedance of an air-cored solenoid also the impedance of a solenoid closely encircling an infinitely long conducting cylinder have been calculated, and the results have been checked against published figures. A good agreement has been obtained. The induced eddy current distributions in the conducting region in both the axial and radial directions are compared with the case when the finite length effects are neglected. For short coils having length/ radius ratio of order of 1.0, a substantial reduction in

the induced current, as compared with infinitely long model, has been observed specially for low frequency situation when the radius/skin depth ratio is of order of 3.0.

For the case when the axial length of the excitation coil is very large as compared to its radius, the finite length effect could be neglected. In such a case, both the electric and magnetic fields are one-dimensional. Analysing an infinitely long model, a simple electromagnetic method has been described for determining the conductivity of 'infinitely' long conducting tubes or solid bars. The method is intended to estimate the conductivity to an accuracy of 1%. The method has been discussed in detail and approximate ranges of the required test frequency has been defined for both thick and thin metallic tubes.

The third general mathematical model of the multiple-shell spherical structure has been considered after that. Only the situation of single phase excitation is considered. The model is useful in representing the practical problems of magnetic (assuming magnetic linearity) and/or eddy current shielding. Also it can represent, to a first order approximation, the practical problem of contamination-free process of melting metals, and in general the applications concerning levitation of spheres by induction forces. In the analysis, the excitation surface current sheet has been replaced by

an infinite series of surface zonal harmonics. It has been shown that the high order surface zonal harmonics have a very little effect on the value of the screening ratio of a thick conducting or magnetic spherical shell. Even if the excitation current sheet is very rich in surface zonal harmonic contents, in some special applications, such as those considered experimentally in chapter 6, the fundamental component only has been found adequate to represent the current sheet waveform.

The transient field problem of some 1-D excitation mathematical models of multi-region cylindrical, multi-layer planar and multiple-shell spherical configuration has been considered.

A method which makes use of the circuit analysis program packages has been adopted. Good agreement has been achieved between the computer results and both the experimental and some close form solution of simple transient field problems of planar models.

Suggestions for future work

* The analysis throughout the thesis assumes isotropic magnetically linear regions. Perhaps, the logical step is to introduce the anisotropy in the double transmission line equivalent network. Also the effect of magnetic non-linearity should be accounted for in any further extension to this work.

* For both the multi-region cylindrical and multi-layer planar models, the effect of finite excitation dimension has been discussed. However, the different layers have been assumed infinitely long and infinitely wide but having finite thickness in a direction normal to the excitation surface. So, it is believed that the finite extension of the regions material should be introduced in any further study.

* It has been shown that the implicit introduction of the effect of motion through the concept of the 'slip frequency' is not generally valid for all cases. The explicit introduction of this effect in the form of $(\bar{V} \times \bar{B})$ product is essential especially if the 'electric field' has a component in the direction of motion. The author feels that the general three dimensional equivalent network developed by Kron should be modified in order to include this motional term explicitly.

References

Chapter 1

1.1 Nasar, S. A.: 'Electromagnetic theory of electrical machines'. Proc. IEE, 1964, 111, (6), pp.1123-1131.

1.2 Discussion contributions on the above paper. Proc. IEE, 1965, 112, (10), pp.1927-1932.

1.3 Howe, G.W.O.:'The application of telephone transmission formulae to skin effect problems'. J. IEE, 1916, 54, pp. 473-480.

1.4 Schelkunoff, S.A.:'Transmission theory of plane electromagnetic waves', Proc. IRE, 1937, 25, (11), pp. 1457-1492.

1.5 Booker, H.G.:'The elements of wave propagation using the impedance concept', J. IEE, 1947, 94, Pt. III, pp. 171-202.

1.6 Kron, G.:'Equivalent circuit of the field equations of Maxwell-I', Proc. IRE, 1944, 32, pp. 289-299.

1.7 Kron, G.:'Electric circuit models of partial differential equations', Elec. Eng., July 1948, pp. 672-684.

1.8 Cooper, W.H.B.:'An approach to the operation of inductors and transformers in terms of the field impedance', Proc. IEE, 1949, 96, Pt. II, pp. 509-517.

1.9 Welsby, V.G.:'Electromagnetic fields in a ferromagnetic medium with particular reference to harmonic distortion due to hysteresis'. Proc. IEE, 1958, 105C, pp. 218-229.

1.10 Cullen, A.L. and Barton, T.H.:'A simplified electromagnetic theory of the induction motor, using the concept of wave impedance', Proc. IEE, 1958, 105C, pp. 331-336.

1.11 Greig, J. and Freeman, E.M.:'Travelling-wave problem in electrical machines', Proc. IEE, 1967, 114, (11), pp. 1681-1683.

1.12 Freeman, E.M.:'Travelling waves in induction machines: input impedance and equivalent circuits', Proc. IEE, 1968, 115, (12), pp. 1772 - 1776.

1.13 Cooper, W.H.B. and Gillespie, A.B.:'The engineering concepts of equivalent networks, transfer functions and field impedance in magnetohydrodynamics', U.K.A.E.A., 1963, Memo. AERE - M 1213, Pt. I.

1.14 Aldridge, E.E.: 'The engineering concepts of equivalent networks, transfer functions and field impedance in magnetohydrodynamics', U.K.A.E.A., 1963, Memo. AERE - M 1213, Pt III.

1.15 Freeman, E.M.:'Levitation force as a function of rate of change of impedance with respect to distance', Proc. IEE, 1969, 116, (6), pp. 1047-1048.

1.16 Freeman, E.M. and Smith, B.E.:'Surface-impedance method applied to multilayer cylindrical induction devices with circumferential exciting currents', Proc. IEE, 1970, 117, (10), pp. 2012 - 2013.

1.17 Freeman, E.M. and Lowther, D.A.: 'Normal force in single-sided linear induction motors', Proc. IEE, 1973, 120, (12), pp. 1499 - 1506.

1.18 Freeman, E.M.:'Equivalent circuits from electromagnetic theory: low-frequency induction devices', Proc. IEE, 1974, 121, (10), pp. 1117-1121.

1.19 Freeman, E.M.:'Wave impedance of induction devices using the scalar Riccati equation', Proc. IEE, 1976, 123, (2), pp. 145-148.

1.20 Postinikov, I.M., Asanbaev, V.N. and Saratov, V.A:'Equivalent circuits and parameters of A.C. machines with "solid wound" rotor', Elektrichestvo, 1973, 17-20, (9), pp. 90-100.

1.21 O'Kelly, D.:'Losses in cylindrical ferromagnetic cores including hysteresis and eddy current effects', J. Phys. D. Appli. Phys., 1975, 8, pp. 568-575.

1.22 Eastham J.F. and Alwash, J.H.:'Transverse flux tubular motors', Proc. IEE, 1972, 119, (12), pp. 1709-1718.

1.23 Williamson, S.:'The anisotropic layer theory of induction machines and induction devices', J. Inst. Maths Applics, 1976, 17, pp. 69-84.

Chapter 2

2.1 Piggott, L.S.:'A theory of the operation of cylindrical induction motors with squirrel-cage rotors', Proc. IEE, 1962, 109C, pp. 270-282

2.2 Freeman, E.M.:'Equivalent circuits from electromagnetic theory: low-frequency induction devices', Proc. IEE, 1974, 121, (10) pp. 1117-1121.

2.3 Freeman, E. M. and Smith, B.E.:'Surface-impedance method applied to multilayer cylindrical induction devices with circumferential exciting currents' Proc. IEE, 1970, 117, (10), pp. 2012-2013.

2.4 Greig, J. and Freeman, E.M.:'Travelling-wave problem in electrical machines', Proc. IEE, 1967, 114, (11), pp. 1681-1683.

2.5 Kirtley, J.L. Jr.:'Surface coefficients for multipole magnetic field boundary condition problems', Trans. IEEE, 1975, PAS-94, pp. 933-938.

2.6 Hughes, A. and Miller, T.J.E.:'Analysis of fields and induction in air-cored and iron-cored synchronous machines', Proc. IEE, 1977, 124, (2), pp. 121-126.

2.7 Hammond, P.:'The calculation of the magnetic field of rotating machines - Pt. 1: The field of tubular current', Proc. IEE, 1959, 106C, pp. 158-164.

2.8 Lawrenson, P.J. and Ralf, M.C.:'General 3-dimensional solution of eddy current and Laplacian fields in cylindrical structures', Proc. IEE, 1970, 117, (2), pp 467-472.

2.9 Endean, V.G. and Allen, J.E.:'Discussion on the above paper', Proc. IEE, 1970, 117, (10), pp. 2059-2060.

2.10 Eastham, J.F. and Alwash, J.H.:"Transverse-flux tubular motors', Proc. IEE, 1972, 119, (12), pp.1709-1718.

2.11 Freeman, E.M.:'Equivalent circuit for the transverse-flux tubular induction motor', Proc. IEE, 1975, 122, (7), pp. 744-745.

2.12 Davies, E. J.:'Air-gap windings for large turbo-generators', Proc. IEE, 1971, 118, (3/4), pp. 529-535.

2.13 Horsley, W.D.: British Patent 837 546 1956.

2.14 Morgan, J.W.H. and Wilkins, J.T.: British Patent 881 468 1958.

2.15 Aichholzer, G:'New ways of building turbogenerators up to 2GVA, 60 KV', Elektrotech. and Machinenbau, 89, pp 1-11.

2.16 Spooner, E:'Fully slotless turbogenerators', Proc. IEE, 1973, 120, (12), pp. 1507-1518.

2.17 Kirtley, J.L. Jr., Smith, J.L. Jr., Thullen, P. and Woodson, H.H.:'MIT-EE1 Program on large superconducting machines', Proc. IEEE, 1973, 61, (1), pp. 112-115.

2.18 Lorch, H.O.:'Feasibility of turbogenerator with superconducting rotor and conventional stator', Proc. IEE, 1973, 120, (2), pp. 221-227.

2.19 Appleton, A.D., Anderson, A.F. and Ross, J.S.H.:'A discussion on large superconducting A.C. generators', Int. Conf. in Elec. Machines, City Univ., London, 1974.

2.20 Lorch, H.O.:'Superconducting turbine-generators', ibid

2.21 Einstein, T.H.:'System performance characteristics of superconducting alternators for electric utility power generation' Trans. IEEE, 1975, PAS-94, (2), pp. 310-319.

2.22 Jackson, R.J.:'The rotating armature superconducting generators', CERL Report, Lab. Note No. RD/L/N 149/75, 1975.

2.23 Parker, J.H. and Towne, R.A.:'Superconducting A.C. generators', Trans. IEEE, 1976, MAG-12, (6), pp. 909-914.

2.24 Luck, D.L. and Thullen,:'Double shielded superconducting field winding', U.S. Patent No. 3, 764, 835, Oct. 1973.

2.25 Furuyama, M. and Kirtley, J.L. Jr.:'Transient stability of superconducting alternators', Trans. IEEE, 1975, PAS-94, (2), pp. 320-328.

2.26 Lawrenson, P.J., Miller, T.J.E., Stephenson, J.M. and Ula, A.H.M.S.:'Damping and screening in the synchronous superconducting generator', Proc. IEE, 1976, 123, (8), pp. 787-794.

2.27 Dagalakis, N. and Kirtley, J.L. Jr.:'Protection of superconducting field windings for electrical machines by the use of an inertial free electromechanical shield', Trans. IEEE, 1975, MAG-11, (2), pp. 650-652.

2.28 Dagalakis, N. and Kirtley, J.L. Jr.:'Design considerations for a 2000 MVA superconducting generator with rotor inertial shielding protection', Elec. mach. and Electromech., 1976, 1, (1), pp. 33-55.

2.29 Russell, R.L. and Norsworthy, K.H.:'Eddy currents and wall losses in screened-rotor induction motors', Proc. IEE, 1958, 105A, pp. 163-175.

2.30 Koch, W.H.:'Equivalent circuits with transformer elements for eddy current rotor induction motor derived from field equations. I - Sleeve rotor motors
II - Drag cup rotor motors', Trans IEEE, 1964, 83, (6), pp. 567-583.

2.31 Hague, P:'The principles of electromagnetism applied to electrical machines', 1962, Dover Pub., N.Y.

2.32 Saunders, R.M.:'Electromechanical energy conversion in double cylindrical structures', Trans. IEEE, 1963, PAS-82, pp. 631-638.

2.33 Nix, G.F. and Laithwaite, E.R.:'Linear induction motors for low-speed and standstill applications', Proc. IEE, 1966, 113, (6), pp. 1044-1056.

2.34 Wood, A.J. and Concordia, C.:'An analysis of solid rotor machines Part III, Finite length effects', Trans. IEEE, 1960, 79, Pt.III pp. 21-26.

2.35 Ashworth, D.S. and Hammond, P.:'The calculation of the magnetic field of rotating machines. Pt. 2 - The field of turbo-generator end windings', Proc. IEE, 1961, 108A, pp. 527-538

2.36 Tegopoulos, J.A.:'Current sheets equivalent to end-winding currents of turbine-generator stator and rotor', Trans. AIEE, 1963, 81, Pt III, pp. 695-700.

2.37 Clarricoats, P.J.B. and Oliner, A.A.:'Transverse-network representation for inhomogeneously filled circular waveguide', Proc. IEE 1965, 112, (5), pp. 883-894.

2.38 Malachlan, N.W.:'Bessel functions for engineering, Clarendon Press, 2nd edition, 1961, pp. 126-129.

2.39, Heaviside, O.:'Electromagnetic theory', Vols. I-III, Dover pub., N.Y. 1950.

2.40 Schelkunoff, S.A.:'Electromagnetic waves', D. Van Nostrand, N.Y., 1943.

2.41 Clarricoats, P.J.B., Olver, A.D. and Wong, J.S.L.:'Propagation in isotropic plasma waveguides', Proc. IEE, 1966, 113, (5), pp. 755-766.

2.42 Oliner, A.A. and Clarricoats, P.J.B.:'Transverse equivalent networks for slotted inhomogeneous circular waveguide', Proc. IEE, 1967, 114, (4), pp. 445-456.

2.43 Clarricoats, P.J.B. and Olver, A.D.:'Propagation in radially stratified isotropic and anisotropic circular waveguides', IEE Conf. Pub. 13, Sept. 1965, pp. 19.

2.44 Oliner, A.A., Bertoni, H.L. and Li, R.C.M.:'A microwave network formalism for acoustic waves in isotropic media', Proc. IEEE, 1972, 60, (12), pp. 1503-1512.

2.45 Oliner, A.A., Li, R.C.M. and Bertoni, H.L.:'Catalog of acoustic equivalent networks for planar interfaces', Proc. IEEE, 1972, 60, (12), pp. 1513-1518.

2.46 Abramowitz, M and Stegun, I.A. (editors):'Handbook of Mathematical Functions', National Bureau of Standards, U.S. - Appl. Math. Ser. - 55, 1965, pp. 378-384.

2.47 Pfaler, C.-E.v.:'A new fundamental system of solutions of Maxwell's equations for a circular cylindrical tube', Siemens Forsch. - u. Entwickl. - Ber. Bd.1, 1972, (2), pp. 197-203.

2.48 Pfaler, C.- E.v.:'A new fundamental system of modified cylindrical functions for an annular region', ibid, 1973, 2, (3), pp. 166-170.

2.49 Roberts, J.:'Analogue treatment of eddy-current problems involving two-dimensional fields', Proc. IEE, 1960, 107C, pp. 11-18.

2.50 Roberts, J.:'Analogue treatment of eddy currents and magnetic flux penetration in saturated iron', Proc. IEE, 1962, 109C, pp. 406-411.

2.51 Oberretl, K.:'Magnetic fields, eddy currents, and losses, taking the variable permeability into acccunt', Trans. IEEE, 1969, PAS-88, pp. 1646-1657.

2.52 Beland, B and Richard, S.:'A new transmission line representation of eddy-current problems in cylinders', Trans. IEEE, 1971, PAS-90, pp. 2181-2185.

2.53 O'Kelly, D. and Salih, A.M.:'Over voltages in reactive circuits due to current-chopping', 1976, 11th Univ. Power Eng. Conf., Southampton, U.K.

2.54 Wall, H.S.:'Analytic theory of continued fractions', D. Van. Nostrand and Co., U.S.A., 1948.

2.55 Weinberg, L.:'Network analysis and synthesis', McGraw-Hill Book Co. U.S.A., 1962.

2.56 Freeman, E.M.:'Computer aided steady-state and transient solutions of quasi-one dimensional field problems in induction devices', Compumag, Oxford, 1976.

2.57 Freeman, E.M.:'Computer-aided steady-state and transient solutions of field problems in induction devices', Proc. IEE, 124, (11), 1977, pp. 1057-1061.

2.58 Johnson, W.C.:'Transmission lines and networks', McGraw-Hill Co., N.Y., 1950, pp. 257-259.

2.59 Wu, K.Y.K.:'A study of the electromagnetic field distribution in multi-region induction devices with particular reference to the screening effect of superconducting generators', M.Sc. thesis, London Univ., Oct. 1977.

Chapter 3

3.1 Tesla, N.:'A new system of alternate current motors and transformers', Trans, AIEE, 1888, 5, pp. 308-324.

3.2 Jaquard, Weaver and Electric Shuttle Co.: British Patent No. 12364, (1895).

3.3 Weeler and Bradley:'Electric transportation system', U.S. Patent No. 448598 (1889).

3.4 Zehden: U.S. Patent No. 772312 (1905).

3.5 Bachelet, E.: (1914)

3.6 Japolski, Ya.S.: Elektrichestvo, 1925, 11

3.7 Japolski, Ya. S.: Engineering, 1926, 122, p. 159

3.8 Trombetta, P.:'The electric hammer', Trans. AIEE, 1922, 41, pp. 233-241.

3.9 'A wound rotor motor 1400 ft. long', Westinghouse Engineer, 1946, 6, p. 160.

3.10 'The first linear motor': An exhibit at the Science Museum, London, U.K.

3.11 Williams, F.C. and Laithwaite, E.R.:'A brushless variable-speed induction motor', Proc. IEE, 1955, 102A, (2), pp. 203-210.

3.12 Laithwaite, E.R.:'Brushless variable speed induction motors involving a new principle', Engineer's Digest, 1956, 17, (8), pp. 329-333.

3.13 Laithwaite, E.R.:'New developments in electromagnetic shuttle propulsion', Textile Weekly, 1957, 57, pp. 234-235.

3.14 Laithwaite, E.R. and Lawrenson, P.J.:'A self-oscillating induction motor for shuttle propulsion', Proc. IEE, 1957, 104A, (14), pp. 93-101.

3.15 Williams, F.C., Laithwaite, E.R. and Piggott, L.S.:'Brushless variable speed induction motors' Proc. IEE, 1957, 104A, (14), pp. 102-118.

3.16 Laithwaite, E.R.:'Linear induction motors', Proc. IEE, 1957, 104 A, (18), pp. 461-470.

3.17 Laithwaite, E.R., Tipping, D. and Hesmondhalgh, D.E.:'The application of linear induction motors to conveyors', Proc. IEE, 1960, 107A, (33), pp. 284-294.

3.18 Nix, G.F. and Laithwaite, E.R.:'Linear induction motors for low speed and standstill applications', Proc. IEE, 1966, 113, (6), pp. 1044-1056.

3.19 Laithwaite, E.R. (editor):'Transportation without wheels', 1977, 1st edition, Elek Books Ltd.

3.20 Liyelpeter, Ya. Ya.:'State of the theory of the MHD induction machines with working media of liquid metal', in 'Movement of conducting bodies in magnetic fields', Institute of Physics of Latvian Academy of Sciences monograph, 1966, (English Translation: NASA TT F-460, 1968, pp 1-12).

3.21 Laithwaite, E.R., Eastham, J.F., Bolton, H.R. and Fellows, T.G.: 'Linear motors with transverse flux', Proc. IEE, 1971, 118, (12), pp. 1761-1767.

3.22 Blake, L.R.:'Conduction and induction pumps for liquid metals', Proc. IEE, 1957, 104A, pp. 49-63.

3.23 Blachford, C.W.:'Induction cup parameters from electromagnetic field theory and experimental analysis', Trans. IEEE, 1965, PAS-84, (11), pp. 1089-1093.

3.24 West, J.C. and Hesmondhalgh, D.E.:'The analysis of thick-cylinder induction machines', Porc. IEE, 1962, 109C, pp. 172-181.

3.25 Veze, A.K. and Ulmanis, L.Ya.:'Electromagnetic process in an ideal induction MHD machine' in 'Movement of conducting bodies in magnetic fields', Institute of Physics of Latvian Academy of Sciences monograph, 1966. (English translation: NASA TT F-460, 1968, pp. 13-37).

3.26 Nonaka, S. and Yoshida, K.:'Analysis of double sided-linear motors', Elec. Eng. in Japan, 1970, 90, (3), pp. 21-31.

3.27 Nonaka, S. and Yoshida, K:'Characteristics of linear motors with sandwich compound conducting plates', ibid, 1971, 91, (1), pp. 183-193.

3.28 Ooi, B.T. and White, D.C.:'Traction and normal forces in the linear induction motor', Trans. IEEE, 1970, PAS-89, (4), pp. 638-645.

3.29 Wang, T.C.:'Linear induction motor for high-speed ground transportation', Trans. IEEE, 1971, IGA-7, (5), pp. 632-642

3.30 Freeman, E.M.:'Travelling waves in induction machines: input impedance and equivalent circuits', Proc. IEE, 1968, 115, (12), pp. 1772-1776.

3.31 Russell, R.L. and Norsworthy, K.H.:'Eddy currents and wall losses in screened-rotor induction motors', Proc. IEE, 1958, 105A, pp. 163-175.

3.32 Bolton, H.:'Transverse edge effect in sheet-rotor induction motors', Proc. IEE, 1969, 116, (5), pp. 725-731.

3.33 Yamamura, S., Ito, H. and Ahmed, F.:'End effect of linear induction motor ', Elec. Eng. in Japan, 1970, 90, (2), pp. 20-30.

3.34 Ooi, B.T.:'A generalised machine theory of the linear induction motor', Trans. IEEE, 1973, PAS-92, pp. 1252-1259.

3.35 Alwash, J.H.H. and Eastham, J.F.:'Permeance harmonic analysis of short-stator machines', Proc. IEE, 1976, 123, (12), pp. 1335-1340.

3.36 Preston, T.W. and Reece, A.B.J.:'Transverse edge effects in linear induction machines', Proc. IEE, 1969, 116, (6), pp. 973-979 (and corrigenda, ibid, 1970, 117, (9), p. 1808).

3.37 Wood, A.J. and Concordia, C.:'An analysis of solid rotor machines: Pt. III - Finite length effects', Trans. IEEE, 1960, 79, Pt. III, pp. 21-26.

3.38 Angst, G.:'Polyphase induction motor with solid rotor; effects of saturation and finite length,', Trans. AIEE, 1961, 80, Pt. III, pp. 902-910.

3.39 Okhremenko, N.M.:'An investigation of the spatial distribution of the magnetic fields and electromagnetic effects in induction pumps', Magnitnaya Gidrodinamika, 1965, 1, (1), pp. 97-109.

3.40 Okhremenko, N.M.:'Transverse fringe effect in flat linear induction pumps', ibid, 1965, 1, (3), pp. 87-95.

3.41 Okhremenko,N.M.:'Travelling-field induction pumps', ibid, 1965, 1, (4), pp. 3 -23.

3.42 Veske, T.A.:'Solution of the electromagnetic field equations for a plane linear induction machine with secondary boundary effects', ibid, 1965, 1, (1), pp. 87-96.

3.43 Parts, I.R.:'Electromagnetic field distribution in liquid metal acyclic converters', ibid, 1965, 1, (3), pp. 127-138.

3.44 Vilnitis, A. Ya.:'Transverse edge effect in plane induction magneto-hydrodynamic machines', in 'Movement of conducting bodies in magnetic fields', Institute of Physics of Latvian Academy of Sciences monograph, 1966, (English translation,: NASA TT F-460, pp. 58-85).

3.45 Freeman, E.M. and Lowther, D.A.:'Transverse edge effects in linear induction motors', Proc. IEE, 1971, 118, (12), pp. 1820-1821.

3.46 Freeman, E.M. and Lowther, D.A.:'Normal force in single-sided linear induction motors', ibid, 1973, 120, (12), pp. 1499-1506.

3.47 Alden, R.T.H. and Nolan, P.J.:'Transfer matrix analysis of linear induction mahcines with finite width and depth', ibid, 1974, 121, (11), pp. 1393-1398.

3.48 Lowther, D.A.:'A study of the 3-axis forces in linear induction machines using electromagnetic scale models', Ph.D. thesis, Brighton Polytechnic, 1973.

3.49 Sudan, R.N.:'Interaction of conducting fluid stream with travelling wave of magnetic field of finite extension', J. Appl. Phys. 1963, 34, (3), pp. 641-650.

3.50 Valdmanis, Ya. Ya.:'Longitudinal edge effect in linear induction MHD machines', see reference (3.25).

3.51 Yamamura, S., Ito, H. and Ishikawa, Y.:'Influence of end effect on characteristics of linear indcution motors', Elec. Eng. in Japan, 1971, 91, (1), pp. 136-147.

3.52 Yamamura, S., Ito, H. and Ishikawa, Y.:'Theories of the linear induction motor and compensated linear induction motor', Trans. IEEE, 1972, PAS-91, pp. 1700-1710.

3.53 Iwamoto, M. and Yamamura, S.:'End effect of high-speed linear induction motors', Elec. Eng. in Japan, 1972, 92, (3), pp. 94-101.

3.54 Engeln, F. and Peschka, W.:'End effect on the linear induction MHD generator calculated by two-sided Laplace transform', Proc. 3rd. Int. Symp. on MHD, Salzburg, 1966,pp. 937-951.

3.55 Nonaka, S. and Yoshida, Y.:'Space harmonic analysis of linear induction motors', Elect. Eng. in Japan, 1973, 93, (2), pp. 42-50.

3.56 Schieber, D.:'Principles of operation of linear induction devices', Proc. IEEE, 1973, 61, (5), pp. 647-656.

3.57 Dukowicz, J.K.:'Analysis of linear induction machines with discrete windings and finite iron length', Trans. IEEE, 1977, PAS-96, (1), pp. 66-73.

3.58 Oberretl, K.:'Three dimensional analysis of the linear motor taking into account edge effects and the distribution of the winding', Arch. Elektrotech., 1973, 55, pp. 181-190.

3.59 Yamamura, S. and Ito, H.:'Three dimensional analysis of linear induction motors', Elec. Eng. in Japan, 1976, 96, (2), pp. 55-61.

3.60 Williamson, S.:'The anisotropic layer theory of induction machines and induction devices',J. Inst. Math. Applics., 1976, 17, pp. 69-84.

3.61 North, G.G.:'Harmonic analysis of short stator linear induction machine using a transformation technique', Trans. IEEE, 1973, PAS-92, pp. 1733-1743.

3.62 Holley, H.J., Nasar, S.A. and Del Cid, L.:'Computations of fields and forces in two-sided linear induction motor', Trans. IEEE, 1973, PAS-92, pp. 1310-1315.

3.63 Foggia, A., Sabonnadiere, J.C. and Silvester, P.:'Finite element solution of saturated travelling magnetic field problems', Trans. IEEE, 1975, PAS-94, (3), pp. 866-871.

3.64 Elliot, D.G.:'Matrix analysis of linear induction machines', 1975, U.S. Dept. of Transp, Report No. FRA-OR and D-75-77.

3.65 Huhns, R. and Pierson, E.S.:'Comparison of different models for the MHD induction generator', Proc. of the 14th Symp.on Engineering Aspects of Magnetohydrodynamics.

3.66 Freeman, E.M.:'Computer-aided steady-state and transient solutions of field problems in induction devices', Proc. IEE, 1977, 124 (11), pp. 1057-1061.

Chapter 4

4.1 Förster, F.:'Non-destructive testing handbook', (ed.: R.C. McMaster), Vol. II, Sections 36-42, Ronald Press Co., N.Y., 1959.

4.2 Hochshild, R.:'Mathematical foundation of non-destructive testing by eddy current methods', U.S. Atomic Energy Commission Report NYO-3576, March, 1953.

4.3 Bareham, F.R.:'Choice of frequency of eddy-current tube testing', Brit. J. Appl. Phys., 1960, 11, pp. 218-223.

4.4 Blitz, J. and Rowse, A.A.:'THe investigation of defects in non-ferromagnetic metal tubes using eddy currents', Appli. materials research, 1964, 3, pp.82-87.

4.5 Lloyd, E.A.:'Impedance of long solenoids with non-ferrous tubular cores', Proc. IEE, 1967, 114, (4), pp. 533-536.

4.6 Freeman, E.M. and Bland, T.G.:'Equivalent circuit of concentric cylindrical conductors in an axial alternating magnetic field', Proc. IEE, 1976, 123, (2), pp. 149-152.

4.7 Freeman, E.M.:'Equivalent circuit from electromagnetic theory: low-frequency induction devices', PRoc. IEE, 1974, 121, (10), pp. 1117-1121.

4.8 Freeman, E.M.:'Travelling waves in induction machines: input impedance and equivalent circuits', Proc. IEE, 1968, 115, (12), pp. 1772-1776.

4.9 Freeman, E.M. and Smith, B.E.:'Surface impedance method applied to multilayer cylindrical induction devices with circumferential exciting currents', Proc. IEE, 1970, 117, (10), pp. 2012-2013.

4.10 Pipes, L.A.:'Applied mathematics for engineers and physicists'. McGraw Hill Co., 2nd edition, 1958, pp. 186- 187.

4.11 Abramowitz, M. and Stegun, I.A.:(editors):'Handbook of mathematical functions', National Bureau of Standards, Appl. Math. series 55, 3rd printing, 1965.

4.12 Woodson, H.H. and Melcher, J.R.:'Electromechanical dynamics: Pt. I - Discrete systems', John Wiley, 1968, p. 268.

Chapter 5

5.1 Nagaoka, H.:'The inductance coefficients of solenoids', J. College of Science, Imp. Univ., Tokyo, Japan, 1909, Vol. 27, aritcle 6, pp. 1-33.

5.2 Moullin, E.B.:'The use of Bessel functions for calculating the self-inductance of single-layer solenoids', Proc. IEE, 1949, 96, Pt. III, pp. 133-137.

5.3 Phillips, F.M.:'A note on the inductance of screened single-layer solenoids', Proc. IEE, 1949, 96, Pt. III, pp. 138-140.

5.4 Bogle, A.G.:'The effective inductance and resistance of screened coil' , J. IEE, 1940, 87, pp. 299-316.

5.5 Butterworth, S.:'Eddy current losses in cylindrical conductors, with special applications to the alternating current resistance of short coils', Phil. Trans. of the Royal Soc. of London, 1921, 222, pp. 57-100.

5.6 Butterworth, S.:'Note on the alternating current resistance of single layer coils', Physical Review, 1924, 23, pp. 752-755.

5.7 Butterworth, S.:'On the alternating current resistance of solenoidal coils', Proc. of the Royal Soc. of London, 1925, A, 107, p. 693.

5.8 Phillips, F.M.:'The eddy current and screen losses of a screened single layer solenoid', Proc. IEE, 1950, 97, Pt. III, pp. 77-87.

5.9 Onoe, M.:'Analysis of a finite solenoid coil near a conductor', Elec. Eng. in Japan, 1968, 88, (10), pp. 59-67.

5.10 Yamamoto, T. and Baba, Y.:'Impedance calculation tables of finite single layer solenoid coil encircling a cylindrical magnetic conductor and their application', Mem. of Sch. of Eng., Okayama Univ., 1977, 11, (2), pp.17-26.

5.11 Balakhotsev, G.A., Zinovev, V.K., Devyatkin, A.B. and Andreev, V.M.: 'Formation of ingot surface during continuous casting', Tsvet. Met., 1970, 8, pp. 64-65.

5.12 Mochalov, P.P. and Getselev, Z.N.:'Continuous casting with the ingot formation in an electromagnetic field', Tsvet. Met., 1970, 8, pp. 62-63.

5.13 Getselev, Z.N.:'The production of continuously cast shapes using electromagnetic forming', J. of Metals, 1971, Oct. pp. 38-39.

5.14 Getselev, Z.N.:'Apparatus for continuous and semi-continuous casting of metals', British Patent Specification No. 1,517,977.

5.15 Fluerasu, C. and Galan, N.:'Eddy currents and the power converted into heat inside a very long cylindrical conductor placed in an a.c. circular coil of finite length', Rev. Roum. Sci. Tech.- Electrotech. et Energ., 1966, 11, (2), pp. 123-141.

5.16 Dodd, C.V.:'Solutions to electromagnetic induction problems', Ph.D. dissertation, Univ. of Tennessee, U.S., 1967.

5.17 McLachlan, N.W.:'Bessel functions for engineers', Oxford Univ. Press, 2nd Edition, p. 128.

5.18 Abramowitz, M. and Stegun, I.A. (editors):'Handbook of mathematical functions', National Bureau of Standards, Appl. Math. series 55, 3rd printing, 1965, p375.

5.19 Freeman, E.M.:'The calculation of harmonics, due to slotting, in the flux-density waveform of a dynamo-electric machine', Proc. IEE, 1962, 109C, pp. 581-588.

Chapter 6

6.1 Okress, E.C., Wroughton, D.M., Comenetz, G., Brace, P.H. and Kelly, J.C.R:'Electromagnetic levitation of solid and molten metals', J. Appl. Phys., 1952, 23, (5), pp. 545-552.

6.2 Brisley, W. and Thornton, B.S.:'Electromagnetic levitation calculations for axially symmetric systems', Brit. J. Appl. Phys. 1963, 14, pp. 682-686.

6.3 Smith, W.E.:'Electromagnetic levitation forces and effective inductance in axially symmetric systems', Brit. J. Appli. Phys., 1965, 16, pp. 377-383.

6.4 Boerdijk, A.H: 'Technical aspects of levitation', Philips Res. Rep., 1956, 11, pp. 45-56.

6.5 Laithwaite, E.R.:'Electromagnetic levitation', Proc. IEE, 1965, 112, (12), pp. 2361-2375.

6.6 Popovic, B.D.:'Introductory engineering electromagnetics', Addison-Wesley Co., U.S.A., 1971, pp. 348-350.

6.7 Smythe, W.R.:'Static and dynamic electricity', McGraw-Hill Co., N.Y., 2nd edition, 1950, pp. 396-400.

6.8 Moon, P. and Spencer, D.E.:'Field theory handbook',Springer-Verlag, 1961, pp. 141-142.

6.9 Spiegel, M.R.:'Mathematical Handbook of formulas and tables', Schaum's series, McGraw-Hill, 1968, p150.

6.10 Lipinski, W., Rolicz, P. and Sikora, R.:'Application of integral transforms to the analysis of the magnetic field of a spherical coil', Trans. IEEE, 1975, MAG-11, (5), pp. 1552-1554.

Chapter 7

7.1 Heaviside, O.:'Electromagnetic theory', Vol. I-III, (Dover pub. N.Y., 1950).

7.2 McLachlan, N.W.:'Complex variables and operational claculus with technical applications', (C.U.P., 1946).

7.3 Carslaw, H.S. and Jaeger, J.C.:'Operational methods in applied mathematics', (O.U.P., 1941).

7.4 Ku, Y.H.:'Transient circuit analysis', (Van Nostrad, N.Y., 1961).

7.5 Rothe, R., Ollendorff, F. and Pohlhausen, K.:'Theory of functions as applied to engineering problems', (Dover pub., N.Y., 1961).

7.6 Miller, K.W.:'Diffusion of electric current into rods, tubes and flat surfaces', Trans. AIEE, 1947, 66, pp. 1496-1502.

7.7 Vallese, L.M.:'Diffusion of pulsed currents in conductors', J. Appl. Phys., 1954, 25, (2), pp. 225-228.

7.8 Grumet, A.:'Penetration of transient electromagnetic fields into a conductor', J. Appl.Phys., 30, (5), pp. 682-686.

7.9 Mocanu, C.I.:'Transient penetration of the electromagnetic field into a conductor excited by a constant electric field', Rev. Roum. Sci. Techn. - Electrotechn. et Energ., 1974, 19 (4), pp. 531-546.

7.10 Chura, V.:'Eddy-current transients', Proc. IEE, 1976, 123, (3), pp. 245-251.

7.11 Vanyan, L.L.:'Electromagnetic depth soundings', selected and translated George V. Keller, Consultants Bureau, N.Y.

7.12 Morrison, H.F., Phillips, R.J. and O'Brien, D.P.:'Quantitative interpretation of transient electromagnetic fields over a layered half space', Geophysical Prospecting, 1969, 17, pp. 82-101.

7.13 Hjelt, S. -E:'The transient electromagnetic field of a two-layer sphere', 1971, Geoexploration, 9, pp. 213-229.

7.14 Bratoljic, T.:'Electromagnetic transients in superconducting turbogenerators', Int. Conf. on Elec. Machines, City Univ., London, 1974, paper A7.

7.15 Miller, T.J.E. and Lawrenson, P.J.:'Penetration of transient magnetic fields through conducting cylindrical structures with particular reference to superconducting a.c. machines', Proc. IEE, 1976, 123, (5), pp. 437-443.

7.16 Baum, C.E.:'Emerging Technology for transient and Broad-Band analysis and synthesis of antennas and scatterers', Proc. IEEE, 1976, 64, (11), pp. 1598-1616.

7.17 IBM:'1620 Electronic circuit analysis program-users manual', IBM Manual GH 20-0170-2.

7.18 Kaplan, G.:'Computer aided design', IEEE Spectrum, October 1975, pp. 40-47.

7.19 Freeman, E.M.:'Computer aided steady-state and transient solutions of field problems in certain induction devices', Proc. IEE, 1977, 124, (11), pp. 1057-1061.

7.20 Lu, H.:'Transient analysis of induction devices using equivalent circuit theory', M.Sc. thesis, London Univ., 1976.

7.21 Carroll, D.P. and Nozari, F.:An efficient computer method for simulating transients on transmission lines with frequency dependent parameters', Trans. IEEE, 1975, PAS-94, (4), pp.1167-1176.

7.22 Ametani, A.:'A highly efficient method for calculating transmission line transients', Trans. IEEE, 1976, PAS-95, (5), pp. 1545-1551.

APPENDIX A

Maxwell field equations in the generalised cylindrical co-ordinate systems

Maxwell equations:

$$\nabla \times \bar{E} = -\frac{\delta \bar{B}}{\delta t}$$

$$\nabla \times \bar{H} = \sigma \bar{E} + \varepsilon \frac{\delta \bar{E}}{\delta t}$$

For a cylindrical coordinate system (u', u^2, z), having z as an axial direction, excited by a travelling wave of the form: $\exp\{j(\omega t - \beta z)\}$, the above curl equations can be expanded in the u'- and u^2- directions as follows:

$$\left.\begin{aligned}
(1/\sqrt{g_{22}}) \cdot \{\frac{\delta}{\delta u^2} E_z + j\beta E_2 \sqrt{g_{22}}\} &= -j\omega\mu H_1 \\
(1/\sqrt{g_{11}}) \cdot \{-j\beta E_1 \sqrt{g_{11}} - \frac{\delta}{\delta u'} E_z\} &= -j\omega\mu H_2 \\
(1/\sqrt{g_{22}}) \cdot \{\frac{\delta}{\delta u^2} H_z + j\beta H_2 \sqrt{g_{22}}\} &= (\sigma + j\omega\varepsilon) E_1 \\
(1/\sqrt{g_{11}}) \cdot \{-j\beta H_1 \sqrt{g_{11}} - \frac{\delta}{\delta u'} H_z\} &= (\sigma + j\omega\varepsilon) E_2
\end{aligned}\right\} \quad (A.1)$$

where the g's are the 'metric coefficients'.

With the appropriate algebraic manipulation of the above four equations, we can write expressions for the transverse field components in terms of its axial components as shown below:

$$
\begin{aligned}
E_1 &= (1/\gamma^2) \cdot \{(j\beta/\sqrt{g_{11}}) \frac{\delta}{\delta u_1} E_z + (j\omega\mu/\sqrt{g_{22}}) \frac{\delta}{\delta u_2} H_z\} \\
E_2 &= (1/\gamma^2) \cdot \{(j\beta/\sqrt{g_{22}}) \frac{\delta}{\delta u_2} E_z - (j\omega\mu/\sqrt{g_{11}}) \frac{\delta}{\delta u_1} H_z\} \\
H_1 &= (1/\gamma^2) \cdot \{-(\sigma_c/\sqrt{g_{22}}) \frac{\delta}{\delta u_2} E_z + (j\beta/\sqrt{g_{11}}) \frac{\delta}{\delta u_1} H_z\} \\
H_2 &= (1/\gamma^2) \cdot \{(\sigma_c/\sqrt{g_{11}}) \frac{\delta}{\delta u_1} E_z + (j\beta/\sqrt{g_{22}}) \frac{\delta}{\delta u_2} H_z\}
\end{aligned}
\qquad \text{(A.2)}
$$

Where:

$$\sigma_c = \sigma + j\omega\varepsilon$$

$$\gamma^2 = \beta^2 - \omega^2\mu\varepsilon + j\omega\mu\sigma$$

Again, the above equation can be written in the vector form as follows:

$$
\left.
\begin{aligned}
\bar{E}_t &= (1/\gamma^2) \cdot \{ j\beta \nabla_t E_z - j\omega\mu \bar{a}_z \times \nabla_t H_z \} \\
\bar{H}_t &= (1/\gamma^2) \cdot \{ \sigma_c \bar{a}_z \times \nabla_t E_z + j\beta \nabla_t H_z \}
\end{aligned}
\right\} \qquad \text{(A.3)}
$$

Where

$\bar{E}_t$ and $\bar{H}_t$ are the components of the electric and magnetic vector fields transverse to the axial direction.

∇_t is the Nabla operator in the transverse direction to z, and is given by:

$$\nabla_t = \nabla - \frac{\delta}{\delta z}$$

Equations (A.2) or (A.3) exhibit the distinct feature of the cylindircal coordinates systems, which is the possibility of expressing the transverse components of the electric and magnetic fields in terms of its axial components only. It is common practice in microwave theory, where similar equations arise when studying waveguides or cavity resonators, to consider the solution obtained by equations (A.2) as composed of two basic modes or wave types. One is known as E-wave or TM-wave, where all field components are given in terms of E_z only as shown below in equation (A.4). While the other is known as H-wave or TE-wave, where the solutions for all field components are given in terms of H_z only as shown in equation (A.5).

(I) <u>The electric and magnetic fields components of the E-wave</u>

$$\left.\begin{aligned} E_1 &= j\beta/\gamma^2 \cdot 1/\sqrt{g_{11}} \cdot \frac{\delta}{\delta u'} E_z \\ E_2 &= j\beta/\gamma^2 \cdot 1/\sqrt{g_{22}} \cdot \frac{\delta}{\delta u^2} E_z \\ E_3 &= E_z \end{aligned}\right\} \quad (A.4)$$

$$
\left.
\begin{aligned}
H_1 &= -(\sigma + j\omega\varepsilon)/\gamma^2 \cdot 1/\sqrt{g_{22}} \cdot \frac{\delta}{\delta u^2} E_z \\
H_2 &= (\sigma + j\omega\varepsilon)/\gamma^2 \cdot 1/\sqrt{g_{11}} \cdot \frac{\delta}{\delta u'} E_z \\
H_3 &= 0
\end{aligned}
\right\} \quad (A.4)
$$

(II) <u>The electric and magnetic fields components of the H-wave</u>

$$
\left.
\begin{aligned}
H_1 &= j\beta/\gamma^2 \cdot 1/\sqrt{g_{11}} \cdot \frac{\delta}{\delta u'} H_z \\
H_2 &= j\beta/\gamma^2 \cdot 1/\sqrt{g_{22}} \cdot \frac{\delta}{\delta u^2} H_z \\
H_3 &= H_z \\
E_1 &= j\omega\mu/\gamma^2 \cdot 1/\sqrt{g_{22}} \cdot \frac{\delta}{\delta u^2} H_z \\
E_2 &= -j\omega\mu/\gamma^2 \cdot 1/\sqrt{g_{11}} \cdot \frac{\delta}{\delta u'} H_z \\
E_3 &= 0
\end{aligned}
\right\} \quad (A.5)
$$

It is quite obvious from the decomposition of the main field into two basic modes, that each mode will depend only on one scalar quantity, i.e. TM-wave depends on E_z, while the TE-wave depends on H_z. The coupling between these two modes is usually introduced in order to satisfy the boundary conditions.

List of papers accepted for publication

1. Freeman, E.M. and El-Markabi, M.H.S.:'Two dimensional field analysis and input impedance of a finite length solenoidal coil'.
   To be published in Proc. IEE , 1978

2. Freeman, E.M. and El-Markabi, M.H.S.:'A simplified computational technique for longitudinal H-field shielding'.
   To be publsihed in Trans. IEEE, Electromagnetic Compatability, 1978.

3. El-Markabi, M.H.S.and Freeman, E.M.:'The electromagnetic field and shielding effect of a three phase helical winding placed coaxially inside a multiregion cylindrical structure' .
   To be published in the proceedings of"International Conference on electrical machines', Brussels, 11-13 Sept. 1978.

4. El-Markabi, M.H.S. and Freeman, E.M.:'The impedance of a finite length coil immersed in a circular cylindrical conducting structure'.
   To be published in Trans. IEEE, MAG-14, (5), 1978.

5. Freeman, E.M. and El -Markabi, M.H.S.:'Digest of reference 4 mentioned above', Intermag Conf. 1978, Flourence, Paper No. 4-3.